A study of Gamma-Ray Bursts and Soft Gamma Repeaters Detected with the INTEGRAL Burst Alert System

Diego Götz

Università degli Studi di Milano Bicocca
Facoltà di Scienze Matematiche, Fisiche e Naturali
Dottorato di Ricerca in Astronomia e Astrofisica
XVII ciclo

A Study of Gamma-Ray Bursts and Soft Gamma Repeaters Detected with the *INTEGRAL* Burst Alert System

Supervisor: Dr. Sandro Mereghetti
Tutor: Prof. Francesco Haardt
Coordinatore: Prof. Guido Chincarini

PHD thesis of:
Diego Götz
Matricola R00186

Contents

Introduction: The Highly Variable Gamma-Ray Sky

Soon after the astronomers took a first glance at the high-energy sky,, during the '60 of the last century, it became evident, that the picture of a quiet, slowly changing sky was disrupted.

The sky at X and γ ray wavelenghts can be observed only with experiments flown above the Earth atmosphere: the first experiments were mounted on balloons or rockets, and their short lifetime (minutes to hours) was not enough to study the variability phenomenon. With the beginning of satellite borne astronomy (*UHURU, Ariel V, SAS-3* in X-rays and *OSO-3, SAS-2, COS-B* in γ-rays), longer exposure times and regular scans of the sky could be performed and the variability was discovered. Since then our sky maps have been quickly populated with thousands of new sources detected at energies > 0.1 keV. The vast majority of them have variable fluxes: some are *transients*, in the sense that their flux has increased just once over the sensitivity thresholds our instruments, while others are detected periodically (*recurrent transients*). Also in the domain of the *persistent* sources the flux variations can be of the order of 80% of the average flux. In fact it is hard to find a calibration source with a constant flux at these energies. Some sources can indeed be identified thanks to their specific temporal variability signatures. For instance the discovery of eclipses, allowed to confirm the binary nature of many of them, while the detection of regular pulsations indicates the presence of a highly magnetized neutron star.

The flux variations observed in the high-energy sky appear in the observer's frame on all time scales, from milliseconds to years. The physical mechanisms that induce such variations have been studied ever since their discovery. In many cases the identification of the source at other wavelengths (radio, optical, etc.) is a critical issue, in order to build a complete physical picture of the studied object. However, often the identification is not an easy task, since the error boxes provided by high-energy instruments (especially in γ rays) are typically too large (from a few arcmin to a degree) to uniquely identify an optical/radio counterpart. In these cases the detection at different wavelengths of related flux variations in the candidate sources are very useful to derive to a successful identification.

A clear example in this respect is given by Gamma-Ray Bursts (GRBs, see

Chapter 1). They are intense flashes of γ-rays that appear randomly in the sky. They can last from a few ms to hundreds of seconds, druing which they are the most intense sources in the sky, and present flux variations over all timescales. They were discovered by the Vela satellites (Klebesadel et al., 1973) (that aimed to the monitoring of nuclear explosions on Earth) and remained an intriguing mystery for a few decades, until, thanks to the Italian-Dutch satellite *BeppoSAX* , the first counterparts at X-ray wavelengths were discovered (Costa et al., 1997). The low-energy counterparts of GRBs have a rapidly (hours to days) fading behavior: the quick re-pointing of the satellite made it possible to discover an X-ray source within the error box, which could thus be reduced to the arcsec size,leading to the discovery of the fading optical (van Paradijs et al., 1997) and radio (Frail et al., 1997) counterparts. Finally the first redshift measurement (Metzger et al., 1997) closed the long lasting debate on the distance scale of GRBs, indicating that these are the most powerful cosmic explosions since the Big Bang. The first results and the developments of this multi-wavelength observation strategy have represented the major breakthrough in the GRB science, allowing to associate these enigmatic sources to the death of massive stars in distant ($0.1< z <4.5$) galaxies, and to start to depict a complete theory on them.

INTEGRAL , launched in October 2002, is an ESA γ-ray (15 keV-10 MeV) satellite. The characteristics of its coded mask imaging telescope (IBIS) (energy range, large field of view ($29°\times29°$) and good location accuracy down to 30 arcsec), make it an excellent instrument for the detection of GRBs. To allow for their rapid detection and localization a software system, running at *INTEGRAL* Science Data Centre (ISDC), has been developed: the *INTEGRAL* Burst Alert System (IBAS; Mereghetti et al. (2003e)). Thanks to the fact that the telemetry of the satellite reaches the ISDC in real time, such a localization can occur within a few tens of seconds and follow-up observations with robotic telescopes can potentially start while the burst is still active (Chapter 2). A total of 18 GRBs have been detected thanks to IBAS in the *INTEGRAL* data, the majority of them within a few seconds from the cosmic event. The results on these bursts will be presented here as part of this Thesis (Chapter 3).

While the observation strategy for GRBs, based on quasi-simultaneous multi-wavelength observations, has been successfully exploited for the understanding of these sources, other transient and variable sources still lack of multi-wavelength information during their outbursts. An example is the peculiar class of neutron stars known as Soft Gamma Repeaters. These source alternate active periods, during which they emit aperiodic short ($\sim$0.1 s) bursts, to periods of quiescence. The results on the *INTEGRAL* observation of one of these sources (SGR 1806–20), concerning in particular the discovery the spectral evolution within the bursts, will be presented here (Chapter 4).

Part I

IBAS and Gamma-Ray Bursts

Chapter 1

Gamma-Ray Bursts: the Astrophysical Scenario

In this Chapter the main observational properties of Gamma-Ray Bursts will be presented. For the details on the theoretical aspects the reader is addressed to the many recent rewievs on this subject (e.g. Hurley et al. (2003b); Piran (2004)).

1.1 Introduction

Gamma-Ray Bursts (GRBs) are short and intense pulses of soft γ-rays. The bursts last from a fraction of a second to several hundred seconds. GRBs arrive from cosmological distances from random directions in the sky. The overall observed fluences range from 10^{-7} to 10^{-4} erg cm^{-2} (the lower limit depends, of course, on the characteristics of the detectors and not on the bursts themselves). This corresponds to isotropic luminosity of $10^{51} - 10^{52}$ erg s^{-1}, making GRBs the most luminous objects in the sky. However, we know today that most GRBs are narrowly beamed and the corresponding emitted energies are "only" around 10^{51}ergs (Frail et al., 2001; Panaitescu & Kumar, 2001; Piran et al., 2001), making them comparable to Supernovae in the total energy release.

The GRBs are followed by afterglows - lower energy, long lasting emission in the X-ray, optical and radio. The radio afterglow was observed in some cases several years after the bursts. The accurate afterglow positions enabled the identification of host galaxies in almost all cases when afterglow was detected and this in turn enabled the determination of the corresponding redshifts that range from 0.105 (or possibly even down to 0.0085) to 4.5. Within the host galaxies there is evidence that (long duration) GRBs arise within star forming regions and there is evidence that the redshift distribution follows the star formation rate.

While not all observed features are understood, there is an overall agreement between the observations and the fireball model. According to the fireball model GRBs are produced when the kinetic energy of an ultra-relativistic flow is dissi-

pated. The GRB itself is produced by internal dissipation within the flow while the afterglow is produced via external shocks with the circum-burst medium.

The numerous observations of the GRB and the observations of the afterglow constrain the fireball model that describes the emitting regions. The evidence on nature of the inner engine that powers the GRB and produces the ultra-relativistic flow is however, indirect. The energetic requirements and the time scales suggest that GRB involve the formation of a black hole via a catastrophic stellar collapse event or possibly a neutron star merger. Additional indirect evidence arises from the requirement of the fireball model of long (several tens seconds) activity of the inner engine. This hints toward an inner engine involving an accreting black hole. On the other hand, the evidence for an association of GRBs with star forming regions indicates that GRBs progenitors are massive stars. Finally, the appearance of Supernova bumps in the afterglow light curve (most notably in GRB 030329) suggests association with Supernovae and stellar collapse.

1.2 Observations

1.2.1 Prompt Emission

Here the so called *prompt emission* will be presented, namely the GRB itself, including the emission at other wavelengths but emitted simultaneously to the γ-rays. This includes the X-ray emission that generally accompanies the γ-ray emission as a low energy tail. In some cases, called X-ray flashes (XRFs), the γ-ray signal is weak and comparable to or smaller than the X-ray signal. Prompt (operationally defined as the time period when the γ-ray detector detects a signal above background) longer-wavelength emission may also occur at the optical and radio but it is harder to detect. So far optical flashes were observed in three cases (Akerlof et al., 1999; Fox et al., 2003b; Li et al., 2003) simultaneously with the γ-ray emission.

Spectrum

The spectrum is non thermal. The energy flux peaks at a few hundred keV and in many bursts there is a long high energy tail extending in cases up to GeV energies. The spectrum varies strongly from one burst to another. A phenomenological function to fit the photon spectrum was introduced by Band et al. (1993) consisting of two power laws joined smoothly at a break energy $(\alpha - \beta)E_0$:

$$N(E) = N_0 \begin{cases} E^{\alpha} \exp(-\frac{E}{E_0}), & \text{for } E < (\alpha - \beta)E_0; \\ \left[(\alpha - \beta)E_0\right]^{(\alpha-\beta)} E^{\beta} \exp(\beta - \alpha), & \text{for } E > (\alpha - \beta)E_0 \end{cases} \tag{1.1}$$

There is no particular theoretical model that predicts this spectral shape. Still, this function provides an excellent fit to most of the observed spectra. For

most observed values of α and β, the spectral energy distribution $\nu F_\nu \propto \nu^2 N(\nu)$ peaks at $E_p = (\alpha + 2)E_0$. For about 10% of the bursts the upper slope is smaller than -2 and there is no peak for νF_ν within the observed spectrum. Another group of bursts, NHE bursts, (no high energy) (Pendleton et al., 1997) does not have a hard component (which is reflected by a very negative value of β). Band et al. (1993) present a catalogue of the spectra of 52 bright bursts which they analyze in terms of the Band function. Preece et al. (2000) present a larger catalogue with 156 bursts selected for either high flux or fluence. They consider several spectral shape including the Band function.

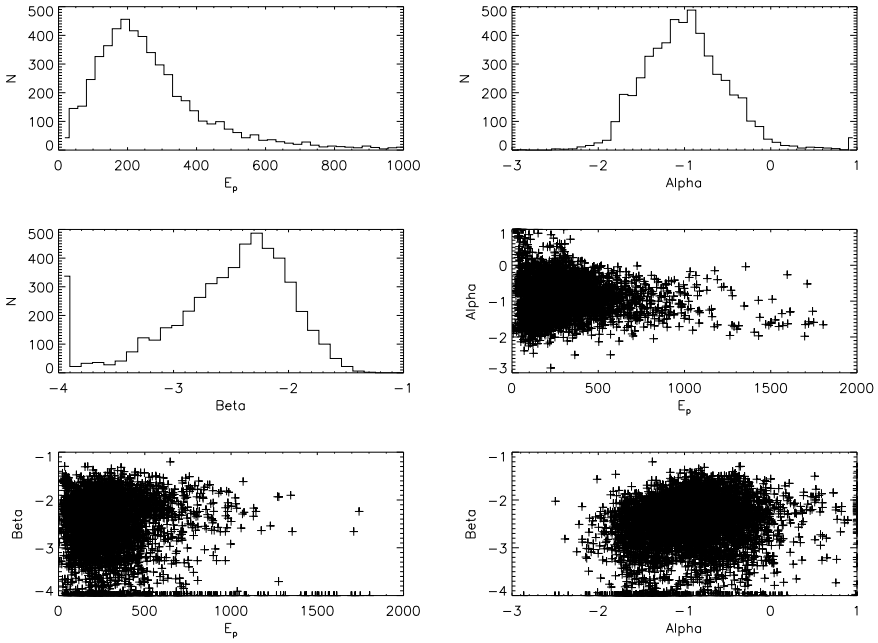

Figure 1.1: Distribution of the observed parameters of the Band function in a sample of bright bursts. The values are taken from Preece et al. (2000). The parameters are represented also in form of scatter plots as a function, in turn, of two of them.

Fig. 1.1 shows the distribution of observed values of the break energy, $(\alpha - \beta)E_0$, in a sample of bright bursts (Preece et al., 2000). For most of the bursts $(\alpha-\beta)E_0$ lies in the range 100-400 keV, with a clear maximum in the distribution around $(\alpha-\beta)E_0 \sim 250$keV. There are not many soft GRBs - that is, GRBs with peak energy in the tens of keV range. However, the discovery (Heise et al., 2001) of XRFs - X-ray flashes with similar temporal structure to GRBs but lower typical energies - shows that the low peak energy cutoff is not real and it reflects the lower sensitivity of BATSE in this range (Kippen et al., 2002).

Similarly, it is debatable whether there is a real paucity in hard GRBs and

there is an upper cutoff to the GRB hardness or it just happens that the detection is optimal in this (a few hundred keV) band. BATSE triggers, for example, are based on the count rate between 50 keV and 300 keV. BATSE is, therefore, less sensitive to harder bursts that emit most of their energy in the MeV range. Using BATSE's observations alone one cannot rule out the possibility that there is a population of harder GRBs that emit equal power in total energy which are not observed because of this selection effect

There is some evidence of a correlation between E_p and the observed peak flux (Mallozzi et al., 1995, 1998). More recently Amati et al. (2002) reported on a correlation between E_p and the isotropic equivalent energy seen in 12 *BeppoSAX* bursts. They also report on a correlation between E_p and the redshift as, the bursts with higher isotropic equivalent energy are typically more distant. These three different correlations are consistent with each other if the observed peak flux of bursts is determined by their intrinsic luminosity more than by the distance of the bursts. In such a case (because of the larger volume at larger distances) the observed more distant bursts are on average brighter than nearer ones.

Even though the burst hardness distribution shows a single population a plot of the hardness vs. temporal duration shows that short bursts (see Fig. 1.2) are typically harder (Dezalay et al., 1996; Kouveliotou et al., 1993). EGRET (The

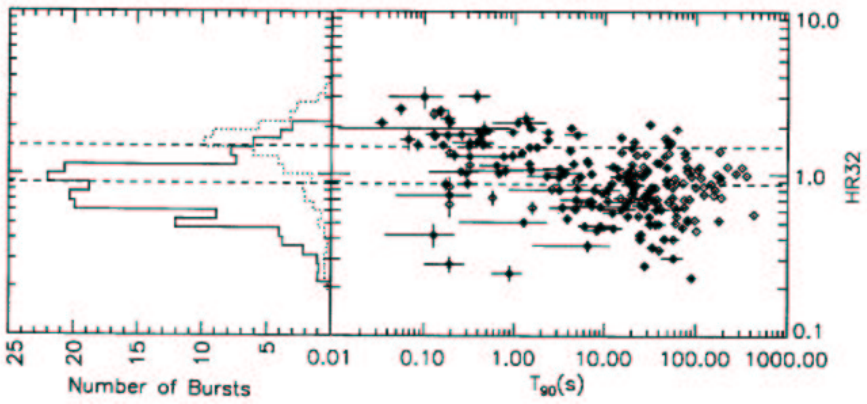

Figure 1.2: The hardness-duration correlation for BATSE bursts. HR is the ratio of fluence between BATSE channels 3 and 2. Left: Separate HR for the two duration classes. The solid line shows events with durations larger than 2 s, and the dotted line depicts events shorter than 2 s. Right: HR vs. duration scatter plot. The dashed lines on both plots correspond to the mean hardness ratio of the two duration classes (from Kouveliotou et al. (1993).)

Energetic Gamma Ray Experiment Telescope) the high energy γ-ray detector on Compton - GRO detected seven GRBs with photon energies ranging from 100 MeV to 18 GeV (Dingus & Catelli, 1998). In some cases this very high

energy emission is delayed more than an hour after the burst (Hurley, 1994; Sommer et al., 1994). No high-energy cutoff above a few MeV has been observed in any GRB spectrum. Recently, (González et al., 2003) have combined the BATSE (30keV -2MeV) data with the EGRET data for 26 bursts. In one of these bursts, GRB 941017, they have discovered a high energy tail that extended up to 200 MeV and looked like a different component. This high energy component appeared 10-20 s after the beginning of the burst and displayed a roughly constant flux with a relatively hard spectral slope ($F_\nu \propto \nu^0$) up to 200 s. At late time (150 after the trigger) the very high energy (10-200 MeV) tail contained 50 times more energy than the "main" γ-ray energy (30keV-2MeV) band. Another puzzle is the low energy tail. Cohen et al. (1997) analyze several strong bursts and find that their low energy slope is around -2/3 to -3/2. However, Preece et al. (1998, 2002) suggest that about 1/5 of the bursts have a the low energy power spectrum, α, flatter than -2/3 (the synchrotron slow cooling low energy slope). A larger fraction is flatter than -3/2 (the fast cooling synchrotron low energy slope). However, this is not seen in any of the HETE spectra whose low energy resolution is somewhat better. HETE bursts with good statistics have a low energy spectrum that is within the range -3/2 and -2/3 (Barraud et al., 2003). As both BATSE and HETE use NaI detectors that have a poor low energy resolution (Cohen et al., 1997), this problem might be resolved only when a better low energy spectrometer will be flown.

Temporal Structure

The observed durations of the bursts span five orders of magnitude, ranging from less than 0.01 s to more than 100 s. Common measures for the duration are T_{90} (T_{50}) which correspond to the time in which 90% (50%) of the counts of the GRB are accumulated. The bursts are divided to long and short bursts according to their T_{90} (see below). Most GRBs are highly variable, showing 100% variations in the flux on a time scale much shorter than the overall duration of the burst. Fig 1.3 depicts the light curves of some GRBs. The variability time scale, δt, is determined by the width of the peaks. δt is much shorter (in some cases by a more than a factor of 10^4) than T, the duration of the burst. Variability on a time scale of milliseconds has been observed in some long bursts (Nakar & Piran, 2002; McBreen et al., 2001). However, $\sim$ 80% of the bursts show substantial substructure in their light curves, while the rest are rather smooth, typically with a FRED (Fast Rise Exponential Decay) structure. The bursts seem to be composed of individual pulses, with a pulse being the "building block" of the overall light curve. Individual pulses display a hard to soft evolution with the peak energy decreasing exponentially with the photon fluence (Liang & Kargatis, 1996; Norris et al., 1996; Ford et al., 1995). The pulses have the following temporal and spectral features. (i) The light curve of an individual pulse is a FRED - fast rise exponential decay - with an average rise to decay ratio of 1:3 (Norris et al., 1996).

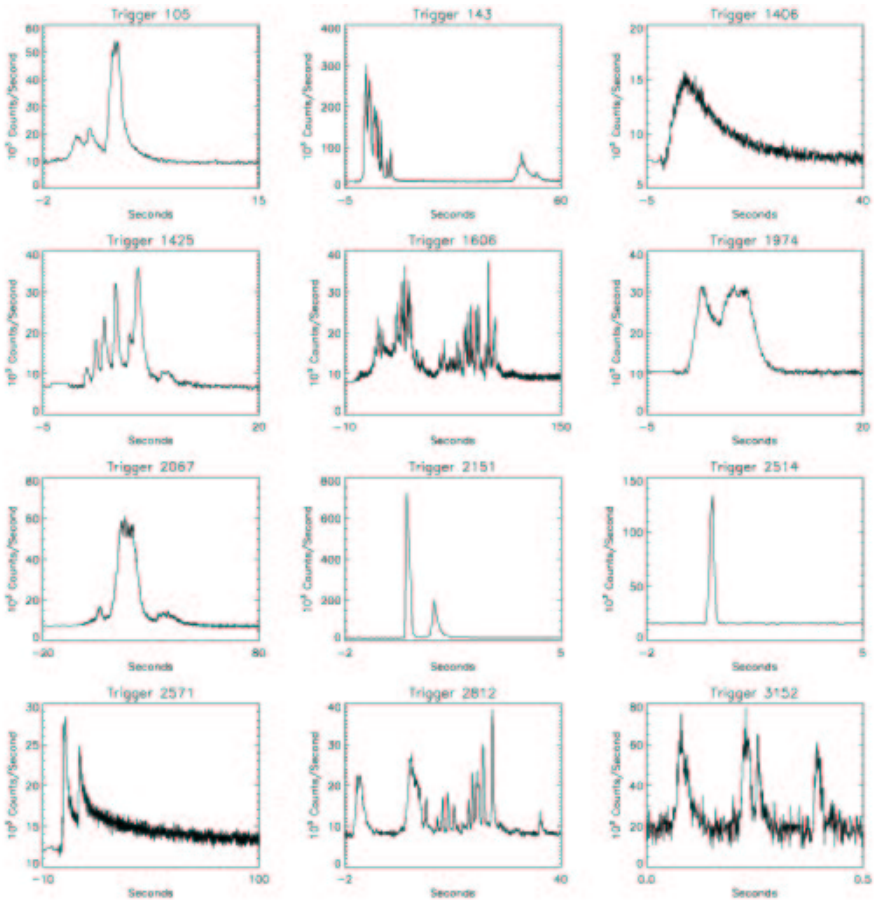

Figure 1.3: Some examples of BATSE GRB light curves. From HEASARC Web Pages.

(ii) The low energy emission is delayed compared to the high energy emission[1] (Norris et al., 1996). Norris et al. (2000) have found that these spectral lags are anti-correlated with the luminosity of the bursts: luminous bursts have long lags. This lag luminosity relation provides another way to estimate the luminosity of a burst from its (multi-spectra) light curve. (iii) The pulses low energy light curves are wider compared to the high energy light curves. The width goes as $\sim E^{-0.4}$(Fenimore et al., 1995). (iv) There is a Hardness-Intensity correlation. The instantaneous spectral hardness of a pulse is correlated to the instantaneous intensity (the pulse become softer during the pulse decay) (Borgonovo & Ryde, 2001).

[1]Low/high energy implies the low vs. the high BATSE channels. The four BATSE channels at 20-50keV, 50-100keV, 100-300keV and $>$ 300keV.

Populations

Long and Short Bursts The clearest classification of bursts is based on their duration. Kouveliotou et al. (1993) have shown that GRB can be divided to two distinct groups: long bursts with $T_{90} > 2$s and short bursts with $T_{90} < 2$s.

Short bursts are typically harder (Dezalay et al., 1996; Kouveliotou et al., 1996). The duration-hardness distribution (see Fig. 1.2) shows clearly that there are not soft short bursts. So far afterglows were detected only from long bursts. It is not clear whether this is an observational artifact or a real feature. However, there was no X-ray afterglow observed for the only well localized short hard burst: GRB 020531 (Hurley et al., 2002d). *Chandra* observations show an intensity weaker by at least a factor of 100-300 than the intensity of the X-ray afterglow from long bursts at a similar time (Butler et al., 2002). No afterglow was not observed in other wavelength as well (Klotz et al., 2003)

As identification of hosts and redshift determination depend on the detection of afterglow this implies that nothing is known about the distance, progenitors, environment etc.. of short burst. These bursts are still waiting for their afterglow revolution.

X-ray Flashes (XRFs) are X-ray bursts with a similar temporal structure to GRBs but lower typical energies. Heise et al. (2001) discovered these flashes by comparing GRBM (GRB Monitor), with sensitivity above 40 keV, and WFC (Wide Field Camera) triggers on *BeppoSAX*. In 39 cases the WFCs were triggered without GRBM triggers, implying that these "flashes" have a weak hard component and most of their flux is in X-rays. The duration of these transients, denoted X-rays flashes (XRFs), is comparable to the duration of the X-ray emission accompanying GRBs. The peak fluxes of the XRFs are similar to the X-ray fluxes observed during GRBs in the WFCs ($\sim 10^{-8}$ergs/sec/cm^2) but their peak energy is clearly below 40 keV. These finding confirmed the detection of Strohmayer et al. (1998) of 7 GRBs with $E_p < 10$ keV and 5 additional GRBs with $E_p < 50$ keV in the *Ginga* data.

Barraud et al. (2003) analyze 35 bursts detected on HETE II. They find that XRFs lie on the extension of all the relevant GRB distributions. Namely there is a continuity from GRBs to XRFs. Detailed searches in the BATSE data revealed that some of these bursts had also been detected by BATSE (Kippen et al., 2002). In 6 years of *BeppoSAX* observations 32 XRFs have been observed above a threshold peak-luminosity of 5×10^{-9}erg/s/cm^2 in the 2-25 keV range compared with 54 GRBs (all GRBs above BATSE thresholds are observed if in the field of view).

Soderberg et al. (2002) discovered an optical afterglow from XRF 020903 and they suggest that the burst was at $z = 0.25$. They also suggest a hint of an underlying SN signal (see Section 1.2.3) peaking between 7-24 days after the initial XRF trigger. An afterglow was discovered from XRF 030723 as well (Fox et al., 2003a).

Polarization

Recently, Coburn & Boggs (2003) reported the detection of a very high (80% ± 20%) linear polarization in the prompt γ-ray emission of GRB 021206 recorded by the Reuven Ramaty High Energy Solar Spectroscopic Imager (RHESSI). This burst was extremely powerful, with an observed fluence of 1.6×10^{-4} erg s^{-1}in the energy range of 25-100 keV (Hurley et al., 2002b,c). This puts GRB 021206 as one of the most powerful bursts, and the most powerful one (a factor of 2-3 above GRB 990123) after correcting for the fact that it was observed only in a narrow energy band (compared to the wide BATSE band of 20-2000keV). The polarization is measured in RHESSI by the angular dependence of the number detection of simultaneous pairs of events that are most likely caused by a scattering of the detected γ-rays within the detector. Coburn & Boggs (2003) rejected the hypothesis of no polarization at confidence level of 5.7σ.

Rutledge & Fox (2004) reanalyzed this data and pointed out several inconsistencies within the methodology of Coburn & Boggs (2003). Their upper limit on the polarization (based on the same data) is $\sim 4\%$. In their reply Boggs & Coburn (2003) point out that the strong upper limit (obtained by Rutledge & Fox (2004) is inconsistent with the low S/N estimated by these authors. However, they do not provide a clear answer to the criticism of the methodology raised by Rutledge & Fox (2004). This leaves the situation, concerning the prompt polarization from this burst highly uncertain.

Prompt Optical Flashes

The Robotic telescope ROTSE (Robotic Optical Transient Search Experiment) detected a 9^{th} magnitude optical flash that was concurrent with the GRB emission from GRB 990123 (Akerlof et al., 1999). The six snapshots begun 40 s after the trigger and lasted until three minutes after the burst. The second snapshot that took place 60 s after the trigger recorded a 9^{th} magnitude flash. While the six snapshots do not provide a "light curve" it is clear that the peak optical flux does not coincide with the peak of the γ-ray emission that takes place around the first ROTSE snapshot. This suggests that the optical flux is not the "low energy tail" of the γ-ray emission. Recently, Fox et al. (2003b) reported on a detection of 15.45 magnitude optical signal from GRB 021004 193 s after the trigger. This is just 93 s after the 100 s long burst stopped being active. Shortly afterwards Li et al. (2003) reported on a detection of 14.67 magnitude optical signal from GRB 021211 105 s after the trigger. Finally, Price et al. (2003) detected a 12th magnitude prompt flash, albeit this is more than 1.5 hours after the trigger. Similar prompt signal was not observed from any other burst in spite of extensive searches that provided upper limits. Kehoe et al. (2001) searched 5 bright bursts and found single-image upper limits ranging from 13^{th} to 14^{th} magnitude around 10 s after the initial burst detection and from 14 to 15.8 magnitudes one hour

later. These upper limits are consistent with the two recent detections which are around 15^{th} mag. The recent events of rapid detection suggest that we should expect many more such discoveries in the near future.

The GRB-Afterglow Transition - Observations

There is no obvious direct correlation between the γ-ray fluxes and the X-ray (or optical) afterglow fluxes. The extrapolation of the X-ray afterglow fluxes backwards generally does not fit the γ-ray fluxes. Instead they fit the late prompt X-ray signal. These results are in nice agreement with the predictions of the Internal - External shocks scenario in which the two phenomena are produced by different effects and one should not expect a simple extrapolation to work.

The expected GRB-afterglow transitions have been observed in several cases. The first observation took place (but was not reported until much later) already in 1992 (Burenin et al., 1999). *BeppoSAX* data show a rather sharp transition in the hardness that takes place several dozen seconds after the beginning of the bursts. This transition is seen clearly in the different energy bands light curves of GRB 990123 and in GRB 980923 (Giblin et al., 1999). Connaughton (2002) have averaged the light curves of many GRBs and discovered long and soft tails: the early X-ray afterglow. Additional evidence for the transition from the GRB to the afterglow is inferred from significant spectral changes within the same GRB (Preece et al., 2002).

1.2.2 The Afterglow Revolution

No known counterparts to GRBs in other wavelengths were known before 1997. On Feb 28 1997 the Italian satellite *BeppoSAX* detected the X-ray afterglow from GRB 970228 (Costa et al., 1997). The resulting precise position given by *BeppoSAX* led to the discovery of the optical afterglow (van Paradijs et al., 1997). A radio afterglow was discovered, again following a *BeppoSAX* precise localization, in GRB 970508 (Frail et al., 1997). By now more than forty X-ray afterglows have been observed[2]. About half of them have optical and radio afterglows. The accurate positions given by the afterglow enabled the identification of the host galaxies of many bursts. In twenty or so cases the redshift has been measured. The observed redshifts range from 0.105 for GRB 031203 (or 0.0085 for GRB 980425) to a record of 4.5 (GRB 000131).

The X-ray afterglow

The X-ray afterglow is the first, most energetic, but shortest signal. In fact it seems to begin already while the GRB is going on (see Section 1.2.1). The light

[2]see http://www.mpe.mpg.de/~jcg/grb.html for a complete up to date tables of well localized GRBs with or without afterglow, maintained by Jochen Greiner

curve observed several hours after the burst can in some cases be extrapolated backward to the late parts of the prompt emission.

The X-ray afterglow fluxes from GRBs have a power law dependence on ν and on the observed time t (Piro, 2001): $f_\nu(t) \propto \nu^{-\beta} t^{-\alpha}$ with $\alpha \sim 1.4$ and $\beta \sim 0.9$. The distribution of X-ray fluxes, when normalized to a fixed time after the burst, is a rather narrow. A cancellation of the k corrections and the temporal decay makes this flux, which is proportional to $(1+z)^{\beta-\alpha}$, insensitive to the redshift. Using 21 *BeppoSAX* bursts (Piro, 2001), Piran et al. (2001) find that the 1-10 keV flux, 11 hours after the burst is 5×10^{-13}ergs cm^{-2}s^{-1}. The distribution is log-normal with $\sigma_{f_x} \approx 0.43 \pm 0.1$. De Pasquale et al. (2003) find a similar result for a larger sample. However, they find that the X-ray afterglows of GRBs with optical counterparts are on average 5 times brighter than those of "dark" GRBs (GRBs with no detected optical afterglow). The overall energy emitted in the X-ray afterglow is generally a few percent of the GRB energy. Berger et al. (2003) find that the X-ray luminosity is indeed correlated with the opening angle and when taking the beaming correction into account they find that $L_X = f_b L_{X,iso}$, is approximately constant, with a dispersion of only a factor of 2.

X-ray lines were seen in 8 GRBs: 970508 (Amati et al., 1999), 970828 (Yoshida et al., 1999), 990705 (Amati et al., 2000), 991216 (Piro et al., 2000), 001025a (Watson et al., 2002), 000214 (Antonelli et al., 2000), 011211 (Reeves et al., 2002), 030227 (Watson et al., 2003). The lines were detected using different instruments: *BeppoSAX* , *ASCA* (Advanced Satellite for Cosmology and Astrophysics), *Chandra* and *XMM-Newton* . The lines were detected around 10 hours after the burst, with typical luminosity in the lines around $10^{44} - 10^{45}$ergs s^{-1}, corresponding to a total fluence of about 10^{49}ergs. Most of the lines are interpreted as emission lines of Fe Kα. However, there are also a radiative-recombination-continuum line edge and Kα lines of lighter elements like Si, S, Ar and Ca (seen in the afterglows of GRB 011211 and GRB 030227). In one case (GRB 990705, Amati et al. (2000)) a transient absorption feature, corresponding to Fe Kα, has been detected within the prompt X-ray emission. The statistical significance of the detection of these lines is of some concern (2-5 σ), and even though the currently used instruments on *XMM-Newton* and *Chandra* are much more sensitive than those of previous satellites, all the line detections remain at this low significance level. Rutledge & Sako (2003) and Sako et al. (2004) expressed concern about the statistical analysis of the data and claim that none of the observed lines is statistically significant. The theoretical implications are far reaching. Not only the lines require, in most models, a very large amount of Iron at rest (the lines are quite narrow), they most likely require (Ghisellini et al., 2002) a huge energy supply ($> 10^{52}$ergs), twenty times larger than the typical estimated γ-ray energy ($\sim 5 \cdot 10^{50}$ergs).

Optical and IR afterglow

About 50% of well localized GRBs show optical and IR afterglow. The observed optical afterglow is typically around 19-20 mag one day after the burst (see Fig. 1.4). The signal decays, initially, as a power law in time, $t^{-\alpha}$ with a typical value of $\alpha \approx 1.2$ and large variations around this value. In all cases the observed optical spectrum is also a power law $\nu^{-\beta}$. Generally absorption lines are superimposed on this power law. The absorption lines correspond to absorption on the way from the source to earth. Typically the highest redshift lines are associated with the host galaxy, providing a measurement of the redshift of the GRB. In a few cases emission lines, presumably from excited gas along the line of site were also observed.

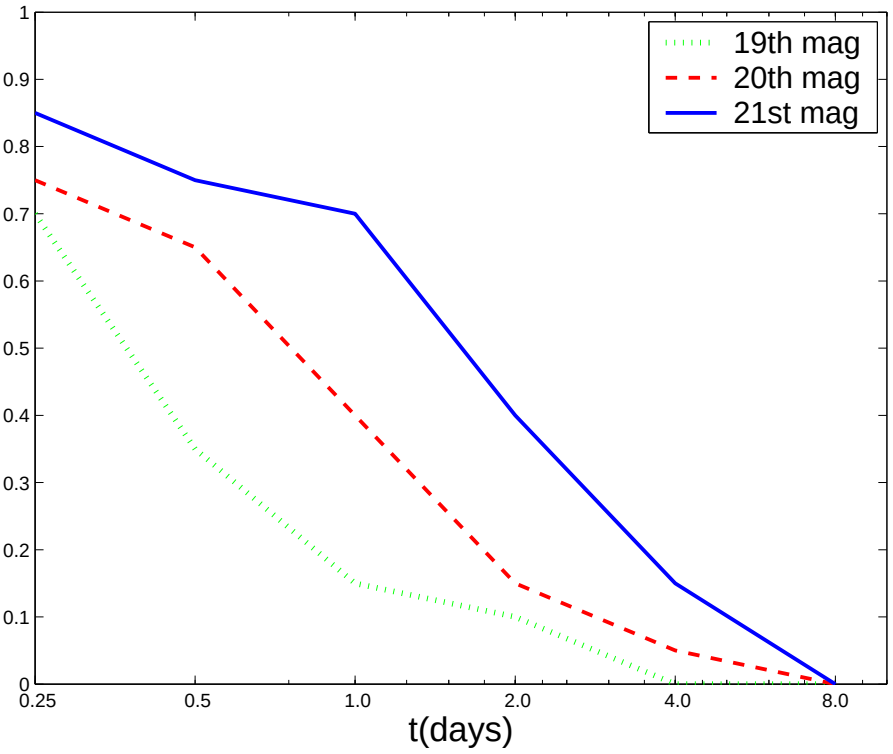

Figure 1.4: The fraction of bursts with optical afterglow above three limiting magnitudes as a function of time (compared to the total number of bursts with optical afterglow). From Piran (2004)

Technical difficulties led a gap of several hours between the burst and the detection of the optical afterglow, which could be found only after an accurate position was available. The rapid localization provided by IBAS (see Chapter 2) and HETE II are helping to close this gap.

Many afterglow light curves show an achromatic break to a steeper decline

with $\alpha \approx 2$. The best example of such a break was seen in GRB 990510 (Harrison et al., 1999; Stanek et al., 1999) and it is shown here in Fig. 1.5. This break

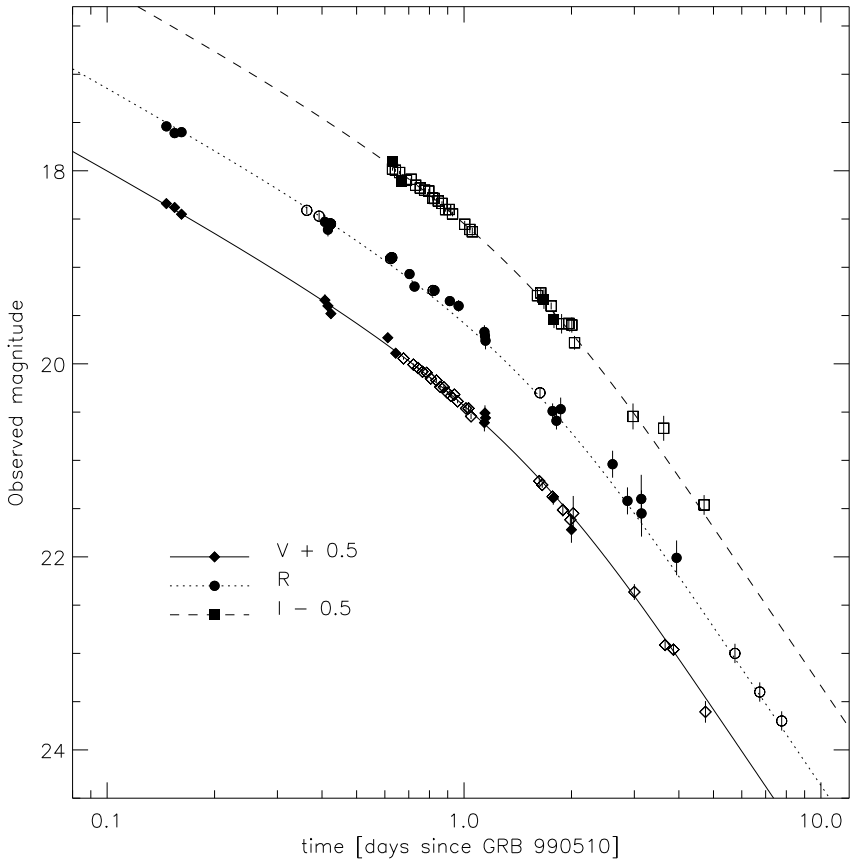

Figure 1.5: The optical light curves of GRB 990510. (from Harrison et al. (1999)).

is commonly interpreted as a jet break that allows us to estimate the opening angle of the jet (Rhoads, 1999; Sari et al., 1999) or the viewing angle within the standard jet model (Rossi et al., 2002) (see below).

The optical light curve of the first detected afterglow (from GRB 970228) could be seen for more than half a year (Fruchter et al., 1998). In most cases the afterglow fades faster and cannot be followed for more than several weeks. At this stage, the afterglow becomes significantly dimmer than its host galaxy and the light curve reaches a plateau corresponding to the emission of the host.

In several cases: e.g. GRB 980326 (Bloom et al., 1999), GRB 970228 (Reichart, 1999), GRB 011121 (Bloom et al., 2002b; Garnavich et al., 2003), red bumps are seen at late times (several weeks to a month). These bumps are usually interpreted as evidence for an underlying SN. A most remarkable Supernova signature was seen recently in GRB 030329 (Stanek et al., 2003; Hjorth et al.,

2003). This supernova had the same signature as SN98bw that was associated with GRB 990425.

Varying polarization at optical wavelengths has been observed in GRB afterglows at the level of a few to ten percent (see e.g. Covino et al. (1999)).

Dark GRBs

Only $\sim 50\%$ of well-localized GRBs show an optical afterglow (OA), whereas an X-ray counterpart is present in 90% of cases. Several possible explanations have been suggested for this situation. It is possible that late and shallow observations could not detect the OAs in some cases; several authors argue that dim and/or rapid decaying transients could bias the determination of the fraction of truly obscure GRBs (Fynbo et al., 2001; Berger et al., 2002). However, recent reanalysis of optical observations (Ghisellini et al., 2001; Lazzati et al., 2002) has shown that GRBs without OA detection (called dark GRBs, FOAs Failed Optical Afterglows, or GHOSTs, Gamma ray burst Hiding an Optical Source Transient) have had on average weaker optical counterparts, at least 2 magnitudes in the R band, than GRBs with OAs. Therefore, they appear to constitute a different class of objects, albeit there could be a fraction undetected for bad imaging.

The nature of dark GRBs is not clear. So far three hypothesis have been put forward to explain the behavior of dark GRBs. First, they are similar to the other bright GRBs, except for the fact that their lines of sight pass through large and dusty molecular clouds, that cause high absorption (Reichart & Price, 2002). Second, they are at $z \geq 5$, more distant than GRBs with OAs, (Fruchter et al., 1999; Lamb & Reichart, 2000), so that the Lyman break is redshifted into the optical band. However, the distances of a few dark GRBs have been determined and they do not imply high redshifts (Djorgovski et al., 2001; Antonelli et al., 2000; Piro et al., 2002). A third possibility is that the optical afterglow of dark GRBs is intrinsically much fainter (2-3 mag below) than that of other GRBs.

De Pasquale et al. (2003) find that GRBs with optical afterglows show a remarkably narrow distribution of flux ratios, which corresponds to an average optical-to-x spectral index 0.794 ± 0.054. They find that, while 75% of dark GRBs have flux ratio upper limits still consistent with those of GRBs with optical transients, the remaining 25% are 4 - 10 times weaker in optical than in X-rays. This result suggests that the afterglows of most dark GRBs are intrinsically fainter at all wavelengths relative to the afterglows of GRBs with observed OAs. As for the remaining 25%, the spectrum (optical to X-ray ratio) must be different than that of other afterglows with a suppression of the optical band.

Radio afterglow

A radio afterglow was detected in $\sim$ 50 % of the well localized bursts. The observed peak fluxes are at the level of 2 mJy (8 GHz). As the localization is

based on the X-ray afterglow (and as practically all bursts have X-ray afterglow) almost all these bursts were detected in X-rays. $\sim$ 80 % of the radio-afterglow bursts have also optical afterglow. The rest are optically dark. Similarly $\sim$ 80% of the optically observed afterglow have also a radio component.

Several bursts (GRBs 980329, 990123, 91216, 000926, 001018, 010222, 011030, 011121) were detected in radio at around one day. Recent radio observations begin well before that, but do not get a detection until about 24 hrs after a burst. The earliest radio detection took place in GRB 011030 at about 0.8 days after the burst (Taylor et al., 2001). In several cases (GRBs 990123, 990506, 991216, 980329 and 020405) the afterglow was detected early enough to indicate emission from the reverse shock and a transition from the reverse shock to the forward shock.

The radio light curve of GRB 970508 (see fig 1.6) showed early strong fluctuations (of order unity) in the flux (Frail et al., 1997). Goodman (1997) suggested that these fluctuations are due to scintillation and the decrease (with time) in the amplitude of the fluctuations is due to a transition from strong to weak scintillations. Frail et al. (1997) used this to infer the size of the emitting region of GRB 970508 at $\sim$ 4 weeks after the burst as $\sim 10^{17}$cm. This observation provided the first direct proof of relativistic expansion in GRBs.

The light curves evolve on a longer time scale in the radio. Some GRB afterglows have been detected years after the burst even after the relativistic-Newtonian transition. At this stage the expansion is essentially spherical and this enables a direct "calorimetric" estimate of the total energy within the ejecta (Soderberg et al., 2004). The long-lived nature of the radio afterglow allows for unambiguous calorimetry of the blast wave to be made when its expansion has become sub-relativistic and quasi-spherical.

1.2.3 Hosts and Distribution

Hosts

By now (end 2004) host galaxies have been observed for almost all bursts with optical, radio or X-ray afterglow with arcsec localization. While many researchers believe that the GRB host population is representative of the normal star-forming field galaxy population at a comparable redshifts, others argue that GRB host galaxies are significantly bluer than average and their star formation rate is much higher than average.

Totani (1997), Wijers et al. (1998) and Paczynski (1998) suggested that GRBs follow the star formation rate. As early as 1998 Fruchter et al. (1999) noted that all four early GRBs with spectroscopic identification or deep multicolor broadband imaging of the host (GRB 970228 GRB 970508, GRB 971214, and GRB 980703) lie in rapidly star-forming galaxies. Within the host galaxies the distribution of GRB-host offset follows the light distribution of the hosts (Bloom

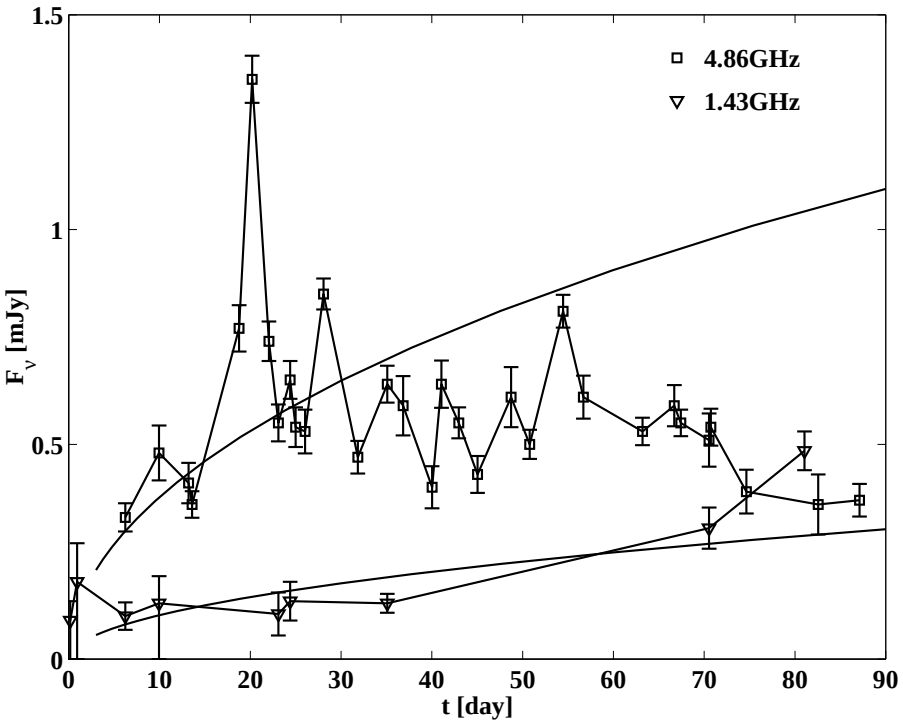

Figure 1.6: Light curves of the radio afterglow of GRB970508 at 4.86GHz and 1.43GHz, compared with the predictions of the adiabatic fireball model (from Frail et al. (1997)).

et al., 2002a). The light is roughly proportional to the density of star formation. Spectroscopic measurements suggest that GRBs are within Galaxies with a higher SFR. However, this is typical for normal field galaxy population at comparable redshifts (Hurley et al., 2002a).

Evidence for a different characteristics of GRB host galaxies arise from the work of Fynbo et al. (2002, 2003) who find that GRB host galaxies "always" show Lyman alpha emission in cases where a suitable search has been conducted. This supports the claim for active star formation and at most moderate metallicity in GRB hosts. It clearly distinguishes GRB hosts from the Lyman break galaxy population, in which only about 1/4 of galaxies show strong Lyman alpha.

The Spatial Distribution

BATSE's discovery that the burst directions are distributed isotropically on the sky (Meegan et al., 1992) was among the first indications of the cosmological nature of GRBs. The isotropic distribution indicated that GRBs are not associated with the Galaxy or with "local" structure in the near Universe.

Magliocchetti et al. (2003) reported that the two-point angular correlation function of 407 short BATSE GRBs reveals a $\sim 2\sigma$ deviation from isotropy on angular scales $2^o - 4^o$. This results is consistent with the possibility that short GRBs are nearer, and the angular correlation is induced by the large scale structure correlations on this scale. Alternatively this indicates repetition of these sources (Magliocchetti et al., 2003). These results, if confirmed, would imply that this sub-group is associated with different objects than the main GRB population, or that, at least they have some specific feature, such as, for example, a different viewing angle.

Cline et al. (2003) studied the shortest GRB population, burst with a typical duration of several tens ms. They find that there is a significant angular anisotropy and the $\langle V/V_{max} \rangle$ distribution provides evidence for a homogeneous sources distribution. They suggest that these features are best interpreted as sources of a galactic origin. However, one has to realize that there are strong selection effects that are involved in the detection of this particular subgroup.

Association with Supernovae

The association of GRBs with star forming regions and the indications that they follow the star formation rate suggest that GRBs are related to stellar death, namely to Supernovae (Paczynski, 1998). Additionally there is some direct evidence of association of GRBs with Supernovae.

GRB 980425 and SN98bw: The first indication of an association between GRBs and SNes was found when SN 98bw was discovered within the error box of GRB 980425 (Galama et al., 1998). This usual type Ic SN was much brighter than most SNs. Typical ejection velocities in SN1998bw were larger than usual ($\sim 2 \cdot 10^4$ km/sec), corresponding to a kinetic energy of $2 - 5 \times 10^{52}$ ergs, more than ten times larger than previously known energy of SNes, (Iwamoto et al., 1998). Additionally, radio observations suggested a component expanding sub relativistically with $v \sim 0.3c$ (Kulkarni et al., 1998). Thus, 1998bw was an unusual type Ic supernova, involving a much higher energy, and suggesting that GRBs are associated with the most powerful SNes. Indeed all other claims of SN signatures in afterglow light curves use SN 98bw as a template. The accompanying GRB, 980425 was also unusual: it had a smooth FRED light curve and no high energy component in its spectrum. Other bursts like this exist but they are rare. The redshift of SN98bw was 0.0085 implying an isotropic equivalent energy of $\sim 10^{48}$ergs, weaker by several orders of magnitude than a typical GRB.

The *BeppoSAX* Wide Field Cameras localized GRB 980425 with a 8 arcmin radius accuracy. In this circle, the *BeppoSAX* NFI (Narrow Field Instrument) detected two sources, S1 and S2, with error circles of 1.5 arcmin radius. The position of SN1998bw is consistent only with the error circle of S1. Therefore, Pian et al. (2000) identified S1 with X-ray emission from SN1998bw, although this was of course no proof of association between SN and GRB. It was difficult, based

only on the *BeppoSAX* NFI data, to characterize the behavior and variability of S2 and it could not be excluded that S2 was the afterglow of GRB 980425. The *XMM-Newton* observations of March 2002 (Pian et al., 2003) seem to have brought us closer to the solution. *XMM-Newton* detects well S1, and its flux is lower than in 1998: the SN emission has evidently decreased. On the other hand, the better angular resolution allowed to resolve S2 into a number of fainter sources. Their random variability (typical fluctuations of X-ray sources close to the level of the background) may have caused the flickering detected for S2 by *BeppoSAX* . This demolishes the case for the afterglow nature of S2, and strengthens in turn the case for association between GRB 980425 and SN 1998bw.

Red Bumps: Late time red bumps (see Section 1.2.2) have been discovered in several GRB light curves (Bloom et al., 1999; Reichart, 1999; Bloom et al., 2002b; Garnavich et al., 2003). These bumps involve both a brightening (or a flattening) of the afterglow as well as a transition to a much redder spectrum. These bumps have been generally interpreted as due to an underlying SN (Bloom et al., 1999). In all cases the bumps have been fit with a template light curve based on that of SN 1998bw, which was associated with GRB 980425. For most GRBs there is only an upper limit to the magnitude of the bump in the light curve.

GRB 030329 and SN 2003dh: The confirmation of the GRB-SN association was finally obtained recently (Stanek et al., 2003; Hjorth et al., 2003) for the very bright GRB 030329 that is associated with SN 2003dh (Chornock et al., 2003). For the first time, in the afterglow a classical GRB, besides a red bump, it was found that a SN 1998bw like spectrum dominated the optical light curve at later times (see Fig. 1.7). The spectral shapes of 2003dh and 1998bw were quite similar.

It is interesting to compare SN 1999bw and SN 2003dh. Basically, at all epochs Matheson et al. (2003) find that the best fit to spectra of 2003dh is given by 1998bw at about the same age . The light curve is harder, as the afterglow contribution is significant, but using spectral information they find that 2003dh had basically the same light curve as 1998bw. Mazzali et al. (2003) model the spectra and find again that it was very similar to 1998bw. They find some differences, but some of that might be due to a somewhat different approach to spectral decomposition, which gives somewhat fainter supernova.

GRB 031203 and SN 2003lw: Another GRB, this time a faint one, for which there is a spectroscopical unambiguous identification with a SN, is 03123, detected by *INTEGRAL* . For details see Section 3.9.

1.2.4 Energetics

Before redshift measurements were available, the GRB energy was estimated by modeling with an (isotropic) luminosity function the Log N-Log S distribution of the bursts observed by BATSE. This lead to a statistical estimate of the bursts

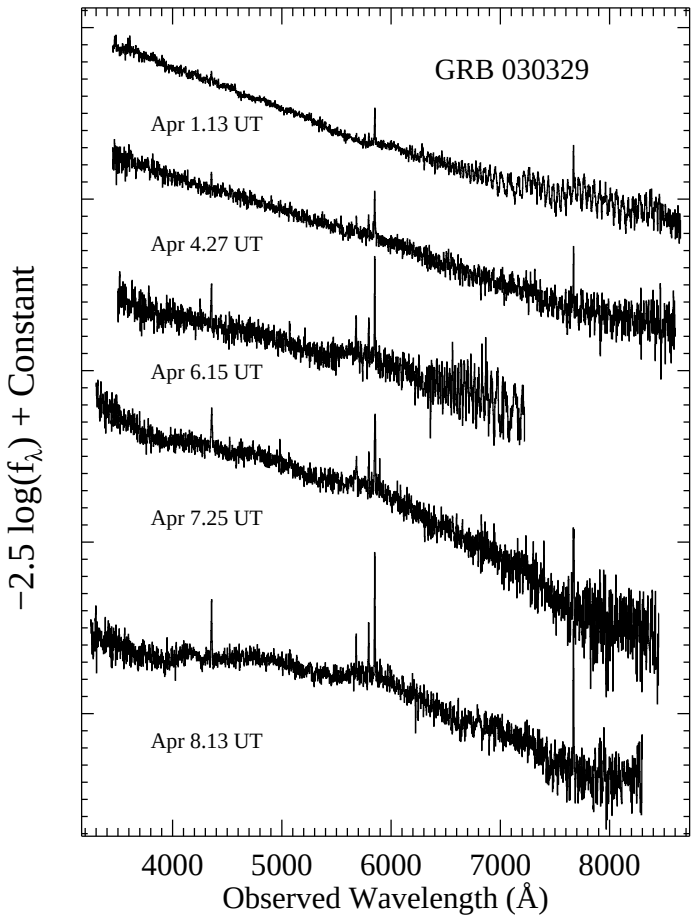

Figure 1.7: Evolution of the GRB 030329/SN2004dh spectrum, from April 1.13 UT (2.64 days after the burst), to April 8.13 UT (6.94 days after the burst). The early spectra consist of a power law continuum ($F_\nu \propto \nu^{-0.9}$) with narrow emission lines originating from HII regions within the host galaxy at redshift z=0.168. Spectra taken after April 5 show the development of broad peaks characteristic of a supernova (from Stanek et al. (2003)).

luminosity.

These estimates were revolutionized with the direct determination of the redshift for individual bursts, which allowed a direct measure of the energetics of specific bursts. Given an observed γ-ray fluence and the redshift to a burst, one can easily estimate the energy emitted in γ-rays, $E_{\gamma,iso}$ assuming that the emission is emitted isotropically (see Bloom et al. (2001) for a detailed study including k corrections). The energy of the first burst with a determined redshift, GRB 970508, was $E_{\gamma,iso} \simeq 10^{51}$ergs. However, as afterglow observations proceeded,

alarmingly larger values (*e.g.* 3.4×10^{54} ergs for GRB 990123) were measured for $E_{\gamma,iso}$, implying a distribution of values spanning three orders of magnitude.

However, there is now strong evidence (Rhoads, 1999; Sari et al., 1999) that GRBs are beamed. $E_{\gamma,iso}$ is not then a good estimate for the total energy emitted in γ-rays, which is instead given by $E_\gamma \equiv (\theta^2/2)E_{\gamma,iso}$, where θ is the effective angle in which γ-rays are emitted. It can be estimated from t_b, the time of the break in the afterglow light curve (Sari et al., 1999):

$$\theta = 0.16(n/E_{k,iso,52})^{1/8} t_{b,days}^{3/8} = 0.07(n/E_{k,\theta,52})^{1/6} t_{b,days}^{1/2}, \tag{1.2}$$

where $t_{b,days}$ is the break time in days. $E_{k,iso,52}$ is "isotropic equivalent" kinetic energy, discussed below, in units of 10^{52} ergs, while $E_{k,\theta,52}$ is the real kinetic energy in the jet i.e: $E_{k,\theta,52} = (\theta^2/2)E_{k,iso,52}$.

Frail et al. (2001) estimated E_γ for 18 bursts, finding typical values around 10^{51}ergs (see also Panaitescu & Kumar (2001)). Bloom et al. (2003) find $E_\gamma = 1.33 \times 10^{51}\, h_{65}^{-2}$ erg and a burst–to–burst variance of a factor of 2.2, three orders of magnitude smaller than the variance in $E_{\gamma,iso}$. A compilation of the beamed energies from (Bloom et al., 2003), is shown in Figs. 1.8 and 1.9. It demonstrates nicely this phenomenon. The constancy of E_γ is remarkable, as it involves the product of a factor inferred from the GRB observation (the γ-ray flux) with one inferred from the afterglow observations (the jet opening angle). However, E_γ might not be a good estimate for E_{tot}, the total energy emitted by the central engine. First, an unknown conversion efficiency of energy to γ-rays has to be considered: $E_{tot} = \epsilon^{-1}E_\gamma = \epsilon^{-1}(\theta^2/2)E_{\gamma,iso}$. Second, the large Lorentz factor during the γ-ray emission phase, makes the observed E_γ rather sensitive to angular inhomogeneities of the relativistic ejecta (Kumar & Piran, 2000). The recent early observations of the afterglow of GRB 021004 indicate that indeed a significant angular variability of this kind exists (Nakar & Piran, 2003).

The kinetic energy of the flow during the adiabatic afterglow phase, E_k is yet another useful measure of the GRB energetics. This energy (per unit solid angle) can be estimated from the afterglow light curve and spectra. Specifically, it is rather closely related to the observed afterglow X-ray flux (Kumar, 2000; Freedman & Waxman, 2001; Piran et al., 2001). As this energy is measured when the Lorentz factor is smaller, it is less sensitive than E_γ to angular variability. The constancy of the X-ray flux (Piran et al., 2001) suggests that this energy is also constant. Estimates of $E_{k,\theta}$ (Panaitescu & Kumar, 2001) show that $\bar{E}_\gamma \approx 3\bar{E}_{k,\theta}$, namely the observed "beamed" GRB energy is larger than the estimated "beamed" kinetic energy of the afterglow. Frail et al. (2001), however, find that $\bar{E}_\gamma \approx \bar{E}_{k,\theta}$, i.e. that the two energies are comparable.

An alternative interpretation of the observed breaks is that we are viewing a "universal"jet from different viewing angles (Lipunov et al., 2001; Rossi et al., 2002; Zhang & Mészáros, 2002). It is supposed that in these "structured" jets, the energy is not uniformly distributed, but is a function of the jet angle. The

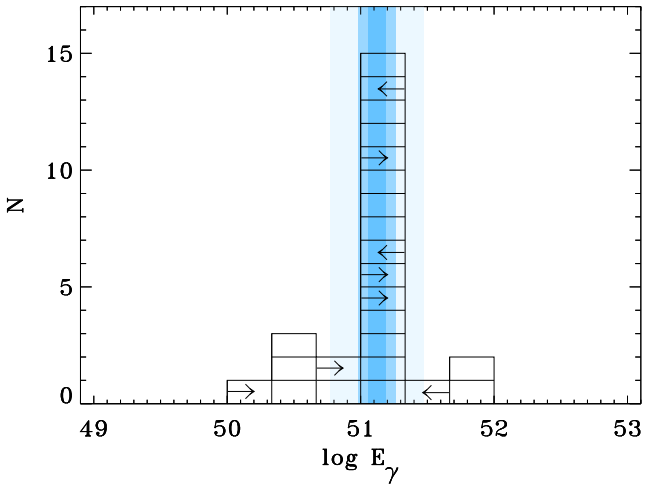

Figure 1.8: A histogram of GRB energies (E_γ) in bins of equal logarithmic spacings. The histogram shows a narrow distribution of GRB energies around the standard energy $E_\gamma = 1.33 \cdot 10^{51}$ ergs , with an error of $\sigma = 0.07$ dex. The observed burst–to–burst rms spread is 0.35 dex (a factor of 2.23) about this value. Bands of 1, 2, and 5 σ about the standard energy are shown. There are five identifiable outliers, which lie more than 5 σ from the mean, however, there is currently no basis other than discrepant energy to exclude these bursts from the sample (Bloom et al., 2003).

observed break corresponds, in this model, to the observing angle θ and not to the opening angle of the jet, which should be the same in all GRBs. This interpretation means that the GRB beams are wide and hence the rate of GRBs is smaller than the rate implied by the usual beaming factor. On the other hand it implies that GRBs are more energetic. Guetta et al. (2003) estimate that this factor (the ratio of the fixed energy of a "structured" jet relative to the energy of a uniform jet is ~ 7. However, they find that the observing angle distribution is somewhat inconsistent with the simple geometric one that should arise in universal structured jets. The energy-angle relation discussed earlier requires an angle-dependent jet with $E(\theta) \propto \theta^{-2}$.

Regardless of the nature of the jet (universal structured jet or uniform with a opening angle that differs from one burst to another), at late time it becomes non relativistic and spherical. With no relativistic beaming every observer detects emission from the whole shell. Radio observations at this stage enable us to obtain a direct calorimetric estimate of the total kinetic energy of the ejecta at late times (Frail et al., 2000) Estimates performed in several cases yield a comparable value for the total energy.

If GRBs are beamed we should expect "orphan" afterglows: events in which

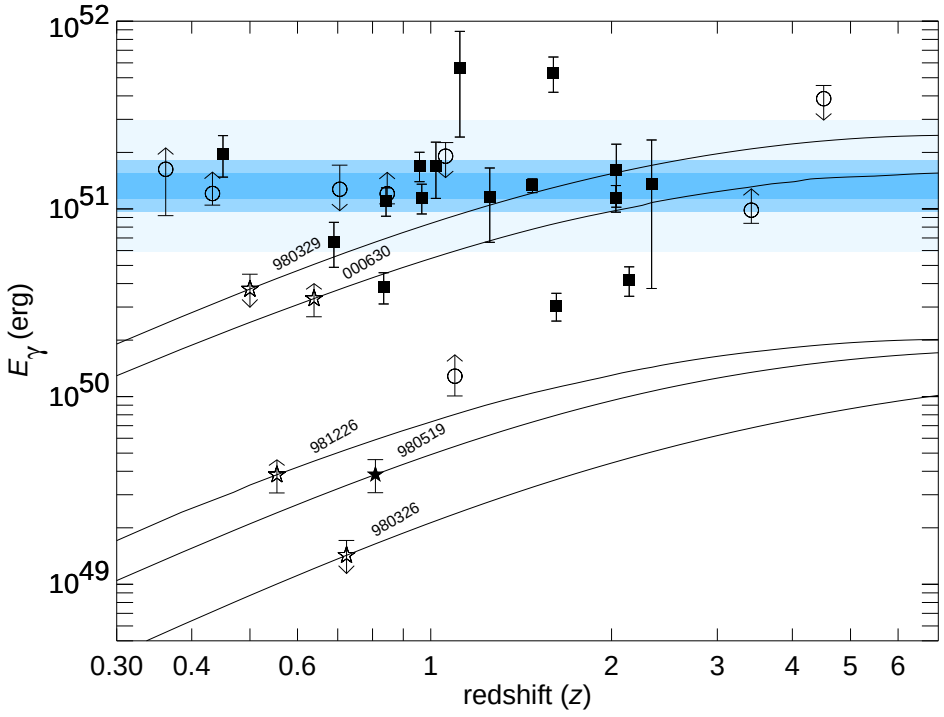

Figure 1.9: GRB energy release versus redshift. Bands of 1, 2, and 5 σ about the mean energy $E_\gamma = 1.33 \cdot 10^{51}$ ergs are shown. Plotted are the possible positions of five GRBs with no known spectroscopic redshift (labeled with star symbols). While the energies of GRB 980329 and GRB 000630 could be consistent with the standard value at redshifts beyond $z \sim 1.5$, at no redshift could the energies of GRB 980326 and GRB 980519 be consistent (Bloom et al., 2003).

we will miss the GRB, but we observe the late afterglow that is not so beamed. A comparison of the rate of orphan afterglows to GRBs will give us a direct estimate of the beaming of GRBs (and hence of their energy). Unfortunately there are not even good upper limits on the rate of orphan afterglows.

When considering the energy of GRBs one has to remember the possibility, as some models suggest, that additional energy is emitted which is not directly visible in the GRB itself or in the afterglow. van Putten & Levinson (2001), for example, suggest that a powerful Newtonian wind collimates the less powerful relativistic one. The "standard jet" model also suggests a large amount of energy emitted sideways with lower energy per solid angle and a lower Lorentz factors. It is interesting to note that the calorimetric estimates mentioned earlier limit the total amount of energy ejected regardless of the nature of the flow. More generally, typically during the afterglow, matter moving with a lower Lorentz factor emits at lower frequencies. Hence by comparing the relative beaming of

afterglow emission in different wavelength one can estimate the relative beaming factors, $f_b^{-1}(E)$, at different wavelength and hence at different energies.

These observations won't limit, of course, the energy emitted in gravitational radiation, neutrinos, Cosmic Rays or very high energy photons that may be emitted simultaneously by the source and influence the source energy budget without influencing the afterglow.

1.3 Theoretical Aspects

There are several generally accepted ingredients in practically all current GRB models.

1.3.1 Relativistic Motion

Relativistic motion with a Lorentz factor, $\Gamma, > 100$, is essential to overcome the compactness problem (see below). At first this understanding was based only on theoretical arguments. However, now there are direct observational proofs of this concept: it is now generally accepted that both the radio scintillation (Goodman, 1997) and the low frequency self-absorption (Katz & Piran, 1997) provide independent estimates of the size of the afterglow, $\sim 10^{17}$cm, two weeks after the burst. These observations imply that the afterglow has indeed expanded relativistically with $\Gamma \sim 100$.

The relativistic motion implies that we observe blue shifted photons, which are significantly softer in the moving rest frame. It also implies that when the objects have a size R the observed emission arrives on a typical time scale of $R/c\Gamma^2$. Relativistic beaming also implies that we observe only a small fraction $(1/\Gamma)$ of the source.

Compactness and relativistic motion

The first theoretical clues of the necessity of relativistic motion in GRBs arose from the Compactness problem (Ruderman, 1975). The conceptual argument is simple. GRBs show a non-thermal spectrum with a significant high-energy tail (see Section 1.2.1). On the other hand, a simple calculation shows that the source is optically thick. The fluctuations on a time scale δt imply that the source is smaller than $c\delta t$. Given an observed flux F, a duration T, and an distance d we can estimate the energy E at the source. For a typical photon's energy $\bar{E}_\gamma$ this yields a photon density $\approx 4\pi d^2 F/\bar{E}_\gamma c^3 \delta t^2$. Two γ-rays can annihilate and produce e^+e^- pairs, if the energy in their CM frame is larger than $2m_e c^2$. The optical depth for pair creation is:

$$\tau_{\gamma\gamma} \approx \frac{f_{e^\pm}\sigma_T 4\pi d^2 F}{\bar{E}_\gamma c^2 \delta t} \tag{1.3}$$

where, $f_{e^\pm}$ is a numerical factor denoting the average probability that a photon collides with another photon whose energy is sufficient for pair creation. For typical values and cosmological distances, the resulting optical depth is extremely large $\tau_{\gamma\gamma} \sim 10^{15}$ (Piran, 2004). This is, of course, inconsistent with the non-thermal spectrum.

The compactness problem can be avoided if the emitting matter is moving relativistically towards the observer, with Lorentz Γ. Two corrections appear in this case. First, the observed photons are blue shifted and therefore, their energy at the source frame is lower by a factor Γ. Second, the implied size of a source moving towards us with a Lorentz factor Γ is $c\delta t\Gamma^2$ (e.g. Piran (2004)). The first effect modifies $f_{e^\pm}$ by a factor $\Gamma^{-2\alpha}$ where α is the photon index of the observed γ-ray spectrum. The second effect modifies the density estimate by a factor Γ^{-4} and it influences the optical depth as Γ^{-2}. Together one finds that for $\alpha \sim 2$ one needs $\Gamma \gtrsim 100$ to obtain an optically thin source.

The requirement that the source is optically thin can be used to obtain direct limits on the minimum Lorentz factor within specific bursts (Piran, 2004). A complete calculation requires a detailed integration over angular integrals and over the energy dependent pair production cross section. The minimum Lorentz factor depends also on the maximum photon energy, $E_{\max}$, the upper energy cutoff of the spectrum. Lithwick & Sari (2001) provide a detailed comparison of the different calculations and point our various flaws in some of the previous estimates. They find that:

$$\tau_{\gamma\gamma} = \frac{11}{180}\frac{\sigma_T d^2 (m_e c^2)^{-\alpha+1}\mathcal{F}}{c^2\delta T(\alpha-1)}\left(\frac{E_{\max}}{m_e c^2}\right)^{\alpha-1}\Gamma^{2\alpha+2}(1+z)^{2\alpha-2} , \qquad (1.4)$$

where the high end of the observed photon flux is given by $\mathcal{F}E^{-\alpha}$ (photons per cm^2 per sec per unit photon energy). A lower limit on Γ is obtained by equating Eq. 1.4 to unity.

Relativistic Beaming and the Patchy Shell Model

The radiation from a relativistic source is beamed with a typical beaming angle $1/\Gamma$. This implies that if the source is expanding radially with an ultra-relativistic speed, a given observer "sees" radiation only from a region that is within Γ^{-1} from its line of sight to the source. If the radius of the emitting region is R the observer will see radiation from a region of size R/Γ. Since Γ is extremely large during the GRB we observe emission only from a small fraction of the emitting shell. It is possible, and even likely, that the conditions within the small region that we observe will be different from the average ones across the shell. This means that the conditions that we infer won't necessarily reflect the true average conditions within this particular GRB.

An interesting point related to the internal shocks model in this context is the following. According to the internal shocks model individual pulses are obtained

by collisions between individual shells. Here the inhomogeneity of individual shells could be wiped out when the contributions of different hot spots from different shells is added. Alternatively the "inner engine" may produce a consistent angular pattern in which the hot spot is in the same position in all shells and in this case averaging won't lead to a cancellation of the patchy shell structure.

In the internal-external model the GRB is produced by internal shocks in which only the relative motion within the flow is dissipated. The bulk Lorentz factor remains unchanged. During the afterglow the shell is slowed down by external shocks. As the Lorentz factor decreases with time, we observe a larger and larger fraction of the emitting region until $\Gamma \approx \theta^{-1}$, where θ is the angular size of the whole emitting region - the GRB jet. This has several unavoidable implications: if the initial relativistic flow is inhomogeneous on a small angular scale then different observers looking at the same GRB (from different viewing angles) will see different γ-ray light curves. A strong burst for one observer might look weak for another one if it is located at an angle larger than $1/\Gamma$ from the first. The two observers will see similar conditions later on, during the afterglow, as then they will observe the same angular regions. This has the following implications: (i) Given that the GRB population originates from some 'typical' distribution we expect that fluctuations between different bursts at early time during the GRB will be larger than fluctuations observed at late times during the afterglow (Kumar & Piran, 2000). A direct consequence of this behavior is the appearance of a bias in the observations of GRBs. As we are more likely to detect stronger events we will tend to identify bursts in which a 'hot spot' was pointing towards us during the GRB phase. If the original GRB shells are inhomogeneous this would inevitably lead to a bias in the estimates of the GRB emission as compared to the kinetic energy during the afterglow. (ii) As the afterglow slows down we observe a larger and larger region. The angular structure would produce a variability in the light curve with a typical time scale of t, the observed time. These fluctuations will decay later as the Lorentz factor decreases and the observations are averaged over a larger viewing angle. Nakar et al. (2003) have suggested that this is the source of the early fluctuations in the light curve of GRB 021004.

1.3.2 Dissipation and Relativistic Shocks

In most models the energy of the relativistic flow is dissipated and this provides the energy needed for the GRB and the subsequent afterglow. The dissipation is in the form of (collisionless) shocks, possibly via plasma instability. There is a general agreement that the afterglow is produced via external shocks with the circumburst matter. There is convincing evidence (see *e.g.* Fenimore et al. (1996); Sari & Piran (1997); Ramirez-Ruiz & Fenimore (2000)) that in most bursts the dissipation during the GRB phase takes place via internal shocks, namely shocks within the relativistic flow itself.

1.3.3 Synchrotron Radiation

Most models (both of the GRB and the afterglow) are based on Synchrotron emission from relativistic electrons accelerated within the shocks. There is a reasonable agreement between the predictions of the synchrotron model and afterglow observations (Wijers & Galama, 1999; Granot et al., 1999; Panaitescu & Kumar, 2001). These are also supported by measurements of linear polarization in several optical afterglows (see Section 1.2.2). As for the GRB itself there are various worries about the validity of this model. In particular there are some inconsistencies between the observed spectral slopes and those predicted by the synchrotron model (see (Preece et al., 2002) and Section 1.2.1). The main alternative to Synchrotron emission is synchrotron-self Compton (Waxman, 1997; Ghisellini & Celotti, 1999) or inverse Compton of external light (Shemi, 1994; Brainerd, 1994; Shaviv & Dar, 1995; Lazzati et al., 2004). The last model requires, of course a reasonable source of external light.

1.4 Models of Inner Engines

If one accepts the beaming interpretation of the breaks in the optical light curve, the total energy release in GRBs is $\sim 10^{51}$ergs (Frail et al., 2001; Panaitescu & Kumar, 2001). It is higher if, as some models suggest, the beaming interpretation is wrong, or, if a significant amount of additional energy (which does not contribute to the GRB or to the afterglow) is emitted from the source. An energy of $\sim 10^{51}$ ergs corresponds to the energy released in a typical Supernova. The short timescales indicate that the process must involve a compact object. No other known source can release so much energy within such a short time scale. The process requires a dissipation of $\sim 0.1\ M_{\odot}$ within the central engine over a period of a few seconds. The sudden appearance of so much matter in the vicinity of the compact object suggests a violent process, one that most likely involves the birth of the compact object itself.

Afterglow observations, which exist for a subset of relatively bright long bursts, show that GRBs arise within galaxies with a high star formation rate. Within the galaxies the bursts distribution follows the light distribution (Bloom et al., 2002a). This has lead to the understanding that (long) GRB arise from the collapse of massive stars . This understanding has been confirmed by the appearance of SN bumps in the afterglow light curve (see Section 1.2.3 earlier) and in particular by the spectroscopic identifications of SN 2003dh in GRB 030329 and SN 2003lw in GRB 031203.

The Fireball model tells us how GRBs operate. However, it does not answer the most interesting astrophysical question: what produces them? which astrophysical process generates the energetic ultrarelativistic flows needed for the Fireball model?

Black hole accretion - Several scenarios could lead to a black hole - massive accretion disk system: mergers (NS-NS binaries Eichler et al. (1989); Narayan et al. (1992), NS-BH binaries Paczynski (1991) WD-BH binaries Fryer et al. (1999), BH-He-star binaries Fryer & Woosley (1998)) and models based on "failed supernovae" or "Collapsars" Woosley (1993); Paczynski (1998); MacFadyen & Woosley (1999). Narayan et al. (2001) have recently shown that accretion theory suggests that among all the above scenarios only Collapsars could produce long bursts and only NS-NS (or NS-BH) mergers could produce short bursts. The basic idea is that the duration of the accretion depends on the size of the disk. So short burst must be produced by small disks and those are naturally produced in mergers. On the other hand long burst require large disks. However, those are inefficient. One can overcome this, if we have a small disk that is fed continuously. In this case the efficiency can be large and the duration long. This happens naturally within the collapsar model.

The Pulsar Model - Several "inner engine" models involve pulsar-like activity of the inner engine which is directly connected to a Poynting flux dominated relativistic flow (in a contrast to a baryonic flux dominated flow). Energy considerations require an extremely large magnetic field of the order of 10^{15} G within such sources.

Usov (1992) suggested that GRB arise during the formation of rapidly rotating highly magnetized neutron stars. Such objects could form by the gravitational collapse of accreting white dwarfs with anomalously high magnetic fields in binaries, as in magnetic cataclysmic binaries. The rapidly rotating and strongly magnetized neutron stars would lose their rotational kinetic energy on a timescale of seconds or less in a pulsar like mechanism. The energy available in this case is the rotational and magnetic energy of the neutron star, that are of the order of a few $\times 10^{51}$ ergs for a neutron star rotating near breakup. The rotation of the magnetic field creates a strong electric field and an electron-positron plasma which is initially optically thick and in quasi-thermodynamic equilibrium. Additionally a very strong magnetic field forms. The pulsar produces a relativistic Poynting flux dominated flow.

Rotating black holes and the Blandford-Znajek mechanism - It is possible and even likely that the process of energy extraction involves the Blandford-Znajek mechanism Blandford & Znajek (1977) in which the black hole - torus system is engulfed in a magnetic field and the rotational energy of the black hole is extracted via this magnetic field.

The Collapsar (Hypernova) Model - The evidence for the association of (long) GRBs with supernovae (see Bloom et al. (2002a) and Section 1.2.3) provides a strong support for the Collapsar model. Woosley (1993) proposed that GRBs arise from the collapse of a single Wolf-Rayet star characterized by fast rotation ('failed' Type Ib supernova). Paczynski (1998) pointed out that there is tentative evidence that the GRBs 970228, 970508, and 970828 were close to star-forming regions and that this suggests that GRBs are linked to cataclysmic

deaths of massive stars.

According to the Collapsar model the massive iron core of a rapidly rotating massive star, of mass $M > 30\ M_{\odot}$, collapses to a black hole (either directly or during the accretion phase that follows the core collapse). An accretion disk forms around this black hole and a funnel forms along the rotation axis, where the stellar material has relatively little rotational support. The mass of the accretion disk is around $0.1\ M_{\odot}$. Accretion of this disk onto the black hole can last several dozen seconds and powers the GRB. Energy can be extracted via neutrino annihilation (MacFadyen & Woosley, 1999) or via the Blandford-Znajek mechanism. The energy deposited in the surrounding matter will preferably leak out along the rotation axis producing jets with opening angles of $<10^{\circ}$. If the jets are powerful enough they would penetrate the stellar envelope and produce the GRB.

The processes of core collapse, accretion along the polar column (which is essential in order to create the funnel) and the jet propagation through the stellar envelope take together ~ 10 s (MacFadyen & Woosley, 1999). The duration of the accretion onto the black hole is expected to take several dozen seconds. These arguments imply that Collapsars are expected to produce long GRBs.

The Supranova Model - Vietri & Stella (1998) suggested that GRBs take place when a "supermassive" (or supramassive as Vietri & Stella (1998) call it) neutron star (namely a neutron star that is above the maximal cold nonrotating neutron star mass) collapses to a black hole. The collapse can take place because the neutron star looses angular momentum via a pulsar wind and it looses the extra support of the centrifugal force. Alternatively the supramassive neutron star can simply cool and become unstable if rotation alone is not enough to support it. The neutron star could also become over massive and collapse if it accretes slowly matter from a surrounding accretion disk (Vietri & Stella, 1999). In this latter case the time delay from the SN could be very large and the SNR will not play any role in the GRB or its afterglow.

The Supranova model is a two step event. First, there is a supernova, which may be more energetic than an average one, in which the supermassive neutron star forms. Then a few weeks or months later this neutron star collapses producing the GRB. While both the Supranova and the Collapsar (or hypernova) events are associated with Supernovae or Supernova-like events, the details of the model are very different. First, while in the Collapsar model one expect a supernova bump on the afterglow light curve, such a bump is not expected in the Supranova model unless the time delay is a few days. On the other hand while it is not clear in the Collapsar model how does the Fe needed for the Fe X-ray lines reach the implied large distances form the center, it is obvious in this model, as the supernova shell was ejected to space several month before the GRB. As mentioned earlier the association of GRB 030329 with SN 2003dh (Stanek et al., 2003; Hjorth et al., 2003) is incompatible with the Supranova model. Proponents of this model, argue however, that there might be a distribution of delay times between the first and second collapses.

The models are also very different in their physical content. First in the Supranova model the GRB jet does not have to punch a whole through the stellar envelope. Instead the ejecta propagates in almost free space polluted possibly by a pulsar wind (Königl & Granot, 2002; Guetta & Granot, 2003). In both models, like in many other models, the GRB is powered by accretion of a massive accretion disk surrounding the newborn black hole. This accretion disk forms, from the debris of the collapsing neutron star at the same time that the black hole is formed. Again, the time scale of the burst is determined by the accretion time of this disk. Narayan et al. (2001) point out however that long lived (50 s) accretion disks must be large and hence extremely inefficient. This may pose a problem for this model.

Chapter 2

IBAS: The *INTEGRAL* Burst Alert System

In this Chapter I will briefly describe the *INTEGRAL* satellite (Section 2.1) and its instruments, concentrating in IBIS (Section 2.3), which is the telescope used by IBAS (Section 2.4) to localize Gamma-Ray Bursts. Before I will describe the basic principles of imaging with coded mask telescopes (Section 2.2).

2.1 *INTEGRAL*

The INTErnational Gamma Ray Astrophysics Laboratory (INTEGRAL; Winkler et al. (2003)) is a satellite mission of the European Space Agency, with contributions from Russia (launcher) and NASA (Goldstone ground station). The observatory is dedicated to fine imaging and spectroscopy in the 15 keV-10 MeV range. The satellite was launched on the 17^{th} of October 2002 from the Russian Space Center in Baikonur with a Proton rocket, which injected it in an ex-centric (perigee at 9000 km; apogee at 153000 km) orbit with an inclination of 52°. Thanks to this orbit the satellite spends most of the time (∼90%) outside the Earth radiation belts, and is in continuous contact with one of the two ground stations (Redu in Belgium and Goldstone in California). This allows a real time down-link of the telemetry of the satellite, which from the Mission Operations Control (MOC in Darmstadt, Germany) is directly sent to the *INTEGRAL* Science Data Centre (ISDC; Courvoisier et al. (2003)) in Versoix (Switzerland).

INTEGRAL carries two main instruments: the spectrometer SPI (Vedrenne et al., 2003) - optimized for the high-resolution gamma-ray line spectroscopy (20 keV-8 MeV), and the imager IBIS (Ubertini et al., 2003) - optimized for high-angular resolution imaging (15 keV-10 MeV). Besides the two main instruments, there are two monitoring instruments operating at lower energies: JEM-X (3-35 keV; Lund et al. (2003)) and an Optical Monitoring Camera (OMC, Mas-Hesse

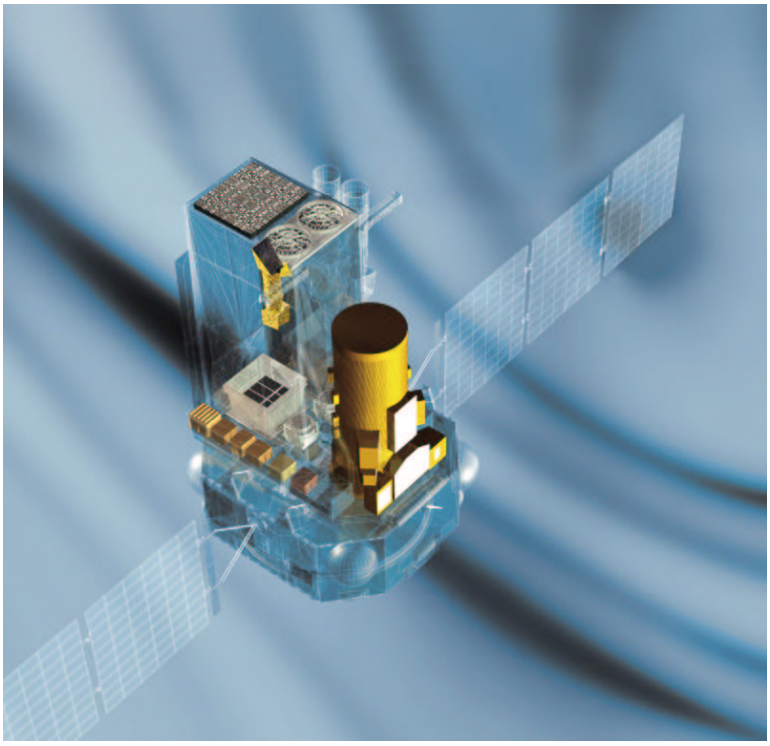

Figure 2.1: The *INTEGRAL* satellite (Credits ESA).

et al. (2003)). All instruments point in the same direction, but their fields of view have different dimensions (see Fig.2.2). The main characteristics of the instruments are presented in Tab. 2.1.

2.2 Coded Mask Telescopes

Since at energies > 10 keV, the traditional photon focusing techniques can hardly be applied (the radiation wavelength is as short as the atomic dimensions), the coded mask telescopes have been developed in order to obtain images also at these energies. This kind of telescopes consists of a mask with elements opaque and transparent to the radiation, and of a position sensitive detector. From the shadow of the mask, recorded on the detector, one can reconstruct the direction of the source(s) and hence the image of the sky. The angular resolution $d\theta$ of such a device is determined by the size of the elements of the coded mask C and by the distance between the mask and the detector, H:

$$d\theta = \arctan\left(\frac{C}{H}\right) \tag{2.1}$$

Different designs of the mask pattern can be used. A particularly interesting pattern is the MURA (Modified Uniformly Redundant Array; Gottesman &

Parameter	SPI	IBIS
Energy range	18 keV–8 MeV	15 keV–10 MeV
Detector	19 Ge detectors, each (6 × 7) cm cooled @ 85 K	16384 CdTe dets, each (4 × 4 × 2) mm 4096 CsI dets, each (8.4 × 8.4 × 30) mm
Detector area (cm^2)	500	2600 (CdTe), 2890 (CsI)
Spectral resolution (FWHM)	3 keV @ 1.7 MeV	8 keV @ 100 keV
Continuum sensitivity (photons cm^{-2} s^{-1} keV^{-1}) ($\Delta E = E/2$, 3σ, 10^6 s)	5.5×10^{-6} @ 100 keV 1.2×10^{-6} @ 1 MeV	6×10^{-7} @ 100 keV 5×10^{-7} @ 1 MeV
Line sensitivity (photons cm^{-2} s^{-1}) (3σ, 10^6 s)	3.3×10^{-5} @ 100 keV 2.4×10^{-5} @ 1 MeV	1.9×10^{-5} @ 100 keV 3.8×10^{-4} @ 1 MeV
Field of view (fully coded)	16° (corner to corner)	9° × 9°
Angular resolution (FWHM)	2.5° (point source)	12′
Source location (radius)	≤1.3° (depending on source strength)	≤1′ (for 10σ source)
Absolute timing accuracy (3σ)	≤200 μs	≤200 μs
Mass (kg)	1309	746
Power [max/average] (W)	385/110	240/208
Parameter	**JEM–X**	**OMC**
Energy range	4 keV–35 keV	500 nm–600 nm
Detector	Microstrip Xe/CH_4–gas detector (1.5 bar)	CCD + V-filter
Detector area (cm^2)	500 for each of the two JEM-X detectors[a]	CCD: (2061 × 1056) pixels Imaging area (1024 × 1024) pixels
Spectral resolution (FWHM)	2.0 keV @ 22 keV	–
Continuum sensitivity[b] (photons cm^{-2} s^{-1} keV^{-1}) (3σ, 10^6 s)	1.2×10^{-5} @ 6 keV 1.3×10^{-5} @ 30 keV	– –
Line sensitivity[b] (photons cm^{-2} s^{-1}) (3σ, 10^6 s)	1.9×10^{-5} @ 6 keV 8.5×10^{-5} @ 30 keV	– –
Limiting magnitude (mag) (3σ, 5000 s)	–	17.8
Field of view (fully coded)	4.8°	5° × 5°
Angular resolution (FWHM)	3′	25″
10σ source location (radius)	≤30″	6″
Absolute Timing accuracy (3σ)	≤200 μs	≥1 s
Mass (kg)	65	17
Power [max/average] (W)	50/37	20/17

[a] At the moment, only one of the two JEM-X detectors is being operated.
[b] Assumes operation of both detectors.

Table 2.1: INTEGRAL payload: key parameters (Winkler et al., 2003)

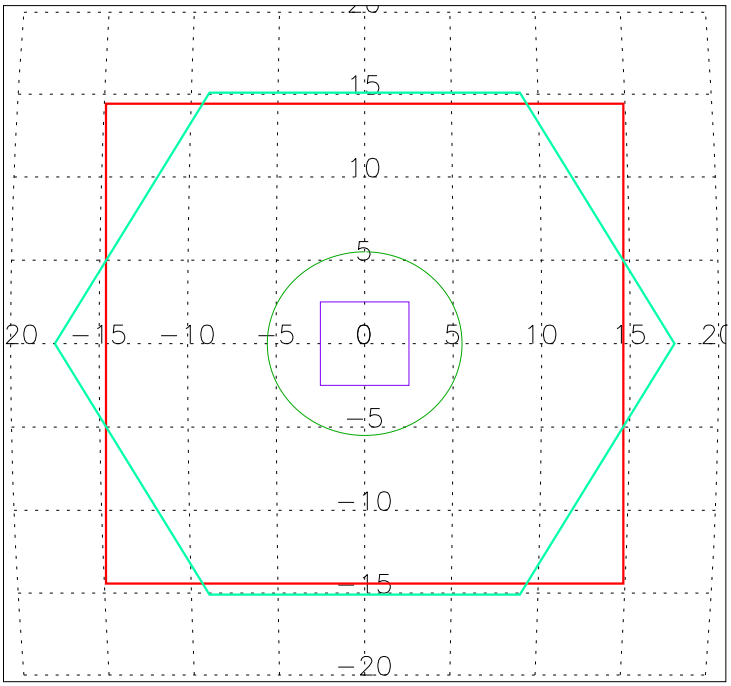

Figure 2.2: The Fields of View of the different *INTEGRAL* instruments. IBIS (large square), SPI (hexagon), JEM-X (circle) and OMC (small square). The units of the grid are degrees.

Fenimore (1989)) The important feature of MURA arrays is that their autocorrelation function is a delta (Fenimore & Cannon, 1978), which results in good quality imaging performances.

In a coded mask instrument configured as IBIS (i.e. with a mask 1.8 times larger than the detector, see Section 2.3), there are different ways in which a source can cast a shadow on the detector. If the detector is fully illuminated, the recorded shadow is a complete (and unique) permutation of the mask base pattern: we say that the source is in the Fully Coded Field Of View (FCFOV). On the other hand, if only a part of the detector is illuminated by the source flux, as it happens if the source is at a large off-axis angle, the recorded shadow is only a part of the complete pattern of the mask. In this case the source is said to be in the Partially Coded Field Of View (PCFOV). The effective area is nearly constant inside the FCFOV, while it goes linearly to zero in the PCFOV.

As mentioned, the autocorrelation function of a MURA pattern is a delta function: this property alone is sufficient to produce raw sky image S of the FCFOV from direct cyclic deconvolution of the detector shadowgram D and the mask base pattern M:

$$S = D \circ M, \tag{2.2}$$

where $\circ$ ($S[k,l] \simeq \sum_i \sum_j D[i,j]M[i+k,j+l]$) is the correlation operator

Usually a slightly different decoding matrix G is used in place of M (Fenimore & Cannon, 1978). G is obtained by setting the closed elements of M to -1 and the open ones to +1 and setting one of the open pixels to close. This produces a single valued background level in the FCFOV and enhances the peak significance. This standard deconvolution method is good for its simplicity and speed of computation, and produces good results in the FCFOV. There is an improved and more general method to extend the deconvolution technique to the PCFOV: the *weighted balanced correlation* (Fenimore & Cannon, 1978; Rideout & Skinner, 1996).

This is an improved version of the method discussed above. The main difference is that for every direction of the PCFOV the signal is obtained using only the modulated part of the detector (via a weighting matrix W), and that the positive and negative contributions are taken into account separately in a balanced way. Three main matrices are used:

- M^+: the full mask pattern, with values set to +1 where pixels are open and 0 elsewhere
- M^-: the full mask pattern, with values set to -1 where pixels are closed and 0 elsewhere
- W: the weight matrix, set to 1 in the central part corresponding to the detector and 0 elsewhere

all matrices are padded with 0 elements up to the total FOV dimensions. The sky is then obtained by:

$$S = (D \times W) \circ M^+ - b \times ((D \times W) \circ M^-) \tag{2.3}$$

where

$$b = \frac{M^+ \circ W - 1}{M^- \circ W} \tag{2.4}$$

and $\times$ a simple multiplication operator (i.e. A[i,j]=B[i,j]·C[i,j]). In Eq. 2.3 the first term is the positive contribution through the mask's open elements (source+background), while the second term is the negative (background) contribution through the mask's closed elements, weighted by the ratio, b, of open and closed elements.

2.3 IBIS

The IBIS telescope, see Fig. 2.3, is the high angular resolution γ-ray instrument on board *INTEGRAL* . The IBIS imaging system is based on two independent detector arrays optimized for low (15-1000 keV; ISGRI; Lebrun et al. (2003)) and

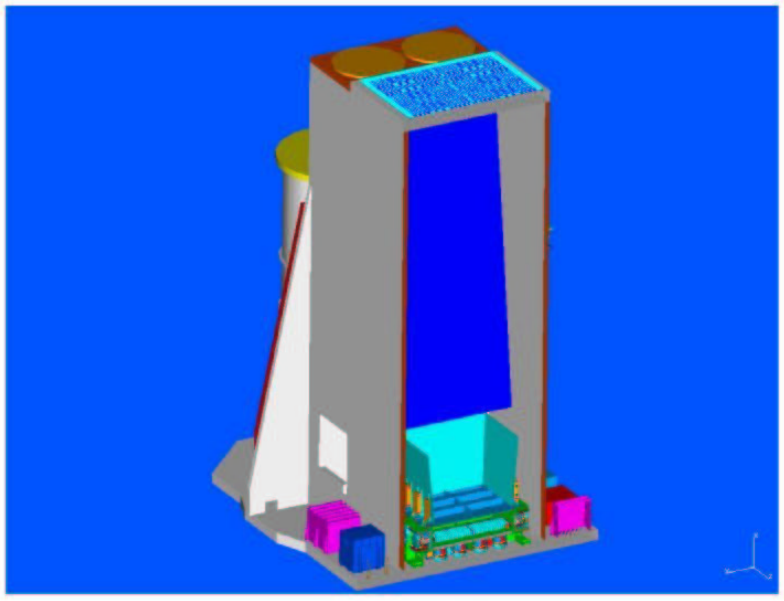

Figure 2.3: The IBIS telescope (Credits ESA).

high (0.175-10 MeV; PICsIT; Labanti et al. (2003)) energies. Both are surrounded by an active VETO System. This high efficiency shield is essential to reduce the background induced by high-energy particles. A Tungsten Coded Aperture Mask, 16 mm thick and $\sim$ 1 squared meter in dimension, is the imaging device.

ISGRI is made of 128×128 CdTe pixels (4×4×2 mm each), giving a geometric area of $\sim$2600 cm^2. PICsIT is made of 64×64 CsI(Tl) pixels (9.2×9.2×30 mm each) resulting in a geometric area of $\sim$3200 cm^2. Both detectors are subdivided in 8 nearly identical units called modules. The two detection planes are separated by 90 mm allowing to use the telescope also in Compton mode.

2.3.1 Scientific Performances

The IBIS scientific performances are summarized in Tab. 2.1. A few aspects will be pointed out here.

Field of View and Angluar Resolution

The Field of View of IBIS is 29×29°(PC) and 9×9°(FC). The mask pattern chosen for IBIS is based on a cyclic replication of a MURA of order 53, expanded to 95 pixels (see Fig. 2.4) The mask closed pixel size is 11.2 mm and the mask-detector distance in the case of ISGRI is 3203 mm, which yields an angular resolution of $\sim 12'$ according to Eq. 2.1. The reason for an incomplete replication (95 instead of $53 \times 2 = 106$) is not accidental but was made for a specific purpose (see Section 2.3.2).

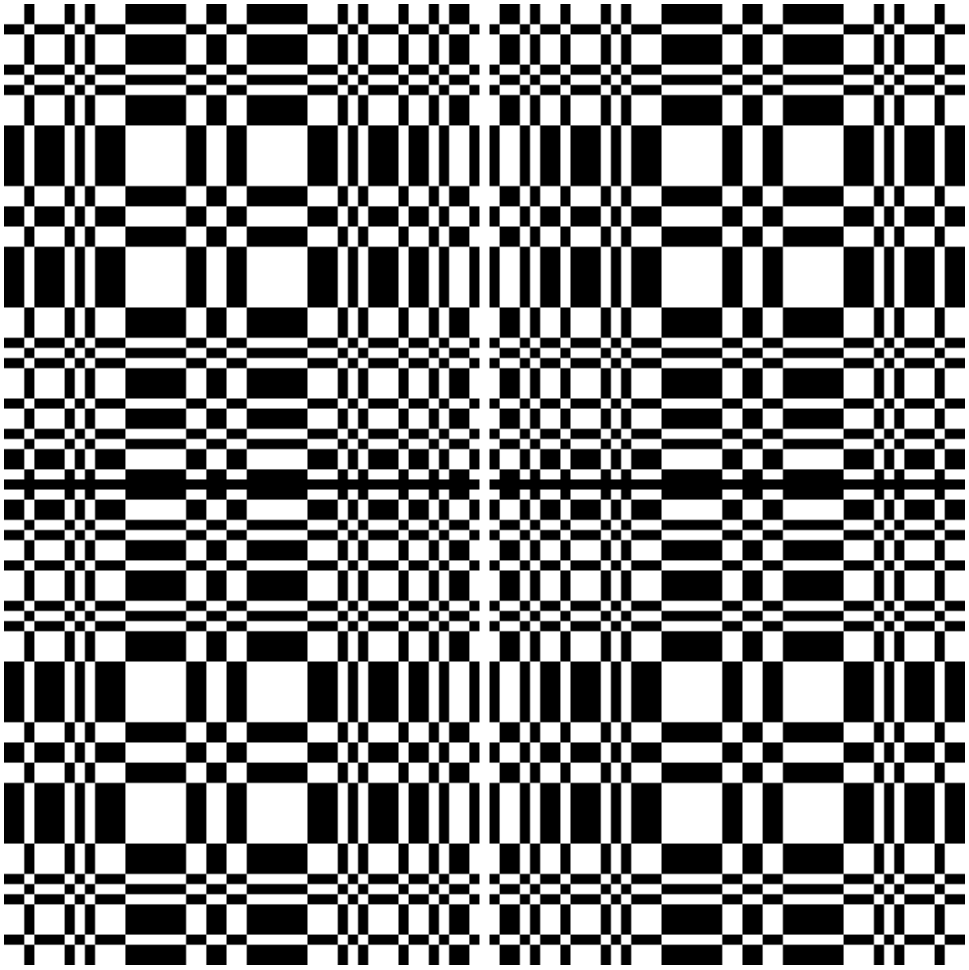

Figure 2.4: IBIS mask pattern.

The closed elements are 16 mm thick and made of Tungsten (W), while the open ones are not fully transparent at low energies due to the presence of the mask support structure, see Fig. 2.5. Since the detector pixel size is smaller than that of the mask it is possible to improve the imaging capabilities (namely the Point Source Location Accuracy; PSLA) since the shadow borders can be recorded at a finer resolution, but not the instrument intrinsic spatial resolution, which is limited by the mask pixel size and the mask-detector distance (see Eq. 2.1). The PSLA depends on the signal-to-noise ratio and for ISGRI it can be as good as $30''$ (Gros et al., 2003).

Spectral Resolution

PICSIT: this detector plane is made of CsI(Tl) crystals. The detection of the photons is based on the scintillation process.

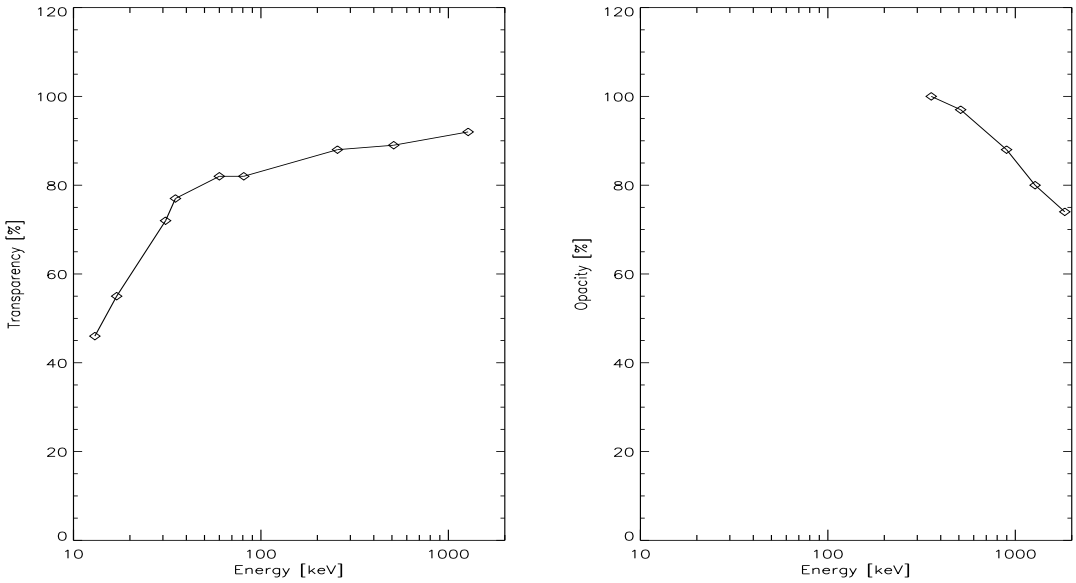

Figure 2.5: Left Panel: Transaprency of IBIS mask open pixels vs. Energy for on axis-sources. Data from Reglero et al. (2001). Right Panel: Opacity of IBIS mask closed elements vs. Energy for on-axis sources (IBIS Scientific Performance Report 5.0).

For PICsIT the spectral resolution can be expressed by the following relation

$$\left(\frac{\Delta E}{E}\right)_{FWHM} = 2.35\frac{\sqrt{nE+N^2}}{nE} + k \tag{2.5}$$

where n is the number of electrons/keV, E is the energy in keV and $k \sim 1.7$ is a term that accounts for the inhomogeneity of the scintillation process and of the light propagation in the crystal. For PICsIT $n = 33$ e^{-1}/keV (IBIS Scientific Performance Report 4.0).

ISGRI: the lower energy detector is made of CdTe, a semiconductor. These kind of devices are similar to scintillators: the difference lies in the fact that the energetic electron does not generate *fluorescence* but a number of charge-hole pairs along its trajectory. Charges and holes drift along the applied electric field in opposite direction. This motion produces a current, which is used to determine the energy of the incident photon. The time the pairs used to reach the extremes (anode and cathode) of the detector is different, due to the different mobility (speed per electric field unit) and distance they have to travel. In addition, part of the holes is lost during the drift due to their shorter lifetime with respect to the charges. The deeper is the interaction (i.e. the larger is the photon energy), the larger will be the *charge loss*, because the larger will be the distance the holes

have to cover. This effect can be corrected measuring the difference of the arrival time between holes and charges, called *rise time*. Events induced by cosmic rays are likely associated with short *rise time* events.

The ISGRI spectral resolution is influenced at energies larger than ∼50 keV by the *charge loss*. Once this effect is taken into account, the relation that represents the spectral resolution is

$$\left(\frac{\Delta E}{E}\right)_{FWHM} = 2E^{-0.7} \tag{2.6}$$

where E is the photon energy expressed in keV(IBIS Scientific Performance Report 4.0).

Operation Modes

IBIS can be operated in different modes: the standard one is to operate ISGRI in photon-by-photon mode, where for each event energy, time, interaction pixel are recorded. PICsIT is usually operated in histogram mode (PICsIT is operated in photon-by-photon mode during satellite slews). In this mode the number of events per pixel is integrated for a characteristic time in 256 energy bands and the time resolution is given by the integration time. This is done in order to reduce the telemetry amount requested by the whole instrument. The loss of time resolution is the reason why PICsIT data are not suitable for GRB detection and hence are not used by IBAS.

2.3.2 Imaging

As already said, the IBIS mask consists of (almost) four cyclic repetitions of the base pattern. This implies that when the detector shadowgram is deconvolved to obtain the sky image, a shadow cast from a given sky position produces significant signal also at positions offset by the mask base pattern. In other words, a point source does not produce a single narrow peak at its true position, but also other spurious peaks at well defined offset positions called *ghosts* (see Fig. 2.6). In the case of the source in the FCFOV there are 8 *ghosts*. *Ghosts* are less intense than the source since only at the correct position the whole flux is taken into account. In the PCFOV, on the other hand, every source has just 3 *ghosts*, but the four peaks have almost exactly the same intensity, since the recorded mask pattern matches the same subset of all four possible patterns. This is true for the mask which is a fully replication of the base pattern, but thanks to the fact that IBIS mask has been chosen to be an incomplete repetition, the true peak has a higher significance than the *ghosts*.

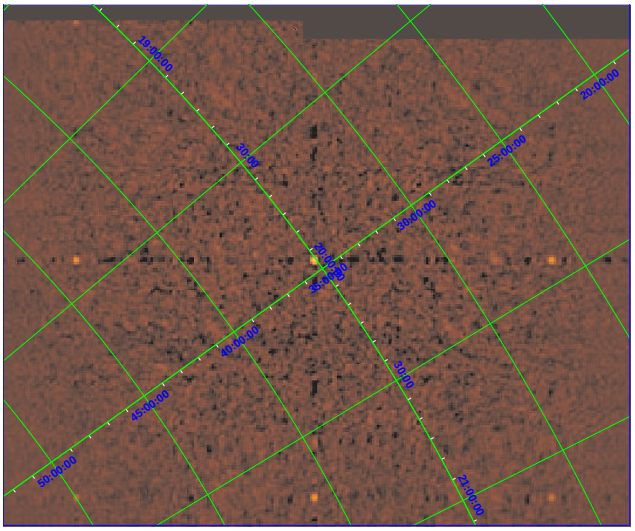

Figure 2.6: Cyg X-1 (at the center of the image) and its 8 *ghosts*. ISGRI (15-300 keV), PV phase data.

2.3.3 Point Source Analysis

In the case of an ideal instrument, the units in the deconvolved sky image can be easily converted to represent source $counts/sec/cm^2$. Unfortunately, detector imperfections and deconvolution algorithm aspects (e.g. re-binning, presence of ghost peaks and systematic coding noise) make this conversion non trivial: a better approach would be fitting to the deconvolved image a model of the (position and energy dependent) Point Spread Function (PSF) (Goldwurm et al., 2003). An alternative, though very similar, approach is to perform the fit before the deconvolution directly to the detector shadowgram with a (position and energy dependent) model of the source contribution. A mixed approach is also possible, where the source position is obtained from the deconvolved image and its flux from the detector shadowgram.

PIF

First let's assume that we already know the source position in the FOV; it is quite trivial to compute, for each detector pixel, which fraction of it is illuminated by the source, or in other words, the Pixel Illuminated Function (PIF) (Skinner, 1995). Computing this value for each detector pixel one obatins a matrix of the same dimensions as the detector shadowgram, whose values range from 0 (fully shaded pixels) to 1 (fully illuminated pixels). One example for a source in the PCFOV is shown in Fig. 2.7.

Following Skinner (1995), we can compare directly our PIF and the recorded shadowgram, plotting the number of events recorded in each pixel versus the PIF

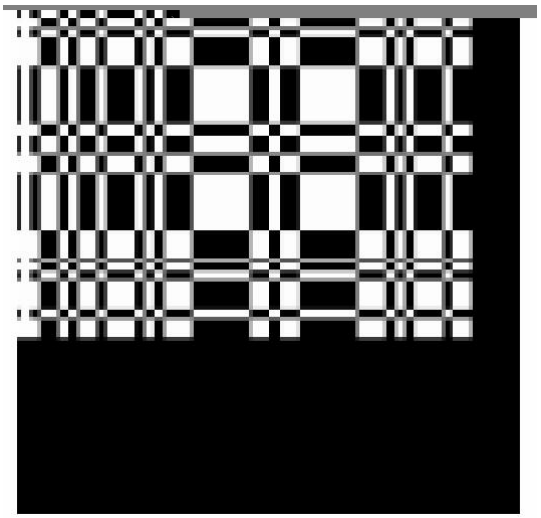

Figure 2.7: Pixel Illumination Function (PIF) for a source in the PCFOV. The source is GRB 040422.

value of each pixel. Performing a linear regression on these points we obtain the parameters of the best fit line $y = A \cdot x + B$. The linear slope coefficient A is the best estimate of the source flux F, while the intercept term B is a measure of the background flux (fluxes units are $cts/(pixelarea)$). The linear coefficients A and B can be computed with their uncertainties. In theory one could think of modeling the source contribution by taking into account something more than the plain geometry, namely the mask transparency/opacity vs. energy and incident angle, the detector efficiency and energy resolution and all sort of instrumental effects: in this case the resulting coefficients would directly represent the incident photons/pixel. On the other hand, with a simple geometry modeling all we retrieve are counts/pixel and the instrumental effects are taken into account (as a global undefined entity) by experimentally derived response matrices; the incident source properties can then be reconstructed by spectral fitting.

Since this method returns an estimate of the source flux and the associated error, the significance of the detection is trivially $F/\sigma F$. An important application when this comes into play is in the discrimination between source and *ghosts* (see below).

2.4 The *INTEGRAL* Burst Alert System

The good Source Location Accuracy of IBIS, its large Field Of View and its energy range, make it an excellent GRB detector. Due to the lack of a GRB triggering system on board *INTEGRAL* , a software system is running at ISDC to detect and quickly localize GRBs. IBAS (*INTEGRAL* Burst Alert System; Mereghetti et al.

(2003e)) achieves this by analyzing (in near real time) the incoming telemetry stream at ISDC. Once a potential GRB is detected and localized, IBAS generates and delivers one or more GRB alerts to a list of recipients (clients). In addition, for GRBs located inside the OMC field of view, IBAS delivers to MOC a special file containing a telecommand to define one OMC window centered on the GRB position.

The search for GRBs is performed by different programs that run simultaneously in parallel. These programs analyze the light curve of the different instruments, on different time scales and energy ranges, looking for significant excesses. In positive cases an imaging algorithm is invoked (where applicable) in order to localize the GRBs. In addition to this traditional algorithm, another one based only on imaging has been developed. Of course the different programs will generate multiple triggers for each GRB. In order to distribute the minimum number of alerts with the largest amount of information, the triggers are filtered and combined by a dedicated program before they are sent via Internet to the clients. Before sending the alerts, the derived positions are compared to a list of variable sources to avoid distributing Alerts not due to GRBs. All these processes are usually completed within a few tens of seconds from the GRB start (see Section 2.5). This allows especially robotic telescopes to quickly react and to potentially observe the GRB while it is still active.

In the following Sections the *INTEGRAL* Burst Alert System will be described in detail.

2.4.1 The IBAS structure

Fig. 2.8 shows the main components of IBAS. The IBAS system interfaces directly in input with the Near Real Time Data Receipt (NRTDR) subsystem and in output with the ISDC Alert Management and IFTS subsystems (shown on the picture, but not part of IBAS) and with IBAS Clients. Basically, IBAS consists of several detector processes and the process `ibasalertd`. All processes run in parallel. The detector processes have the task to trigger on possible GRB events and perform preliminary checks to filter out, as much as possible, spurious events. They do not communicate with each other, but they just communicate with the `ibasalertd` process. The `ibasalertd` process has the task to further filter out triggers (taking into account all the information received from several detector programs) and to send GRB Alerts out. An additional program continuously stores the incoming events, that can be used for the off-line interactive analysis, if needed.

All IBAS processes are multi-threaded applications written in C and/or C++. They run as daemon processes, which means they do not perform any terminal I/O and run in background. IBAS processes perform several subtasks in parallel. Each subtask is handled by a separate thread. With some unavoidable exceptions, subtasks are independent and do not block each other.

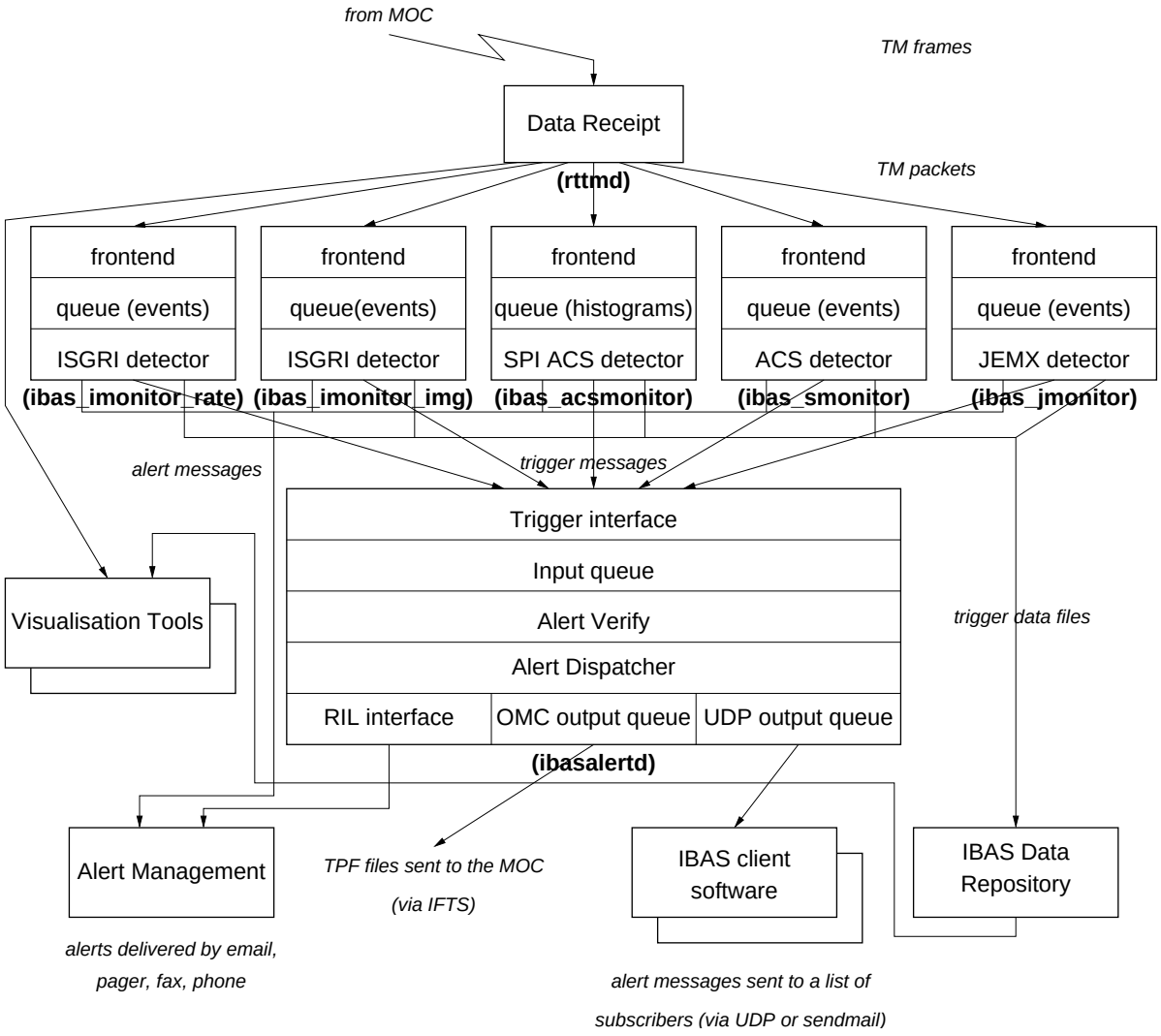

Figure 2.8: *INTEGRAL* Burst Alert System main components (from Borkowski et al. (2002)).

IBAS uses only IBIS/ISGRI data (PICsIT data are transmitted to ground already binned as shadowgrams and hence with no timing information) to localize GRBs. The Anti-Coincidence System of SPI is used by IBAS to detect GRBs, but it has no localization capabilities. On this subject see von Kienlin et al. (2003b). It is possible, in principle, to add detection programs based on data from SPI and JEM-X to localize GRBs: thanks to the modularity of IBAS they can easily integrated into the system, but this has not been done yet. There is also a number of IBAS visualization tools that are used to analyze quickly IBAS data off-line in order to confirm or deny an Alert.

For a detailed explanation of the real time telemetry decoding process see Borkowski et al. (2002). He we present in detail only the IBIS/ISGRI detector

programs.

2.4.2 GRB detector programs

At the time of writing two kinds of programs have been implemented and are used to search for GRBs in the ISGRI data.

2.4.3 GRB search in ISGRI count rates: `imonitor_rate` program

The `imonitor_rate` program searches for GRBs in the ISGRI photon mode data stream. When an excess is found in the light curve a quick imaging analysis is performed to verify the presence of a new point source in the field of view. The search can be done on a number of different timescales simultaneously. Selection on the energy and rise time (see Section 2.3.1) of the accepted events can be done. IBAS reconstructs the energy of each photon using PHA and rise time information *on-the-fly*. This means that the differences between the individual pixels are not taken into account, but only average values are used. This provides a good broad band energy correction (see Fig. 2.9) and does not require large computing time. To simultaneously search with different selection settings,

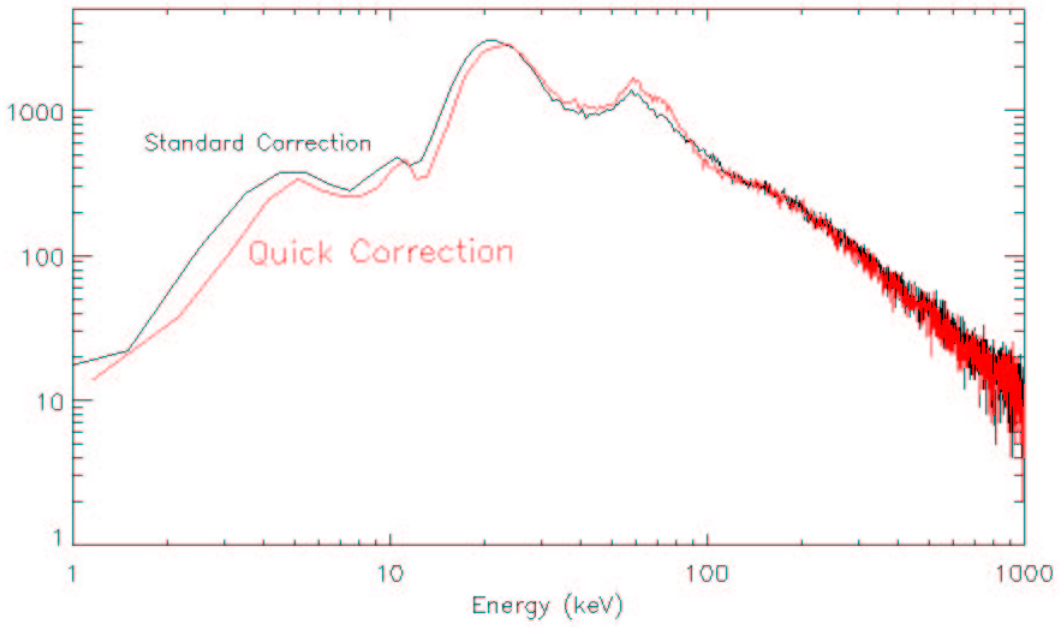

Figure 2.9: Comparison between the standard accurate energy correction (black spectrum), used in IBAS off-line analysis tools, and the quick IBAS correction (red spectrum).

different instances of `imonitor_rate` run in parallel. The logical functions of the `imonitor_rate` program, explained in more detail in the following subsections, are:

- Input parameters and initialization
- light curve analysis (check for the presence of a *potential trigger*)
- imaging analysis (promote a *potential trigger* to a *good trigger*)
- GRB localization for *good triggers*
- production of output files

In case of a Good Trigger a *Trigger Message* is prepared and delivered to the `ibasalertd` program (see Section 2.4.5). In general, more than one *Trigger Message* is expected for the same GRB (e.g., due to the different timescales analyzed, or due to a complex light curve). The `ibasalertd` process filters these *Trigger Messages* in order to produce a limited number of *Alert Messages*. The content of the *Trigger Message* is the following:

```
IbasAlert.det_flags = IBAS_ALERT_DETF_HAVE_POSITION;
IbasAlert.grb_timescale = ttscale; [seconds]
IbasAlert.grb_time_err = pars.imit*pars.sit; [seconds]
IbasAlert.grb_y = srcpy*MASK_PIXEL_SIZE/MASK_CDTE_DISTANCE; [tan(offaxis
angle)]
IbasAlert.grb_z = srcpz*MASK_PIXEL_SIZE/MASK_CDTE_DISTANCE; [tan(offaxis
angle)]
IbasAlert.monitor = IBAS_ALERT_MONITOR_ISGRI_RATE;
IbasAlert.grb_dy = dsrcpy; [arcmins] burst position error
IbasAlert.grb_dz = dsrcpz; [arcmins] burst position error
IbasAlert.grb_sigma = snr;
IbasAlert.magic_num = 1229078867;
IbasAlert.grb_obt = tstart; [seconds]
IbasAlert.pkt_type = IBAS_ALERT_PKTYPE_TRIGGER;
IbasAlert.test_flag = testflag;
```

The program `imonitor_rate` can also write several output files in case of a trigger. These files consist of the triggering image(s), the light curves and the event file for each trigger, and can then be used in a rapid off-line analysis.

Processing

The search for GRBs is performed by comparing the number of counts detected in the current time interval (SIT) with that expected from the average count

rate measured previously during a reference time interval (LIT). The detector programs can compute the background level over the LIT continuously (every SIT) or just once per pointing at the starting of the pointing. The second method can be used either when the background variations are small, or when the telemetry quality is not constant during the pointing. In the currently running version of the programs, the first method is used. After a program restart, some time must therefore be spent (SIT+DIT+LIT) to accumulate and measure the reference count rate. The time boundaries of the reference interval relative to the current time interval are specified by the parameters LIT and DIT (see also Fig. 2.10). The duration of the time interval ΔT over which counts are

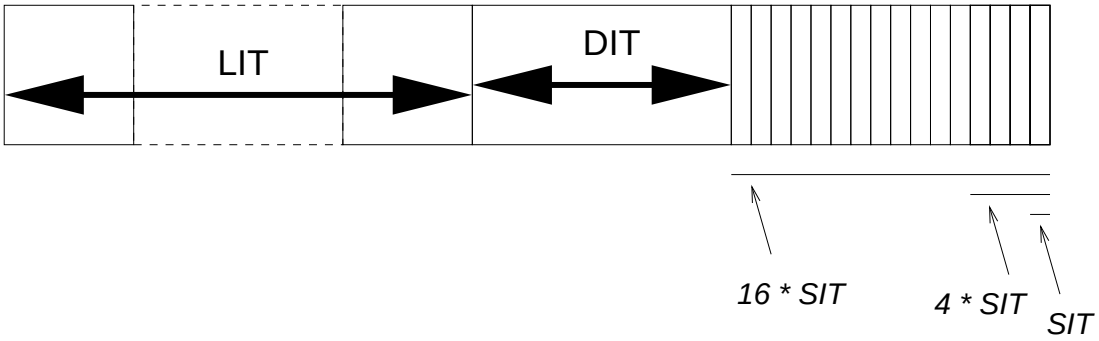

Figure 2.10: Time intervals used in the triggering algorithm of *imonitor_rate*.

accumulated to check for the presence of an excess is a critical parameter in any triggering algorithm. In principle, the sensitivity increases as $\Delta T^{1/2}$ for a source with constant flux. However, GRBs are by definition variable sources and they have a broad distribution of durations and rise times (see Chapter 1). Therefore the overall sensitivity is optimized by searching GRB with different ΔT values. For example, the BATSE on board triggering scheme was based on the values ΔT = 64 , 256, and 1024 ms (Fishman et al., 1994). The program `imonitor_rate` is optimized to perform simultaneously the search in a number of timescales. The shortest ΔT value is set by the parameter SIT. The other values are given by the relation:

$$\Delta T_i = SIT \times TIMEPOWERBASE^i \tag{2.7}$$

with i=0,1,2,...$TIMESCALES$-1. $TIMESCALES$ and $TIMEPOWERBASE$ are parameters. The $TIMEPOWERBASE$ value currently used in IBAS is 4 (as shown in Fig, 2.10). Obviously a different threshold level is associated to the different ΔT_i. After initialization, the main program task is to ingest the data and bin them on the minimum timescale, SIT. Every time a SIT is elapsed, the search for *potential triggers* is done by comparing the number of counts C_i present in the time intervals ΔT_i with the reference values. A potential trigger occurs if:

$$C_i - RATE \cdot \Delta T_i > LCTHRESH_i \cdot (RATE \cdot \Delta T_i)^{1/2} \tag{2.8}$$

where $RATE$ is the average count rate measured in the current LIT interval. After each SIT also the value of $RATE$ is updated. Since the imaging analysis requires a longer computing time, it is not convenient to perform it every SIT (even when a potential trigger has occurred). For this reason the parameter $IMIT$ has been introduced. This is the minimum time interval that must elapse before the imaging analysis is performed. This also ensures that enough photons are collected.

Let's assume, for example that a potential trigger occurs at T_{trig}. Then several imaging analysis are repeated at times T_{trig} + j×$IMIT$ (j=1,2,3,... until the intensity of the light curve returns below the threshold levels).

The image analysis can be performed in two ways:

1. the pre-burst and burst light curve (i.e. the time interval starting at DIT+LIT before the current time) is examined to define ON-BURST and OFF-BURST intervals. This is done comparing the light curve with two values ($SKYTHRESH$ and $BKGTHRESH$ in Fig. 2.11) that are specified with the $IMTRHESH$ parameter. ON-BURST and OFF-BURST

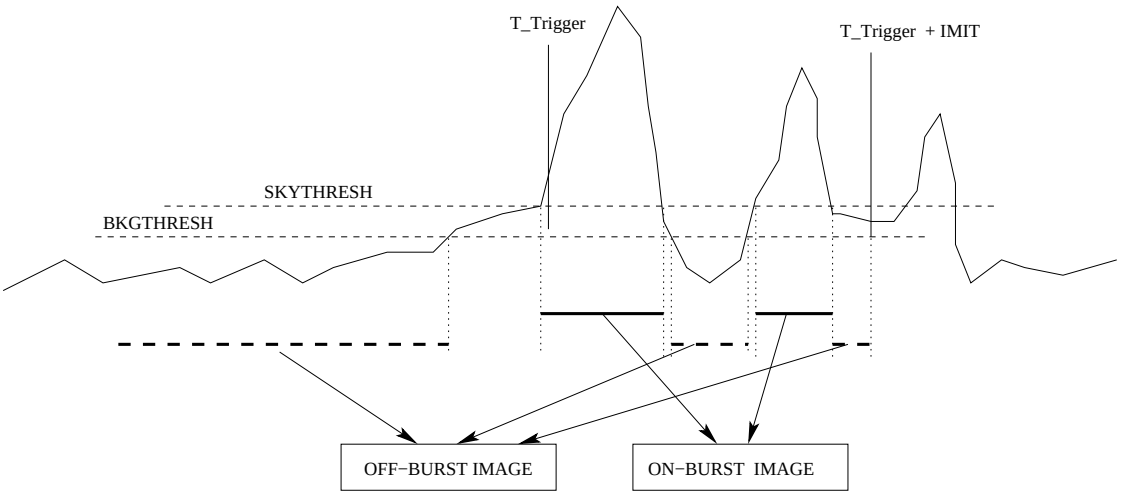

Figure 2.11: Time intervals used in the triggering algorithm of `imonitor_rate`.

detector images (shadowgrams) are accumulated, cleaned from noisy pixels (they are eliminated by substituing their values with the mean value of the shadowgram, if their value is larger than 9 σ above the mean level), normalized for the different exposure times, and deconvolved; only the FCFOV is considered in order to reduce the computing time. The difference sky image (SKY_ON-BURST – SKY_OFF-BURST) is computed and examined to look for the highest peak. If the peak is below a given threshold the potential trigger is considered *bad*. If a significant peak is found the trigger is promoted to the *good* class.

2. the pre-burst image is accumulated at the beginning of a pointing for an integration time corresponding to the entire event buffer (*SIT+DIT+LIT*), during which the triggering is inhibited. This allows to have a better quality background image due to the longer exposure times, and hence to better resolve faint sources. The position of the source found in the ON-BURST image is compared to the most significant peak found in the pre-burst image. In case they match no trigger is issued, in the opposite case the trigger is considered *good*. This method has been developed, because, in case of very short events (<1 s), the signal-to-noise of the peak is worsened by the subtraction algorithm. (An almost empty detector produces a *flatter* image than a statistically uniformly filled one).

In the current version of IBAS the second method has been chosen, in order to increase the sensitivity to short bursts. This method allowed to detect several short (∼0.1 s) bursts from SGR 1806–20 (see Chapter 4).

Concerning the imaging part and the shadowgram treatments, it has to be pointed out that before the correlation with the mask pattern (deconvolution) is applied, some correction steps are performed: the shadowgrams are expanded from their original pixel size (128×128) in order to include the 2 pixles wide gaps between the modules (see Section 2.3). The gaps are filled with the mean value of the shadowgram, and the shadowgrams are then cut back to their original size. This procedure is applied as a whole only to the OFF-BURST shadowgrams and to all the shadowgrams of the `imonitor_img` program (see Section 2.4.4). For the ON-BURST image, on the other hand, the gaps are just filled with 0s, since it was realized that the signal-to-noise ratio of the sky images obtained from shadowgrms with few counts is better in without the averaging process. In addition, since periodically the on-board software switches off one of the modules, this issue is checked and the triggering is inhibited, because in these situations the localization of the source cannot be performed properly and this could give rise to false triggers from known sources.

Only when a *good* trigger is detected, the program performs the actual source localization part. A *good* trigger means that a new, statistically significant peak has appeared in the FCFOV (the significance threshold is tunable by parameter). It could be due to a source in the FCFOV, but, most likely, it will be the ghost image of a source in the PCFOV[1]. Therefore, the aim of the localization part is to locate the true source position by discriminating among the 8+1 (3+1) possible ones. Rather than performing an imaging analysis of the whole field of view, this is done only by computing the PIF corresponding to the possible positions and taking the one with the best significance as the most likely GRB localization (see Section 2.3.3). The starting position of the function which discriminates between the different ghosts is determined with a 2-D gaussian fitting algorithm

[1]Sources in the PCFOV have always a *ghost* in the FCFOV.

that starts from the integer values of the pixels where the maximum in the image was found and returns a *best fit* couple. This is done because obviously the center of the PSF (which is larger than a single pixel) does not usually correspond to the center of the pixel where the maximum was found. A 2-D gaussian function represents sufficiently well the IBIS PSF shape at this stage.

The main triggering parameters that are used for the 3 instances of `imonitor_rate` currently running are reported in Tab. 2.2. As can be seen the instance 200 is

ID	Times Scales	Energy Range	IMIT	LIT	DIT	LCTHRESH$_i$
200	2,8,32 ms	15-200 keV	2 s	20 s	12 s	7.5 6 6
201	0.08, 0.32, 1.28, 5.12 s	15-200 keV	8 s	40 s	20 s	7 7 6 6
202	10, 40, 160, 640 ms	40-200 keV	2 s	20 s	6 s	7.5 6 6 6

Table 2.2: Main Triggering Parameters for the 3 instances of `imonitor_rate`

optimized for very short events and instance 202 has been optimized for events with hard spectra, as expected for short GRBs (Pendleton et al., 1994).

2.4.4 GRB search in ISGRI images: `imonitor_img` program

The `imonitor_img` program searches for GRBs in the ISGRI photon mode data stream by continuously comparing sky images accumulated over a single timescale (defined by the input parameter *IIT*). Selection on the pulse height and rise time of the accepted events can be done as in the case of `imonitor_rate`. To search in different energy ranges and/or timescales different instances of `imonitor_img` run in parallel.

This program is more efficient than `imonitor_rate` to detect GRBs in conditions of time variable background. However, its performance is limited by the time required to deconvolve images. This sets the minimum timescale of the GRB time trigger interval (equal of the image integration time, typically of the order of several seconds). This program can also be useful to discover long (and/or slowly rising) GRBs.

The Input and Output phases are exactly the same as described for `imonitor_rate`. Note that in general several *Trigger Messages* will be sent at times T_{trig}+j×IIT (j=1,2,...) until the GRB light curve returns below the pre-burst threshold level. The `ibasalertd` process will filter these *Trigger Message* in order to produce a limited number of *Alert Messages*. Four images are stored as output files for each trigger.

Processing

Incoming counts are binned to produce detector images integrated on time intervals given by the parameter IIT. During program initialization, i.e. the first part of a new pointing, these images are summed to produce a *reference sky image*. After the initialization phase, a new detector image is accumulated and deconvolved each IIT. The resulting *sky image* is then compared to the *reference sky image* by subtraction. The subtraction is done in order to subtract the contribution from persistent sources, which can be present in the field of view. If no peaks are present above the threshold value, the current *sky image* is added to the *reference image* and the latter is normalized for the exposure time. If a peak is found a process of source localization is started. This is done as explained above for `imonitor_rate`, since also in this case the imaging analysis is done only in the FCFOV. Before promoting a trigger to a good one an additional check is performed: it may happen that a persistent *strongly variable* source is present in the FOV (like e.g. Cyg X-1, GRS 1915+105 or 4U 1700-37). In this case the normalization process is not enough and after the subtraction of the two images a residual peak can be present at the position of the persistent source. So the position of the new peak is compared to the position of the peak in the reference image. If these two match, than no *Trigger message* is produced.

In case of *good trigger* four images are stored: the *sky image*, its *shadowgram*, the *reference image* and the difference image where the peak has been searched for.

The main triggering parameters of the 5 currently running instances of this program are reported in Tab. 2.3.

ID	Times Scales	Energy Range
300	10 s	15-200 keV
301	20 s	15-200 keV
302	40 s	15-200 keV
303	10 s	15-40 keV
304	100 s	15-200 keV

Table 2.3: Main Triggering Parameters for the 5 instances of `imonitor_img`

The instance 303 is optimized for the detection of events with soft spectra like X-ray Flashes, but also for type-I X-ray bursts, while 304 is optimized for slowly rising faint GRBs (Götz & Mereghetti, 2003), but has detected also several Galactic transient sources.

2.4.5 Alert verification and delivery

The IBAS GRB detector programs described in the previous sections operate independently from each other. Thus it is quite probable that more than one trigger is generated for the same GRB. Since IBAS should send out as few alerts per GRB as possible, it is necessary to have a final alert verification phase which takes into account the information from all the detector programs. `ibasalertd` is the program which takes care of that (see Fig. 2.12).

The advantage of having a final verification phase is that the GRB detector programs are allowed to be more *verbose*, i.e., they are free to generate triggers even for events of relatively low statistical significance.

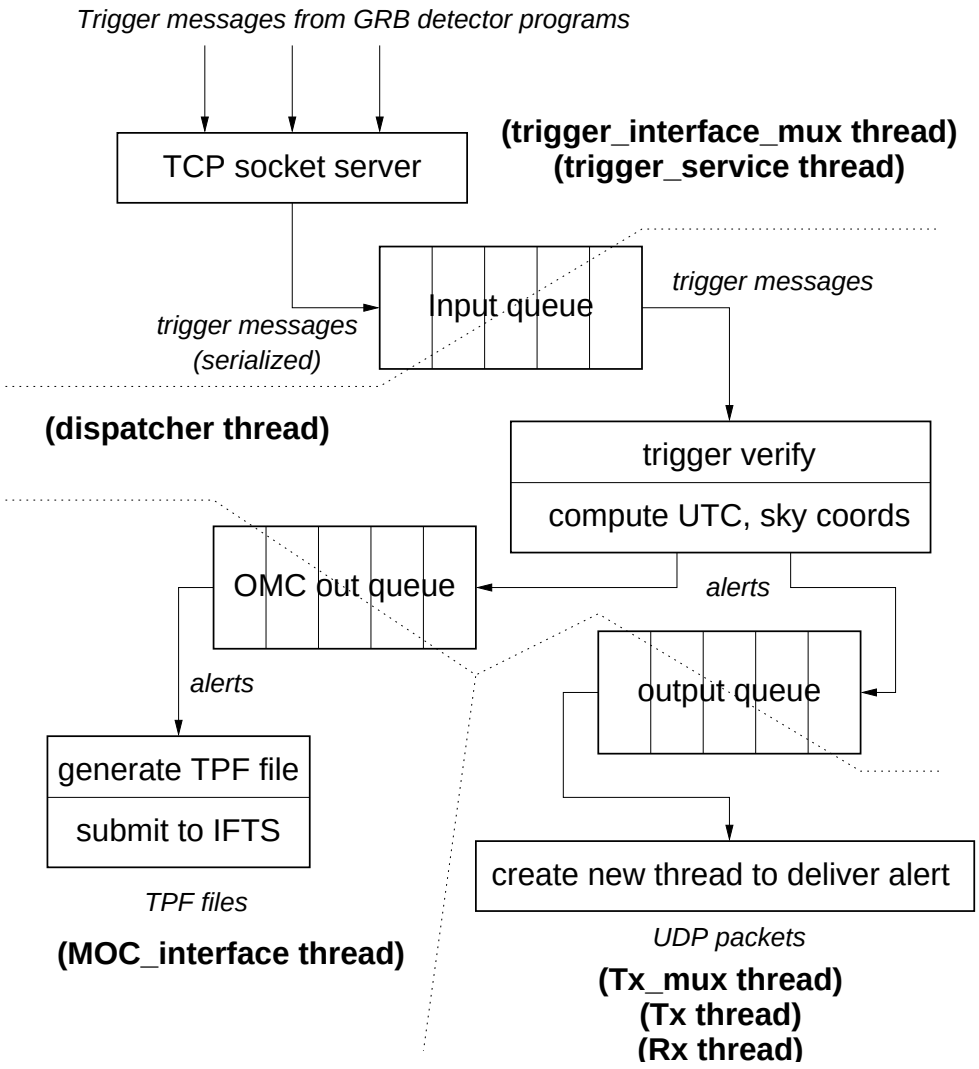

Figure 2.12: `ibasalertd` program functional diagram (Borkowski et al., 2002).

The dispatcher thread is the real *decision making* thread. It works in a loop

and hangs until the new trigger in the input queue is available. Next, the program verifies whether an alert can be sent out immediately (see Fig. 2.13). In

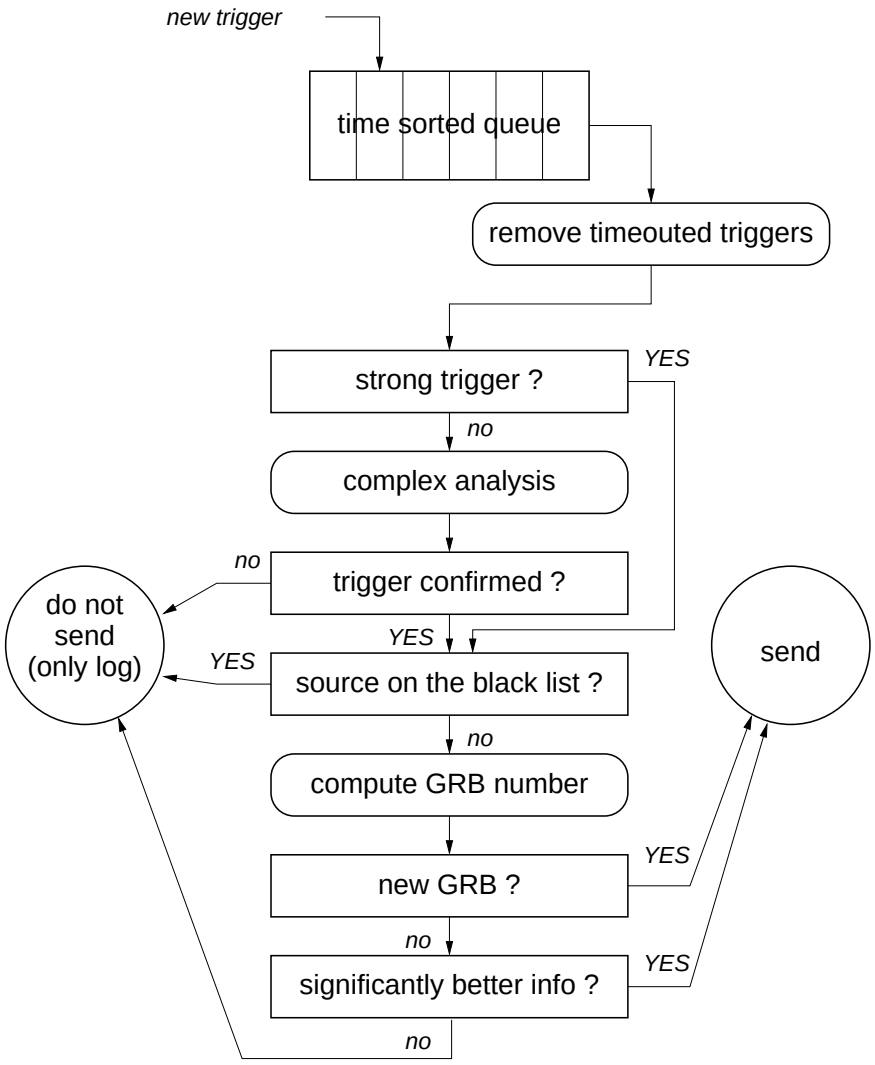

Figure 2.13: Alert verification algorithm (Borkowski et al., 2002).

the first step the new trigger is inserted into a time sorted queue. Triggers do not necessarily come sorted in time, since GRB detection delay varies with GRB detector program or time bin used in computations and algorithm. It is expected however that, most of the time, triggers will be coming time sorted. The verification process involves several checkpoints. The result of each checkpoint can be:

- SEND - positive verification, no need to check further. Alert will be sent.
- DO NOT SEND - negative verification, no need to check further. Alert will NOT be sent.

- YES - positive verification but still uncertain, continue with next checkpoint.
- NO - negative verification but still uncertain, continue with next checkpoint.

The following checkpoints are defined (given in the order they are called) :

- **strong trigger** - if the `significance` value in the trigger is above a predefined level (tunable in the parameter file, now set to 8.0), the trigger is considered *strong*. The threshold level is tunable for each GRB detector program, but at the moment is kept the same for each one. If the trigger is strong, then there is no need to do more complex analysis.
- **complex analysis** - if the trigger is not found *strong*, but above the *possible* level (now set to 6.5) then the queue of triggers shall be rescanned to check if there are any further indications that there is real a GRB. The current implementation is very simple: if there are other independent triggers in the queue (besides the new one just inserted) with the same position but generated from a different instrument[2], then this checkpoint returns YES (trigger confirmed). Otherwise it returns NO. In any case a *possible* trigger, confirmed or not, produces a low level alert, which reaches the members of the IBAS Team, but a quick reaction can be achieved only during working hours. Triggers with significance below the *possible* level are discarded.
- **black list source** - the position of the new trigger is converted to sky coordinates and is compared against a list of known non-GRB sources and to their possible *ghosts* positions. If a match is found (small error margin is allowed) this checkpoint returns NO. Otherwise it returns YES. Of course IBAS should not send alerts for events associated with known sources.
- **new GRB** - the time of the new trigger and its position are compared with the time of the last alert sent. If they differ by more than certain value (tunable via parameter file) then it is assumed that the trigger corresponds to a new GRB. An Alert is sent out.
- **significantly better info** - this step is called only when a given trigger is not the first one for a given GRB. It is checked whether the new trigger has much better info in terms of position accuracy then the last alert sent. The threshold level (how much better info is needed) is tunable.

Once the alert is verified, the dispatcher thread converts Central On Board Time to UTC and computes the sky coordinates of the GRB. These computations must

[2]Currently, since only IBIS/ISGRI programs are running, possible triggers cannot be confirmed automatically.

use the best attitude information available at that time: either the *predicted* one, or the *NRT* (Near-Real Time attitude, based on the star trackers snapshot images) one, if available.

The main IBAS GRB Alert delivery method is via UDP packets. This method was chosen for the following reasons :

- Alerts can be delivered to the recipient within 1 second. The actual delay depends on Internet interconnection between ISDC and the recipient. Simple tests show that for majority of astronomical institutions the delay is less than 0.2 s. This number is valid for nominal conditions, if networks are full operational and there is no traffic congestion.
- Alerts can be delivered to the recipients independently
- Alerts can be delivered to the recipients in parallel. The delivery of alerts in parallel should not consume too much resources (processes, memory, etc).
- the programmatic interface to the IBAS alerts can be simple (from the recipients perspective).

2.4.6 IBAS Alerts

IBAS sends to the outside world different types of Alert Packets. Each packet type is identified by a number. The following packet types have been defined:

Alert type number	name	purpose
1	POINTDIR	allows automated telescopes to get pre-GRB data
2	SPIACS	GRBs detected by them SPI ACS (no position available)
3	WAKEUP	first message of each GRB with positional info
4	REFINED	subsequent messages giving better info
5	OFFLINE	results of interactive analysis

Clients can decide to subscribe in order to receive only to alert packets of a given type(s). Each packet type has a fixed format, consisting of several fields. Some fields can be empty for particular packet types. The Gamma-Ray Coordinates Network (GCN; Barthelmy et al. (1995)) itself is a client of IBAS and re-broadcasts IBAS Alerts (Barthelmy, 2002).

Thanks to POINTDIR Alerts, automated telescopes can exploit the knowledge of the INTEGRAL pointing direction in order to:

- reduce the slew time to the GRB position in case of an alert
- obtain reference images of the pre-GRB sky
- monitor at other wavelengths interesting and/or potential INTEGRAL sources

Packets of type WAKEUP are generated only once for each GRB and only if the GRB positional information is available. These are the alerts with the shortest time delay (and consequently the highest chance of not being due to a real GRB event). Although IBAS is performing several checks to reduce the occurrence of false triggers, there is a compromise between sensitivity and confidence in the real astrophysical nature of the event. Clients can use the information on significance and location uncertainty to decide the actions to take. A given (potential) GRB will generate only one WAKEUP packet, IBAS will then automatically distribute more refined information as soon as it becomes available using packets of type 4 (REFINED). IBAS is designed to generate always a REFINED packet, after a fixed time span from the WAKEUP packet, with the best available information (smallest positional uncertainty, i.e. highest detection significance) among all the triggers registered from a GRB event. This is suppressed only if the best available information is already contained in the WAKEUP packet.

Packets of type OFFLINE are generated manually after interactive analysis of the data performed off-line by a member of the IBAS Team. The time delay might be from one to a few hours (or even longer in some cases). Typically only one OFFLINE packet is expected for each GRB, but the possibility of more than one is allowed for exceptional cases. The OFFLINE alert packet represents the final confirmation (or rejection) of a GRB and contains the most accurate GRB properties distributed by IBAS.

For the detailed description of IBAS Alert fields see Appendix B.

2.5 IBAS Performances and Results

IBAS has localized 18 GRBs so far, about one per month in agreement with pre-launch predictions (Mereghetti et al., 2001). Preliminary peak fluxes in the 20-200 keV band,the T_{90} durations and the delays between the GRB start time and the IBAS Alert (or GCN circular when IBAS was not running) are reported in Tab. 2.5. The positions of the GRBs in instrumental and Galactic coordinates are reported in Figs. 2.14 and 2.15.

The first two GRBs have been discovered during the satellite Performance and Verification (PV) phase, during which the automatic sending of IBAS Alerts to the external clients was disabled. This because at the beginning of the mission, the parameters and detection algorithms were being tuned and optimized and the in-flight instrument misalignment was not calibrated yet. These two reasons

GRB	Peak Flux [ph cm^{-2} s^{-1}]	Peak Flux [erg cm^{-2} s^{-1}]	T_{90} [s]	Delay	Refs.
021125	22	2×10^{-6}	25	0.9 days	Bazzano & Paizis (2002)
021219	4.0	4.4×10^{-7}	5.5	5 hr	Mereghetti et al. (2002)
030131	1.9	1.7×10^{-7}	124	2 hr	Borkowski et al. (2003)
030227	1.1	1.0×10^{-7}	33	48 min	Götz et al. (2003a)
030320	3.6	4.0×10^{-7}	48	6 hr[2]	Mereghetti et al. (2003c)
030501	2.7	2.3×10^{-7}	40	24 s	Mereghetti et al. (2003d)
030529	0.4	3.0×10^{-8}	20	-	discovered offline
031203	1.7	1.6×10^{-7}	39	18 s	Götz et al. (2003b)
040106	1.0	1.0×10^{-7}	47	19 s	Mereghetti et al. (2004c)
040223	0.4	4.0×10^{-8}	258	210 s	Götz et al. (2004a)
040323	1.6	2.0×10^{-7}	14	30 s	Mereghetti et al. (2004a)
040403	0.5	5.0×10^{-8}	19	21 s	Götz et al. (2004b)
040422	3.5	2.8×10^{-7}	10	17 s	Mereghetti et al. (2004e)
040624	0.5	3.5×10^{-8}	35	6 hr[1,2]	Mereghetti et al. (2004b)
040730	0.4	2.2×10^{-8}	43	35 s	Götz et al. (2004h)
040812	0.6	5.0×10^{-8}	19	30 s	Götz et al. (2004i)
040827	0.6	6.0×10^{-8}	49	1.5 hr[2]	Mereghetti et al. (2004d)
040903	0.4	2.0×10^{-8}	10	32 s	Götz et al. (2004g)

[1]IBAS was not running due to telemetry problems.
[2]Below the threshold for automatic Alert Packet delivery.

Table 2.4: Peak Fluxes, durations, and announcement delays for all *INTEGRAL* GRBs.

explain the relatively large delays between the GRBs and their public announcements (and also the large uncertainties on their positions, see Fig. 2.17). After the automatic distribution of Alerts to the outside had been enabled (17^{th} of January 2003, exactly 3 months after launch) the delays (and the error boxes) have become always smaller reaching a few tens of seconds, which represents the limit of the system considering all the unavoidable delays. These are due to buffering on board the satellite ($\sim$5 s), earth reception time ($\sim$0.6 s maximum), delays induced between the ground stations and ISDC ($\sim$3 s for Redu, $\sim$6 s for Goldstone) and the time (few seconds) to analyze the data, which depends on the algorithm which triggers, which in turn depends on the time history of the burst. Finally the conversion to sky coordinates, the Alert production, and the delivery take about 2 s.

Today IBAS is providing the best performances in terms of GRB localization accuracy and speed ever, see Figs. 2.16, 2.17. As can be seen the IBAS Alerts delivered after April 2003 have very small error radii, of the order of $\sim$3 arcmin (90% c.l.). The size of the boxes is usually reduced after a few hours by interactive

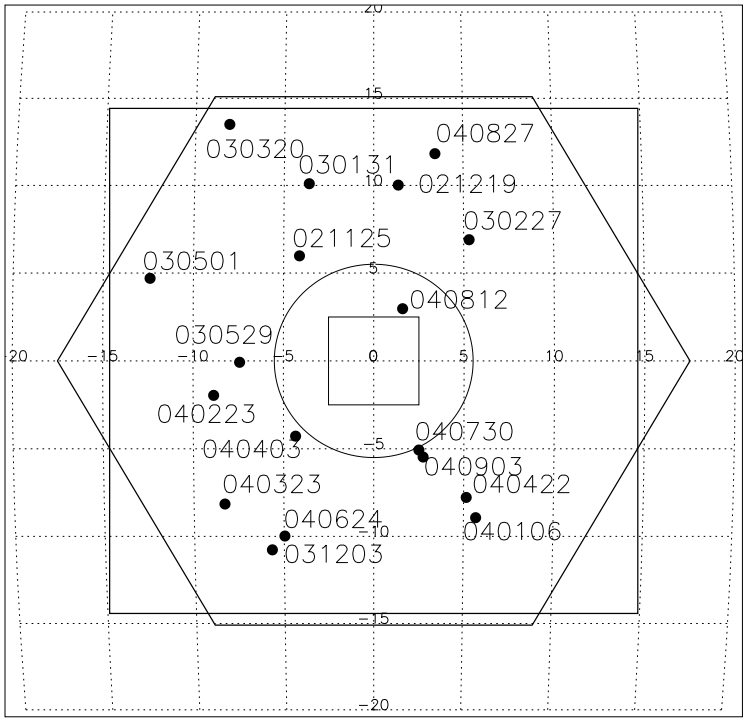

Figure 2.14: Positions of the GRBs detected with *INTEGRAL* in instrumental coordinates.

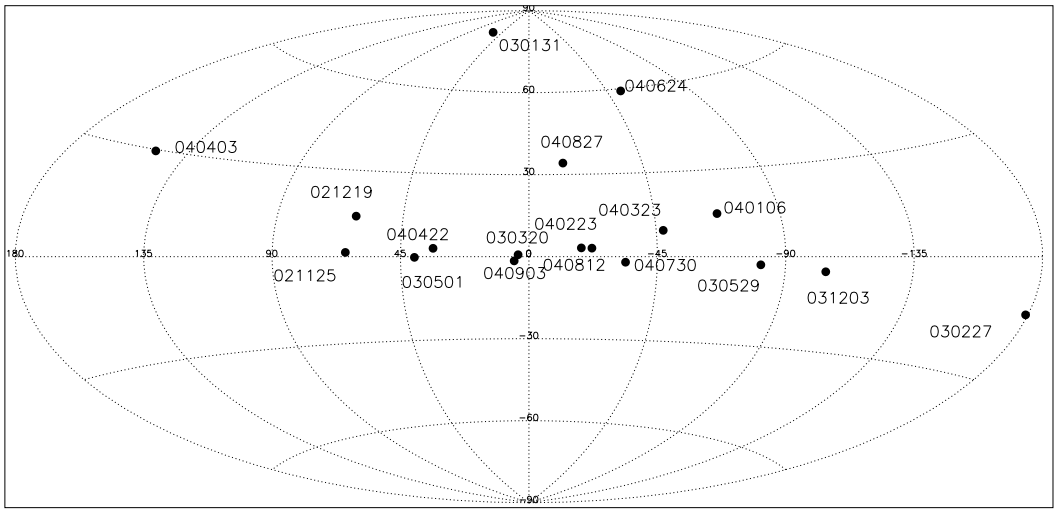

Figure 2.15: Positions of the GRBs detected with *INTEGRAL* in Galactic coordinates. The bias toward the Galactic Plane is due to the fact that *INTEGRAL* spends most of its observing time pointing Galactic sources.

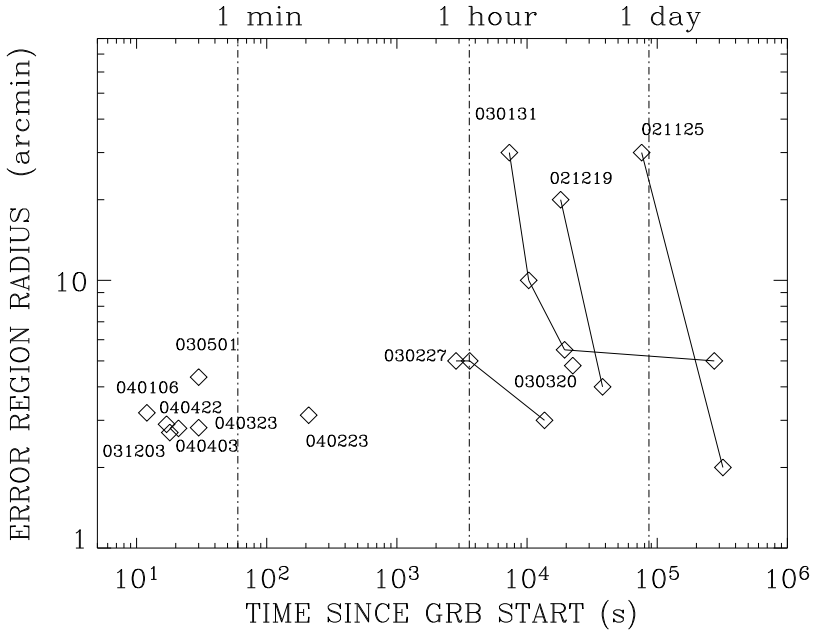

Figure 2.16: IBAS localization speed vs. accuracy (Mereghetti et al., 2004f).

analysis to ∼2 arcmin.

Despite the rapid communication, counterparts at other wavelengths, especially at optical ones, have been found for only a few of the *INTEGRAL* GRBs, see Tab.2.5 and Fig. 2.17. This can be due to the fact that some are intrinsically dark or faint, but also to the fact that the satellite spends most of its observing time on Galactic targets (see Fig. 2.18), where the optical extinction may be severe. On the other hand each time an X-ray counterpart has been looked for, it has been found.

The accuracy of the localizations by the IBAS automatic software can be estimated by looking at the trigger IBAS produces on known variable sources like Vela X-1, Cyg X-1 or Sco X-1. From the curves shown in Fig. 2.5, we can estimate the location accuracy as a function of the signal-to-noise ratio (S/N). This is reported in the second plot, where it can be seen that the 90% c.l. error radius is smaller than 2.5 arcmin for S/N $>$ 10. Being the current threshold for automatic delivery S/N=8.0, the first alert sent out (very often the only one, because the error box does not shrink enough during the bursts themselves) is the first one which exceeds this value, for which the error is about ∼3 arcmin.

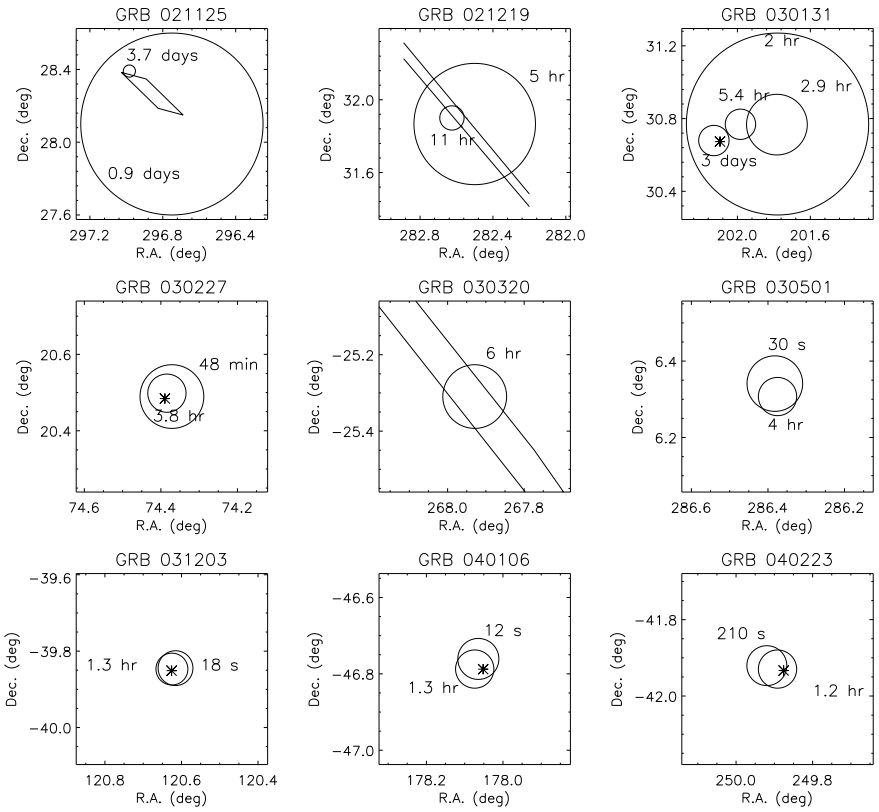

Figure 2.17: Error boxes for the first nine *INTEGRAL* GRBs. The corresponding time delays are also indicated. The parallelogram and the straight lines indicate error regions independently derived from the IPN. The asterisks mark the positions of the X-ray and/or optical transients.

GRB	X	Optical	IR	Radio
021125	-	-	-	-
021219	-	-	-	-
030131	-	Götz et al. (2003e)	-	-
030227	Mereghetti et al. (2003g)	Castro-Tirado et al. (2003)	-	-
030320	-	-	-	-
030501	-	-	-	-
030529	-	-	-	-
031203	Watson et al. (2004)	Cobb et al. (2004)	Malesani et al. (2004)	Soderberg et al. (2004)
040106	Ehle et al. (2004)	Masetti et al. (2004)	-	-
040223	Tiengo et al. (2004)	-	-	-
040323	-	Gal-Yam et al. (2004)	-	-
040403	-	-	-	-
040422	-	-	-	-
040624	-	-	-	-
040730	-	-	-	-
040812	Patel et al. (2004)	-	-	-
040827	De Luca et al. (2004)	Berger et al. (2004)	-	-
040903	-	-	-	-

Table 2.5: Counterparts of *INTEGRAL* GRBs.

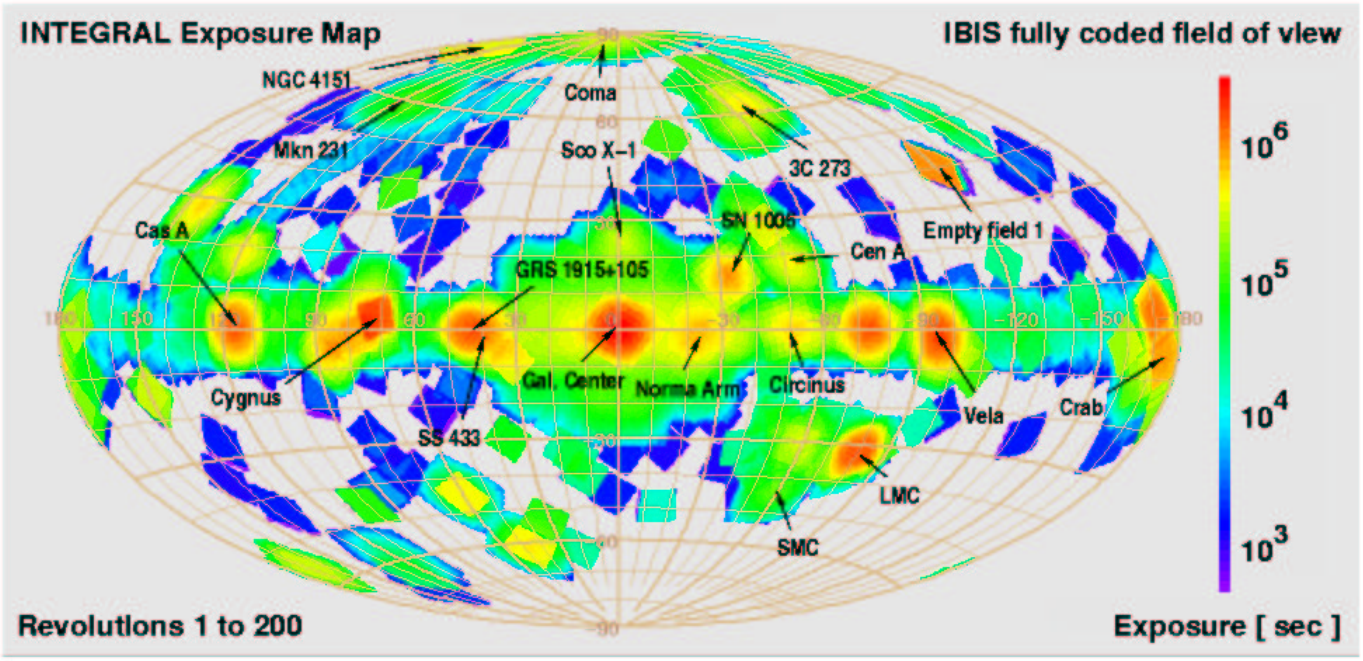

Figure 2.18: IBIS FCFOV exposure map for orbits 1-200 in Galactic coordinates. Courtesy Nami Mowlavi (ISDC).

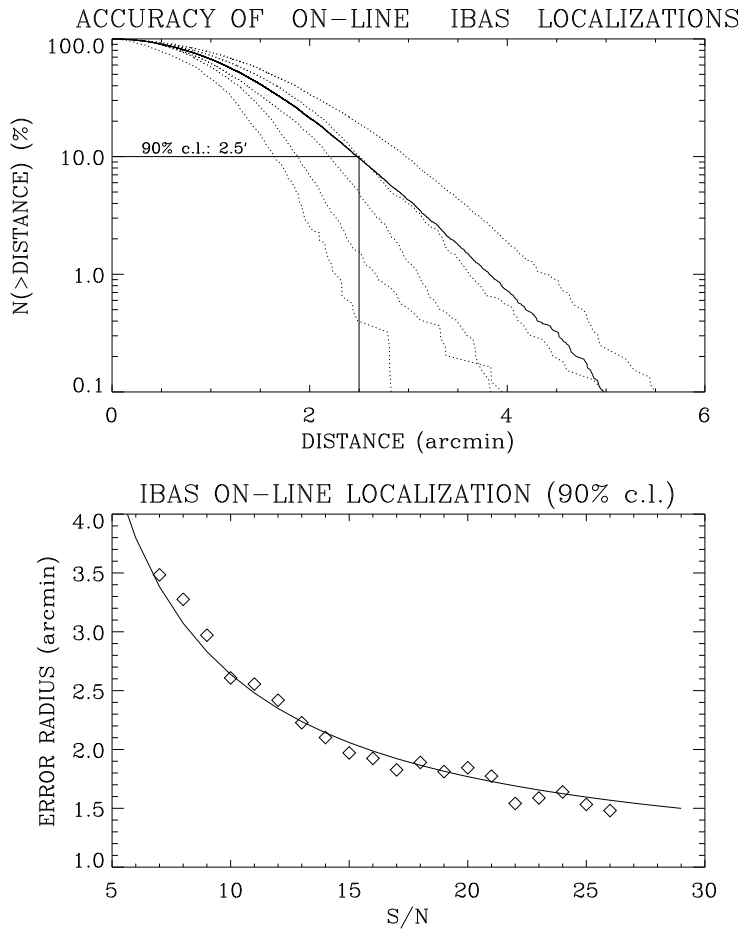

Figure 2.19: Upper panel: integral distribution of the angular difference between the true coordinates of known sources and those derived on-line by IBAS. The solid line is the total distribution of all the triggers. The dotted lines refer to the triggers with signal-to-noise values in different ranges (from top to bottom: 8-10, 10-12, 12-15,15-20, >20). Bottom panel: error on the coordinates derived by the on-line IBAS imaging program as a function of the signal-to-noise ratio. The diamonds are the experimental data derived from the observation of known sources. The line is an eye-fit with a simple analytical law.

Chapter 3

Results on Gamma-Ray Bursts

In this Chapter we present the results of the analysis of the GRBs detected by IBAS (see Chapter 2). For some of these GRBs preliminary results, derived as part of this thesis, have been already published (see Appendix A). The IBIS data, have been all re-analyzed with the most recent tools and calibration information and are presented in this Chapter. This allows a better direct comparison between the different properties of the GRBs, especially from the spectral point of view.

3.1 Data Analysis

The localizations (*hh:mm:ss, +/-dd:mm:ss*; J2000) have been recomputed using the best available attitude information and instrument misalignment matrix. The uncertainties are given at 90% confidence level and are computed adding in quadrature the statistical uncertainties to a conservative systematic error of $1'$.

The light curves (15-300 keV) presented here for the GRBs detected by *INTEGRAL* have been recomputed. All of them are given in units of equivalent counts: these units represent the vignetting corrected counts. In other words, the raw counts have been multiplied by the ratio between the total geometric area and the area effectively illuminated by the GRB. In addition, to improve the signal-to-noise ratio, the light curves have been extracted only from the pixels that were illuminated by the GRB for at least half their surface (with exception of 030131, see Section 3.4) and they were background subtracted. The background level was determined using data before and after the GRB. From these light curves the T_{90}[1] duration of each burst has been computed.

The light curves have been also extracted in two bands (S 15-40 and H 40-300 keV): these data have been used to compute time-resolved hardness ratio ($HR = (H - R)/(H + R)$). These hardness ratios have been used to investigate the spectral evolution of the burst and are reported here if not already published.

[1] The time during which the 90% of the total count are accumulated

A peak spectrum (integrated over 1 s) and an average spectrum have been extracted for each burst and fitted with the latest available response matrices. The low-energy different absorption at various off-axis angles due to the *nomex* mask support structure has been taken into account. The response matrix, on the other hand is the one for on-axis sources, so these results may still be affected by some systematic uncertainties. The spectra have been extracted in 64 logarithmically binned channels between 13 keV and 1 MeV and rebinned in order to have at least 20 counts per bin. All the peak fluxes and fluences are given, unless where indicated differently, in the 20-200 keV energy range.

3.2 GRB 021125

This is the first GRB detected by *INTEGRAL* still during PV phase. Despite its brightness, it was difficult to detect with the automatic software, due to a peculiar configuration of IBIS during that observation. In fact, due to calibration purposes, most of the telemetry of the instrument was allocated to PICsIT, which was operated in photon-by-photon mode. This implied that the information obtainable from ISGRI is very limited (see Fig. 3.1). Due to the poor quality of the data, IBAS was idle during this observation. On the other hand this is the

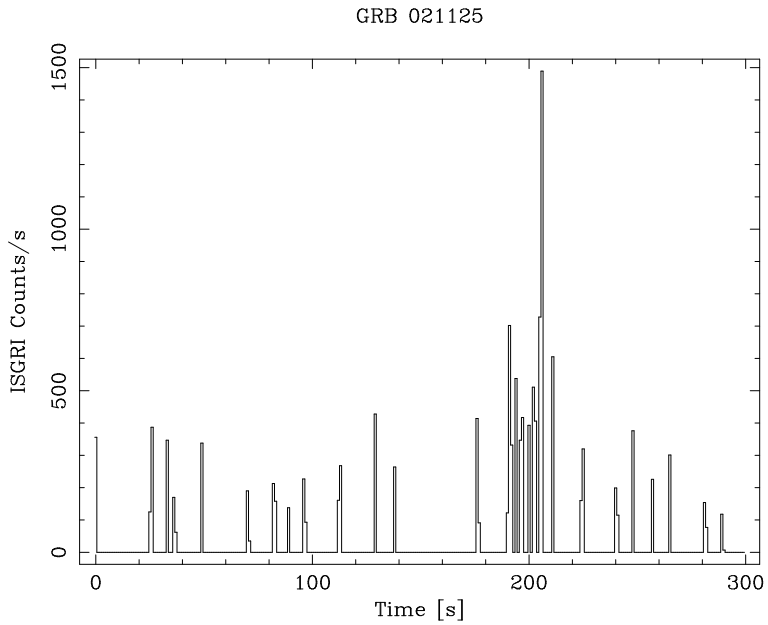

Figure 3.1: Raw light curve of GRB 021125. The data is binned over 1 s interval. The GRB corresponds to the data around 200 (the time scale is arbitrary). As can be seen there are gaps in the data of the order of tens of seconds.

only *INTEGRAL* GRB, for which broad band coverage is available, thanks to the

combined detection with ISGRI and PICsIT, see Malaguti et al. (2003).

Localization: R.A. = 19:47:57; Dec. = +28:23:35; Uncertainty = 1.2′

Time History: Due to the missing data the T_{90} cannot be computed. Its approximate duration is 25 s.

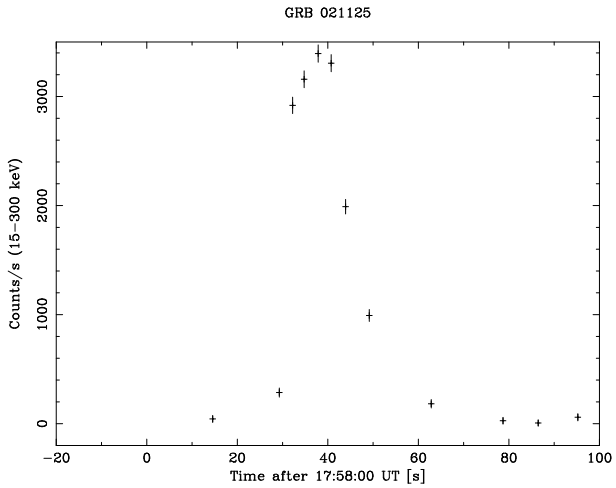

Figure 3.2: Time history of GRB 021125.

Spectrum: Only the total spectrum is shown. The fit with a single power law is unacceptable (χ^2/d.o.f.= 127.25/39). Using a Band (Band et al., 1993) model we get a better fit (χ^2/d.o.f. = 45.87/37). The derived parameters are $\alpha = 0.62^{+0.27}_{-0.17}$, $\beta = 2.2^{+0.14}_{-0.25}$ and $E_0 = 56^{+32}_{-20}$ keV. The peak flux and fluence are the ones derived for publication in Malaguti et al. (2003) in the whole IBIS range (20-500 keV): 2×10^{-6}erg cm^{-2} s^{-1} and 5.1×10^{-5}erg cm^{-2} , respectively.

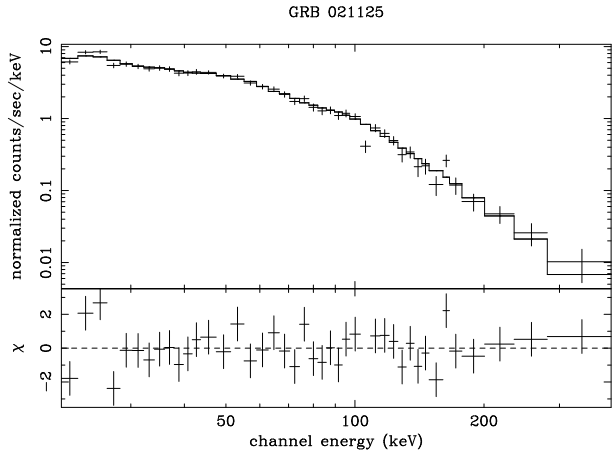

Figure 3.3: Average Spectrum of GRB 021125.

Spectral Evolution: Due to the poorness of the data no spectral evolution could be computed for this burst.

Afterglow: No search for afterglows has been performed for this burst.

3.3 GRB 021219

This GRB was detected by IBAS in near real time (with a delay of ∼10 s), but the Alert was issued only internally, because the system was still under testing. The public announcement was given 5 hours later after the verifications of the position derived automatically (the satellite was still in PV phase). This is the event that validated IBAS and allowed to start with the public distribution of the Alerts soon after. The preliminary results are published in Mereghetti et al. (2003b).

Localization: R.A. = 18:50:27; Dec. = +31:57:17; Uncertainty = 1.5′

Time History: T_{90} = 5.5 s, single peak.

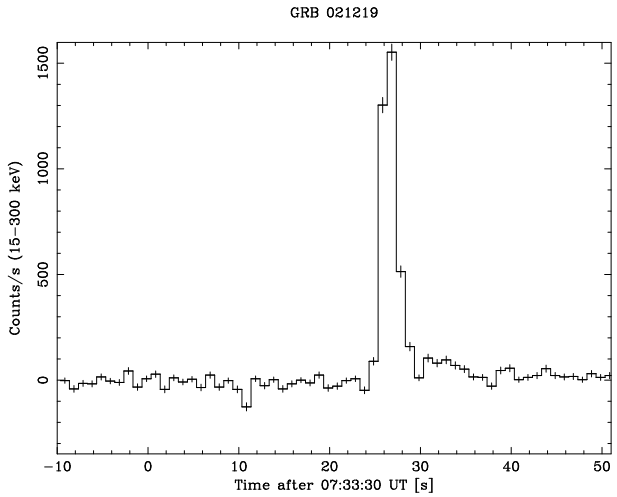

Figure 3.4: Time history of GRB 021219.

Spectrum: The fluence is 9.5×10^{-7} erg cm^{-2} . In this case a simple power-law model describes better the data than a Band model. The derived photon index is: Γ=1.67±0.15. The peak flux of this burst is 4 ph cm^{-2} s^{-1}(4.4×10^{-7}erg cm^{-2} s^{-1}).

Spectral Evolution: Clear hard to soft evolution is found.

Afterglow: No afterglow candidate found.

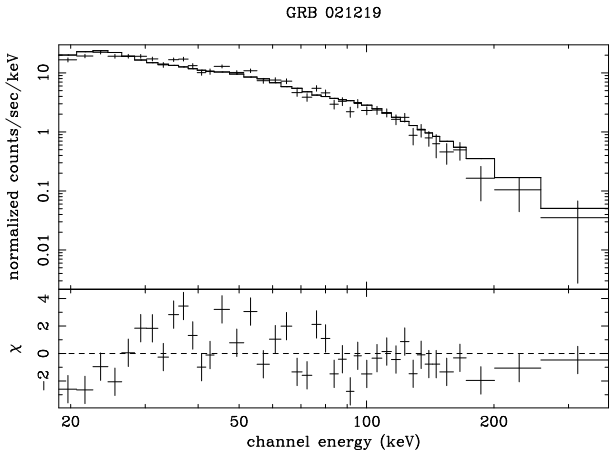

Figure 3.5: Average Spectrum of GRB 021125.

3.4 GRB 030131

This burst has been detected during a satellite slew. This made its analysis very difficult. Hence the results given below are the same that can be found in Götz et al. (2003e) (see Appendix A).

Localization: R.A. = 13:28:21; Dec. = +30:40:43; Uncertainty = 2.5′

Time History: T_{90} = 124 s. Structured light curve with several peaks.

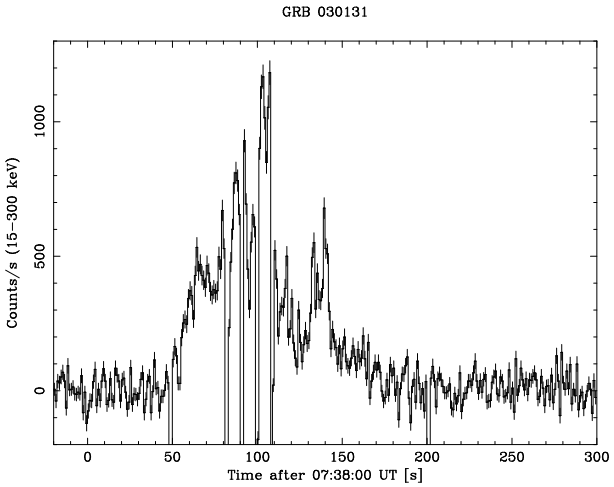

Figure 3.6: Time history of GRB 030131.

Spectrum: The peak flux is 1.9 ph cm^{-2} s^{-1}(1.7×10^{-7} erg cm^{-2} s^{-1}) and the fluence is 7×10^{-6} erg cm^{-2} . The Band spectral parameters derived for this burst are: α=1.4±0.2, β=3.0±1.0, E_0=70±20.

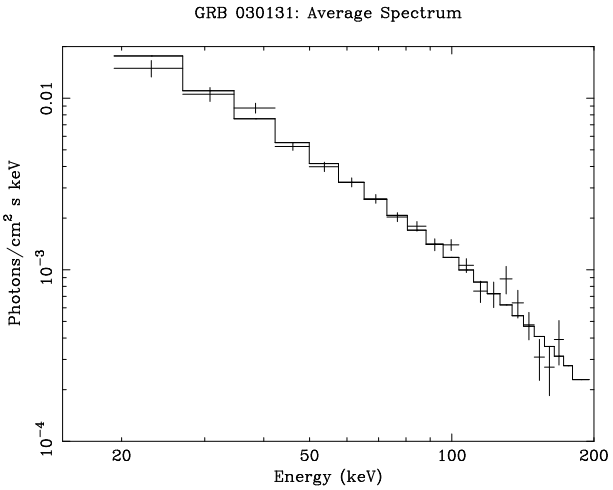

Figure 3.7: Average Spectrum of GRB 030131. From Götz et al. (2003e)

Spectral Evolution: A general hard-to-soft spectral evolution is associated to this GRB, but also a correlation between light curve peaks and spectral hardening (Hardness-Intensity correlation) can be noticed.

Afterglow: A faint ($R \sim 21.2$ mag after 3.62 hours) optical transient at R.A. = 13:28:22.29; Dec. = +30:40:23.7, has been reported.

3.5 GRB 030227

The analysis of the γ and X-ray data are presented in Mereghetti et al. (2003g). Using the same *XMM-Newton* data Watson et al. (2003) claim the detection of soft X-ray lines in the afterglow of this GRB, but this finding is still controversial (see e.g. Sako et al. (2004))

Localization: R.A. = 04:57:34; Dec. = +20:28:16; Uncertainty = $1.5'$

Time History: T_{90} = 33 s. FRED profile.

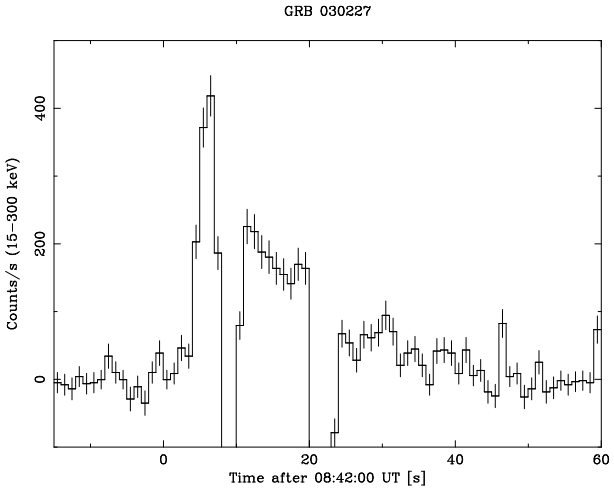

Figure 3.8: Time history of GRB 030227. The data gaps are due to satellite telemetry saturation.

Spectrum: The averages spectrum is well described by a power law with photon index $\Gamma = 1.72 \pm 0.09$. The fluence is 8.8×10^{-7}erg cm^{-2} . The peak flux is 1.2 ph cm^{-2} s^{-1}(1.1×10^{-7}erg cm^{-2} s^{-1}).

Spectral Evolution: Hard to soft evolution.

Afterglow: This is the first *INTEGRAL* GRB for which an X-ray counterpart has been found. The X-ray afterglow was detected only $\sim$8 hours after the burst with the *XMM-Newton* satellite. The 0.2-10 keV flux decreased with time as a power-law with index $\delta = 0.97 \pm 0.07$. The afterglow spectrum can be well fit with a photon index $\Gamma = 2.04 \pm 0.05$ with a hydrogen column density (N_H), larger than the Galactic value in that direction. An acceptable fit could be obtained by fixing the N_H to the Galactic value and adding a red-shifted absorber. Anyway this did not strongly constrain the redshift value. An upper limit to the redshift of $z \leq 3.5$ has been set by optical data (Castro-Tirado et al., 2003). Tentative evidence (3.2

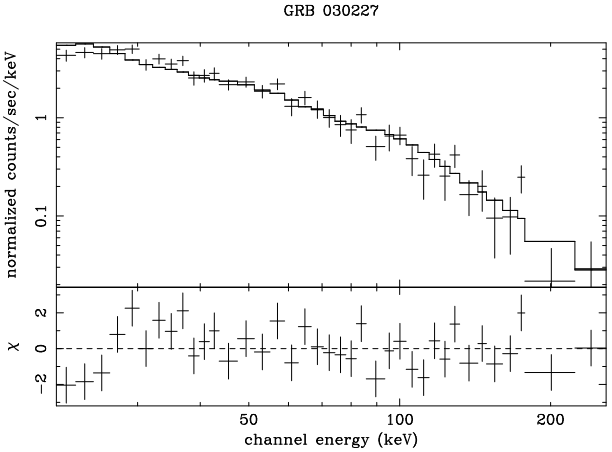

Figure 3.9: Average Spectrum of GRB 030227.

σ) for an emission line at 1.67 keV has been found. If this line is due to Fe, the implied redshift is $\sim$ 2.7-3 depending on the ionization state. Our analysis did not show evidence of thermal emission or any other emission lines. The optical afterglow is described in Castro-Tirado et al. (2003).

3.6 GRB 030320

This burst has been detected with a delay of a few hours, because it produced only low significance (*possible*) triggers. This is due to the fact that it was located close to the edge of IBIS FOV (see Fig. 2.14), where imaging is very difficult due to the coding noise. It is located close to the Galactic Center (∼3.8°). Its analysis is reported in von Kienlin et al. (2003a).

Localization: R.A. = 17:51:36; Dec. = –25:18:52; Uncertainty = 3′

Time History: T_{90} = 48 s. Several peaks.

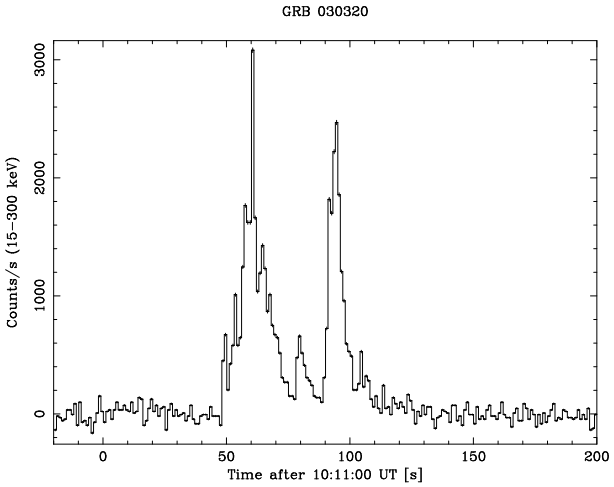

Figure 3.10: Time history of GRB 030320.

Spectrum: The spectral results are quite uncertain because this GRB was detected at very large off-axis angles. The best fit power-law model has a photon index $\Gamma = 1.5 \pm 0.15$. The fluence is 1.2×10^{-5} erg cm^{-2} and the peak flux 3.6 ph cm^{-2} s^{-1}(4×10^{-7} erg cm^{-2} s^{-1}).

Spectral Evolution: A general hard-to-soft spectral evolution is observed, although the second peak (yet being softer compared to the first one) seems not to evolve spectrally.

Afterglow: The optical follow-up, performed by our group at ESO-NTT, did not reveal any afterglow candidate within the IBAS error circle, but the extinction is A_V=10.5±0.5 mag.

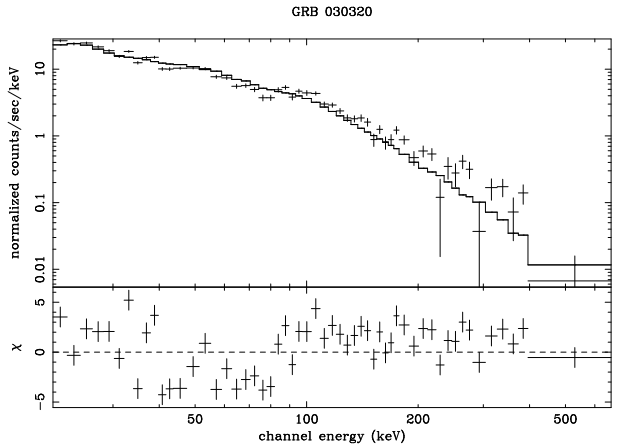

Figure 3.11: Average Spectrum of GRB 030320.

3.7 GRB 030501

This GRB has been localized very quickly and the first optical observations (Boer & Klotz, 2003) started already when the burst was still active, see Fig. 3.12. The

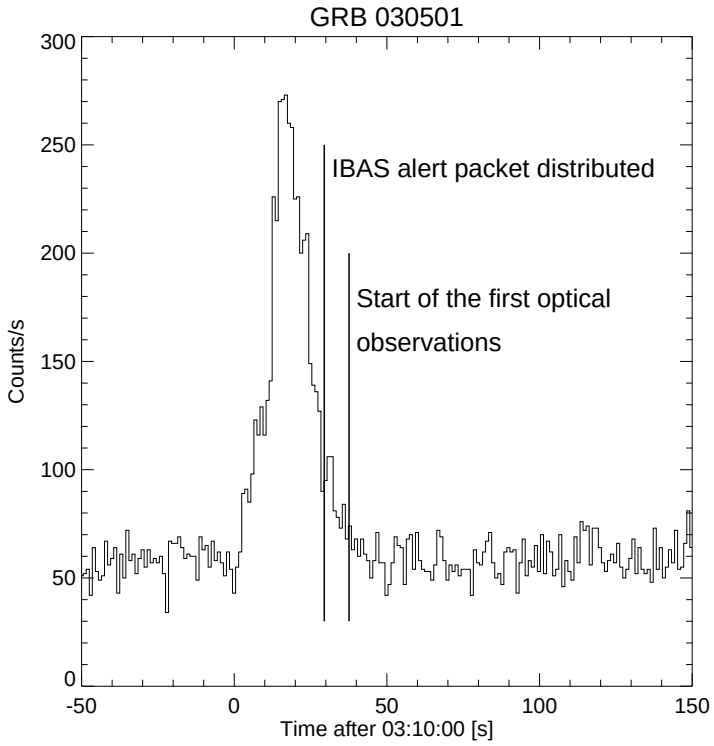

Figure 3.12: Time history of GRB 030501. The delivery of the IBAS Alert Packet (596) and the beginning of the first optical observations are indicated.

analysis based on IBIS, SPI and RHESSI (Ramaty High Energy Solar Spectro-

scopic Imager; Lin et al. (2002)) data is presented in Beckmann et al. (2003).
Localization: R.A. = 19:05:33; Dec. = +06:15:57; Uncertainty = 1.8′

Time History: T_{90} = 24 s. Single peak.

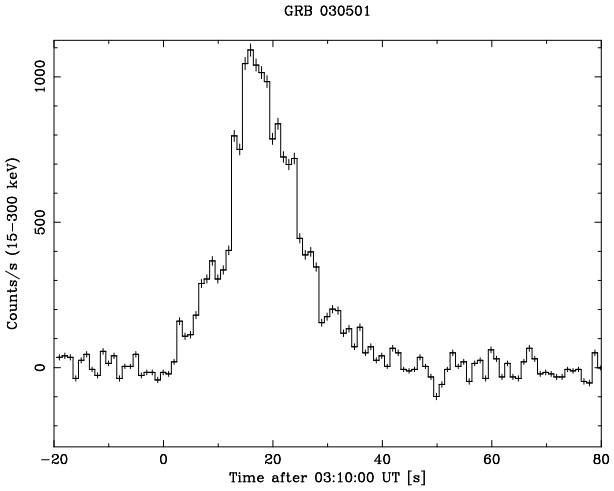

Figure 3.13: Time history of GRB 030501.

Spectrum: Again the large off-axis angle of this burst, makes its spectral analysis difficult. The average spectrum, fitted with a power-law model, yields a photon index $\Gamma = 1.87 \pm 0.15$. The fluence is 3.7×10^{-6} erg cm^{-2} and the peak flux 2.7 ph cm^{-2} s^{-1}(2.3×10^{-7} erg cm^{-2} s^{-1}).

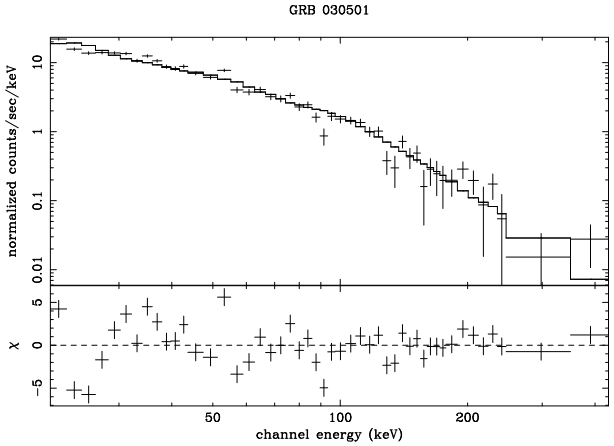

Figure 3.14: Average Spectrum of GRB 030501.

Spectral Evolution: IBIS and SPI data indicate a spectral softening after the peak, while before it they show different results: IBIS indicates a Hardness-

Intensity correlation while SPI a simple hard-to-soft evolution.

Afterglow: Optical follow-up observations were performed, but no optical counterpart has been found.

3.8 GRB 030529

GRB 030529 has been detected during an *off-line* reprocessing of the first 165 orbits of *INTEGRAL* data. This has been done in order to scan also the older data with the most recent and more sensitive versions of the programs. Looking at the raw light curve of GRB 030529 (see Fig. 3.15), it is no surprise that it has not been detected by the early versions of the programs since it is close to very large background variations.

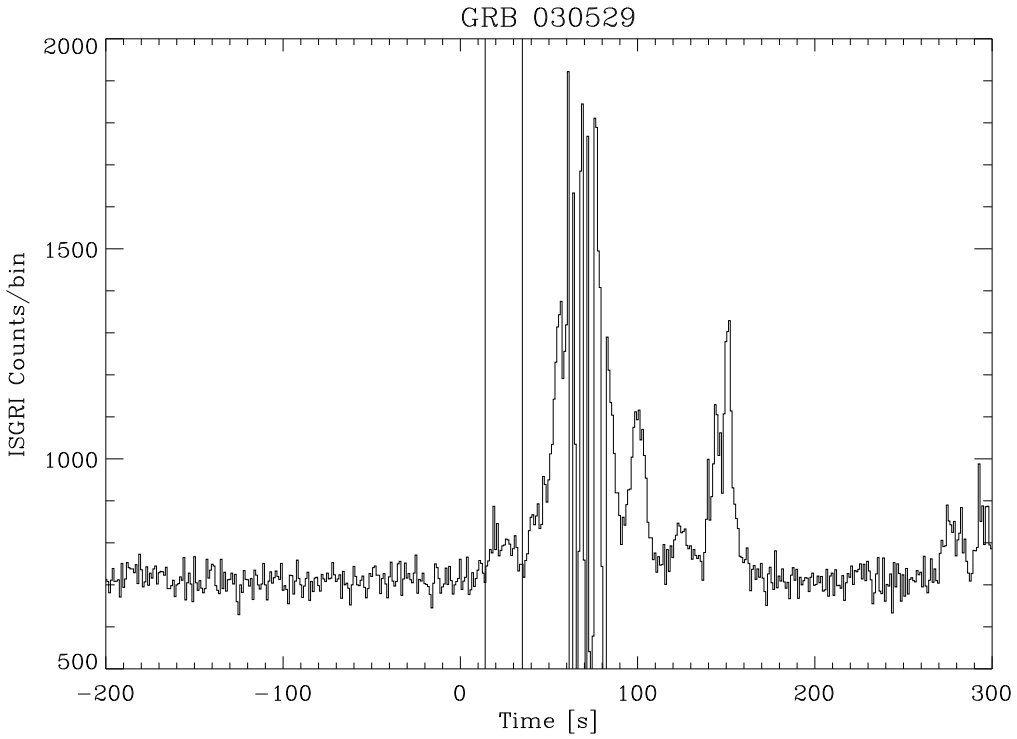

Figure 3.15: Raw light curve of GRB 030529. The duration of the GRB is indicated by two vertical lines. The other variations seen in the light curve are due to particle induced background. Time=0 corresponds to 19:53:00 UT.

Localization: R.A. = 09:40:29.31; Dec. = –56:20:31; Uncertainty = 3′

Time History: T_{90} = 20 s. The burst starts around 19:53:15 UTC and lasts for about 25 s.

Spectrum: The peak flux of this burst, computed over 1 s integration time, is about 0.4 ph cm^{-2} s^{-1} (3×10^{-8} erg cm^{-2} s^{-1}). The average spectrum of the GRB, extracted over the 20-400 keV energy range, is shown in Fig. 3.17. It is well described (χ^2/dof =30.18/31) by a power law model with photon index

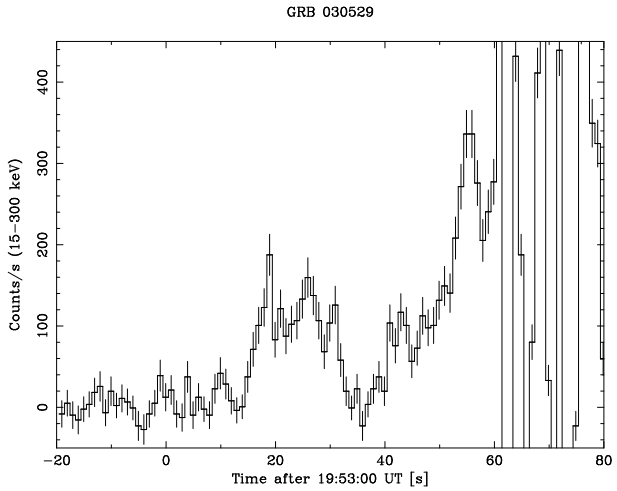

Figure 3.16: Time History of GRB 030539.

Γ=1.71±0.20. The fluence of this weak GRB is 4×10^{-7} erg cm^{-2} .

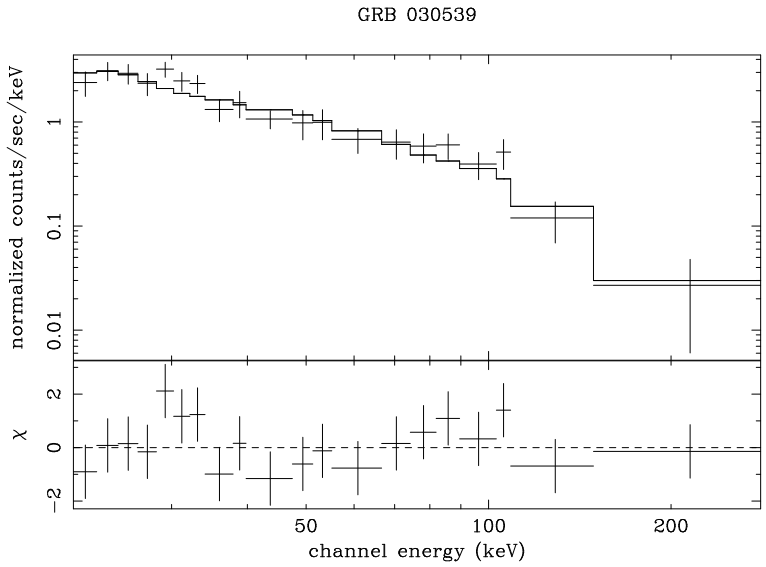

Figure 3.17: Average spectrum of GRB 030529.

Spectral Evolution: As can be seen from Fig. 3.18 no significant spectral evolution is detected in IBIS/ISGRI data.

Afterglow: Search not carried out due to the late discovery of the event.

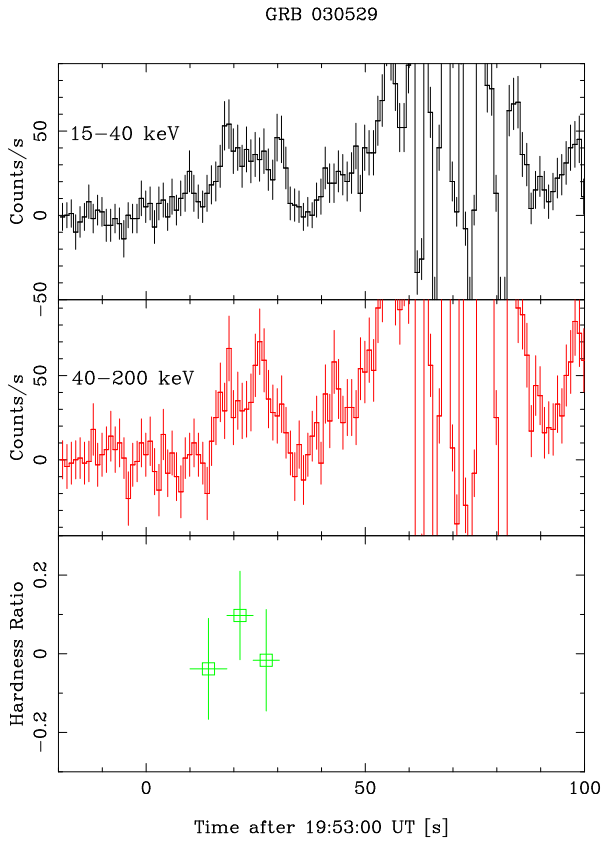

Figure 3.18: Top Panel: background subtracted light curve of GRB 030529 in the 15-40 keV band. Middle Panel: same as above, but in the 40-200 keV band. Lower Panel: Hardness Ratio: the bins have been chosen in order to have at least 225 counts in the total $(H + S)$ band. Note that the bursts lasts only until T $\simeq$ 45 s.

3.9 GRB 031203

GRB 031203 was quickly localized with IBAS within just 18 s from the GRB start (Götz et al., 2003b). The rapid response of *XMM-Newton* made it possible to detect the X-ray afterglow just ∼6 hours after the GRB (Watson et al., 2004).

The γ-ray and X-ray data, already published by other authors, have been re-analyzed and are presented here.
Localization: R.A. = 08:02:32; Dec. = –39:50:47; Uncertainty = 1.5′.

Time History: T_{90} = 39 s. FRED profile.

Spectrum: The average spectrum is well fitted by a single power law with photon index $\Gamma = 1.71 \pm 0.07$. The fluence is 1.5×10^{-6}erg cm^{-2} . The peak flux is

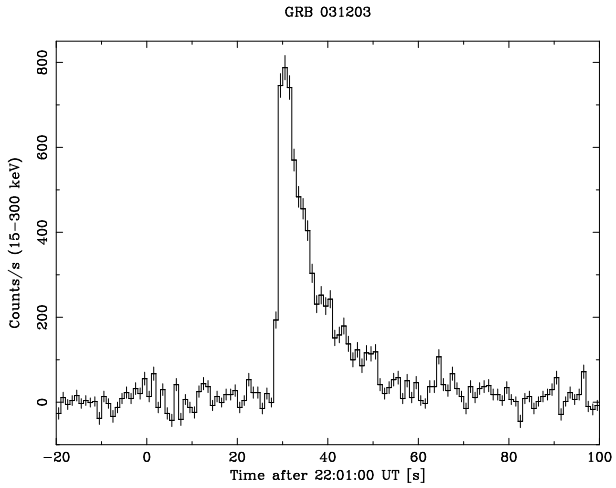

Figure 3.19: Time History of GRB 031203.

1.7 ph cm^{-2} s^{-1}(1.6×10^{-7} erg cm^{-2} s^{-1}).

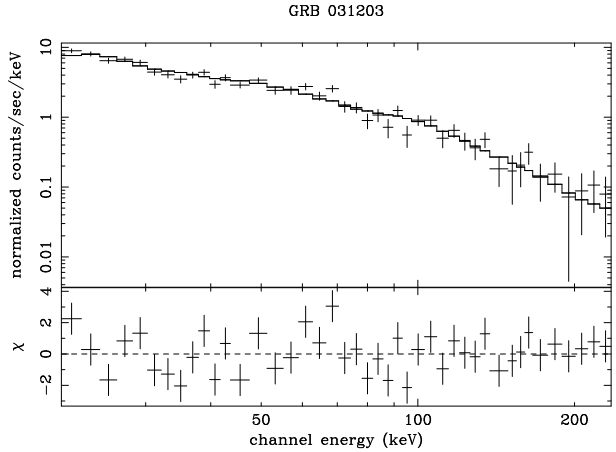

Figure 3.20: Average Spectrum of GRB 031203.

Spectral Evolution: No significant spectral evolution is found, in agreement with the results of Sazonov et al. (2004)

Afterglow: During the *XMM-Newton* observation of the afterglow an expanding X-ray halo, due to dust scattering, was discovered (Vaughan et al., 2004). A radio counterpart to this GRB was found with the VLA (Soderberg et al., 2004). At optical wavelengths no obvious afterglow was found, but both the radio and X-ray positions are consistent with galaxy at redshift z=0.105, making this the closest GRB ever detected. With an energy in γ-rays of $\sim 10^{50}$ erg s^{-1}, Sazonov et al. (2004) conclude that this burst is sub-energetic by a factor 10^2, with respect to classical GRBs (Frail et al., 2001).

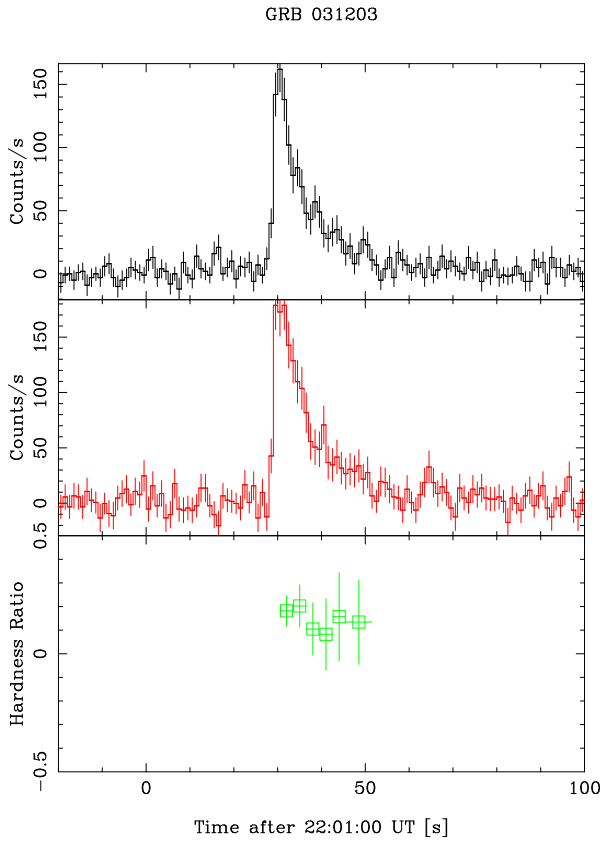

Figure 3.21: Top Panel: background subtracted light curve of GRB 031203 in the 15-40 keV band. Second Panel: same as above, but in the 40-200 keV band. Third Panel: Hardness Ratio: the bins have been chosen in order to have at least 150 counts in the total $(H + S)$ band. Lower Panel: power law photon index obtained from spectral analysis of the three time intervals.

Our results on optical and NIR monitoring of the source (Malesani et al., 2004), indicate that this source is clearly associated with a Supernova explosion, SN2003lw. In fact the light curve and the spectra can be identified (like for SN1998bw) with a peculiar SN of type Ic. In addition looking at the spectral energy distribution from NIR data to X-rays, a discontinuity is apparent, indicating a different origin for the emission in the two bands. The X-ray component has a much harder spectrum than the NIR one.

The X-ray Halo

From the flux measured from the X-ray expanding halo, one can derive the the prompt emission of the GRB in X-rays. This has been done by Watson et al. (2004), who claim that the measured flux is higher than what expected from the

extrapolation of γ-ray data in case of a normal GRB (see Fig. 3.22). So they conclude that GRB 031203 is an X-ray flash. Sazonov et al. (2004) report that the γ-ray fluence of the GRB is $(2.0\pm0.4)\times10^{-6}$ erg cm^{-2} , the duration is about 25 s and the average spectrum has a photon index Γ=1.63±0.06, in agreement with the results derived above.

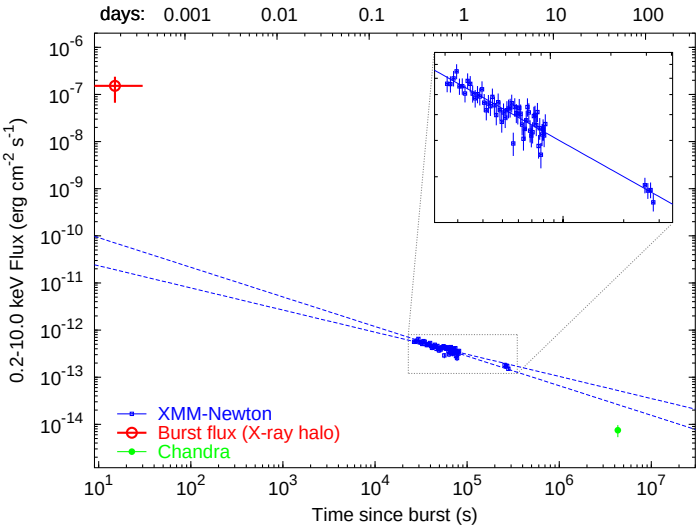

Figure 3.22: X-ray afterglow and halo fluxes (Watson et al., 2004).

We have re-analyzed the *XMM-Newton* data of the X-ray expanding halo. In particular we have used EPIC-PN (Strüder et al., 2001) data. If we define the following quantities:

D = distance Earth - GRB (about 430 Mpc if z=0.105)

d_s = xD =distance Earth-scattering dust

Θ = angular radius of the halo (i.e. from the central source as seen by the observer)

Φ = scattering angle (i.e. angular deviation of the scattered photons)

(1-x)Φ = Θ (see Fig. 3.23)

δ = time delay of the scattered photons

$$\delta = \frac{D}{2c}\frac{x\Theta^2}{1-x} \tag{3.1}$$

in our case x∼0, therefore $\delta=\frac{d_s}{2c}\Theta^2$ and $\Theta=\Phi$.

We derived the ring angular size,Θ, as a function of time since the GRB, obtaining the values reported in table 3.1. The angular velocity of the ring expansion is clearly not constant, but it follows, as expected, the relation $\Theta \propto \delta^{0.5}$. Fitting these data with Eq. 3.1 we can derive the distance of the dust slab, d_s=1.2 kpc. The time evolution of the ring radius is consistent with being the scattered photons emitted at the time of the GRB (actually two rings are seen indicating

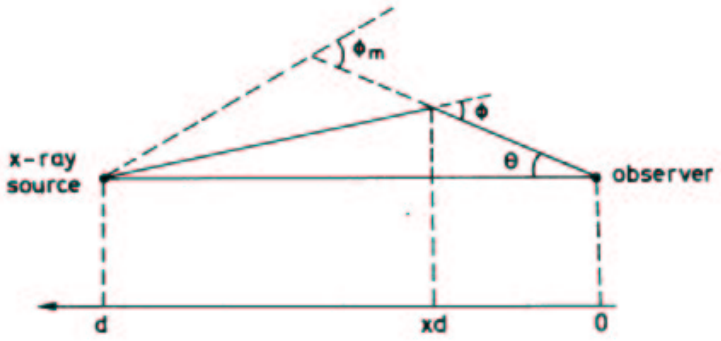

Figure 3.23: Geometrical model of the scattering halo (Trümper & Schönfelder, 1973).

δ [ks]	24	31	43.5	66.25
Θ [arcmin]	2.2	2.5	3	3.4

Table 3.1: Angular size of the halo as a function of time.

that there are two dust slabs at different distances, we will consider here only the brightest one). Therefore, from the scattered flux in the ring we can measure the intensity of the prompt X-ray emission (at a few keV). The problem is to compute the factor f relating these two quantities: $F_{ring} = f \times F_{GRB}$.

We work in term of fluences. If we had an observation starting at the burst time and long enough to see all the scattered halo evolution, we would measure the total fluence (point source+scattered) by counting the photons in a large circular region and integrating on the whole observation. In practice we see only a fraction of the scattered photons, but we can correct for the lost fraction using theoretical halo profiles and assuming a dust grain model (in our case, following Draine (2003), carbonaceous and silicate grains)

$$F_h(< \Theta) = F_{GRB} \tau g(\Theta) \tag{3.2}$$

where

$F_h(< \Theta)$ is the total flux within an angle Θ (the angle must be small enough that the ring has completely passed through it. This is equivalent to say that for the chosen Θ the integration time is long enough to collect all the scattered photons)

$g(\Theta)$ is the fraction of halo photons scattered within Θ, see Fig. 3.24

τ is the scattering optical depth = (0.05-0.1)A_V(mag) E (keV)$^{-2}$. In our case A_V is about 2 mag (Neckel et al., 1980), so we assume $\tau \sim 0.15$ at 1 keV.

Again the measured values are time averaged on the integration time T. Actually the emission is shorter and we must correct by the factor $\Delta t/T$, where Δt

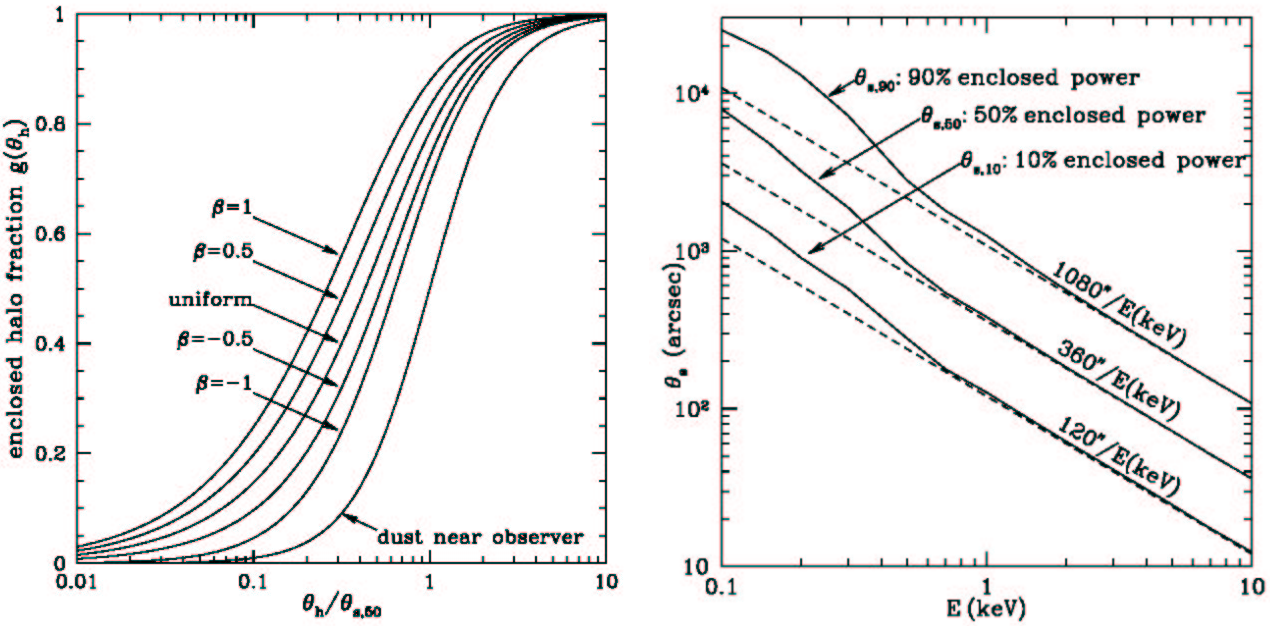

Figure 3.24: Right: Median scattering angle $\theta_{s,50}$ as a function of energy for the assumed grain model. Also shown are scattering angles $\theta_{s,10}$ and $\theta_{s,90}$ for 10% and 90% enclosed power. Dashed lines show asymptotic behavior for E $\geq$ 1 keV. Left: Fraction of the single-scattering halo falling within halo angle θ_h as a function of $\theta/\theta_{s,50}$. (Draine, 2003)

is the GRB duration. Hence the GRB flux is given by

$$F_{GRB} = (T/\Delta t)\overline{F_{ring}(\Theta_1 < \Theta < \Theta_2)}\,\tau^{-1}\,\frac{1}{g(\Theta_1) - g(\Theta_2)} \tag{3.3}$$

For a ring of width $\Theta_1 - \Theta_2$=1′, we have $g(\Theta_1) - g(\Theta_2) \sim$0.1. Therefore

$$\begin{aligned} F_{GRB} &= (40,000/25) \cdot (\overline{F_{ring13}} \times 10^{-13}\ \mathrm{erg\ cm^{-2}s^{-1}})\ 0.15^{-1} \cdot 10 \\ &= \overline{F_{ring13}} \cdot 1.1 \times 10^{-8}\ \mathrm{erg\ cm^{-2}s^{-1}} \end{aligned} \tag{3.4}$$

The spectrum of the ring is very soft: in fact the ring is seen only between 1 and 2 keV. So we extrapolate the 1-2 keV flux to the 2-10 keV range. The measured X-ray flux value, $\overline{F_{ring13}}$, is 2.5, and hence $F_{GRB} = 2.75{\times}10^{-8}$ erg cm^{-2} s^{-1} . This value for the prompt emission in the X-rays is compatible with the value extrapolated back from γ-rays using *INTEGRAL* data, namely $2{\pm}0.4{\times}10^{-8}$ erg cm^{-2} s^{-1} . We can hence confirm that 031203 is a classical, though sub-energetic, GRB and not an X-Ray Flash.

3.10 GRB 040106

Our analysis of GRB 040106 is presented in Moran et al. (2004). For this GRB SPI and IBIS data were available, and for its afterglow in the X-rays *XMM-Newton* data were used, which have been collected just ∼5 hours after the GRB.

Localization: R.A. = 11:52:18; Dec. = –46:47:15; Uncertainty = 2.5′

Time History: T_{90} = 47 s. The GRB has a duration of about 52 s and is composed of two distinct peaks.

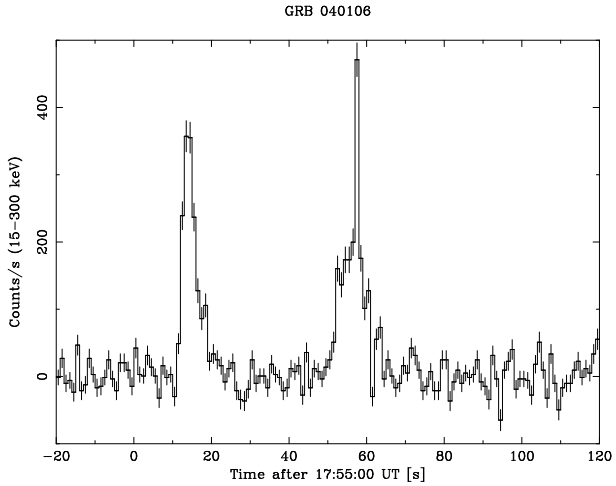

Figure 3.25: Time History of GRB 040106.

Spectrum: The overall spectrum is well described by a power law model with photon index $\Gamma = 1.72 \pm 0.15$. The fluence is 8.3×10^{-7} erg cm^{-2} and the peak flux (second peak) is 1 ph cm^{-2} s^{-1}(1×10^{-7} erg cm^{-2} s^{-1}).

Spectral Evolution: The second peak is harder than the first one, see Fig. 3.27. This evolution is seen from the hardness ratio and is confirmed also by the spectral indexes of the spectra extracted from the first peak (1.69 ± 0.12) and from the second peak (1.41 ± 0.1), and also from the ones extracted on the rise and and fall of the first (1.7 ± 0.2; 1.85 ± 0.2) and of the second peak (1.45 ± 0.2;1.1 ± 0.2).

Afterglow: The X-ray afterglow spectrum is uniquely hard with a photon index of 1.49 ± 0.03, a power law temporal decay of slope 1.46 ± 0.04 and a 2-10 keV flux of 1.1×10^{-12} erg cm^{-2} s^{-1} at 11 hours after the burst.

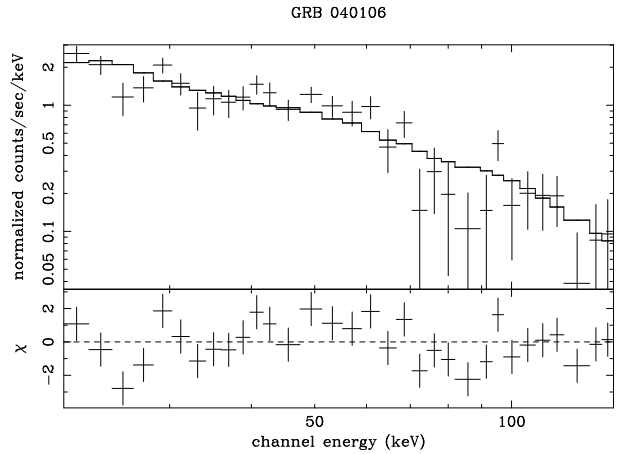

Figure 3.26: Average Spectrum of GRB 040106.

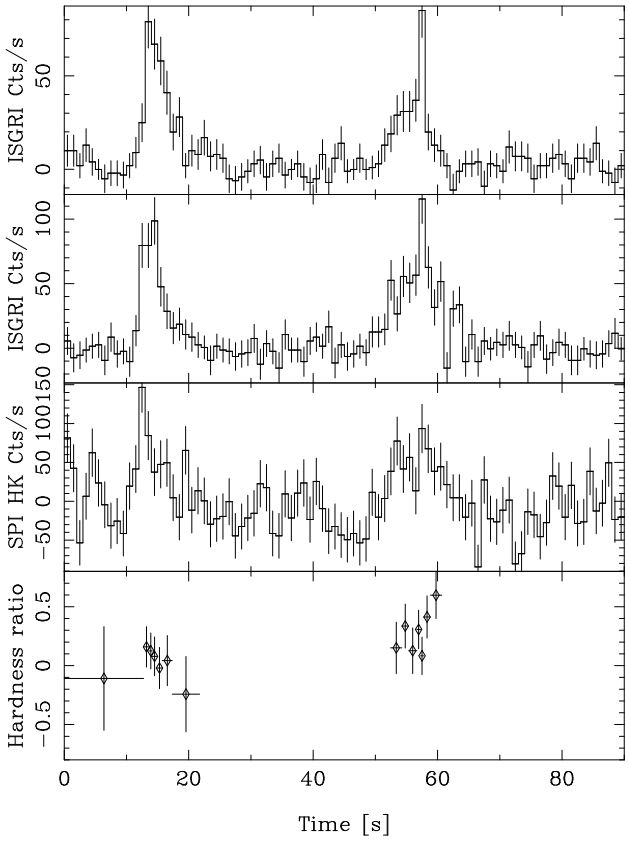

Figure 3.27: Top Panel: background subtracted light curve of GRB 040106 in the 15-40 keV band. Second Panel: same as above, but in the 40-200 keV band. Third Panel: SPI Housekeeping data. Lower Panel: Hardness Ratio.

3.11 GRB 040223

Localization: R.A. = 16:39:31; Dec. = –41:55:47; Uncertainty = 2.2′

Time History: T_{90} = 258 s. Multi-peaked structure. This is the longest GRB seen by *INTEGRAL* .

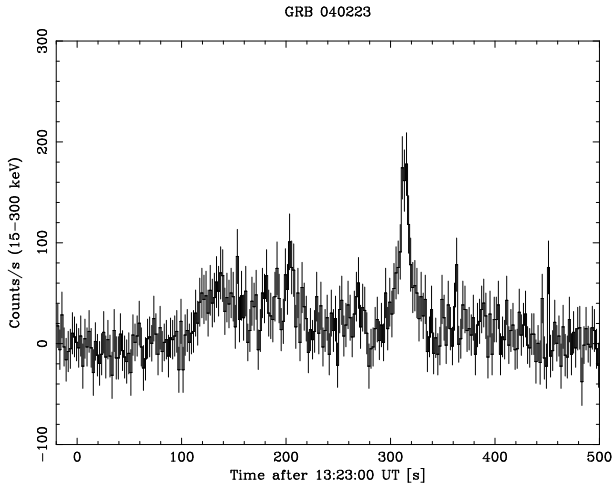

Figure 3.28: Time History of GRB 040223.

Spectrum: The average spectrum, modeled as a power law, yields a photon index of $\Gamma = 2.0 \pm 0.17$. The steep power law spectrum indicates that this is most likely an X-ray rich GRB. In fact $S_{7-30KeV}/S_{30-400KeV} \sim 0.5$, while for classical GRBs this value is smaller than 1/3. The fluence is 2×10^{-6} erg cm^{-2} . The peak flux is 0.4 ph cm^{-2} s^{-1}(4×10^{-8} erg cm^{-2} s^{-1}).

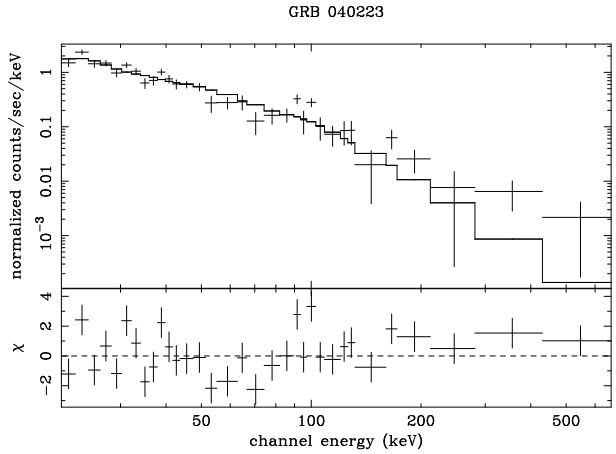

Figure 3.29: Average Spectrum of GRB 040223.

Spectral Evolution: The spectral evolution is rather complicated, see Fig. 3.30. For the last peak a hardness-intensity correlation is seen, while no particular trend can be identified in the first part.

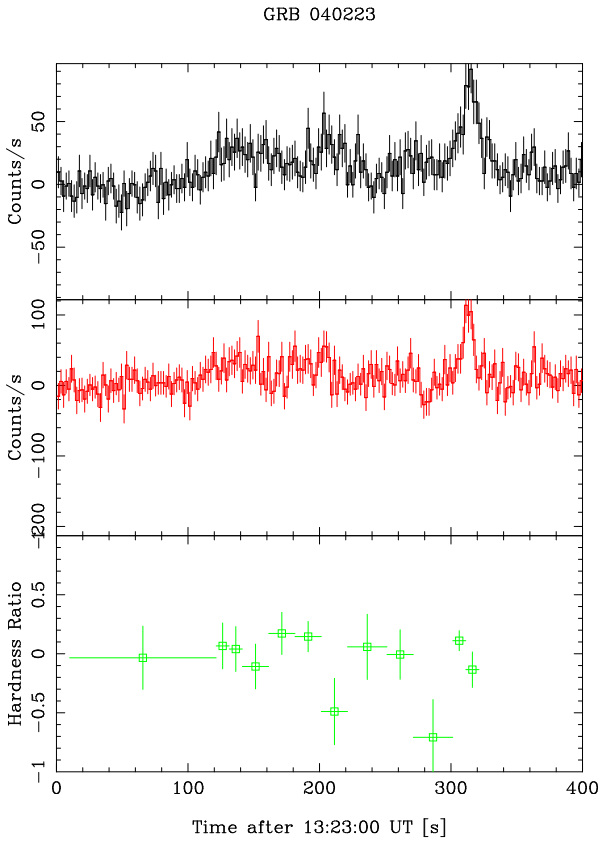

Figure 3.30: Top Panel: background subtracted light curve of GRB 040223 in the 15-40 keV band. Middle Panel: same as above, but in the 40-300 keV band. Lower Panel: Hardness Ratio: the bins have been chosen in order to have at least 250 counts in the total $(H + S)$ band.

Afterglow: *XMM-Newton* started an observation at 18:21 UTC, less than 5 hours after the GRB, being the fastest *XMM-Newton* ToO response to date. Quick look analysis of the first 7 ksec of the observation of the GRB 040223 field showed the presence of a bright source in the EPIC-PN (Strüder et al., 2001) and MOS (Turner et al., 2001) at a position of R.A. = 16:39:29.9, Dec. = -41:56:01.4, with a positional accuracy better than 6 arcsec (Breitfellner et al., 2004), well inside the IBAS error box.

The *XMM-Newton* observation lasted about 42 ks. All three EPIC cameras were operated in Full Frame Mode. For the MOS1 camera the medium optical blocking filter was used, while for the MOS2 and PN camera the thin filter has been chosen.

The afterglow time decay, as measured by all three EPIC instruments (see Fig. 3.31), is well fit by a power law with photon index δ=0.82±0.10

Afterglow spectra from the PN and MOS cameras were obtained after stan-

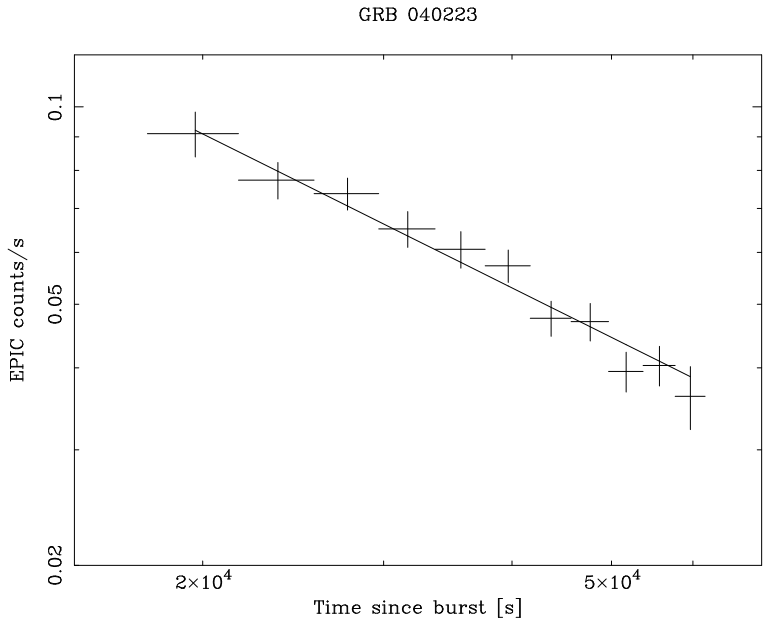

Figure 3.31: EPIC light curve of the afterglow of GRB 040223.

dard data screening. Due to the high background level this resulted in only about 13 ks for the PN and 27 ks for the MOS. The data (see Fig. 3.32) are well described ($\chi^2/dof = 64.48/68$) by an absorbed power law with photon index Γ=2.91±0.22. The hydrogen column density N_H=(1.9±0.3)×10^{22} cm^{-2} is in excess by a factor $\sim$ 3 with respect to the Galactic value in this direction (Dickey & Lockman, 1990). Fixing the absorption value to the Galactic one and adding a redshifted absorber, it turns out that the redshift value is not well constrained due to the poor quality of the data. Assuming a redshift z=1 (roughly the average value for all the GRBs), the local N_H value is (6.7±1.3)×10^{22} cm^{-2}, significantly larger than found in previous studies (De Pasquale et al., 2003). The 2-10 keV average flux is 2.1×10^{-13} erg cm^{-2} s^{-1} (not corrected for absorption).

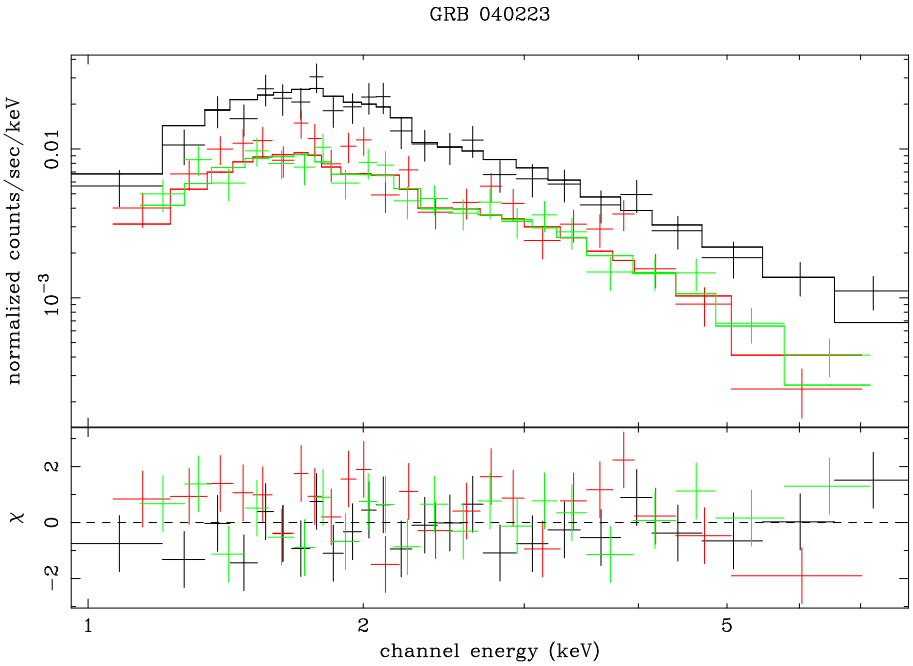

Figure 3.32: Spectrum of the afterglow of GRB 040223 and its best-fit with an absorbed power law model. The upper data points refer to the PN, while the lower ones to MOS1 and MOS2. The residuals are in units of standard deviations.

3.12 GRB 040323

Localization: R.A. = 13:53:49; Dec. = –52:20:45; Uncertainty = 1.7′

Time History: T_{90} = 14 s. Single peak.

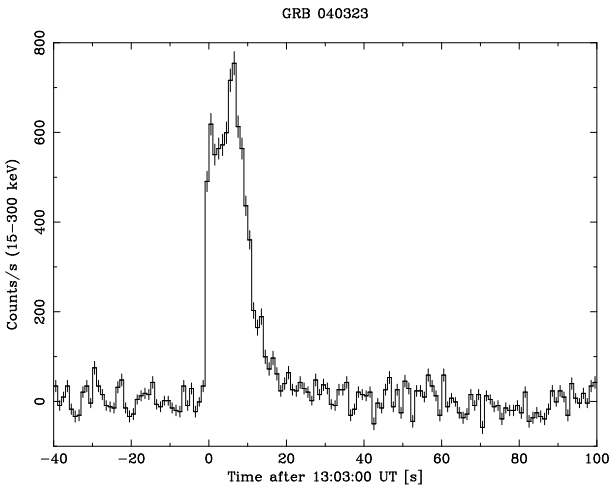

Figure 3.33: Time History of GRB 040323.

Spectrum: The spectrum is better described by a Band model (χ^2/d.o.f =95.46/45) than by a power law (127.35/47). The derived parameters are $\alpha = 0.64 \pm 0.10$, $E_0 = 159 \pm 35$ keV. β poorly constrained with values larger than 3 at a 2 σ level. The fluence is 2×10^{-6} erg cm^{-2} . The peak flux is 1.6 ph cm^{-2} s^{-1}(2×10^{-7} erg cm^{-2} s^{-1}).

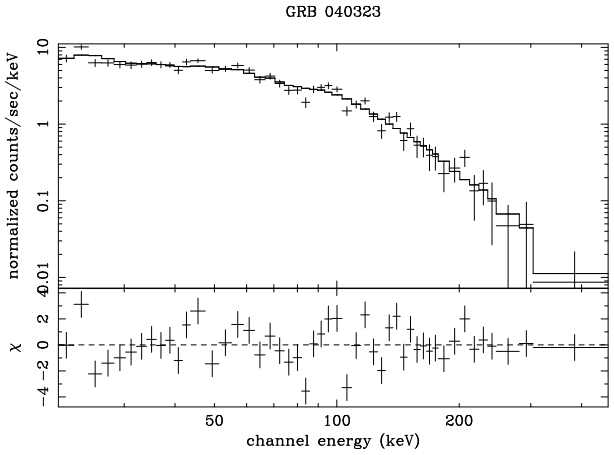

Figure 3.34: Average Spectrum of GRB 040323. Binsize = 2 s.

Spectral Evolution: A clear hard to soft evolution is seen, see Fig. 3.35.

Afterglow: A possible NIR counterpart for this GRB has been reported by Gal-Yam et al. (2004).

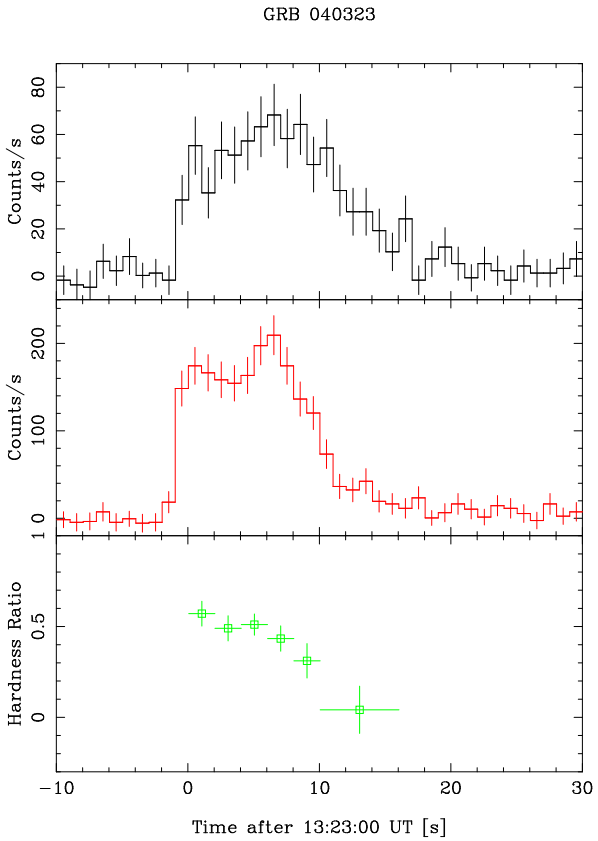

Figure 3.35: Top Panel: background subtracted light curve of GRB 040323 in the 15-40 keV band. Middle Panel: same as above, but in the 40-300 keV band. Lower Panel: Hardness Ratio: the bins have been chosen in order to have at least 250 counts in the total $(H + S)$ band.

3.13 GRB 040403

Localization: R.A. = 07:40:54 ; Dec. = +68:12:55; Uncertainty = $2'$

Time History: T_{90} = 19 s. Single peak.

Spectrum: The average spectrum is well fitted by an single power law with photon index $\Gamma = 1.90 \pm 0.15$, making this GRB X-ray rich. The fluence is 5×10^{-7} erg cm^{-2} . The peak flux is 0.5 ph cm^{-2} s^{-1}(5×10^{-8} erg cm^{-2} s^{-1}).

Spectral Evolution: Hard to soft evolution.

Afterglow: Our optical limit of R>24.2, taken at the Nordic Optical Telescope (NOT) 16.5 hours after the burst, indicates a rather faint afterglow, similar to those seen in the other relatively faint and soft bursts.

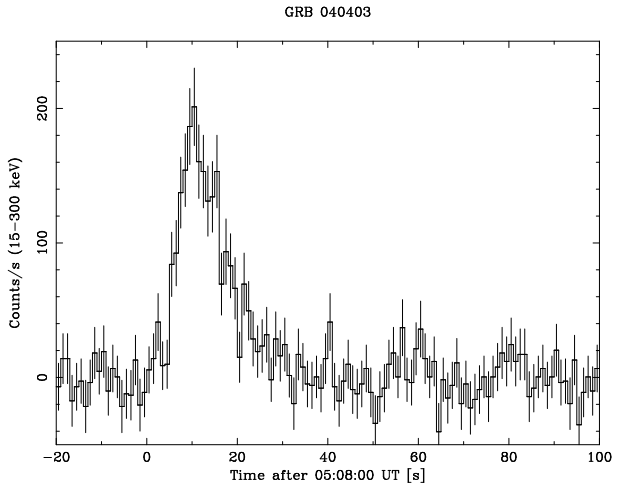

Figure 3.36: Time History of GRB 040403.

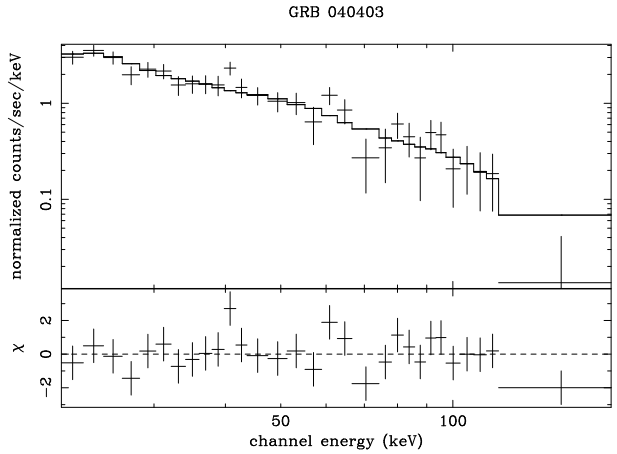

Figure 3.37: Average Spectrum of GRB 040403.

3.14 GRB 040422

Localization: R.A. = 18:42:01; Dec. = +01:59:04; Uncertainty = 1.3′

Time History: T_{90} = 10 s. Double peaked profile.

Spectrum: The average spectrum can be described by a power law model with photon index $\Gamma = 2.07 \pm 0.1$. This makes this burst X-ray rich. The fluence is 8×10^{-7} erg cm^{-2} . The peak flux is 3.5 ph cm^{-2} s^{-1}(2.8×10^{-7} erg cm^{-2} s^{-1}).

Spectral Evolution: The first peak is harder than the second one.

Afterglow: The optical observations performed yielded no afterglow candidate.

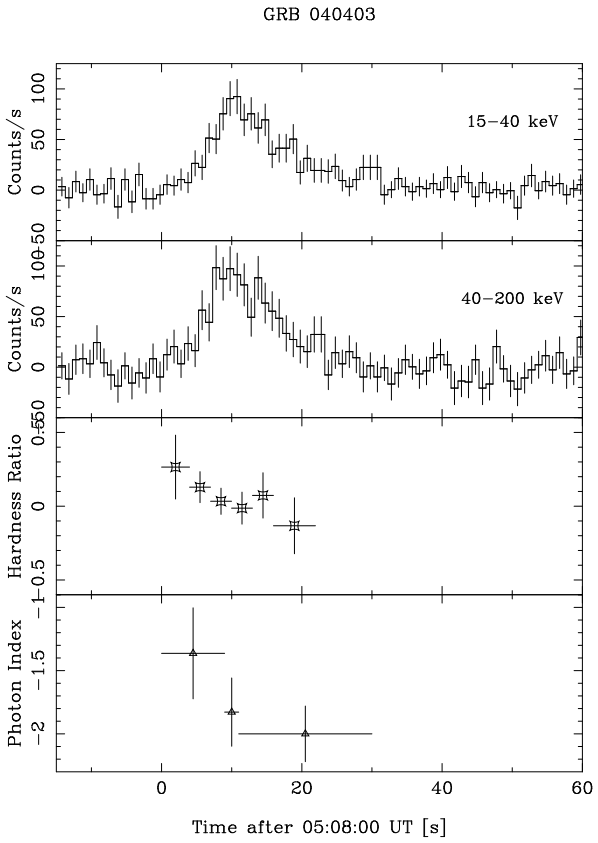

Figure 3.38: Top Panel: background subtracted light curve of GRB 040403 in the 15-40 keV band. Second Panel: same as above, but in the 40-200 keV band. Third Panel: Hardness Ratio: the bins have been chosen in order to have at least 200 counts in the total $(H + S)$ band. Lower Panel: power law photon index obtained from time resolved spectral analysis.

3.15 GRB 040624

This GRB has not been localized in real time, but with a 6 hrs delay due to telemetry problems.
Localization: R.A. = 13:00:08; Dec. = –03:34:08; Uncertainty = $3'$

Time History: T_{90} = 35 s. FRED profile.

Spectrum: The average spectrum can be modeled as a power law with photon index $\Gamma = 2.16 \pm 0.13$, which classifies this GRB as X-ray rich. The fluence is 8×10^{-7} erg cm^{-2} , while the peak flux is 0.5 ph cm^{-2} s^{-1}(3.5×10^{-8} erg cm^{-2} s^{-1}).

Spectral Evolution: The burst has too few counts to achieve statistical signif-

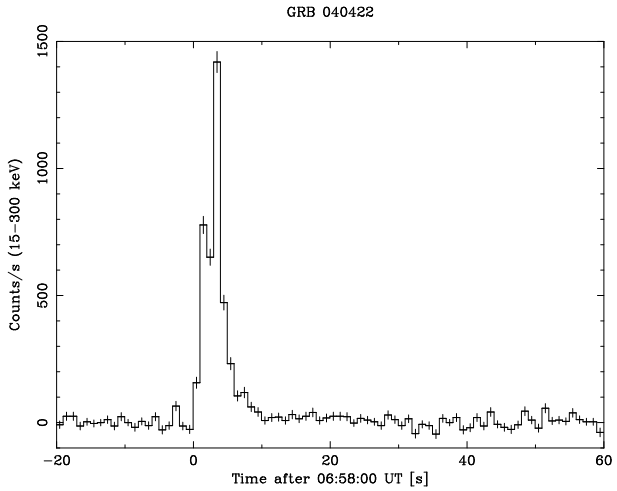

Figure 3.39: Time History of GRB 040422.

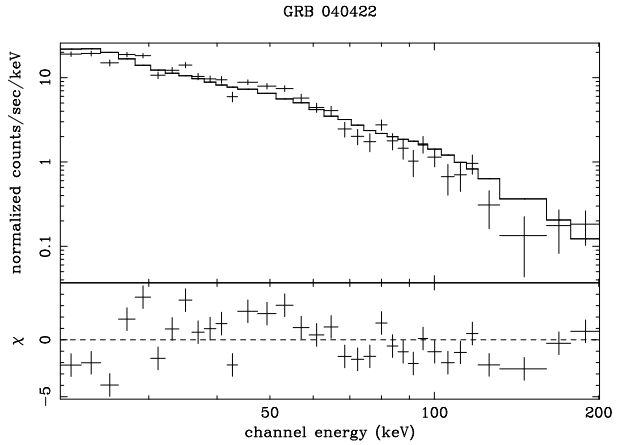

Figure 3.40: Average Spectrum of GRB 040422.

icant Hardness Ratio bins.

Afterglow: The afterglow searches have been unsuccessful, also because of the late discovery of this GRB.

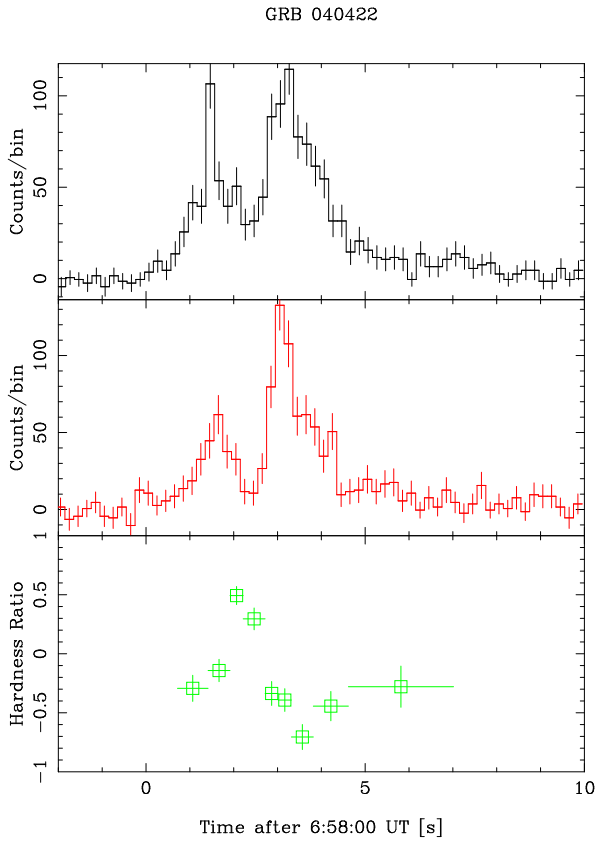

Figure 3.41: Top Panel: background subtracted light curve of GRB 040422 in the 15-40 keV band. Time bin = 0.2 s. Middle Panel: same as above, but in the 40-200 keV band. Bottom Panel Hardness Ratio: the bins have been chosen in order to have at least 200 counts in the total $(H + S)$ band.

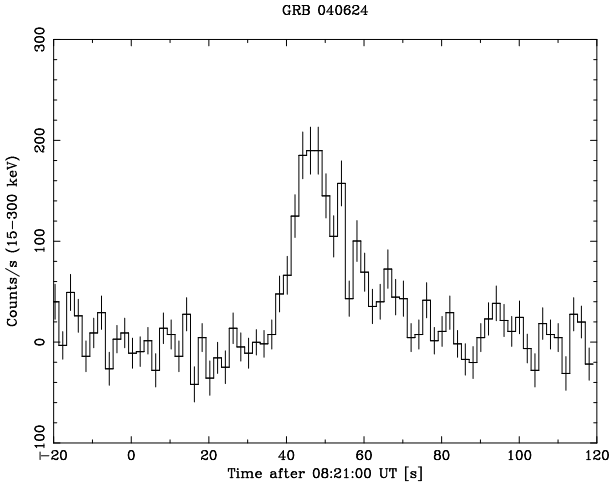

Figure 3.42: Time History of GRB 040624. Binsize = 2 s.

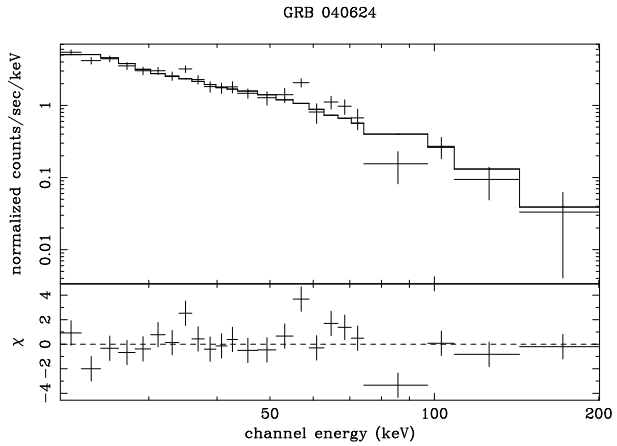

Figure 3.43: Average Spectrum of GRB 040624.

3.16 GRB 040730

Localization: R.A. = 15:53:14; Dec. = –56:28:15; Uncertainty = 1.7′

Time History: T_{90} = 43 s.

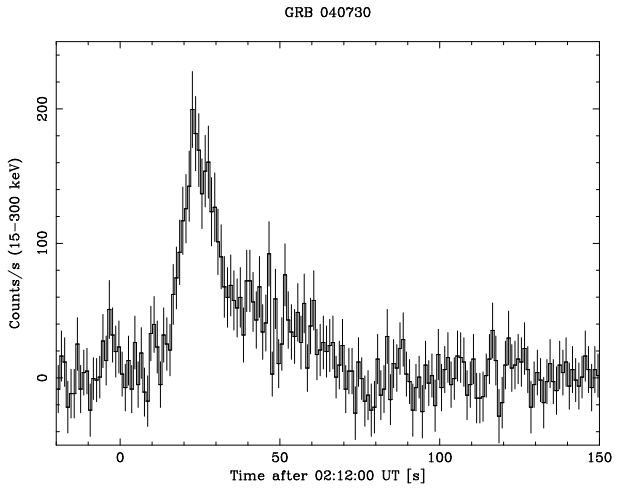

Figure 3.44: Time History of GRB 040730. The small peak around t = -5 is not related to the XRF, but it is due to a background variation.

Spectrum: The average spectrum can be well represented by a power law model with photon index $\Gamma = 1.65 \pm 0.15$. The fluence is 8×10^{-7} erg cm^{-2} , while the peak flux is 0.4 ph cm^{-2} s^{-1}(2.2×10^{-8}erg cm^{-2} s^{-1}).

Spectral Evolution: One of the nest examples in the *INTEGRAL* GRBs of hard to soft evolution, see Fig. 3.46.

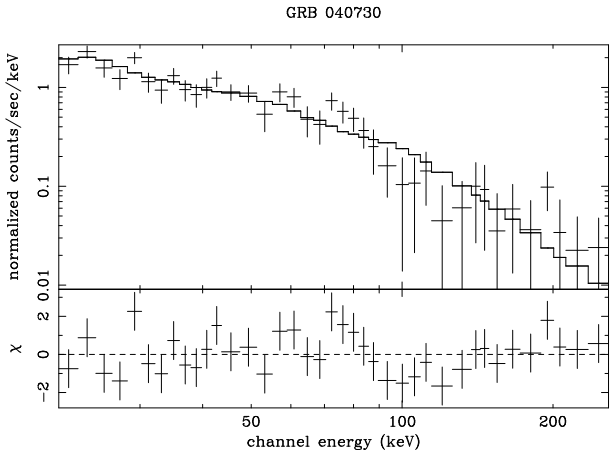

Figure 3.45: Average Spectrum of GRB 040730.

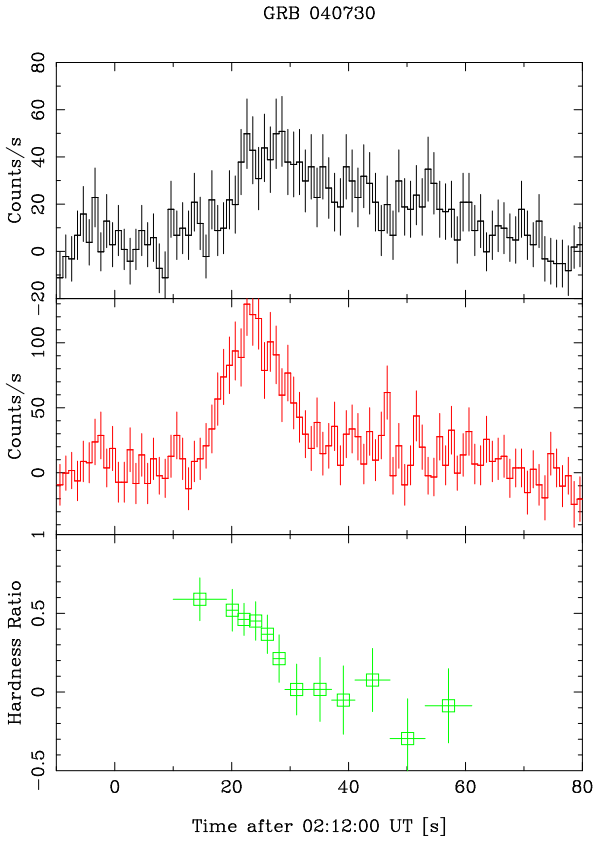

Figure 3.46: Top Panel: background subtracted light curve of GRB 040730 in the 15-40 keV band. Middle Panel: same as above, but in the 40-200 keV band. Bottom Panel: Hardness Ratio: the bins have been chosen in order to have at least 200 counts in the total $(H + S)$ band.

Afterglow: No afterglow has been found for this GRB.

3.17 GRB 040812

This is the only GRB, that was detected at an off-axis angle small enough to be also detected by JEM-X.

Localization: R.A. = 16:26:05; Dec. = –44:42:32; Uncertainty = $2'$

Time History: T_{90} = 19 s. Single peak.

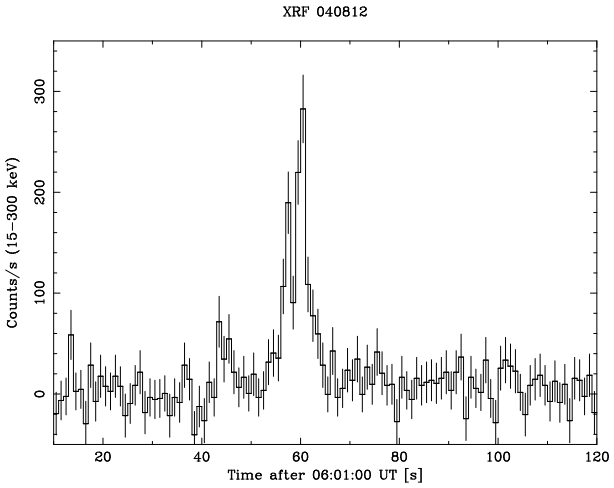

Figure 3.47: Time History of GRB 040812.

Spectrum: This GRB has a very soft spectrum. Actually it can be classified as an XRF. A preliminary spectral fit using only IBIS/ISGRI data shows a power law with photon index $\Gamma = 2.3 \pm 0.34$. The fluence is 2.5×10^{-7} erg cm^{-2} and the peak flux 0.6 ph cm^{-2} s^{-1}(5×10^{-8} erg cm^{-2} s^{-1}).

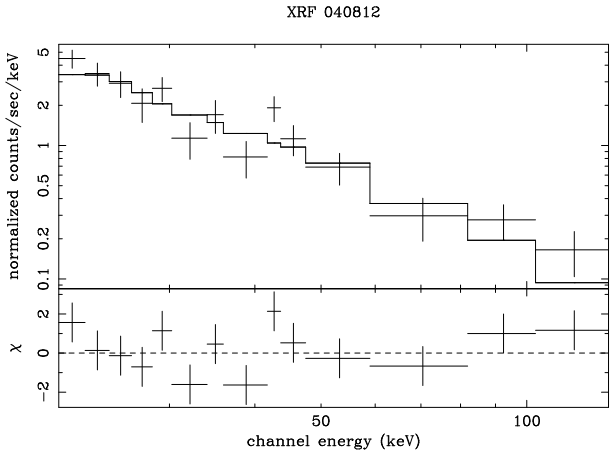

Figure 3.48: Average Spectrum of XRF 040812.

Spectral Evolution: There is an indication of hardness-intensity correlation.

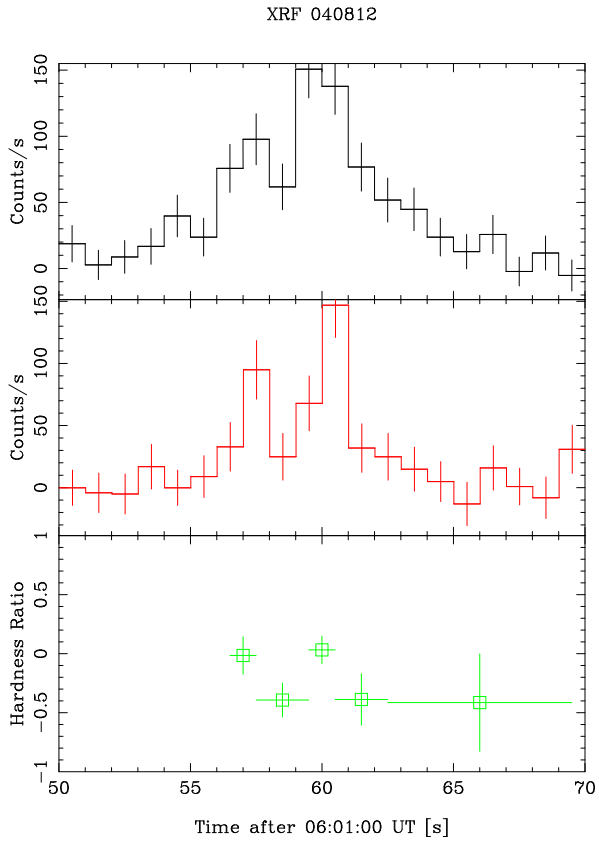

Figure 3.49: Top Panel: background subtracted light curve of GRB 040812 in the 15-40 keV band. Middle Panel: same as above, but in the 40-200 keV band. Bottom Panel: Hardness Ratio: the bins have been chosen in order to have at least 150 counts in the total $(H + S)$ band.

Afterglow: Two *Chandra* observations have been performed as a follow-up to this burst leading to the discovery of a fading source in the IBAS error circle at coordinates R.A.= 16:26:2.25, Dec.= –44:43:49.4 (Patel et al., 2004).

3.18 GRB 040827

Localization: R.A. = 15:17:00; Dec. = –16:08:21; Uncertainty = 2.5′

Time History: T_{90} = 49 s. Single peak.

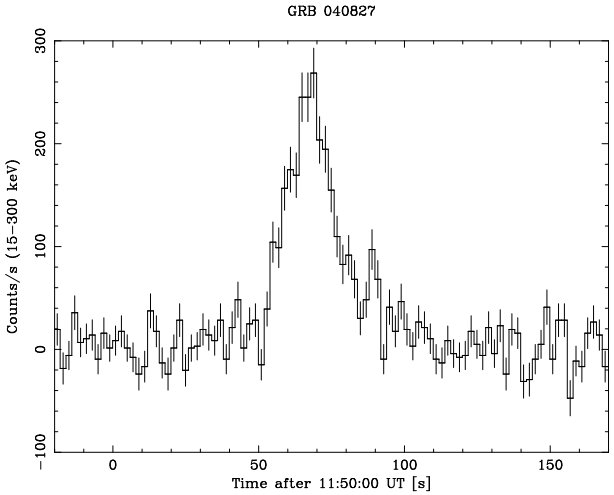

Figure 3.50: Time History of GRB 040827. Binsize = 2 s.

Spectrum: The average spectrum can be well modeled with a power law with photon index $\Gamma = 1.57 \pm 0.1$. The fluence is 1.2×10^{-6}erg cm^{-2} and the peak flux 0.6 ph cm^{-2} s^{-1} (6×10^{-8} erg cm^{-2} s^{-1}).

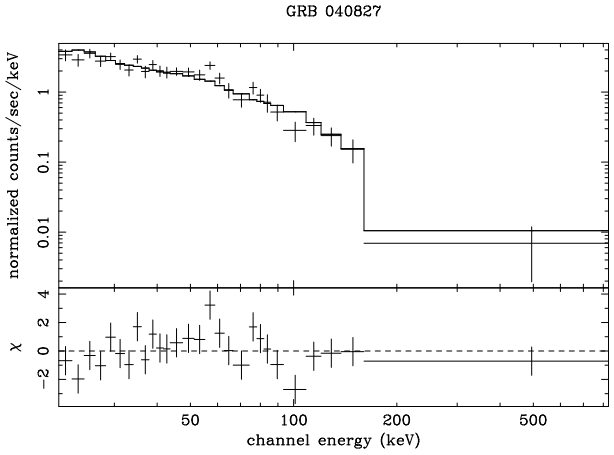

Figure 3.51: Average Spectrum of GRB 040827.

Spectral Evolution: A clear hard to soft evolution is evident from Fig. 3.52.

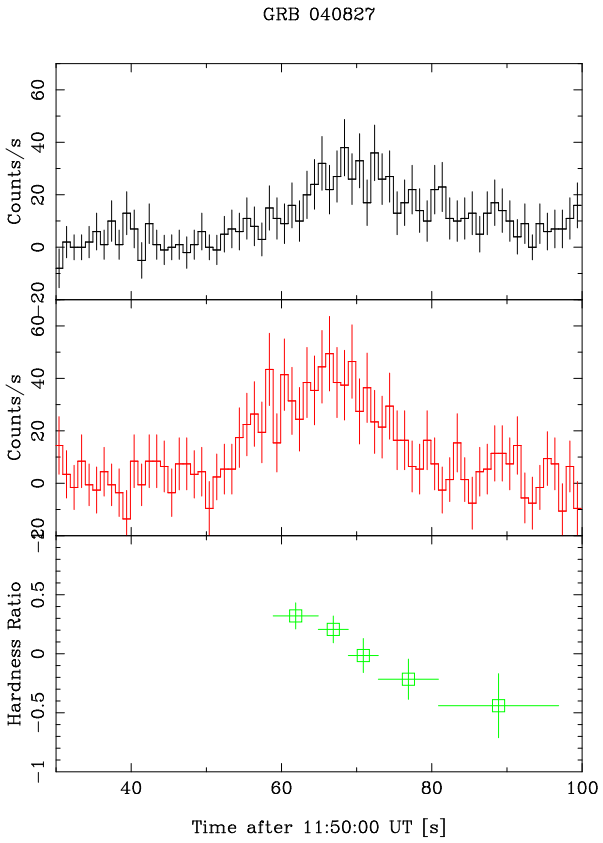

Figure 3.52: Top Panel: background subtracted light curve of GRB 040827 in the 15-40 keV band. Middle Panel: same as above, but in the 40-200 keV band. Bottom Panel: Hardness Ratio: the bins have been chosen in order to have at least 200 counts in the total $(H + S)$ band.

Afterglow: The *XMM-Newton* satellite observed the GRB field for 50 ks, starting ∼6 hr after the prompt IBAS Alert. The observation started on 2004-08-27 at 18:07:56.UT (lasting 54.3 ks). Thanks to quick-look data it was soon realized that an afterglow was present but it was more than 1 arcmin off the camera boresight. Therefore, the telescope was re-pointed during the observation.

The 0.2-10 keV PN light curve shows a clear decay in time. We excluded from this analysis the first 4 ks when the XMM-Newton pointing was not definitive. A power law decay with $t^{-1.6\pm0.2}$ can account for the main decay (see Fig. 3.53).

We extracted spectra from the three EPIC cameras (See Fig. 3.54). A single absorbed power law model provides a good description of the spectra (χ^2_{red}=1.2 with 187 degrees of freedom), however the column density ($N_H=(3.7^{+4.2}_{-1.2})\times10^{21}$ cm^{-2}, errors at 90% c.l.) is much larger than the column density in this direction of the Galaxy (N_H=8x10^{20} cm^{-2}, Dickey & Lockman (1990)). Fixing the column density to N_H=8x10^{20} cm^{-2} results in a unacceptable fit with $\chi^2_{red} = 3.0$.

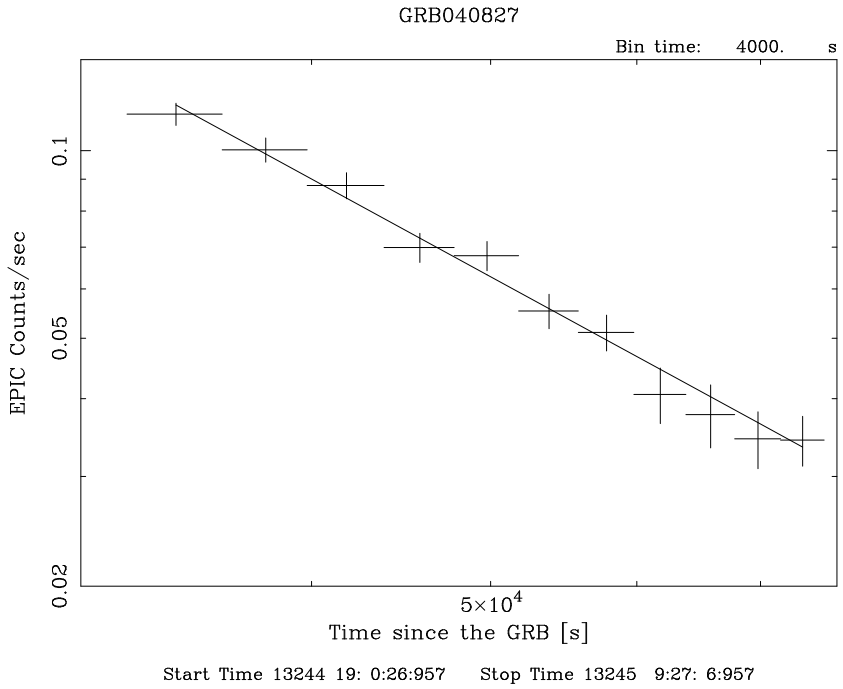

Figure 3.53: EPIC light curve of the afterglow of GRB 040827.

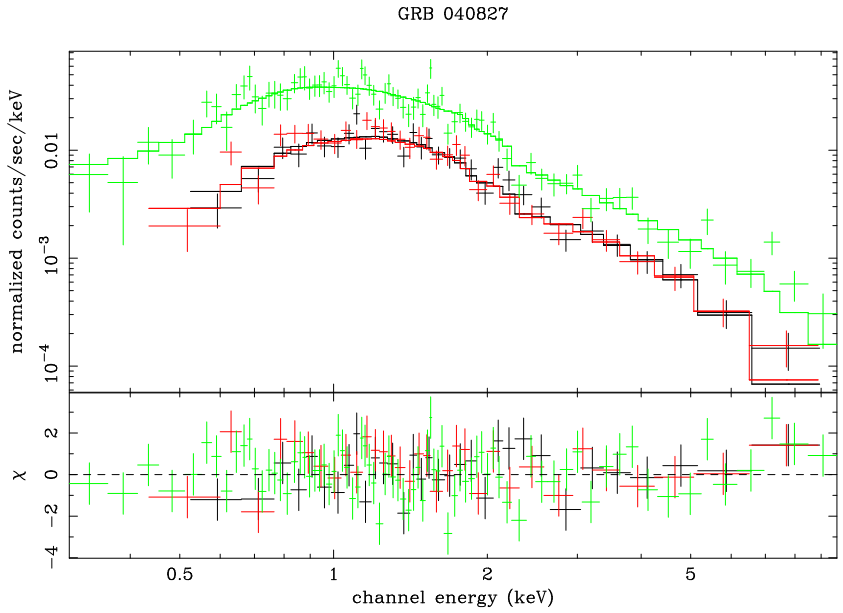

Figure 3.54: EPIC average spectrum of the afterglow of GRB 040827. Green points: PN, Black Points: MOS1, Red Points: MOS2.

We then include a redshifted absorption component, keeping fixed the Galactic column density to N_H=8×10^{20} cm^{-2}. The new fit is good ($\chi^2_{red} = 1.0$) providing an intrinsic value of N_H=$(1.3^{+0.6}_{-0.3})$×10^{22} cm^{-2}. The redshift is relatively well con-

strained (even if more the one minimum is found) to z=$0.9^{+0.9}_{-0.2}$. The power law photon index is $\Gamma = 2.3 \pm 0.1$ and the unabsorbed 0.5-10 keV flux is 3.4×10^{-13} erg cm^{-2} s^{-1} .

A NIR optical counterpart, coincident with the X-ray one, has been reported for this burst (Berger et al., 2004).

3.19 XRF 040903

A very soft high-energy transient, potentially an X-ray Flash, has been detected by IBAS on September 3, 2004. Due to its very soft spectrum and its localization in the Galactic Bulge (R.A. = 18:03:22 Dec. = –25:15:23, uncertainty 2.5 arcmin radius), it is also possible that it could be a previously unknown type-I X-ray burster. Within the IBAS error circle there is a faint *ROSAT* source (1RXS J180326.2-251556) which could be responsible of the burst. However, the analysis of *INTEGRAL* data before and after the burst itself does not reveal any persistent source at the position of 040903 with a 3 σ upper limit of 10 mCrab.

The initial light curve of GRB 040903 shows basically two peaks, which is reminiscent of the hard X-ray light curves of strong X-ray bursts with photospheric radius expansion (e.g., 4U 1812-12, Cocchi et al. (2000)). Also, both the GRB and XRBs reach peak intensities a few seconds after the start of the events. We compared in more detail the spectra and temporal behavior of GRB 040903 with that of one type I X-ray burst from 4U 1812-12, both as seen with the IBIS/ISGRI instrument on board INTEGRAL. The XRBs we focussed on were observed on 2003 April 25 and 27.

The 20-100 keV GRB spectrum of 040903 integrated over the burst can be well fit by a power-law with photon index of 3.5± 0.5 (1 sigma error; χ^2_{red} = 0.6 for 16 dof), although a black-body model cannot be formally ruled out (χ^2_{red} = 1.1 for 16 dof). The latter model gives a temperature of kT = 6.9±1.5 keV, which is significantly higher than the maximum value reached during any XRB (∼3 keV). The 20-100 keV spectrum of the XRB integrated over the burst can be well fit by a black-body model with temperature kT = 2.9±0.3 (χ^2_{red} = 0.5 for 5 dof), whereas a power-law model provides a rather bad fit (χ^2_{red} = 1.6 for 5 dof).

We used three energy bands to investigate the temporal behavior at a time resolution of 1 s: 13-26 keV, 26-60 keV and 60-500 keV. The light curves (and the hardness curve, i.e., the ratio of the counts in the 26-60 keV band to that of the counts in the 13-26 keV band, versus time) are shown in Figs. 3.55 and 3.56. The main differences between GRB 040903 and the XRBs are the following. The GRB is clearly seen in the 13-26 keV and 26-60 keV bands, whereas the XRBs are only seen in the 13-26 keV band. The first peak of the GRB is harder than the second peak, whereas the XRB is soft during both peaks (as well as in between).

We favor GRB 040903 being a XRF, given that

1. GRB 040903 is significantly harder than the XRBs from 4U 1812-12,

2. the spectral evolution of the GRB is unlike that seen for the XRBs, but resembles that of GRBs (and XRFs),

3. the integrated spectrum of the GRB is consistent with being due to power-law emission, but not with black-body emission as expected during XRBs,

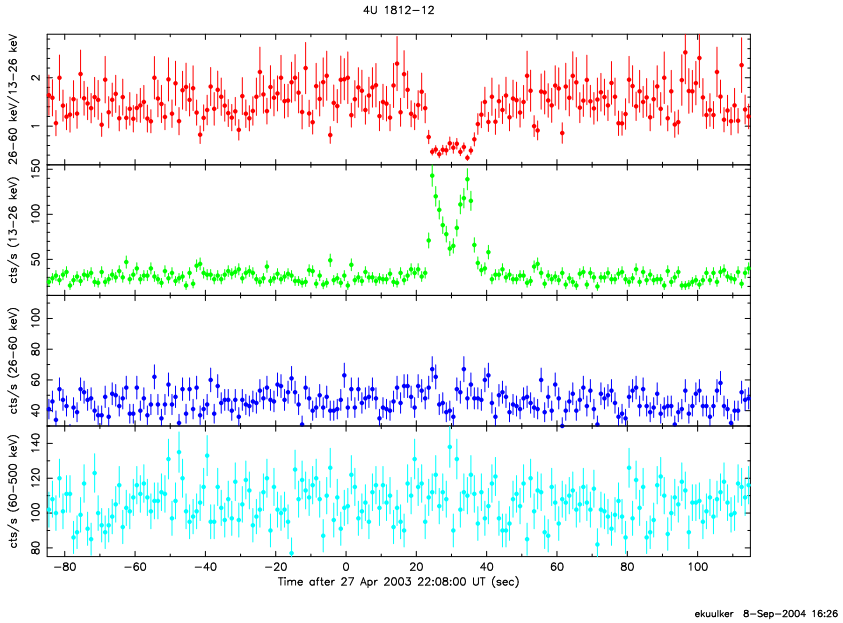

Figure 3.55: Hardness Ratio (upper panel) and light curves in three energy bands for a type I X-ray burst from 4U 1812-12

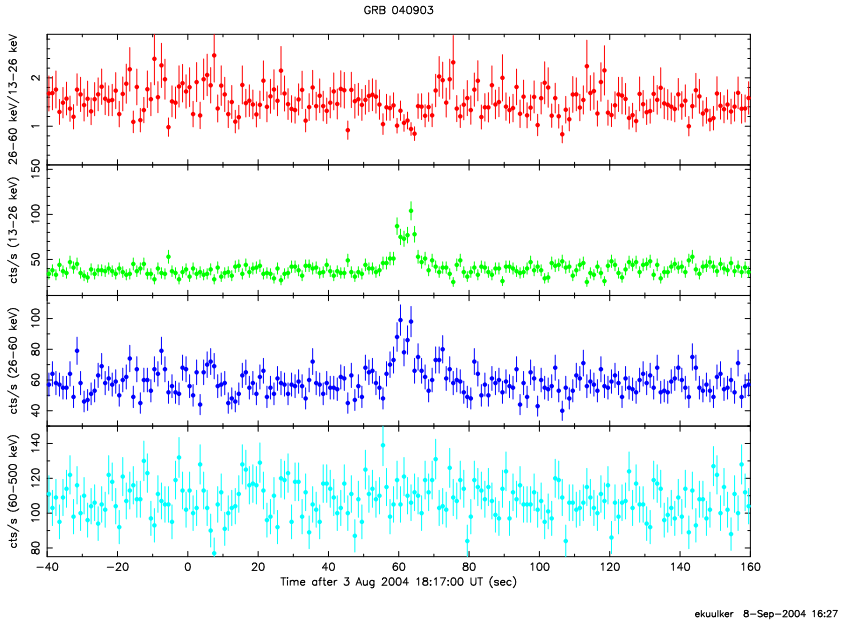

Figure 3.56: Hardness Ratio (upper panel) and light curves in three energy bands for XRF 040903

4. the GRB is not significantly detected above ∼60 keV,

Regime	ISM ρ=const	Jet ρ=const	Wind $\rho \propto \rho^{-2}$
$\nu < \nu_c$ $\alpha = \frac{p-1}{2}$	$C = \delta - \frac{3}{2}\alpha$	$C = \delta - 2\alpha - 1$	$C = \delta - \frac{3}{2}\alpha - \frac{1}{2}$
$\nu > \nu_c$ $\alpha = \frac{p}{2}$	$C = \delta - \frac{3}{2}\alpha + \frac{1}{2}$	$C = \delta - 2\alpha$	$C = \delta - \frac{3}{2}\alpha + \frac{1}{2}$

Table 3.2: Constraints on the fireball models from X-ray afterglows. From Piro (2004). The closure parameter C has to be consistent with 0 for the different cases. p is the spectral index of the electrons parent population. ν_c is the photon frequency that separates the fast cooling ($\nu < \nu_c$) from the slow cooling ($\nu > \nu_c$) synchrotron regime.

3.20 Early Afterglow and Precursor Search

The rapid re-pointing of *XMM-Newton* , in response to the IBAS Alerts has allowed us to study for the first time in detail the early phases of X-ray afterglow. We re-analyzed the five *INTEGRAL* GRB afterglows (030227, 031203, 040106, 040223, 040827), in order to verify if the derived afterglow parameters are consistent with the most popular GRB fireball models.

In addition, thanks to the fact that *INTEGRAL* observes the GRB regions for some time before and after the GRB itself, we have looked for precursors or early high-energy afterglow emission (as in the case of GRB 920723 reported by Burenin et al. (1999) or of GRB 980923 reported by Giblin et al. (1999)) and we have compared, where possible, these results with the *XMM-Newton* ones.

3.20.1 *XMM-Newton* Data Analysis

We can model the temporal and spectral behavior of the afterglow as $F(t, E) = F_0 exp(-\sigma N_H) t^{-\delta} E^{-\alpha}$. Using *XMM-Newton* data we can derive with unprecedented accuracy the temporal decay slope δ, the energy index α, and the hydrogen column density N_H. These values can be compared with the most popular models for GRB fireballs emission: the spherical expansion in a constant medium (ISM), or in a wind-like medium, with a density profile following ρ^{-2}, and the collimated (jet) flow. This is done by the evaluation of the so called closure relationships (Sari et al. (1998), Chevalier & Li (1999)), see Tab. 3.2.

The *XMM-Newton* data have been processed using SAS version 6.0. Only EPIC data have been used, because of its good sensitivity and broad band coverage. The light curves have been extracted summing the counts from all three cameras. The spectra have been extracted after the standard data screening from soft proton flares, and have been fitted simultaneously for PN, MOS1, and MOS2. The results are reported in Tab. 3.3.

GRB	δ	α	N_H^1	2-10 keV Flux @ 10 hrs [erg cm^{-2} s^{-1}]
030227	0.93±0.08	0.91±0.06	0.11	8.0×10^{-13}
031203	0.46±0.05	0.80±0.07	0.18	4.6×10^{-13}
040106	1.44±0.03	0.52±0.03	0	1.2×10^{-12}
040223	0.82±0.10	1.91±0.22	6.6	2.1×10^{-13}
040827	1.6±0.2	1.3±0.1	1.3	1.7×10^{-13}

[1] in excess of the Galactic value in the direction of the GRB (Dickey & Lockman, 1990) (units of 10^{22} cm^{-2}).

Table 3.3: *XMM-Newton* derived parameters for the analyzed afterglows.

If we consider the temporal slope δ and energy index α and apply the likely $\nu > \nu_C$ regime, we see that for 030227 and 040827, the closure parameter C is consistent with 0 in the case of spherical expansion (either Wind or ISM).

For 031203, C is inconsistent with with all the models. But being 031203 associated with a type Ic Supernova, it might be that we are not observing only the GRB afterglow, but also a SN component (see also Malesani et al. (2004)). In addition one can note that the temporal decay slope of this afterglow is unusually flat, by far much flatter than the average value reported for *BeppoSAX* afterglows.

040106 is a particular case, since again none of the models for $\nu > \nu_C$ seems to apply and the energy index is very small. On the other hand, the optical data by Masetti et al. (2004) taken simultaneously with the X-ray data are consistent with the extrapolation of the X-ray spectrum indicating that we are indeed in the $\nu > \nu_C$ regime. This implies a very hard spectrum for the parent electron population (α=$p/2$, in the synchrotron hypothesis) of $\sim$1, significantly flatter than the nearly universal value (2.2-2.3) for charged particles accelerated in ultra-relativistic shocks. However, for a different interpretation of the data (i.e. $\nu < \nu_C$, wind model applies) see Gendre et al. (2004).

In the case of 040223 again none of the model in the $\nu > \nu_C$ regime fits the data (not even in the $\nu < \nu_C$).

In conclusion, in 3 out of 5 cases the data collected by *XMM-Newton* seem to indicate that the standard fireball models fail in describing the early phases of the X-ray afterglow.

In an analogous work based on *BeppoSAX* data (normalized at 11 hours after the bursts, 36 observations) De Pasquale et al. (2003) and Piro (2004) find a narrow distribution for these parameters: $< \alpha >$=1.13±0.07, $< \delta >$=1.2±0.1. They conclude that the fireball expansion is consistent with spherical outflow either in ISM or wind, but as said they are sampling on average later phases of the X-ray afterglow.

As can be seen from Tab. 3.3, the absorption value is compatible with or slightly larger than the Galactic value for 3 out of 5 cases. A word of caution has

to be spent on the value found for 040223, since the data were affected by high background (see Section 3.11). These values can be compared with the mean value found by De Pasquale et al. (2003), namely $0.13^{+0.42}_{-0.13}$ for optically dark GRBs and 0.13 ± 0.06 for GRBs with an optical transient.

3.20.2 *INTEGRAL* Data Analysis

Thanks to the large FOV of *INTEGRAL* and its typically long observations, in many cases the position of a GRB discovered with IBAS can be monitored for few hours up to days after and before the burst itself. We have performed a search for precursors and early γ-ray afterglows in IBIS/ISGRI data using the Off-line Scientific Analysis (OSA) software package version 4.0. In none of the bursts we have analyzed, we have been able to detect any precursors or early high-energy afterglow emission. It must be considered that the bursts we have analyzed are by far much weaker than those for which high energy afterglow has been reported (920723, 980923). In addition, stimulated by the work of Frontera et al. (2000) on *BeppoSAX* data, we have tried to compare, where possible, the X-ray afterglow light curve with the prompt γ-ray emission in order to evaluate which is the relationship between the two. Frontera et al. (2000) report that the X-ray afterglow starts at about 50% of the GRB duration and its fluence, as computed from the WFC light curve, is consistent with the decay law found from the afterglow NFI observations.

In Figs. 3.57-3.60 we show for each GRB

1. the 15-40 keV flux of the GRBs measured with *INTEGRAL* ,
2. the flux of the X-ray afterglow, measured with *XMM-Newton* , extrapolated to the 15-40 keV energy range,
3. the *INTEGRAL* upper limits,
4. the extrapolation of the afterglow light curves back to the time of the GRB.

As can be seen only in one case (030227) out of 4, the afterglow is consistent with the prompt data as in the case of *BeppoSAX* GRBs. It is interesting to note that this is the GRB with the largest delay between the discovery and the *XMM-Newton* observation. In two cases (031203, 040223) the extrapolation of the afterglow is well below the γ-ray flux and points to times earlier than the GRB itself. The case of GRB 040106 is striking: the *INTEGRAL* upper limits indicate that even an early break in the light curve would not be enough to justify a common origin (or a smooth transition) for prompt and afterglow emission.

Again we have to conclude that more data is needed to disentangle this relationship in detail. It may well be that we are sampling a different phase of the X-ray afterglow than the one studied with *BeppoSAX* , which had reaction times always larger than 8 hrs. On the other hand, it has been already reported at

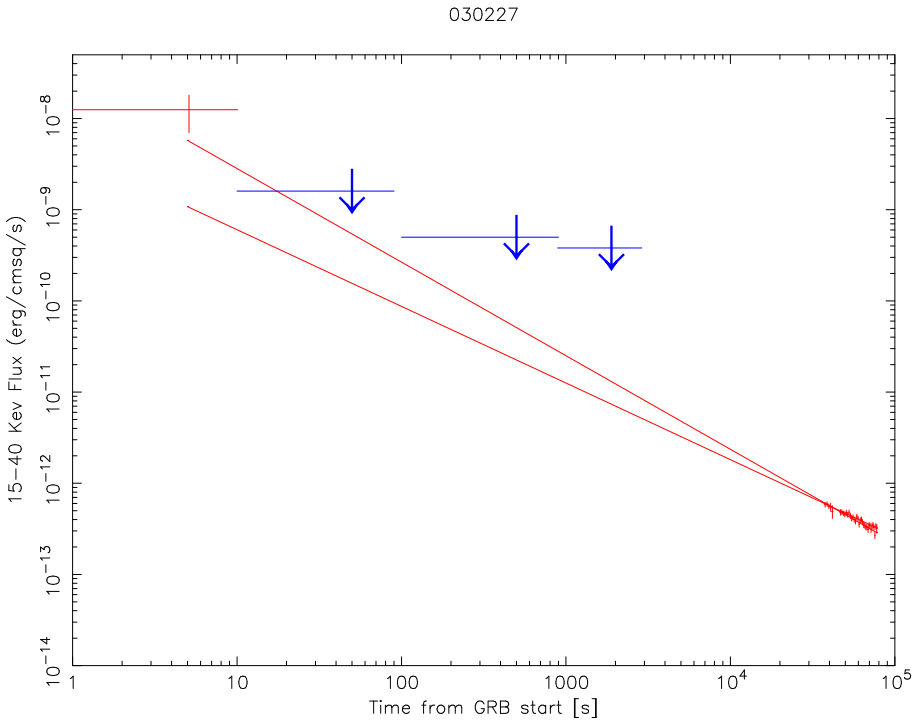

Figure 3.57: Prompt emission measured by *INTEGRAL* compared with X-ray afterglow emission as measured by *XMM-Newton* (extrapolated to the higher energy range). The blue arrows indicate IBIS/ISGRI 5 σ upper limits for the emission in the direction of the GRB. This GRB has been detected close to the end of an orbit, so just a few ks of data are available for the GRB.

least in one case (GRB 970508; Piro et al. (1998)) that the X-ray afterglows do not have a smooth time history, but they can have re-brightening phases.

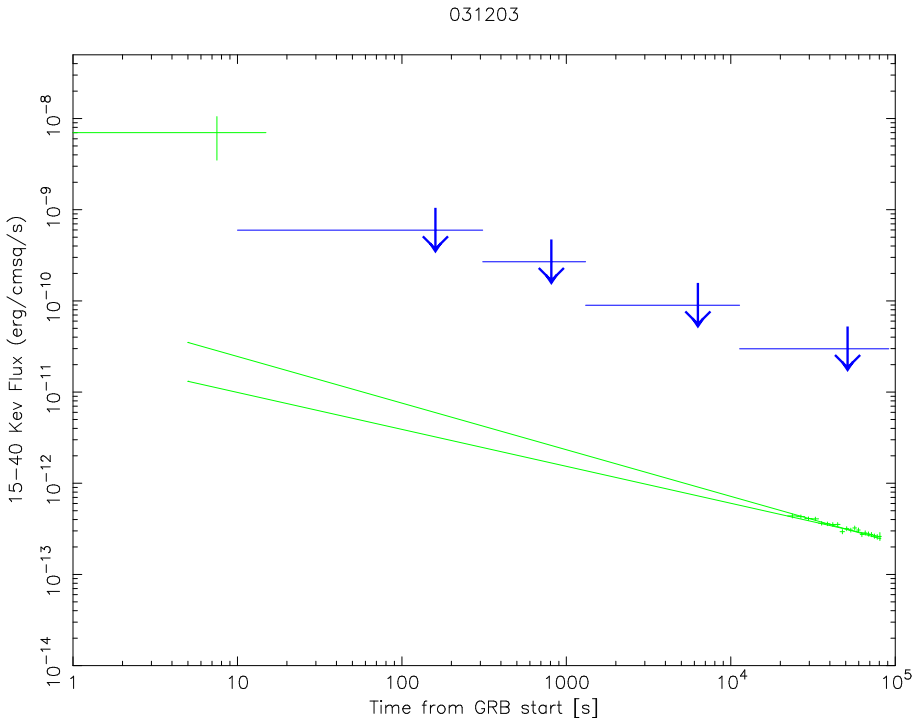

Figure 3.58: Prompt emission measured by *INTEGRAL* compared with X-ray afterglow emission as measured by *XMM-Newton* (extrapolated to the higher energy range). The blue arrows indicate IBIS/ISGRI 5 σ upper limits for the emission in the direction of the GRB.

3.21 The *INTEGRAL* GRB Sample Global Properties

The main properties of *INTEGRAL* GRBs described above are summarized in Tab. 3.21. In Fig. 3.61 the peak fluxes of the *INTEGRAL* are bursts plotted against their T_{90} durations.

As can be seen *INTEGRAL* GRBs sample mainly the faint end of the BATSE population of long duration GRBs. The fact that *INTEGRAL* is sampling a faint population of bursts is confirmed by the comparison between the peak fluxes of HETE-II, *BeppoSAX* and *INTEGRAL* bursts reported in Fig. 3.62.

Plotting the power-law indexes of *INTEGRAL* bursts versus their fluence one can see a correlation between the burst hardness and its fluence, which is analogous to the correlation between E_p and fluence seen e.g by HETE-II (Sakamoto et al., 2004). Also the well known E_p(hardness)-peak flux correlation (Mallozzi et al., 1995, 1998) is seen in *INTEGRAL* bursts. Both plots are shown in Fig. 3.63.

Finally we note that the number of GRBs with a photon index larger than $\sim$ 1.7 (which is, in the IBIS/ISGRI energy range, the limit between classical GRBs

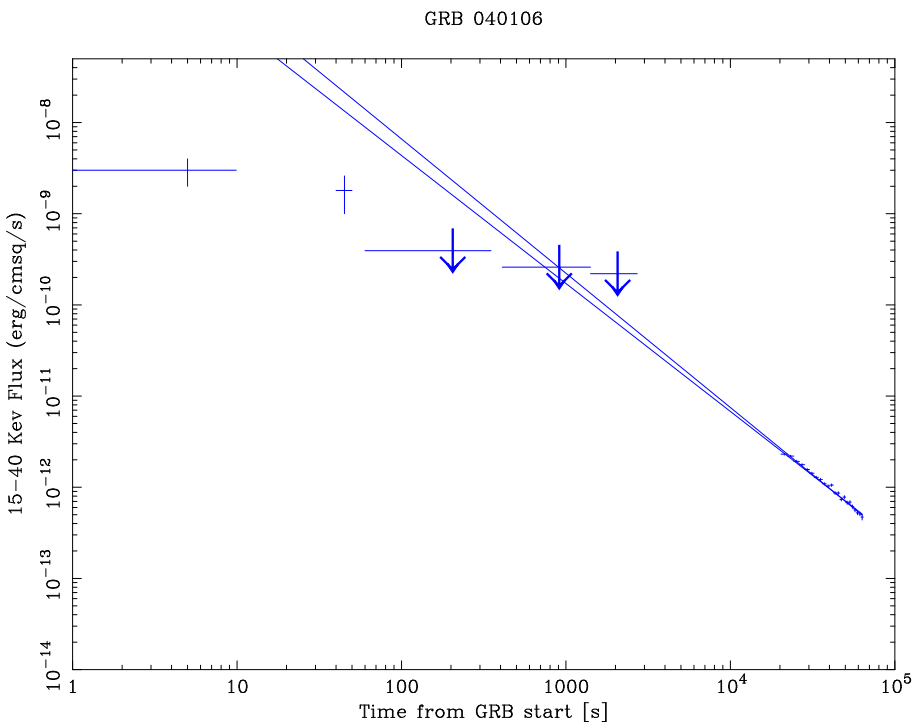

Figure 3.59: Prompt emission measured by *INTEGRAL* compared with X-ray afterglow emission as measured by *XMM-Newton* (extrapolated to the higher energy range). The blue arrows indicate IBIS/ISGRI 5 σ upper limits for the emission in the direction of the GRB. The satellite started a new observation soon after the GRB, so just a few ks of data are available.

and X-ray rich events) is 11 out of 18, which is less than the fraction detected by HETE-II (35 out of 45). This difference is probably due to the fact that the localization instrument on board HETE-II, the WXM, has a lower energy range (2-25 keV), and hence is more sensitive to soft events.

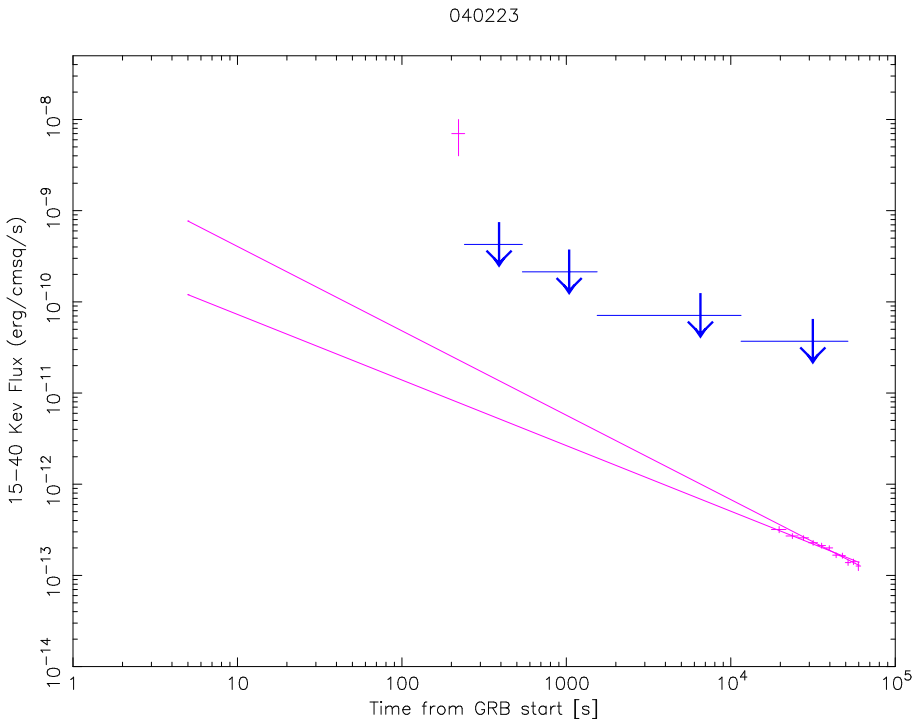

Figure 3.60: Prompt emission measured by *INTEGRAL* compared with X-ray afterglow emission as measured by *XMM-Newton* (extrapolated to the higher energy range). The blue arrows indicate IBIS/ISGRI 5 σ upper limits for the emission in the direction of the GRB.

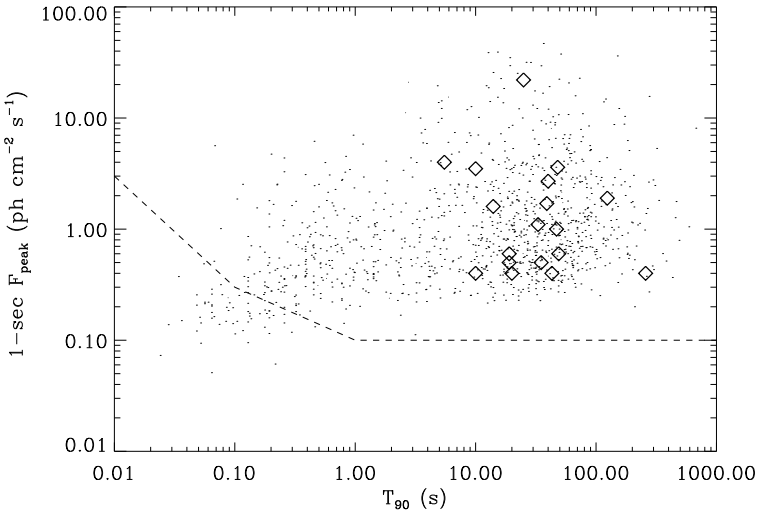

Figure 3.61: Peak flux vs. T_{90} duration for the *INTEGRAL* bursts (diamonds) compared to BATSE bursts (dots) and to the theoretical IBAS sensitivity for on-axis sources as computed by Götz & Mereghetti (2003).

GRB	Fluence [erg cm^{-2}]	Peak Flux [erg cm^{-2} s^{-1}]	T_{90} [s]	Power law photon index[1]	Spectral Evolution
021125	[2]5.1×10^{-5}	2.0×10^{-6}	25	0.62±0.22	-
021219	9.5×10^{-7}	4.4×10^{-7}	5.5	1.67±0.15	H→S
030131	7.0×10^{-6}	1.7×10^{-7}	124	1.4±0.2	H→S
030227	8.8×10^{-7}	1.0×10^{-7}	33	1.72±0.09	H→S
030320	1.2×10^{-5}	4.0×10^{-7}	48	1.5±0.15	H→S
030501	3.7×10^{-6}	2.3×10^{-7}	40	1.87±0.15	H→S
030529	4.0×10^{-7}	3.0×10^{-8}	20	1.71±0.20	-
031203	1.5×10^{-6}	1.6×10^{-7}	39	1.71±0.07	-
040106	8.3×10^{-7}	1.0×10^{-7}	47	1.72±0.15	S→H
040223	2.0×10^{-6}	4.0×10^{-8}	258	2.00±0.17	-
040323	2.0×10^{-6}	2.0×10^{-7}	14	0.64±0.10	H→S
040403	5.0×10^{-7}	5.0×10^{-8}	19	1.90±0.15	H→S
040422	8.0×10^{-7}	2.8×10^{-7}	10	2.07±0.10	H→S
040624	8.0×10^{-7}	3.5×10^{-8}	35	2.16±0.13	H→S
040730	8.0×10^{-7}	2.2×10^{-8}	43	1.65±0.15	H→S
040812	2.5×10^{-7}	5.0×10^{-8}	19	2.30±0.34	-
040827	1.2×10^{-6}	6.0×10^{-8}	49	1.57±0.10	-
040903	1.0×10^{-7}	2.0×10^{-8}	10	3.50±0.50	H→S

[1] or α parameter of the Band function where applicable (021125 and 040323)
[2] 20-500 keV energy range

Table 3.4: Fluences, Peak Fluxes, durations, power law indexes and spectral evolution for all *INTEGRAL* GRBs.

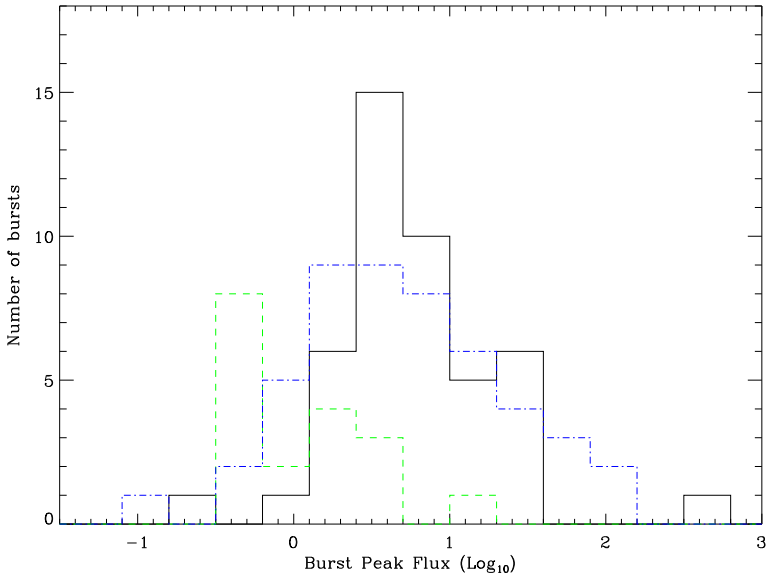

Figure 3.62: Peak fluxes distribution for HETE-II (continuous black line) *BeppoSAX* (dash-dotted blue line) and *INTEGRAL* GRBs (dashed green line). HETE-II data are taken from Sakamoto et al. (2004). *BeppoSAX* data courtesy F. Frontera.

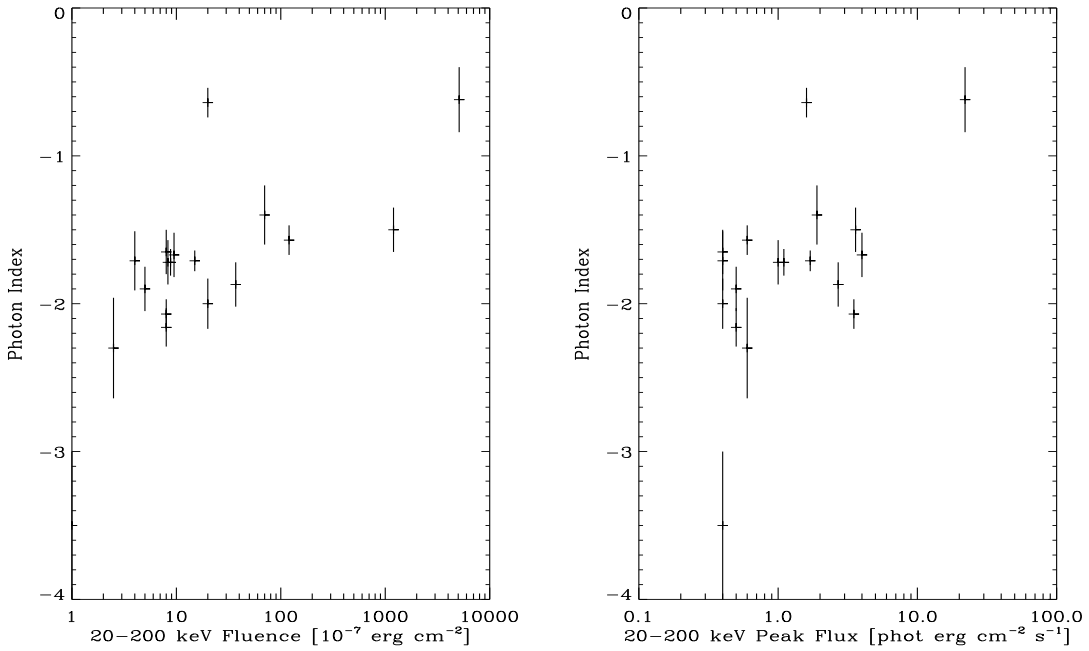

Figure 3.63: Left: photon index vs. fluence for *INTEGRAL* GRBs. Right: photon index vs. peak flux.

Part II

Soft Gamma Repeaters

Chapter 4

Soft Gamma Repeaters

In this Chapter the results on the bursting activity of SGR 1806–20, detected with IBAS, and its persistent emission, as measured with *INTEGRAL* , are presented. Some of the work presented here has been published in Götz et al. (2004e), that can be found in Appendix A.

4.1 Introduction

Soft Gamma Repeaters (SGRs) are a class of peculiar high-energy sources discovered through their recurrent emission of soft ($\leq$ 100 keV) γ-ray bursts. These sources undergo sporadic, unpredictable periods of activity, which last days to months, often followed by long periods (up to years or decades) during which no bursts are emitted. The bursts have typical durations of $\sim$0.1 s and luminosities in the range 10^{39}-10^{42} ergs s^{-1} (see Hurley (2000); Woods & Thompson (2004) for recent reviews of this class of objects). Occasionally, SGRs also emit giant bursts that last up to a few hundred seconds and exhibit remarkable pulsations that reveal their spin periods (e.g. Mazets et al. (1979), Hurley et al. (1999a)).

SGR also exhibit persistent (quiescent) X-ray emission, where the spin period of these objects can also be measured. Typical luminosities (0.5-10 keV) of these heavily absorbed sources is of the order of a few 10^{35} ergs s^{-1}.

The bursting activity and the persistent emission are generally explained in the framework of the "Magnetar" model (see e.g. Duncan & Thompson (1992a), Paczynski (1992), Thompson & Duncan (1995)), as caused by a highly magnetized ($B \sim 10^{15}$ G) slowly rotating ($P \sim$ 5-8 s) neutron star.

The recent detection of X-ray bursts similar to those of SGRs from at least one, and possibly two, Anomalous X-ray Pulsars (AXPs) (Gavriil et al., 2002; Kaspi et al., 2003) indicates that these sources are also Magnetar candidates.

Up to now 4 confirmed sources belonging to this class have been discovered: 0526-66, 1627-41, 1806-20, 1900+14[1]. Precise localizations (accuracy $< 1''$, see

[1]Two bursts have been recorded in 1997 from a fifth candidate source, 1801-23 (Cline et al.,

Tab. 4.1) have now been obtained for all the four SGR. Their distances have been estimated in several different ways, with widely varying degree of precision: one SGR (0526-66) is located In the Large Magellanic Cloud and has a well-determined distance. Both 1806-20 and 1900+14 may be associated with massive star clusters, each of which has an estimated distance. Other distances measurements rely on the value of interstellar absorption from X-ray spectra.

Source	Right Ascension (J2000)	Declination (J2000)	Associated SNR/Cluster	Distance (kpc)
SGR 0526−66	$05^h\ 26^m\ 00.89^s$	$-66^\circ\ 04'\ 36.3''$	N49/cluster?	50
SGR 1627−41	$16^h\ 35^m\ 51.84^s$	$-47^\circ\ 35'\ 23.3''$	...	11
SGR 1806−20	$18^h\ 08^m\ 39.32^s$	$-20^\circ\ 24'\ 39.5''$	cluster	15
SGR 1900+14	$19^h\ 07^m\ 14.33^s$	$+09^\circ\ 19'\ 20.1''$	cluster	15

REFERENCES – (SGR 0526) Kulkarni et al. 2003; Klose et al. 2004; (SGR 1627) Wachter et al. 2004; Corbel et al. 1999; (SGR 1806) Kaplan et al. 2001; Fuchs et al. 1999; Corbel & Eikenberry 2004; (SGR 1900) Frail et al. 1999; Vrba et al. 2000;

Table 4.1: The X-ray positions, reported associations, and the inferred distances of the SGRs.

4.2 Short Bursts

The most common SGR bursts have short durations (~ 0.1 s), thermal spectra, and peak luminosities reaching up to 10^{41} ergs s^{-1} — well above the standard Eddington limit of $\sim 2 \times 10^{38}$ ergs s^{-1} for a 1.4 $M_\odot$ neutron star.

The properties of the most common SGR bursts do not appear to vary greatly between different periods of activity, or indeed between different sources (e.g.Aptekar et al. (2001); Göğüş et al. (2001)). A burst typically has a faster rise than decay, and lasts ~ 100 ms. Four examples from SGR 1806–20, SGR 1900+14, and AXP 1E2259+586 are shown in Fig. 4.1. A number of bursts are multi-peaked, like the two shown from SGR 1806–20 and SGR 1900+14. The intervals between sub-peaks have a broad distribution, suggesting that these multi-peaked bursts are a superposition of two (or more) single-peaked bursts close in time (Göğüş et al., 2001).

2000). One burst has been detected from a sixth candidate, 1808-20 (Lamb et al., 2003), localized very near to, but formally inconsistent with, the direction of 1806-20, during one of its active phases. None of these candidates has been confirmed up to now.

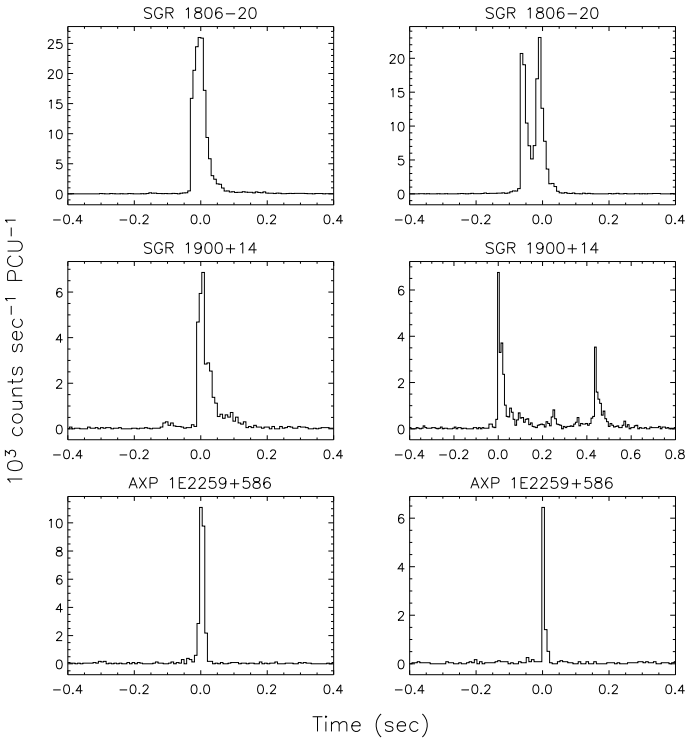

Figure 4.1: A selection of common burst morphologies recorded from SGR 1806–20, SGR 1900+14 and AXP 1E2259+586, as observed with the *RXTE* PCA. All light curves display counts in the energy range 2−20 keV, with a time resolution of 7.8 ms. From Woods & Thompson (2004).

The burst durations have a narrow distribution: they show a mild positive correlation with burst fluence (Göğüş et al., 2001), but do not vary significantly with photon energy.

The burst activity in SGRs tends to be concentrated in time. These episodes of enhanced burst activity are referred to as active periods. They occur at irregular intervals with variable duration and intensity. The recurrence patterns of individual bursts are just as irregular as those of the outbursts themselves, and differ dramatically from what is observed in X-ray bursts (of either Type I or II) in accreting neutron stars. There is no correlation between the energy of a given burst and the time to the next burst (Laros et al., 1987; Göğüş et al., 1999).

4.2.1 Spectral Properties

Bursts from SGRs were discovered using all-sky detectors with little sensitivity below ~ 30 keV. Above this photon energy, SGR burst spectra are well modeled by optically thin thermal bremsstrahlung (OTTB). The temperatures so obtained

fall within the narrow range $kT = 20 - 40$ keV, indicative of the spectral uniformity of SGR bursts. The spectra of SGR bursts vary weakly with intensity – not only from burst to burst within a given source, but also between sources.

A shortcoming of the OTTB model is that it over-predicts the flux of photons with energies below $\sim$ 15 keV (Fenimore et al., 1994). It is doubtful that this spectral rollover is due to a thick column of absorbing material, since the requisite $N_{\rm H}$ is an order of magnitude greater than what is deduced from the persistent X-ray emission. Recently, a $7 - 150$ keV *HETE-II* spectrum of a high-fluence burst from SGR 1900+14 was successfully fit by the sum of 2 blackbodies of 4.1 keV and 10.4 keV (Olive et al., 2003). A similar result was obtained with $1.5 - 100$ keV *BeppoSAX* spectra of 10 bursts also from SGR 1900+14 (Feroci et al., 2004). The temperatures of these lower peak flux bursts are consistent with the *HETE-II* burst spectrum – so that the flux ratio of the two blackbody components is approximately constant. Furthermore, the absorbing column measured during the bursts is consistent the value obtained in quiescence.

The energies radiated during the common ($\sim$ 0.1 s) SGR bursts follow a power-law distribution, $dN/dE \propto E^{-5/3}$. Cheng et al. (1996) first uncovered this distribution in SGR 1806–20, and pointed out the similarity with the Gutenburg-Richter law for earthquakes. Similar distributions are measured in a variety of other physical systems, including Solar flares and avalanches.

4.3 Giant Flares

The luminosity of SGR giant flares peaks peaks above a million times the Eddington luminosity of a neutron star. The flares begin with a $\sim$ 1 second spike of spectrally hard emission which decays rapidly into a softer, pulsating tail that persists for hundreds of seconds. These coherent pulsations are at the spin period of the underlying neutron star. The giant flares are rare: only two have been detected from the four known SGRs over 20 years of observation, so the corresponding rate is approximately once per 50−100 yrs (per source).

The first giant flare was recorded on 1979 March 5 from SGR 0525-66 (Mazets et al., 1979). The source is well localized in the LMC, and so the isotropic energy of the flare could immediately be estimated as 5×10^{44} ergs – some ten thousand times larger than a typical thermonuclear flash. The initial peak of this flare lasted $\sim$ 0.2 s and had significant structure on time scales shorter than $\sim$ 2 ms. It was spectrally harder ($kT \sim 250 - 500$ keV) than the common SGR bursts, and reached a peak luminosity of 4×10^{44} ergs s^{-1} (Mazets et al., 1979; Fenimore et al., 1981). Thereafter, the flux decayed in a quasi-exponential manner over the next $\sim$2-3 minutes. The pulsations during this phase of the burst had a period of 8.00 ± 0.05 s (Terrell et al., 1980). The pulse profile showed two clear peaks per cycle and a change in morphology during the first few cycles. The spectrum of the decaying tail had an OTTB temperature of $\sim 30 - 38$ keV, consistent with

the spectra of the recurrent burst emissions from this SGR.

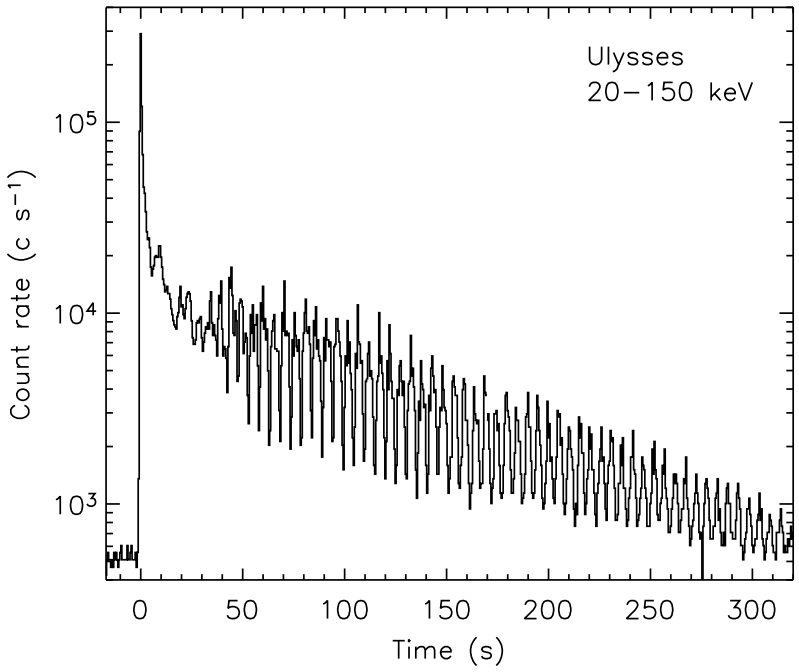

Figure 4.2: The giant flare from SGR 1900+14 as observed with the gamma-ray detector aboard Ulysses (20−150 keV). Note the strong 5.16 s pulsations clearly visible during the decay. From Woods & Thompson (2004).

The second giant flare (see Fig. 4.2) was not recorded until almost 20 years later, on 1998 August 27 and it occurred in the SGR 1900+14 (Hurley et al., 1999a; Feroci et al., 1999; Mazets et al., 1999b; Feroci et al., 2001). This burst was similar to the 0525-66 one. It began with a bright spike lasting ~ 0.35 s, and the X-ray spectrum contained a very hard power-law component $dN/dE \propto E^{-1.5}$ in the initial stages. Only a lower bound of 3×10^{44} ergs s^{-1} was obtained for its peak luminosity, because the flare saturated every detector that observed it. In fact, it was the brightest extra-Solar gamma-ray transient ever recorded. In contrast with the previous flare, the decline in the flux from the August 27 flare was followed by a well-defined termination some 400 s after the initial spike (Feroci et al., 2001). The spectrum after the first 50 s levelled to a (OTTB) temperature of ~ 30 keV, even while the luminosity continued to decrease by more than an order of magnitude. During this same phase, the light curve maintained large-amplitude pulsations with a 5.16 s period, precisely equal to the periodicity that had been previously detected in the persistent X-ray emission of SGR 1900+14 (Hurley et al., 1999b). The pulse maintained a complex four-peaked pattern that gradually simplified into a smooth single pulse during the final stages of the flare (Mazets et al., 1999b).

4.4 Intermediate Bursts

Intermediate bursts are intermediate in duration, peak luminosity and energy between the common recurrent SGR bursts and the extremely rare giant flares. Their durations range from ∼1 to 40 s and their isotropic energies from $10^{41}-10^{43}$ ergs. The spectra of most intermediate bursts are consistent with the spectra of the short, recurrent bursts and the pulsating tails of the giant flares. The spectrum does not vary much, either from burst to burst or within individual bursts. A striking exception to this rule was a very intense ($L_{\rm peak}$ ∼10^{43} ergs s^{-1}) and spectrally hard ($kT_{\rm peak}$ ∼120 keV) burst detected from SGR 1627-41 (Mazets et al., 1999a; Woods et al., 1999b). This burst lasted ∼0.5 s and was similar both spectrally and temporally to the initial peaks of the giant flares – but without the extended softer pulsations. Two bursts recorded from SGR 1900+14 during the 1998−1999 activation were also spectrally much harder than all other burst emission from this SGR (Woods et al., 1999a) with the exception of the initial spike of the August 27 flare. These bursts are, in fact, spectrally and temporally indistinguishable from classical GRBs. They were not exceptionally bright and had durations lasting ∼1 s with a fast rise and exponential decay. Their spectra were consistent with a power law (photon index ∼ −2) whose hardness was anti-correlated with X-ray flux (see Fig. 4.3).

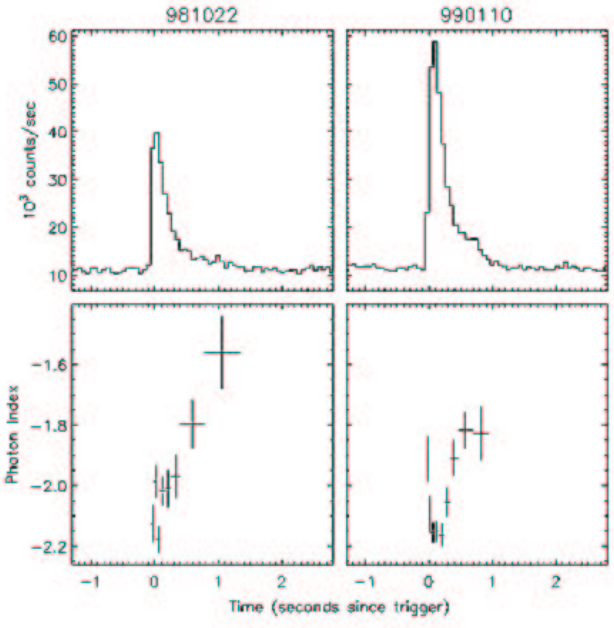

Figure 4.3: Light curves and time resolved power-law indexes for two hard bursts from SGR 1900+14. From Woods et al. (1999a).

SGR bursts which last longer than a second (but less than the rotation period of several seconds) tend to have abrupt onsets and end points, while their flux

varies modestly in between. By contrast, the light curves of the short, recurrent bursts (e.g.Göğüş et al. (2001)) are usually more irregular, which suggests that the emitting particles cool more rapidly.

4.5 X-ray Spectra

The X-ray spectra of the counterparts of SGRs (and AXPs) (0.5−10 keV) are usually well fit by a two-component model, a blackbody plus a power law, modified by interstellar absorption (see Tab.4.2). The soft blackbody component is not required in a few sources, but these tend to be dim and/or heavily absorbed (e.g. SGR 1627-41). During quiescence (i.e., outside of bursting activity), the blackbody temperature does not vary greatly between different members of the class (Marsden & White, 2001). On the other hand, the non-thermal component does show significant variations between different sources (Marsden & White, 2001).

Source[a]	N_H	Blackbody Temperature	Photon Index	Unabsorbed[b] Flux	Luminosity[c]
	10^{22}			10^{-11}	10^{35}
	(cm^{-2})	(keV)		(ergs cm^{-2} s^{-1})	(ergs s^{-1})
SGR 0526−66	0.55	0.53	3.1	0.087	2.6
SGR 1627−41	9.0	−	2.9	0.027−0.67	0.04−1.0
SGR 1806−20	6.3	−	2.0	1.2−2.0	3.2−5.4
SGR 1900+14	2.6	0.43	1.0−2.5	0.75−1.3	2.0−3.5

a – Spectral values given for quiescent state only (i.e. periods with no *detected* burst activity)
b – All fluxes and luminosities integrated over 2.0−10.0 keV
c – Assumed distances given in Table 4.1

REFERENCES – (SGR 0526) Kulkarni et al. 2003; (SGR 1627) Kouveliotou et al. 2003; (SGR 1806) Mereghetti et al. 2000; (SGR 1900) Woods et al. 2001;

Table 4.2: X-ray spectral properties of the SGRs and AXPs.

Very little is known about the X-ray spectra of magnetar candidates above ∼10 keV due to the limitations of past and current instrumentation. Knowledge of the photon distribution with energy above 15 keV is crucial in determining the underlying emission mechanism (see Section 4.7).

4.5.1 X-ray Afterglows

Extended X-ray afterglows have been detected following four different bursts from SGR 1900+14. The first such detection followed the giant flare of 1998 August 27 (Woods et al., 2001). Half an hour after the flare, the persistent X-ray flux from 1900+14 remained ∼700 times brighter than the pre-flare level. The X-ray flux decayed over the next 40 days approximately as a power law in time ($F \propto t^{-\alpha}$ with an exponent $\alpha = 0.71$). The blackbody component of the X-ray spectrum was hotter ($kT = 0.94$) one day into the afterglow phase (Woods et al., 2003) than it was before the burst ($kT = 0.5$ keV); but eighteen days later the power-law component of the spectrum was again dominant.

Afterglows have also been detected from SGR 1900+14 following bursts on 1998 August 29 (Ibrahim et al., 2001; Lenters et al., 2003), 2001 April 18 (Feroci et al., 2003), and 2001 April 28 (Lenters et al., 2003). A power-law decay is also seen in these cases, with a return to the pre-burst flux level between 10^4 and 10^6 s following the burst. Enhanced thermal emission is typical, with temperatures as high as $\sim$ 4 keV (corresponding to a hot spot covering $\sim$ 1 percent of the neutron star surface). In fact, the afterglow of the 2001 April 28 burst involved only enhanced thermal emission. Within this small sample of afterglows from SGR 1900+14, the $2-10$ keV afterglow energy is about 2% of the $25-100$ keV burst energy (Lenters et al., 2003).

4.6 Timing

The spin periods of the SGRs and AXPs are clustered between 5 and 12 seconds, a very narrow range compared with radio pulsars and accreting X-ray pulsars. These sources are all spinning down rapidly and persistently, with fairly short characteristic ages $P/\dot{P} \sim 10^3 - 10^5$ yrs. The magnitude of the spin-down torque is consistent with magnetic dipole braking of an isolated neutron star with a dipole field of $\sim 10^{14} - 10^{15}$ G (see Fig. 4.4). Although most of the characteristic ages are less than 10^4 yrs, the ages for individual sources should be treated with caution since the spin-down torque has been observed to vary by more than a factor $\sim$ 4 in the SGR 1806–20 and SGR 1900+14.

In addition to rapid spin down, all SGRs and AXPs have shown significant timing noise: an irregular drift of the spin frequency superposed on the secular spin down trend (Woods & Thompson, 2004).

4.7 Magnetar Model

The basic idea of the model is that the variable X-ray emission – the bursts lasting up to $\sim$ 1000 s and the transient changes in persistent emission observed up to $\sim$ 1 yr – are powered by the decay of the star's magnetic field. A field exceeding

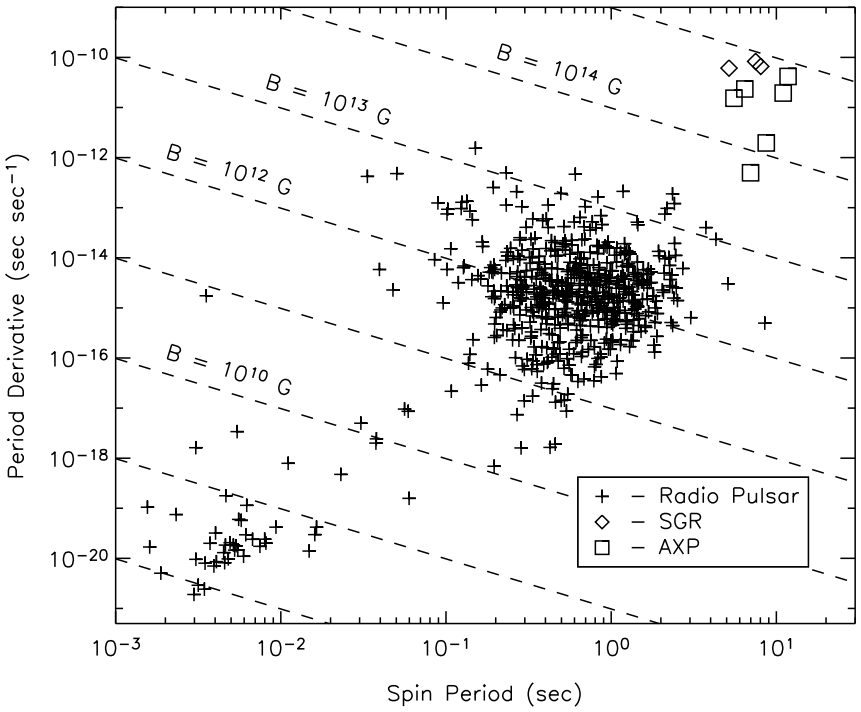

Figure 4.4: Period versus period derivative for radio pulsars (plus signs), Anomalous X-ray Pulsars (squares), and Soft Gamma Repeaters (diamonds). Contours of constant inferred magnetic field strength are drawn as diagonal dashed lines. From Woods & Thompson (2004).

$\sim 10^{15}$ G is needed to supply an output of 10^{35} erg s^{-1} extending over 10^4 yrs. The non-thermal X-ray emission of the SGRs cannot be powered primarily by cooling or by spin-down.

In the magnetar model, this enhanced X-ray emission results from four effects (Thompson & Duncan, 1996; Heyl & Kulkarni, 1998; Colpi et al., 2000; Thompson et al., 2002; Kouveliotou et al., 2003; Arras et al., 2004): i) internal heating by field decay; ii) a modest increase in the thermal transmissivity of the envelope due to the strong surface magnetic field (Heyl & Hernquist, 1998; Potekhin & Yakovlev, 2001); iii) a delay in the transition to core neutron superfluidity caused by magnetic heating (after this transition, a neutron star undergoes a significant drop in surface X-ray flux, Yakovlev et al. (2001)); and iv) surface heating, and cyclotron scattering of thermal surface emission, by charged particles which supply electric currents outside the star.

Both the short and the long outbursts of magnetars are hypothesized to arise from the direct injection of energy into the magnetosphere, through a rearrangement of the magnetic field and the formation and dissipation of strong localized currents.

The initial spikes of the giant flares have been associated with expanding fire-

balls composed of $e^{\pm}$ pairs and non-thermal gamma-rays (Paczynski, 1992), and the pulsating tails with thermalized energy which remains confined close to the neutron star by its magnetic field (Thompson & Duncan, 1995). In the spikes, the combination of rapid (< 0.01 s) variability with a hard non-thermal spectrum points to a low baryon contamination. The argument that most of the flare energy is deposited in the first second comes from i) the near coincidence between the energy of the initial spike and the energy radiated over the remaining ~ 300 s of the burst; and ii) the smooth adiabatic simplification of the pulse profile in the tail of the 27 August 1998 flare, which shows no evidence for secondary impulsive injections of energy that would be associated with a continuing substantial reorientation of the magnetic field. The lower bound on the magnetic moment implied by the confinement of $\sim 10^{44}$ ergs is $BR_{NS}^3 \simeq 10^{14}$G (Thompson & Duncan, 2001).

Large-scale deformations of the crust are constrained by its high hydrostatic pressure, but varying implications have been drawn for its elastic response to evolving magnetic stresses. One possibility is that the crust develops a dense network of small-scale (but macroscopic) dislocations, and that the resulting fast ohmic heating of the uppermost layers of the star is what powers the extended afterglow observed following SGR flares (Lyubarsky et al., 2002). Alternatively Jones (2003) and Lyutikov (2003) raise the possibility that the response of the crust may be more gradual and purely plastic, which would force the main source of energy for an X-ray flare into the magnetosphere. Evidence that the shear deformations of the crust are spatially concentrated comes from the observation of hard thermal X-ray emission – covering $\sim 1\%$ of the surface area of the star – right after the August 29 flare of SGR 1900+14 (Ibrahim et al., 2001).

A trapped thermal fireball (in which the photons have a Planckian distribution at a temperature ~ 1 MeV) is very optically thick to scattering, given the high density of electron-positron pairs. It releases energy through the contraction of its cool surface – in contrast to the cooling of a material body of fixed surface area. Thus, the X-ray flux is predicted to drop rapidly toward the end of a flare, when the external fireball evaporates (Thompson & Duncan, 1995). A simple model of a contracting spherical surface, bounding a fireball with a modest temperature gradient, provides an excellent fit to the 27 August 1998 flare (Feroci et al., 2001).

The temperature of the fireball surface is also buffered by a quantum electrodynamic effect: X-ray photons propagating through intense magnetic fields are able to split in two or merge together. The rate of splitting grows rapidly with photon frequency, but loses its dependence on magnetic field strength when $B \gg B_{QED} = 4.4 \times 10^{13}$ G (Duncan & Thompson, 1992b). Energy and momentum are both conserved in this process, with the consequence that only one polarization mode can split. As a result, splitting freezes out below a characteristic black body temperature of ~ 12 keV in super-QED magnetic fields (Thompson & Duncan, 1995). This is, very nearly, the temperature observed during an extended period of flux decline in the pulsating tail of the 27 August 1998 flare

(Feroci et al., 2001). In some geometries, double Compton scattering can also be a significant source of photon seeds near the scattering photosphere (Lyubarsky, 2002).

One clear prediction of the trapped fireball model is that ~ 1 percent of the trapped energy will be conducted into the surface of the neutron star over the duration of the fireball phase (Thompson & Duncan, 1995). This energy can explain the prompt afterglow observed immediately following the intermediate burst on 29 August 1998 (Ibrahim et al., 2001), but heat conducted into the crust cannot supply afterglow longer than $\sim 10^4$ s following the burst. The relative importance of such conductive heating for the observed afterglow – as compared with direct bulk heating and continuing relaxation of currents outside the star – is not well understood.

Searches for X-ray lines during SGR bursts are potentially diagnostic of the burst mechanism and the strength of the magnetic field. Short, low-energy SGR bursts are probably highly localized on the neutron star surface. The magnetosphere is probably at a higher temperature than the surface during a burst, and so proton cyclotron features may be seen in emission in the keV range (if the surface magnetic field is $\sim 10^{14} - 10^{15}$ G).

4.8 *INTEGRAL* Results on SGR 1806–20

SGR 1806–20 is one of the most active Soft Gamma-ray Repeaters. Here I report new observations of this source obtained with the INTEGRAL satellite in September and October 2003 (from now on referred to as *first dataset*) during a period of moderate bursting activity (Mereghetti et al., 2003f; Götz et al., 2003c; Hurley et al., 2003a; Mereghetti et al., 2003a; Götz et al., 2003d) and in Spring and Summer 2004 (*second dataset*) during a period of high activity (see e.g. Mereghetti et al. (2004h); Golenetskii et al. (2004b)), see Tab. 4.3.

Fig. 4.5 depicts the increase in the bursting activity of the source as observed with *INTEGRAL* . Finally I briefly on the preliminary results of the analysis of the huge outburst of October 5 2004.

These data have two advantages compared to previous observations in the soft γ-ray energy range of bursts from this source. First, they have been obtained with an imaging instrument, thus we can exclude that the bursts originate from a different source in the field. Second, they have a good sensitivity and time resolution which allows us to study the spectral evolution of relatively faint bursts.

4.8.1 First Dataset : Bursts

The analysis and results on the bursts of 2003 are reported in Götz et al. (2004e) (see Appendix A) and Götz et al. (2004f). These bursts, detected during a 240 ks ToO observation and during Core Program (GCDE and GPS) observations, are

INTEGRAL Orbit	Obs. Type	Number of Bursts	Orbit Start Time [UT]
108	TOO	2	2003-09-01T09:41:20
109	TOO	1	2003-09-04T09:26:46
119	CP	1	2003-10-04T07:22:32
120	CP	3	2003-10-07T07:11:55
121	CP	1	2003-10-10T07:02:43
122	CP	16	2003-10-13T06:53:37
171	CP	1	2004-03-07T22:21:10
173	CP	1	2004-03-13T21:54:43
175	CP	2	2004-03-19T21:30:35
181	CP	2	2004-04-06T20:15:13
225	TOO	36	2004-08-16T09:51:26
226	CP	4	2004-08-19T09:37:14
229	CP	1	2004-08-28T08:53:12
232	CP	1	2004-09-06T08:17:45
233	CP	2	2004-09-09T08:04:02
234	CP	1	2004-09-12T07:50:28
235	CP	2	2004-09-15T07:37:33

Table 4.3: Observation summary of the bursts from SGR 1806–20 analyzed here. The horizontal line separates the two datasets (see text).

typical in durations and spectra, and are among the faintest observed at energies > 15 keV. With one exception, they have all been observed only with IBIS/ISGRI being outside of JEM-X field of view, and too faint to be observed with SPI.

The T_{90} duration values, the peak flux and the fluence for the 24 bursts of the first dataset are reported in Tab. 4.4, while their light curves in the 15-100 keV energy band are shown in Fig. 4.6. We have computes integral distributions of peak flux and fluence (Log N-Log S and Log N-Log P). Within the large uncertainties, the fluence distribution is consistent with the power law slope found by Göğüş et al. (2000) using *RXTE* data. Many of these bursts are the faintest ever imaged from SGRs at these energies.

The main result reported in Götz et al. (2004e) is the discovery of the sepctral evolution within the bursts and a hardness-intensity anti-correlation for the bursts of SGR 1806–20. The spectral evolution of short bursts with time has been investigated using time resolved hardness ratios for the bursts with the best statistics (> 200 net counts). Some bursts show significant spectral evolution, while others, particularly those with a "flat topped" profile, do not. Some examples are given in Fig. 4.7.

As said, in addition to the spectral evolution within single bursts, the variation of the hardness ratio versus intensity has been investigated. All the hardness ratio

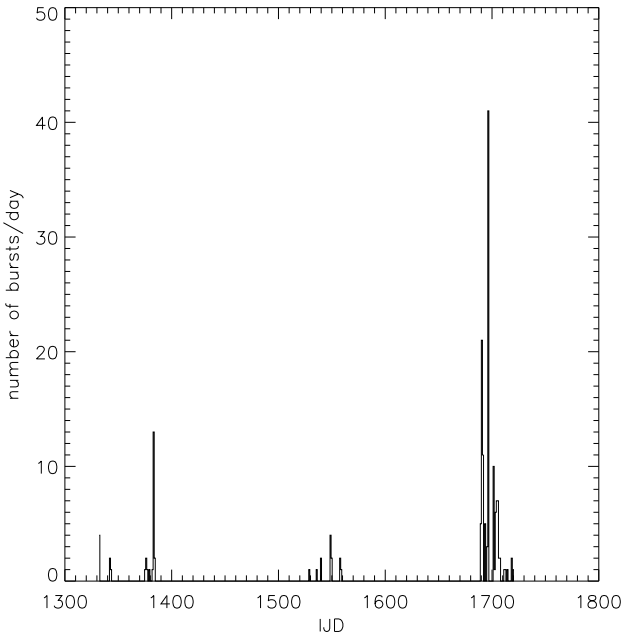

Figure 4.5: IBAS burst detection rate vs. time. SGR 1806–20 is visible by *INTEGRAL* only during Spring and Autumn. The first bunch of data represents the 2003 Autumn observation, while the second and the third, most prominent bunch, represent the 2004 observation. The source activity increased dramatically during Autumn 2004.

individual bins, that had been computed to study the spectral evolution of the bursts, bursts have been plotted versus their vignetting corrected flux. (see Fig. 4.8). Fitting these data, Götz et al. (2004e) found a hardness-intensity anti-correlation. The linear correlation coefficient of the data corresponds to a chance probability smaller than 10^{-5} of being due to uncorrelated data. In addition, according to an F-test, the data are significantly (at a 5.2 σ level) better described by a linear fit than by a constant value.

We have verified that there is no correlation between the hardness ratios of the individual bursts and the off-axis angle at which they have been detected. In addition we have verified that the vignetting correction procedure used in Götz et al. (2004e) is consistent with the values of the flux of the Crab Nebula measured in different positions in the field of view of IBIS.

4.8.2 First Dataset : Persistent Emission

Persistent (quiescent) emission from SGR 1806–20 has been discovered at X-ray (<10 keV) energies (Murakami et al., 1994). Up to now no detection at higher energies has been reported for any of the SGRs. We have analyzed IBIS, JEM-X

Burst Number	Fluence 10^{-8} erg cm^{-2}	Peak Flux 10^{-7} erg cm^{-2} s^{-1}	T_{90} ms
1	1.65 ± 0.16	3.74 ± 0.75	437
2	1.84 ± 0.17	4.26 ± 0.80	69
3	1.97 ± 0.17	2.15 ± 0.57	579
4	4.92 ± 0.27	14.77 ± 1.49	109
5	65.35 ± 0.99	60.73 ± 3.02	179
6	46.58 ± 0.84	50.42 ± 2.75	199
7	5.49 ± 0.28	15.73 ± 1.53	99
8	2.21 ± 0.18	3.67 ± 0.74	169
9	6.15 ± 0.30	12.71 ± 1.38	89
10	2.89 ± 0.21	5.27 ± 0.89	139
11	20.99 ± 0.56	36.40 ± 2.34	169
12	3.17 ± 0.22	9.18 ± 1.17	129
13	3.06 ± 0.21	4.83 ± 0.85	89
14	3.89 ± 0.24	4.86 ± 0.85	489
15	3.94 ± 0.24	15.62 ± 1.53	69
16	3.50 ± 0.23	7.95 ± 1.09	99
17	2.72 ± 0.20	7.21 ± 1.04	189
18	3.62 ± 0.23	9.45 ± 1.19	89
19	2.50 ± 0.19	8.49 ± 1.13	119
20	3.71 ± 0.24	14.33 ± 1.47	159
21	7.88 ± 0.34	8.15 ± 1.11	475
22	27.21 ± 0.64	43.71 ± 2.56	188
23	25.17 ± 0.61	54.80 ± 2.87	288
24	4.29 ± 0.25	4.24 ± 0.80	159

Table 4.4: Fluences (15-100 keV), Peak Fluxes (over 10 ms, 15-100 keV), T_{90} durations.

and SPI data of the ToO, but we did not find convincing evidence of quiescent emission.

On the other hand analyzing IBIS/ISGRI Core Program data (∼1 Msec of exposure on SGR 1806–20), we detect the source at ∼6 σ level in IBIS/ISGRI (see Fig. 4.9) in the 20-40 keV band. The flux is ∼3 mCrab, consistent with an extrapolation of the spectrum measured at lower energies (Mereghetti et al., 2000). Although a detection with such a relatively small significance is also compatible with background systematic noise in the significance maps, the positional coincidence with the X-ray counterpart strengthens the detection.

Also SPI data have been searched for quiescent emission. 482 pointings around the position of SGR 1806–20 (Core Program and TOO data) have been used, yielding a total exposure of ∼0.798 Ms. For the SPIROS (Skinner & Connell,

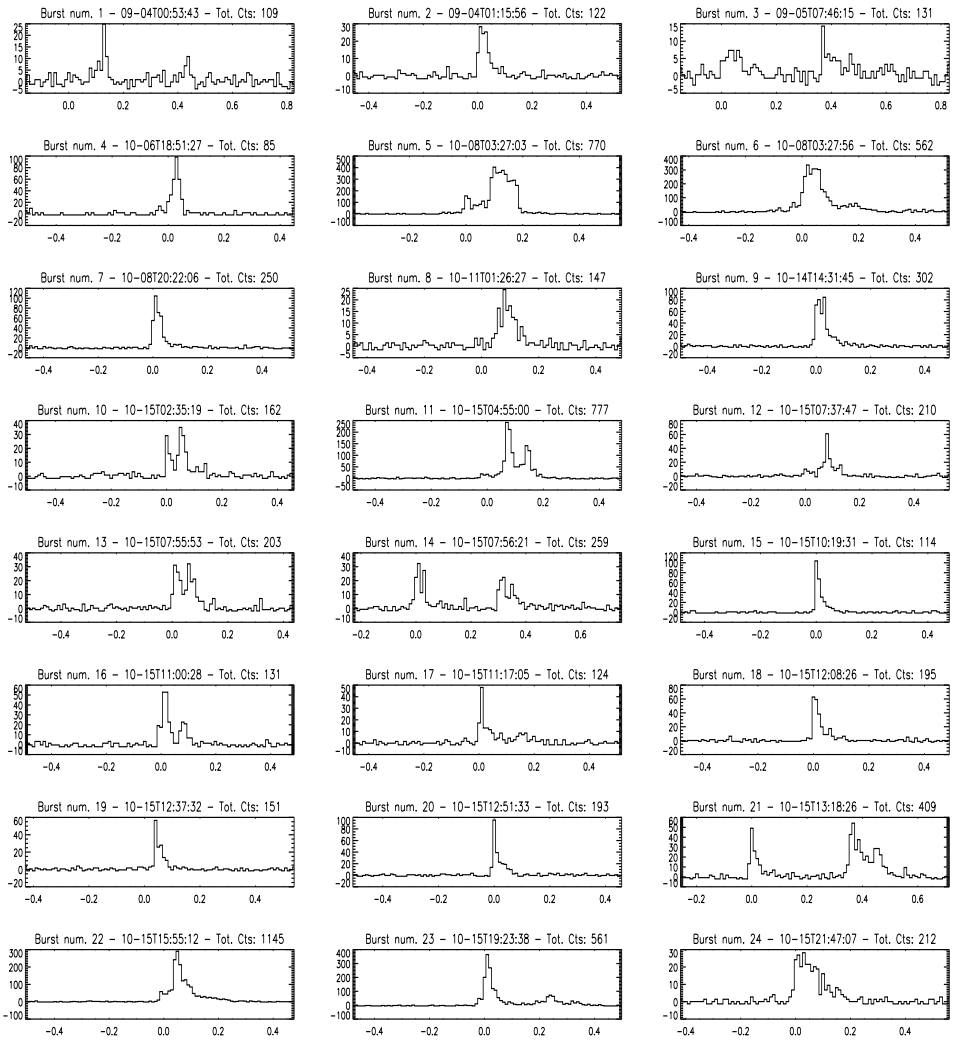

Figure 4.6: 15-100 keV light curves of the bursts from the first dataset.

2003) analysis tool the catalog of the sources detected by IBIS/ISGRI has been used as an input. A significance map was generated in the energy range between 28 and 48 keV. The measured flux is $0.69 \pm 0.15 \times 10^{-3}$ photons cm^{-2} s^{-1}. This flux ($\sim$ 10 mCrab) is slightly higher than the one measured by IBIS, but considering that the SPI detection level is just $\sim 4.4\ \sigma$, and that systematic errors are still present at this stage in the analysis of both instruments, we can consider the two results as consistent with each other.

Concerning JEM-X Core Program data, the analysis has still to be completed and will surely be helpful in order to better asses the possible IBIS and SPI detection.

The detection of pulsed emission is at the moment below our sensitivity.

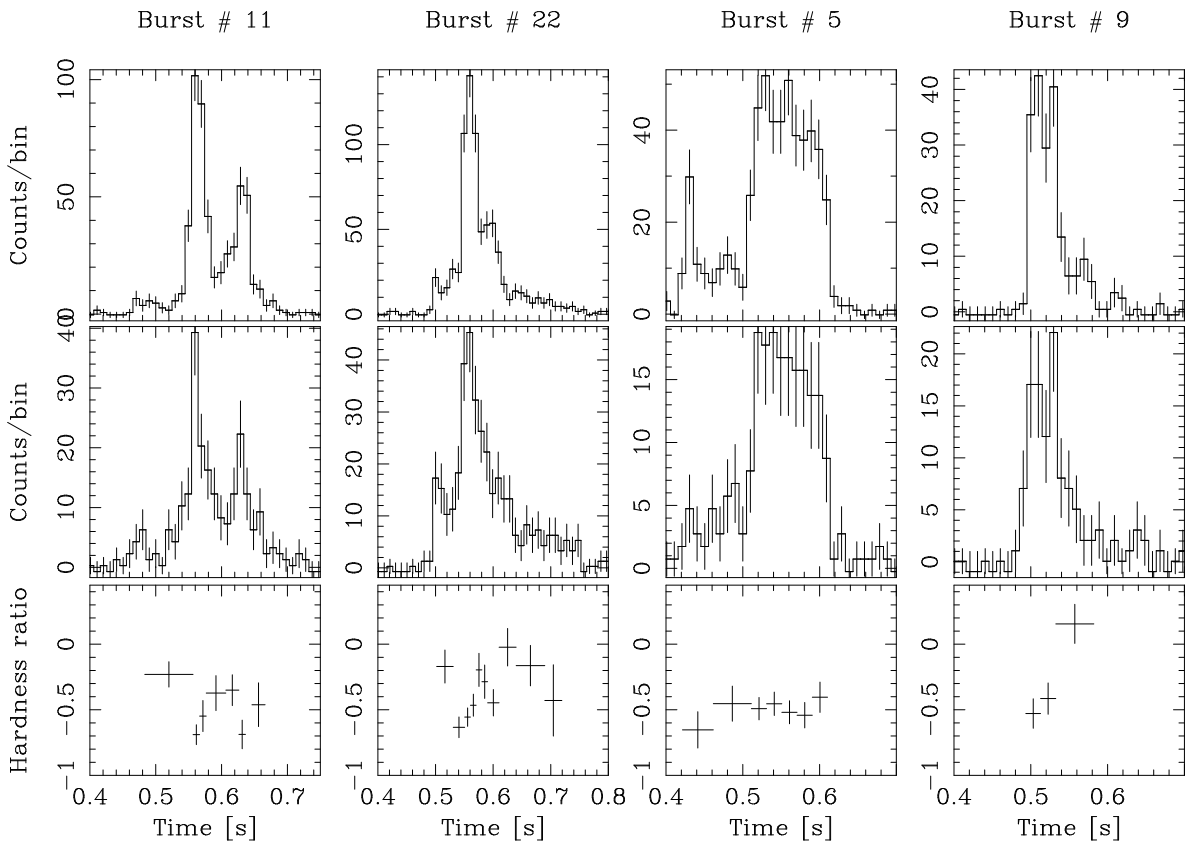

Figure 4.7: 15-40 keV light curve (*Top Panels*), 40-100 keV light curve (*Middle Panels*), and time resolved hardness ratio (*Bottom Panels*) for four bursts with good statistics. The time resolved hardness ratio for bursts number 11,22,9 is inconsistent with a constant value at $\sim$3.5 σ level. From Götz et al. (2004e).

4.8.3 Second Dataset : Bursts

During the 2004 observation IBAS detected 134 bursts from SGR 1806–20. Here we present the analysis of 53 of them, namely the one observed during Core Program observations and during the ToO observation performed during Revolution 225. The 15-100 light curves of these bursts are reported in Figs. 4.10 and 4.11.

The peak fluxes, fluences and T_{90} durations of these burst are reported in Tabs. 4.5 and 4.6.

In Fig. 4.12 we report the integral distribution of the peak flux and fluence for the bursts from both the first and the second dataset. The slope of the fluence distribution is now better determined and is $-0.85^{+0.03}_{-0.05}$, which is inconsistent with the *RXTE* results reported by Göğüş et al. (2000), but in agreement with the –0.9 slope reported by Aptekar et al. (2001) using *KONUS* data, which, however, sample bursts with $\sim$2 orders of magnitude larger fluences.

The search for spectral evolution has been applied also to this second dataset

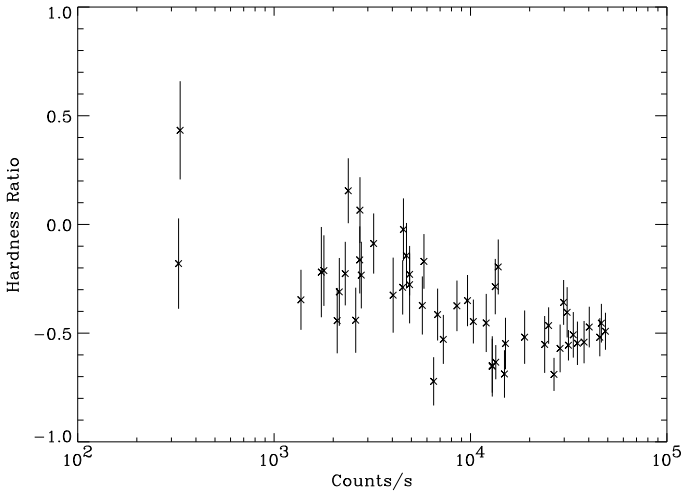

Figure 4.8: Hardness-Intensity plot of the time resolved hardness ratios of the 12 bursts with the best statistics. The hardness ratio is defined as $(H-S)/(H+S)$, where H and S are the background subtracted counts in the ranges 40-100 keV and 15-40 keV respectively. The count rates are corrected for the vignetting and refer to the 15-100 keV range (Götz et al., 2004e).

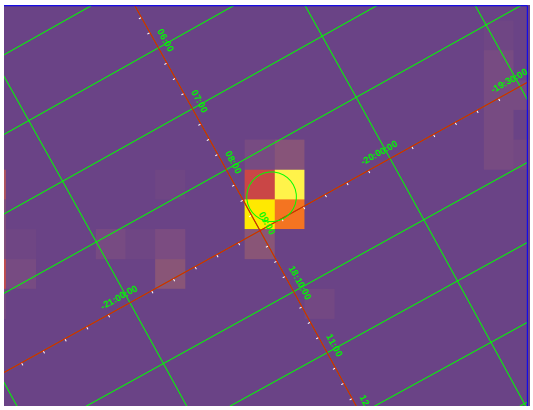

Figure 4.9: IBIS/ISGRI significance map. SGR 1806–20 is detected at $\sim$6 σ level. The circle is centered on the X-ray Chandra position (Kaplan et al., 2002) and has 5 arcmin radius.

of bursts. In this case the hardness ratios have been computed using 15-30 keV and 30-100 keV light curves in order to have more equally distributed statistical significance in the light curves.

The results are similar to what obtained for the first dataset. Some examples for the bursts with the best statistics are shown in Figs. 4.13, 4.14, 4.15, 4.16, 4.17, 4.18. As can be seen also here, short SGR bursts show significant spectral

evolution: in particular there seems to be a soft-to-hard evolution in bursts tails.

We also re-analyzed the data from the first dataset using the new energy bins and then added both dataset to further investigate the hardness-intensity anti-correlation found before. The hardness-intensity plot we obtained is shown in figure 4.19. For the second dataset we analyzed the 16 bursts with more than 300 counts. In this case the linear correlation coefficient of the data corresponds to a chance probability of $\sim 1.6\times10^{-5}$ of being due to uncorrelated data, which is slightly worse, but still consistent for what found for the first dataset.

4.8.4 Second Dataset : persistent emission

The analysis of the second dataset is on going. At the time of writing most of the data has not yet been released. Interestingly, Woods et al. (2004) report that the X-ray flux measured with *Chandra* and *RXTE* has increased by a factor 2 to 3 and the pulsed fraction has risen by 40-50%. Some of the *INTEGRAL* data has been analyzed by Molkov et al. (2004) and they report an increased flux of the source ($\sim$ 5 mCrab) in the 18-70 keV band.

4.8.5 The Huge Outburst of October 5 2004

After the bursts reported in the previous section SGR 1806–20 remained very active (Götz et al., 2004d), culminating in a huge outburst on October 5 at 13:56:47 UT (Mereghetti et al., 2004g; Götz et al., 2004c). This peculiar event (see figure 4.20), lasting about 10 minutes, is characterized by the emission of tens of short bursts close in time. In particular there are two large clusters of bursts: the first around 13:56:43 UT lasting about 20 s and the second one 13:59:33 UT lasting 40 s. Both this events, as can be seen from Fig. 4.20, saturated the telemetry available for IBIS, so only a lower limit to their fluence can be established in 1 and 2×10^{-5} erg cm^{-2} (15-100 keV), respectively. Using *KONUS* data Golenetskii et al. (2004a) derive a fluence of 8.6×10^{-5} erg cm^{-2} (20-200 keV) for all the bursts.

The preliminary IBIS/ISGRI spectral results on the two clusters of bursts reveal that while the first one has a rather common temperature (kT) for SGR bursts (45$\pm$3 keV) the second one is exceptionally hard (57$\pm$3 keV). This hardening is confirmed also by *KONUS* data. Golenetskii et al. (2004a) point out that his series resembles the series of soft bursts from SGR 1900+14 detected on 1998 May 30, three months before giant outburst on 1998 August 27.

To investigate the periods during which IBIS/ISGRI was saturated we have screened the data from different satellite borne instruments. The best data, even if much more less sensitive than IBIS/ISGRI data, is represented by the instruments on board *RHESSI* (Lin et al., 2002). The expanded view of the two

clusters as seen by *RHESSI* are reported in Figs. 4.21 and 4.22. The longest burst is in the first cluster and lasts for about 0.5 s.

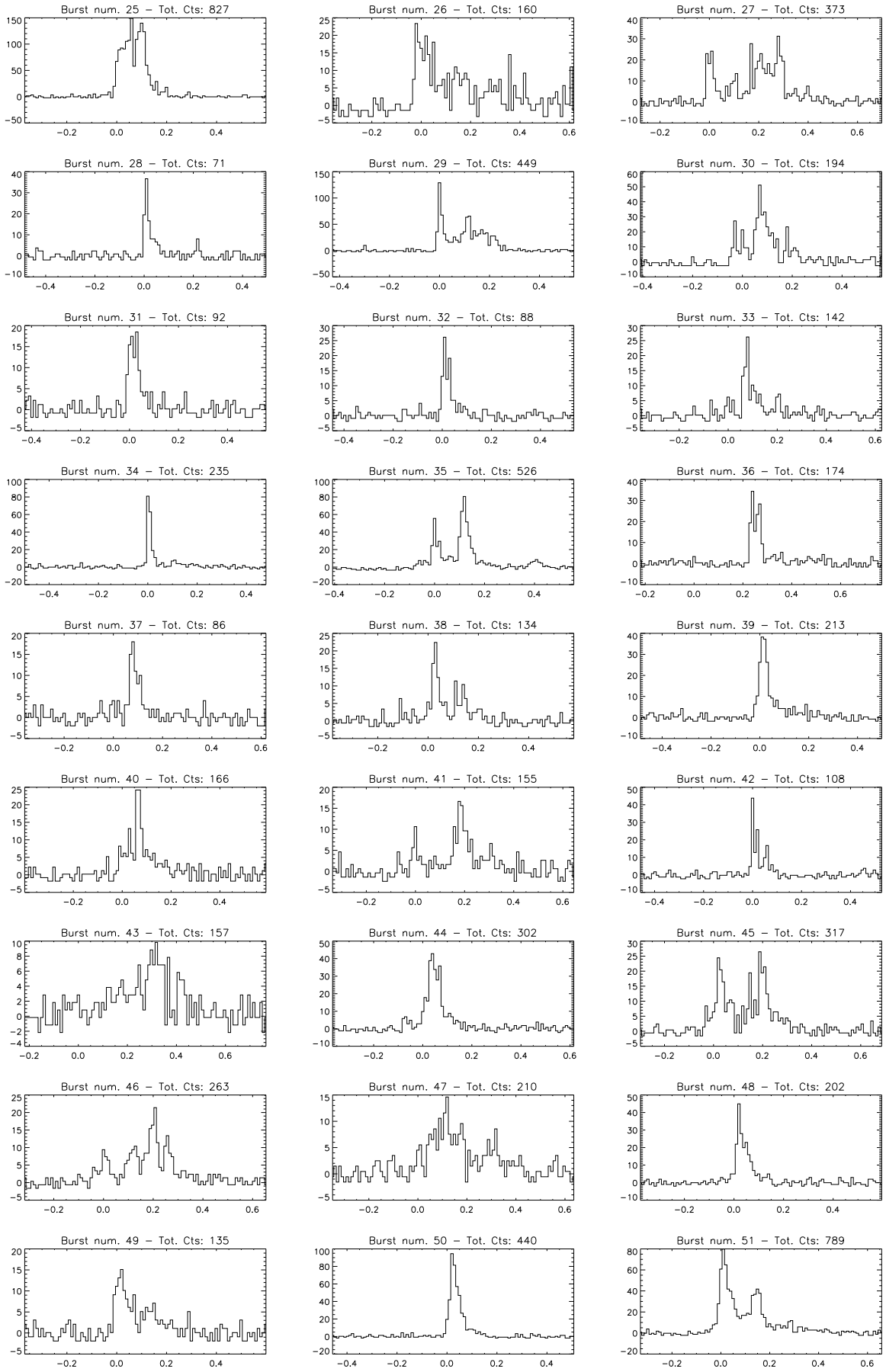

Figure 4.10: 15-40 keV light curves of the bursts of the second dataset. Binsize = 10ms

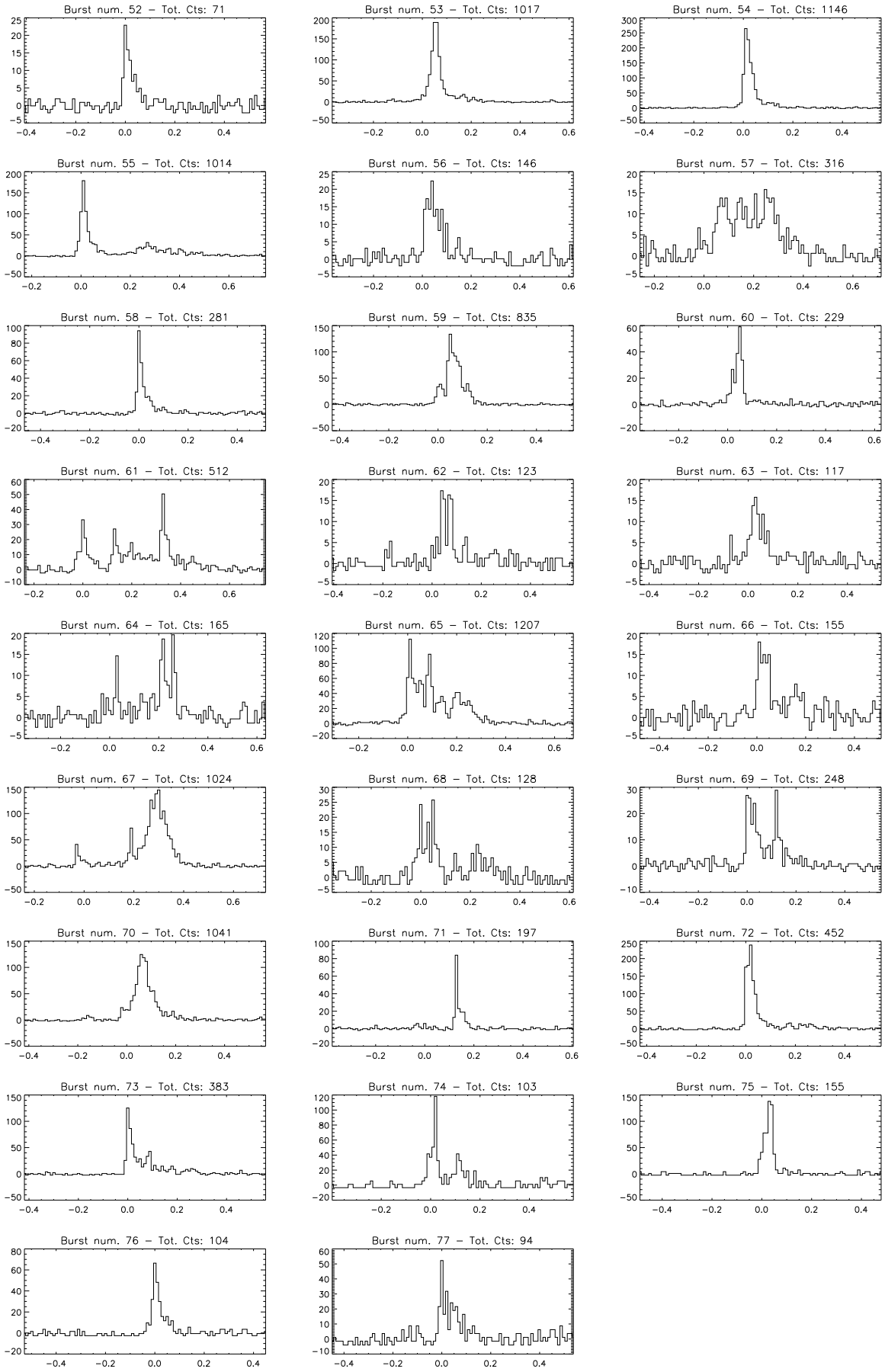

Figure 4.11: 15-40 keV light curves of the bursts of the second dataset. Binsize = 10ms

Burst Number	Fluence 10^{-8} erg cm^{-2}	Peak Flux 10^{-7} erg cm^{-2} s^{-1}	T_{90} ms
25	22.65 ± 0.58	22.40 ± 1.83	159
26	4.27 ± 0.25	3.51 ± 0.72	548
27	6.67 ± 0.31	4.70 ± 0.84	388
28	1.54 ± 0.15	5.51 ± 0.91	69
29	13.41 ± 0.44	19.40 ± 1.70	228
30	5.81 ± 0.29	7.68 ± 1.07	269
31	1.41 ± 0.14	2.77 ± 0.64	69
32	1.33 ± 0.14	3.92 ± 0.76	49
33	2.15 ± 0.17	3.94 ± 0.76	317
34	3.53 ± 0.23	12.16 ± 1.35	169
35	7.91 ± 0.34	12.10 ± 1.34	388
36	2.62 ± 0.19	5.16 ± 0.88	478
37	1.29 ± 0.13	2.70 ± 0.63	119
38	2.02 ± 0.17	3.37 ± 0.71	159
39	3.21 ± 0.21	5.75 ± 0.92	159
40	2.51 ± 0.19	3.63 ± 0.73	269
41	2.34 ± 0.18	2.50 ± 0.61	347
42	1.62 ± 0.15	6.58 ± 0.99	59
43	2.37 ± 0.18	1.47 ± 0.47	476
44	4.55 ± 0.26	6.43 ± 0.98	168
45	4.78 ± 0.26	3.97 ± 0.77	288
46	3.97 ± 0.24	3.21 ± 0.69	425
47	3.20 ± 0.21	2.19 ± 0.57	387
48	3.05 ± 0.21	6.75 ± 1.00	109
49	2.04 ± 0.17	2.27 ± 0.58	199
50	6.72 ± 0.31	14.22 ± 1.46	99
51	11.86 ± 0.422	11.99 ± 1.34	319
52	1.07 ± 0.12	3.44 ± 0.71	49
53	15.29 ± 0.47	28.41 ± 2.06	169
54	17.24 ± 0.50	39.71 ± 2.44	119
55	15.27 ± 0.47	26.87 ± 2.01	449
56	2.22 ± 0.18	3.36 ± 0.71	119
57	4.80 ± 0.26	2.37 ± 0.59	336
58	4.30 ± 0.25	14.16 ± 1.45	99
59	12.71 ± 0.43	20.09 ± 1.73	129
60	3.50 ± 0.22	8.88 ± 1.15	179

Table 4.5: Fluences (15-100 keV), Peak Fluxes (over 10 ms, 15-100 keV), T_{90} durations.

61	7.80 ± 0.34	7.57 ± 1.06	448
62	1.85 ± 0.16	2.60 ± 0.62	267
63	1.77 ± 0.16	2.37 ± 0.59	297
64	2.49 ± 0.19	2.95 ± 0.66	307
65	18.15 ± 0.52	16.87 ± 1.59	268
66	2.33 ± 0.18	2.69 ± 0.63	289
67	22.75 ± 0.58	21.76 ± 1.80	359
68	2.86 ± 0.20	3.87 ± 0.76	248
69	3.73 ± 0.23	4.34 ± 0.80	169
70	15.64 ± 0.48	18.72 ± 1.67	189
71	2.96 ± 0.21	12.61 ± 1.37	168
72	16.45 ± 0.49	35.90 ± 2.32	248
73	8.98 ± 0.36	18.82 ± 1.68	249
74	6.99 ± 0.32	17.77 ± 1.63	199
75	7.83 ± 0.34	20.74 ± 1.76	59
76	3.19 ± 0.21	9.99 ± 1.22	69
77	3.64 ± 0.23	7.85 ± 1.08	488

Table 4.6: Fluences (15-100 keV), Peak Fluxes (over 10 ms, 15-100 keV), T_{90} durations.

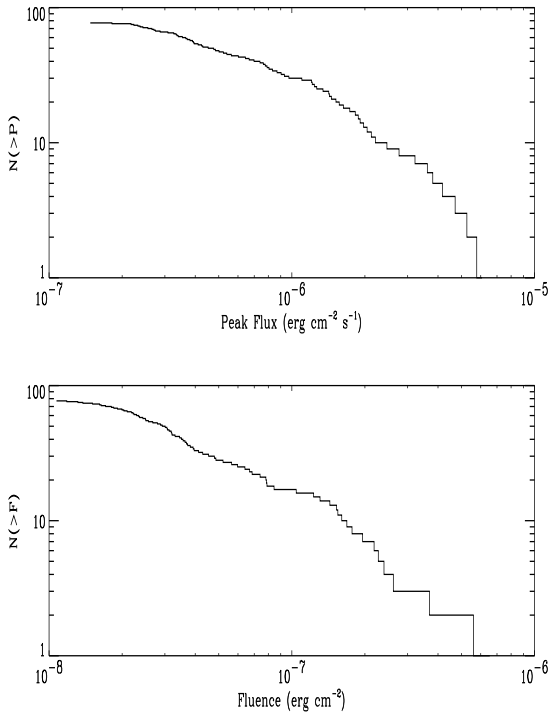

Figure 4.12: Integral distributions of Peak flux (Δt=10 ms, *Upper Panel*) and fluences (*Lower Panel*). Both refer to the 15-100 keV energy range.

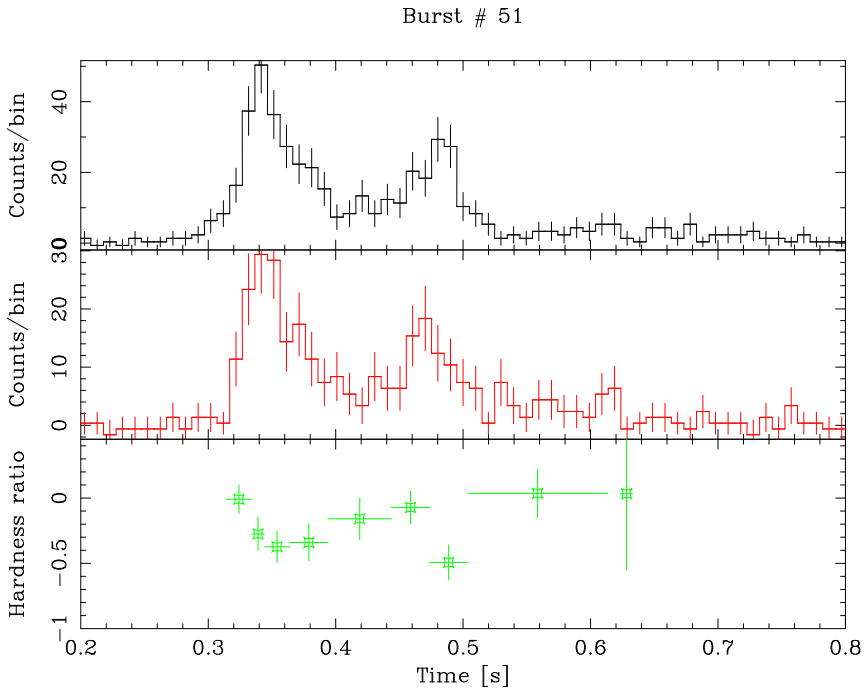

Figure 4.13: 15-30 keV light curve (*Top Panel*), 30-100 keV light curve (*Middle Panel*), and time resolved hardness ratio (*Bottom Panel*) for four burst number 51.

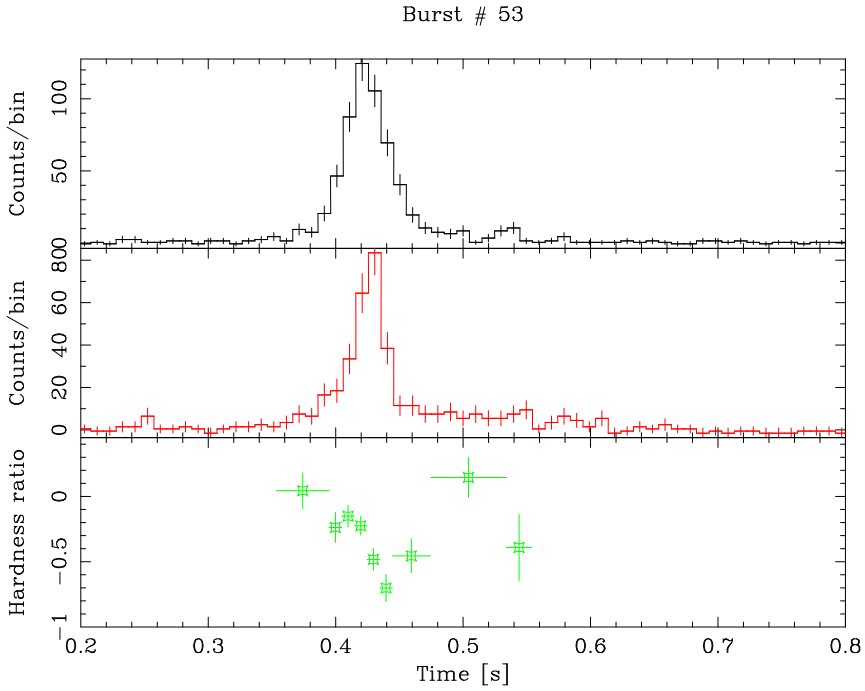

Figure 4.14: 15-30 keV light curve (*Top Panel*), 30-100 keV light curve (*Middle Panel*), and time resolved hardness ratio (*Bottom Panel*) for four burst number 53.

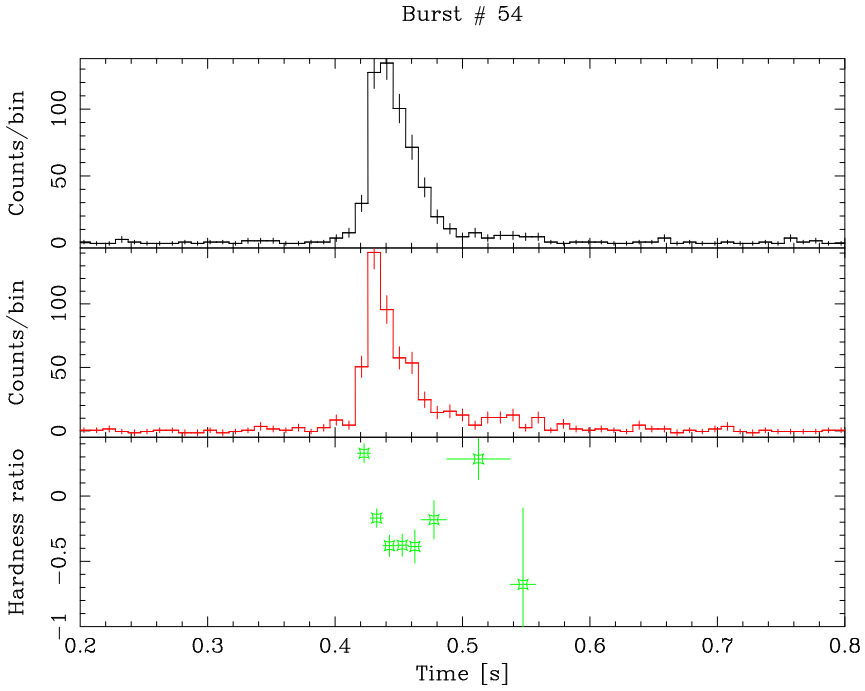

Figure 4.15: 15-30 keV light curve (*Top Panel*), 30-100 keV light curve (*Middle Panel*), and time resolved hardness ratio (*Bottom Panel*) for four burst number 54.

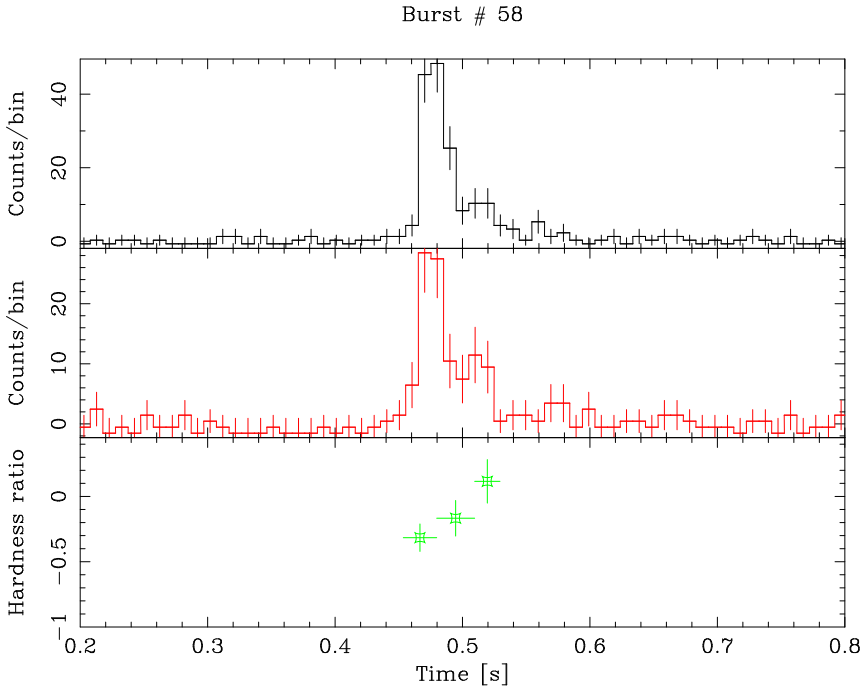

Figure 4.16: 15-30 keV light curve (*Top Panel*), 30-100 keV light curve (*Middle Panel*), and time resolved hardness ratio (*Bottom Panel*) for four burst number 58.

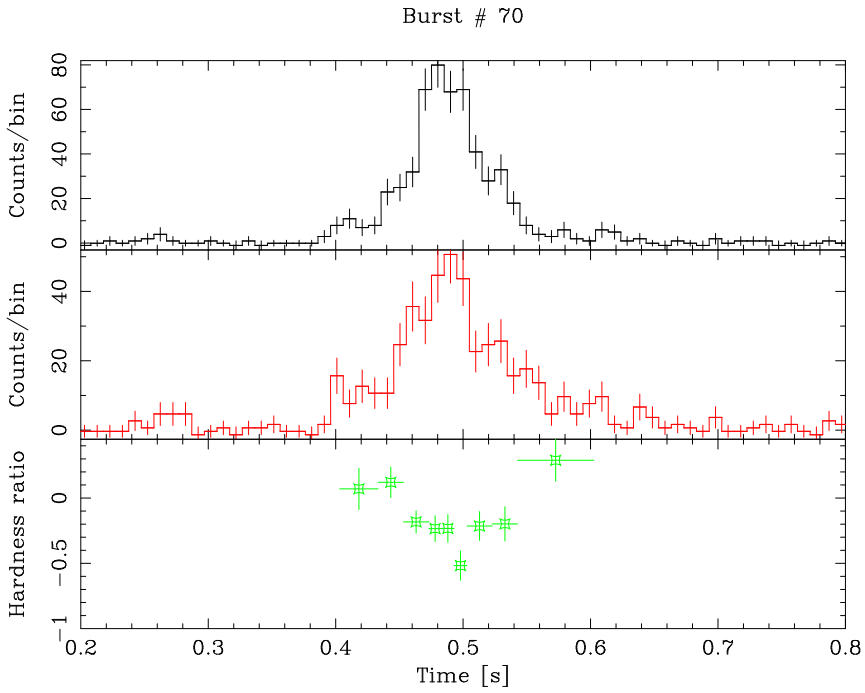

Figure 4.17: 15-30 keV light curve (*Top Panel*), 30-100 keV light curve (*Middle Panel*), and time resolved hardness ratio (*Bottom Panel*) for four burst number 70.

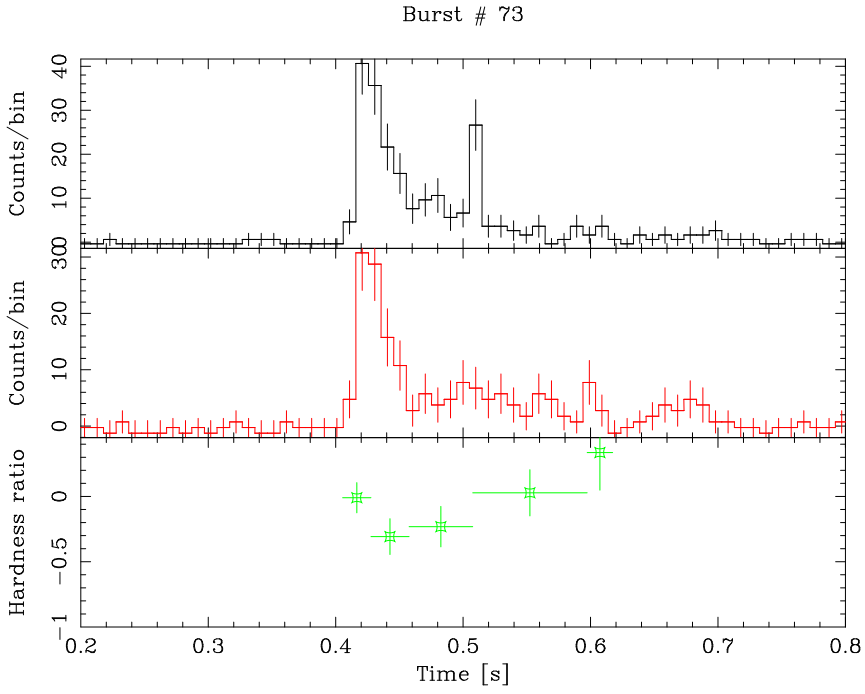

Figure 4.18: 15-30 keV light curve (*Top Panel*), 30-100 keV light curve (*Middle Panel*), and time resolved hardness ratio (*Bottom Panel*) for four burst number 73.

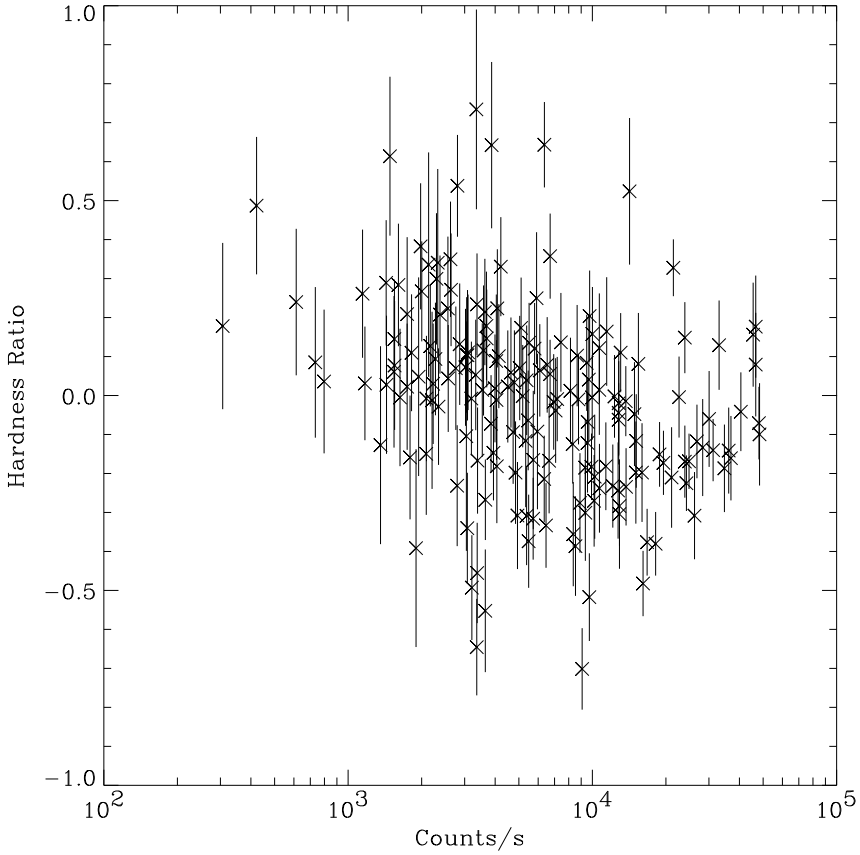

Figure 4.19: Hardness-Intensity plot of the time resolved hardness ratios of the 12+16 bursts with the best statistics (both datasets). The hardness ratio is defined as $(H - S)/(H + S)$, where H and S are the background subtracted counts in the ranges 30-100 keV and 15-30 keV respectively. The count rates are corrected for the vignetting and refer to the 15-100 keV range.

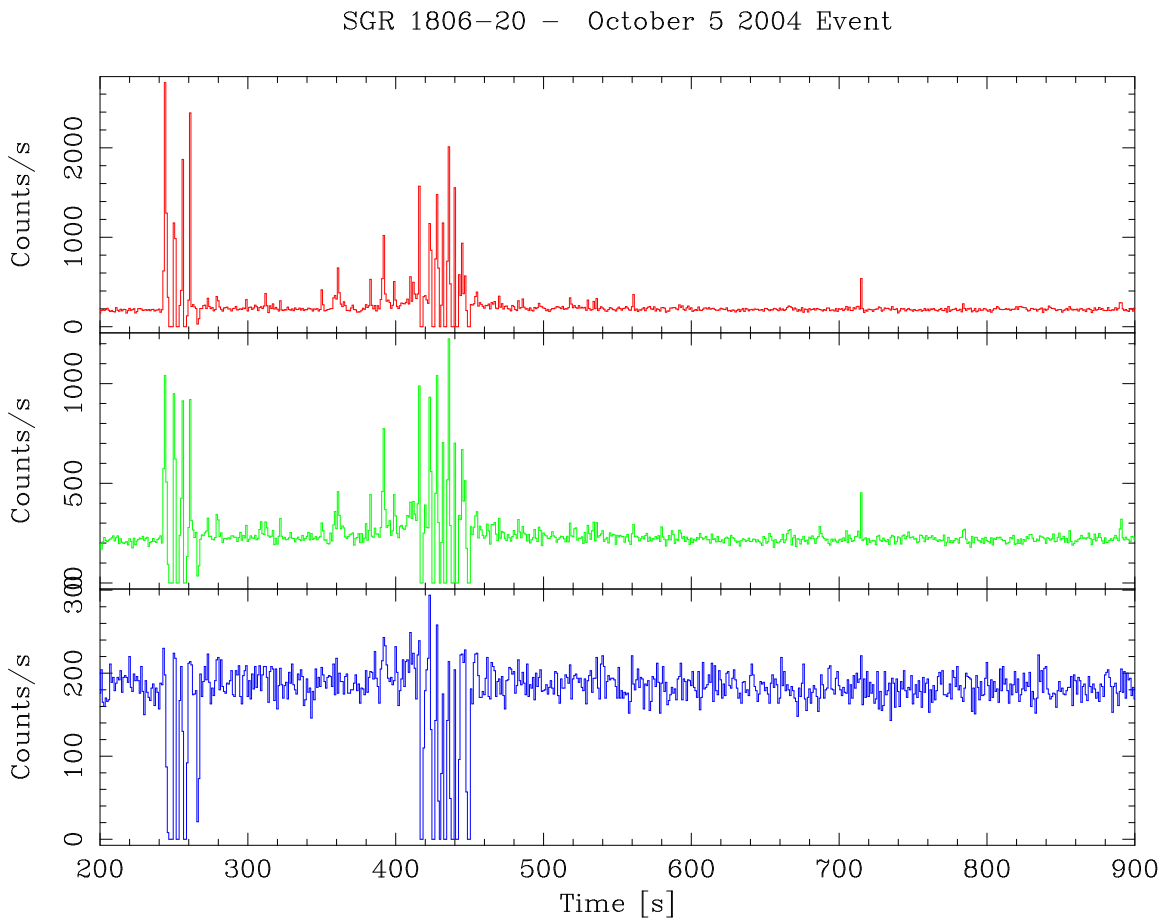

Figure 4.20: IBIS/ISGRI light curves (15-40 keV, upper panel, 40-100 keV, middle panel, 100-300 keV, lower panel) of the huge outburst of SGR 1806–20 on October 5 2004. Time bin is 1 s.

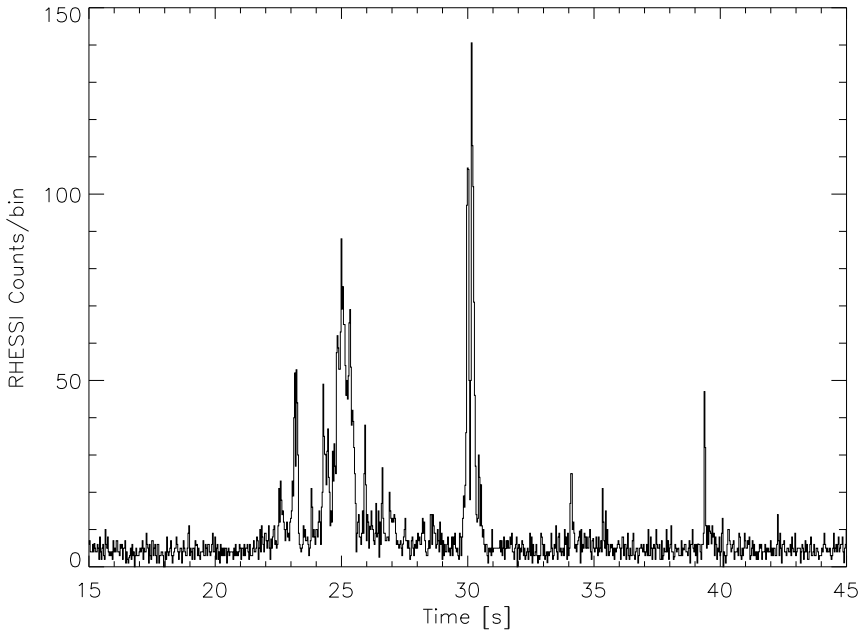

Figure 4.21: *RHESSI* light curve (25-150 keV) of the first cluster of bursts. Time bin is 0.031 s. Data courtesy Kevin Hurley.

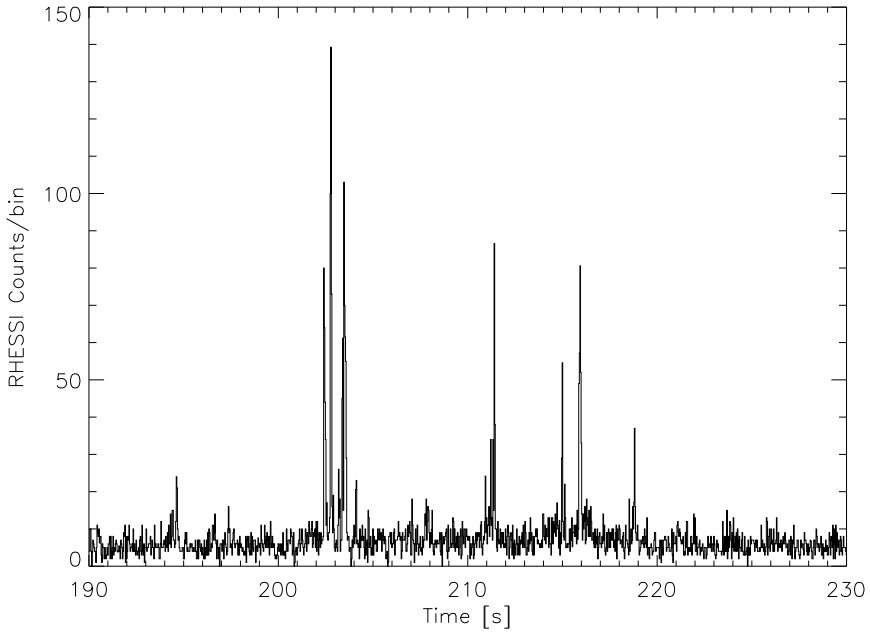

Figure 4.22: *RHESSI* light curve (25-150 keV) of the second cluster of bursts. Time bin is 0.031 s. Data courtesy Kevin Hurley.

Conclusions

One of the aims of the work done in this Thesis was to provide the scientific community with a new tool to study the highly variable γ-ray sky. This tool is the *INTEGRAL* Burst Alert System (IBAS, see Chapter 2), which searches the *INTEGRAL* data for GRBs, localizes them and distributes their coordinates in real time. My contribution to this System has been to perform the simulations of the IBIS/ISGRI instrument before the *INTEGRAL* launch, in order to develop the fast imaging and detection algorithms used by IBAS. In addition some tools to interactively analyze the GRB data (spectra, images and light curves production) have been developed. Besides that, I have tested and integrated also the other parts of the System. After the launch the detection parameters and programs had to be optimized to cope with the flight data. A maintenance and development work (mainly aimed at the enhancement of the System sensitivity and at the lowering of the rate of false Alerts) has been performed and is on-going. Thanks to it, IBAS is now working and providing the best performances in terms of speed and localization accuracy ever.

IBAS has detected 18 GRBs up to now. Their detailed analysis has been presented in Chapter 3. From the prompt emission point of view, *INTEGRAL* GRBs do not reveal any new feature with respect to bursts detected with previous instruments. They are just weaker and our analysis allowed us to confirm that many of the characteristics that apply to stronger bursts, apply also to the weaker ones. It can be pointed out that the relatively small energy range of IBIS/ISGRI does not allow, in most of the cases, to study the typical curvature of GRB spectra, but nevertheless it allows to constrain well the low energy power-law slope. The most interesting results came from the follow-ups at longer wavelength of *INTEGRAL* GRBs. Thanks to the rapid multi-wavelength observation campaigns in response to the IBAS Alerts, we are providing a new insight into the early phases of the afterglows of relatively weak GRBs. The case of GRB 031203 is particularly interesting: during the *XMM-Newton* observation of its afterglow an expanding X-ray scattering halo has been discovered. This burst has been spectroscopically associated with a type Ic Supernova (SN 2003lw), and its redshift (z=0.105) places it among the closest and faintest GRBs with a total energy release in γ-rays of $\sim 10^{50}$ ergs.

IBAS can also provide real time information for other sources, besides GRBs.

Thanks to it, more than 100 short bursts from the Soft Gamma Repeater SGR 1806–20 have been discovered, providing a large database of good quality data. In fact, we have been able to study their spectral and temporal properties in detail (see Chapter 4). We can summarize our results on SGR 1806–20 as follows:

- For the first time good evidence for spectral evolution of weak SGR bursts is detected and a hardness-intensity anti-correlation within the bursts has been found (Götz et al., 2004e). These results represent a new challenge for the *Magnetar* model, which predicts that the effective temperature of the bursts should vary weakly during the bursts, while we detect large spectral variations within the bursts.

- IBAS monitoring of the source indicates that its activity is still growing. A huge ($\sim$ 10 minutes long) outburst from SGR 1806–20, composed of tens of bursts, has been discovered in real-time by IBAS on October 5, 2004.

Appendix A

Refereed Papers

- S. Mereghetti, **D. Götz**, A.Tiengo, V. Beckmann, J. Borkowski, T.J.-L. Courvoisier, A. von Kienlin, V. Schnfelder, J.P. Roques, L. Bouchet, P. Ubertini, A. Castro-Tirado, F. Lebrun, J. Paul, N. Lund, M. Mas Hesse, W. Hermsen, P. den Hartog, C. Winkler, *INTEGRAL and XMM-Newton observations of the weak GRB 030227*, 2003, ApJ, 590, L73

- **D. Götz**, S. Mereghetti, K. Hurley, S. Deluit, M. Feroci, F. Frontera, A. Fruchter, J. Gorosabel, D.H. Hartmann, J. Hjorth, R. Hudec, I.F. Mirabel, E. Pian, G. Pizzichini, P. Ubertini, C. Winkler, *Observation of GRB 030131 with the INTEGRAL satellite*, 2003, A&A, 409, 831

- S. Mereghetti, **D. Götz**, J. Borkowski, R. Walter and H. Pedersen, *The INTEGRAL Burst Alert System (IBAS)*, 2003, A&A, 411, L291

- G. Malaguti, A. Bazzano, V. Beckmann, A.J. Bird, M. Del Santo, G. Di Cocco, L. Foschini, P. Goldoni, **D. Götz**, S. Mereghetti, A. Paizis, A. Segreto, G. Skinner, P. Ubertini, A. von Kienlin, *GRB 021125: the first GRB imaged by INTEGRA*L, 2003, A&A, 411, L307

- S. Mereghetti, **D. Götz**, V. Beckmann, A. von Kienlin, P. Ubertini, A. Bazzano, L. Foschini and G. Malaguti, *GRB 021219: the first Gamma-Ray Burst localized in real time with IBAS*, 2003, A&A, 411, L311

- A. von Kienlin, V. Beckmann, S. Covino, **D. Götz**, G. C. Lichti, D. Malesani, S. Mereghetti, E. Molinari, A. Rau, C. R. Shrader, S. J. Sturner and F. Zerbi, *Integral Results on GRB 030320: a long gamma-ray burst detected at the edge of the field of view*, 2003, A&A, 411, L321

- V. Beckmann, J. Borkowski, T.J.-L. Courvoisier, **D. Götz**, R. Hudec, F. Hroch, N. Lund, S. Mereghetti, S.E. Shaw, C. Wigger, *Time resolved spectroscopy of GRB 030501 using INTEGRAL*, 2003, A&A, 411, L327

- **D. Götz**, S. Mereghetti, I.F. Mirabel, and K. Hurley, *Spectral evolution of weak bursts from SGR 1806-20 observed with INTEGRAL*, 2004, A&A, 417, L45

- D. Malesani, G. Tagliaferri, G. Chincarini, S. Covino, M. Della Valle, D. Fugazza, P.A. Mazzali, F.M. Zerbi, P. D'Avanzo, S. Kalogerakos, A. Simoncelli, L.A. Antonelli, L. Burderi, S. Campana, A. Cucchiara, F. Fiore, G. Ghirlanda, P. Goldoni, **D. Götz**, S. Mereghetti, I.F. Mirabel, P. Romano, L. Stella, T. Minezaki, Y. Yoshii, K. Nomoto, *SN 2003lw and GRB 031203: A Bright Supernova For A Faint Gamma-Ray Burst*, 2004, ApJ, 609, L5

Not Included:

- L. Moran, S. Mereghetti, **D. Götz**, L. Hanlon, A. von Kienlin, B. McBreen, A. Tiengo, R. Preece, O.R. Williams, K. Bennet, R.M. Kippen, S. McBreen, S. McGlynn, *INTEGRAL and XMM-Newton Observations of GRB 040106*, 2004, A&A, in press

- S. Mereghetti, **D. Götz**, M.I. Andersen, A. Castro-Tirado, F. Frontera, D.H. Hartmann, J. Hjorth, R. Hudec, K. Hurley, G. Pizzichini, N. Produit, A. Tarana, M. Topinka, P. Ubertini, *GRB 040403: a faint X-ray rich Gamma-Ray burst discovered by INTEGRAL* , 2004, A&A, submitted

THE ASTROPHYSICAL JOURNAL, 590:L73–L77, 2003 June 20

INTEGRAL AND *XMM-NEWTON* OBSERVATIONS OF THE WEAK GAMMA-RAY BURST GRB 030227[1]

S. MEREGHETTI,[2] D. GÖTZ,[2] A. TIENGO,[2] V. BECKMANN,[3,4] J. BORKOWSKI,[3] T. J.-L. COURVOISIER,[3] A. VON KIENLIN,[5] V. SCHOENFELDER,[5] J. P. ROQUES,[6] L. BOUCHET,[6] P. UBERTINI,[7] A. CASTRO-TIRADO,[8] F. LEBRUN,[9] J. PAUL,[9] N. LUND,[10] J. M. MAS-HESSE,[11] W. HERMSEN,[12] P. R. DEN HARTOG,[12] AND C. WINKLER[13]

Received 2003 March 20; accepted 2003 May 14; published 2003 May 27

ABSTRACT

We present *International Gamma-Ray Astrophysical Laboratory* (*INTEGRAL*) and *XMM-Newton* observations of the prompt γ-ray emission and the X-ray afterglow of GRB 030227, the first gamma-ray burst for which the quick localization obtained with the *INTEGRAL* Burst Alert System has led to the discovery of X-ray and optical afterglows. GRB 030227 had a duration of about 20 s and a peak flux of ~1.1 photons cm^{-2} s^{-1} in the 20–200 keV energy range. The time-averaged spectrum can be fitted by a single power law with photon index ~2, and we find some evidence for a hard-to-soft spectral evolution. The X-ray afterglow has been detected starting only 8 hr after the prompt emission, with a 0.2–10 keV flux decreasing as t^{-1} from 1.3×10^{-12} to 5×10^{-13} ergs cm^{-2} s^{-1}. The afterglow spectrum is well described by a power law with photon index 1.94 ± 0.05 modified by a redshifted neutral absorber with column density of several 10^{22} cm^{-2}. A possible emission line at 1.67 keV could be due to Fe for a redshift $z \sim 3$, consistent with the value inferred from the absorption.

Subject headings: gamma rays: bursts — X-rays: general

1. INTRODUCTION

Our understanding of gamma-ray bursts (GRBs), one of the mysteries of high-energy astrophysics for more than 25 years, advanced dramatically after the discovery of their X-ray, optical, and radio afterglows (see, e.g., van Paradijs, Kouveliotou, & Wijers 2000). Currently, the multiwavelengths study of GRBs is providing a wealth of results relevant for several branches of astrophysics. Besides the study of the prompt emission, a rapid and accurate localization is crucial to pursue these objectives and fully exploit the information on the GRB afterglows and host environment. Such a capability was first achieved by the *BeppoSAX* satellite, which located more than 45 GRBs from 1997 to 2002 (see, e.g., Amati et al. 2002) and is currently provided by the *High Energy Transient Explorer 2*, a satellite specifically devoted to this task (Ricker et al. 2002).

The *International Gamma-Ray Astrophysical Laboratory* (*INTEGRAL*) satellite (Winkler et al. 1999) was successfully launched on 2002 October 17. The *INTEGRAL* payload consists of two γ-ray instruments operating in the ~15 keV–10 MeV range: the Imager on Board the *INTEGRAL* Satellite (IBIS; Ubertini et al. 1999) and the Spectrometer on *INTEGRAL* (SPI; Vedrenne et al. 1999). Both are coded mask telescopes[14] optimized for angular and spectral resolution, respectively.

Although not specifically devoted to GRB studies, thanks to the large field of view and good imaging capabilities of its γ-ray instruments, *INTEGRAL* is able to localize GRBs at an expected rate of 1–2 per month (Mereghetti, Cremonesi, & Borkowski 2001a). The data are immediately transmitted to the ground, and it is possible to derive the coordinates of detected GRBs with very small delays. Automatic software, the *INTEGRAL* Burst Alert System (IBAS; Mereghetti et al. 2001b), has been developed at the *INTEGRAL* Science Data Center (ISDC; Courvoisier et al. 1999) to exploit these capabilities. As soon as telemetry reaches the ISDC, the IBAS software screens the data in real time looking for the presence of potential GRBs, performs a rapid imaging analysis of the candidates, and eventually distributes the positions of the GRBs via the Internet.

In line with prelaunch expectations, five GRBs have been detected to date in the field of view of the *INTEGRAL* instruments: GRB 021125 (Bazzano & Paizis 2002), GRB 021219 (Mereghetti, Götz, & Borkowski 2002), GRB 030131 (Borkowski et al. 2003), GRB 030227 (Götz et al. 2003a), and GRB 030320 (Mereghetti, Götz, & Borkowski 2003). Their positions have been determined with errors in the 2′–4′ range. Here we report on the observations of GRB 030227, the first GRB for which our prompt localization has led to the successful identification of X-ray (Loiseau et al. 2003) and optical afterglows (Castro-Tirado et al. 2003a; Soderberg et al. 2003).

[1] Based on observations with *INTEGRAL*, an ESA project with instruments and science data center funded by ESA member states (especially the PI countries: Denmark, France, Germany, Italy, Switzerland, and Spain), the Czech Republic, and Poland and with the participation of Russia and the US, and *XMM-Newton*, an ESA science mission with instruments and contributions directly funded by ESA member states and the US.

[2] Istituto di Astrofisica Spaziale e Fisica Cosmica, Sezione di Milano "G. Occhialini," CNR, via Bassini 15, I-20133 Milan, Italy; sandro@mi.iasf.cnr.it.

[3] *INTEGRAL* Science Data Center, Chemin d' Écogia 16, CH-1290 Versoix, Switzerland.

[4] Institut für Astronomie und Astrophysik, Universität Tübingen, Sand 1, D-72076 Tübingen, Germany.

[5] Max-Planck-Institut für extraterrestrische Physik, Postfach 1312, D-85741 Garching, Germany.

[6] Centre d'Etude Spatiale des Rayonnements, 9, Avenue du Colonel Roche, BP 4346, 31028 Toulouse Cedex 4, France.

[7] Istituto di Astrofisica Spaziale e Fisica Cosmica, CNR, via del Fosso del Cavaliere, I-00133 Rome, Italy.

[8] Instituto de Astrofísica de Andalucía (IAA-CSIC), P.O. Box 03004, 18080 Granada, Spain.

[9] Centre d'Etudes de Saclay, DAPNIA/Service d'Astrophysique, Batiment 709, Orme des Merisiers, Gif-sur-Yvette Cedex 91191, France.

[10] Danish Space Research Institute, Juliane Maries Vej 30, Copenhagen 0 DK-2100, Denmark.

[11] Centro de Astrobiología, Instituto Nacional de Técnica Aeroespacial (CSIC-INTA), Ctra. de Ajalvir, E-28850 Torrejon de Ardoz, Spain.

[12] Space Research Organization of the Netherlands, National Institute for Space Research, 3584 Utrecht, Netherlands.

[13] European Space Research and Technology Center, Research and Scientific Support Department, Keplerlaan 1, 2201 AZ Noordwijk, Netherlands.

[14] With the coded mask technique, it is possible to obtain images at energies at which photons cannot be easily reflected by interposing a partially absorbing mask between the source and a position-sensitive detector (see, e.g., Dean 1983).

2. *INTEGRAL* OBSERVATION

IBIS detected GRB 030227 with its low-energy detector ISGRI (*INTEGRAL* Soft Gamma-Ray Imager; Lebrun et al. 2001), an array of 128 × 128 CdTe crystals sensitive in the energy range from ~15 keV to 1 MeV. ISGRI has an effective area of the order of 1000 cm^2 and provides an angular resolution of ~12′ over a 29° × 29° field of view. Bright sources can be located with good accuracy (for example, the 90% confidence level [c.l.] error radius for a source with a signal-to-noise ratio of ~10 is as small as 1′). The SPI instrument observes with a coarser angular resolution (~2°) the same region of sky covered by IBIS, providing a better energy resolution (FWHM = 2.5 keV at 1 MeV). The detector consists of 19 Ge crystals cooled to 85 K, surrounded by a thick anticoincidence shield (ACS) of BGO scintillation crystals.

GRB 030227 was detected by the IBAS program based on the analysis of the IBIS/ISGRI data, consisting of positional, timing, and energy information of each detected photon. The IBAS alert message with the preliminary position of the burst (R.A. = $4^h57^m24^s$, decl. = +20°28′24″, J2000.0) was delivered to the IBAS Team at 08:42:38 UT on 2003 February 27, only 35 s after the start of the burst (most of this delay was due to buffering of the telemetry on board the satellite and to data transmission between the ground station and the ISDC). Unfortunately, the Internet message with these coordinates could not be distributed in real time.[15] Nevertheless, this information was distributed within less than 1 hr, after the GRB had been confirmed by an interactive analysis of the data (Götz et al. 2003a). Further analysis resulted in an improved localization at R.A. = $4^h57^m32\overset{s}{.}2$, decl. = +20°29′54″ (Götz et al. 2003b), with an error of 3′ dominated by systematic uncertainties. This position differs by only 50″ from that of the optical transient (Castro-Tirado et al. 2003a).

The IBIS/ISGRI light curve of GRB 030227 is shown in Figure 1*a*. The burst, which started approximately at 08:42:03 UT, had a typical fast rise and exponential decay profile, with a rise to the peak in 2 s and a decay well described by an exponential with *e*-folding decay time of 11 ± 1 s. The peak flux, integrated over 1 s, is 1.1 photons cm^{-2} s^{-1} in the 20–200 keV energy range. The fluence, in the same range and assuming the average spectrum discussed below, is 7.5 × 10^{-7} ergs cm^{-2}.

GRB 030227 was detected with a signal-to-noise ratio of ~20 at off-axis angles $Z = 5\overset{\circ}{.}3$, $Y = 6\overset{\circ}{.}9$. Since a fully calibrated response matrix valid at these off-axis angles is not yet available, we derived the spectrum of GRB 030227 by comparing its count rate in different energy bins to the corresponding values obtained from the Crab Nebula observed at a similar position in the field of view. With this procedure we extracted the average burst spectrum for the time interval 08:42:04–08:42:26 UT, which is well described by a single power law with photon index 1.85 ± 0.2 over the 20–200 keV energy range.

GRB 030227 was also detected by SPI with a significance of 7.7 σ in the 20–200 keV range and localized (R.A. = $74\overset{\circ}{.}766$, decl. = $+20\overset{\circ}{.}531$) only $0\overset{\circ}{.}36$ off the IBIS position, owing to the less accurate location precision of SPI.

A spectrum was extracted for a time interval of 18 s starting at 08:42:04 UT. The background was estimated from a time interval of 35 minutes around the GRB but excluding the time span of the event itself. A power law with photon index of 1.9 ± 0.3 and 20–200 keV flux of 4.7 × 10^{-8} ergs cm^{-2} s^{-1} gives a good fit to these data. These values are consistent with those obtained with IBIS, confirming that the method used in the IBIS spectral analysis does not introduce important systematic effects.

To study the spectral evolution as a function of time, we defined a hardness ratio HR = $(H - S)/(H + S)$ based on the background-subtracted count rates in the ranges H = 40–100 keV and S = 20–40 keV. From the HR values of both SPI and IBIS, we found evidence for a hard-to-soft evolution. A time-resolved spectral analysis gave the power-law indices shown in Figure 1*b*, which confirm the indication of a possible spectral softening during the decaying part of the event.

The overall veto count rate of SPI's ACS showed no count rate increase that could be associated with the GRB. This is consistent with the fluxes quoted above and the low effective area of the ACS for directions corresponding to the SPI field of view (von Kienlin et al. 2001).

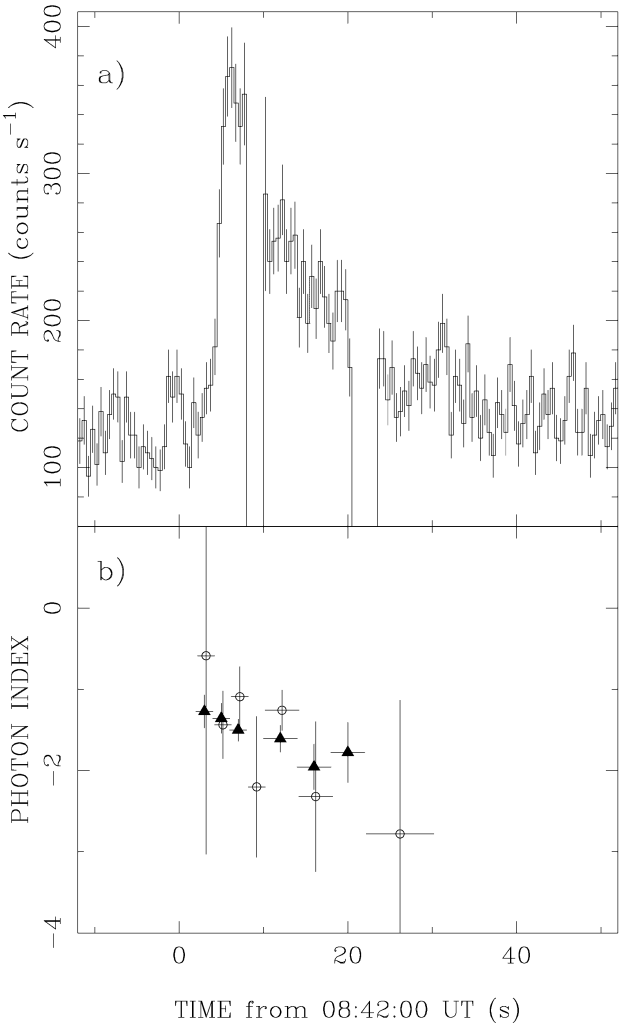

FIG. 1.—(*a*) IBIS/ISGRI light curve of GRB 030227 in the energy range 15–300 keV binned in 0.5 s intervals. The two small gaps at $t \sim 10$ and 20 s are artifacts due to telemetry saturation. (*b*) Power-law index as a function of time for IBIS (*triangles*) and SPI (*circles*). Error bars are at 1 σ.

[15] The detection of GRB 030227 occurred during a calibration observation of the Crab Nebula. Since the instrument configuration during these observations caused some spurious IBAS triggers, the automatic delivery of the alerts to external clients had been temporarily disabled.

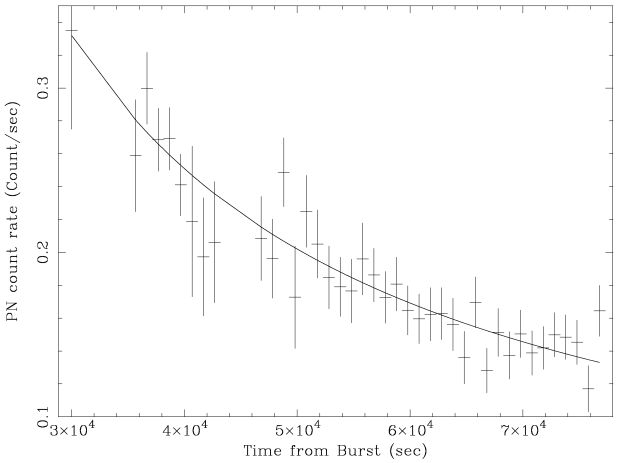

FIG. 2.—Light curve of the GRB 030227 afterglow fitted by a power-law function $F \propto t^{-\delta}$ with $\delta = 0.97$. All the points are from the PN, except for the first one obtained with the MOS (the remaining MOS points, consistent with the PN ones, are not plotted for clarity).

3. *XMM-NEWTON* OBSERVATION

XMM-Newton observed the position of GRB 030227 for ~13 hr, starting on February 27 at 16:58 UT. Because of the presence of a high particle background, the observation had to be interrupted twice, resulting in net exposures of 33 and 36 ks, respectively, in the PN and MOS cameras of the European Photon Imaging Camera (EPIC; Strüder et al. 2001; Turner et al. 2001). All the cameras operated in Full Frame mode and with the thin optical blocking filter. The data were processed using SAS version 5.4.1.

A bright and variable source was detected at R.A. = $04^{h}57^{m}33\overset{s}{.}1$, decl. = $+20°29'05''$ (error radius of 4″), well within the IBIS error circle of GRB 030227. The flux variability immediately suggested that this source was the GRB afterglow (Loiseau et al. 2003), as it was later confirmed by the discovery of a fading optical transient within its small error region. Figure 2 shows the background-subtracted PN light curve in the 0.2–10 keV energy range. The figure also shows the first flux measurement (at ~17:00 UT) obtained with the MOS camera, which started the observation earlier than the PN. The X-ray flux decay is well described by a power-law function, $F \propto t^{-\delta}$, with $\delta = 0.97 \pm 0.07$.

The source spectra were extracted from a circle of radius 40″ and rebinned to have at least 20 counts per channel and to oversample by a factor of 3 the instrumental energy resolution. For the PN, the background was extracted from a nearby rectangular region (1.′5 × 2′) in the same chip as the source and for the MOS from an annulus (radii of 1′ and 2′) centered on the source. All the errors on the spectral parameters given below are at the 90% c.l.

After checking that no significant variations in the best-fit parameters, except for the flux value, occurred during the observation, we performed a spectral fit of the whole PN data set. An absorbed power law gave an unacceptable fit (χ^2/degree of freedom [dof] = 272/209) with photon index $\Gamma = 2.04 \pm 0.05$ and $N_{\rm H} = 3.6^{+0.3}_{-0.2} \times 10^{21}$ cm^{-2}, larger than the Galactic absorption in this direction ($N_{\rm H} = 1.75 \times 10^{21}$ cm^{-2}; Hartmann & Burton 1997). An acceptable fit (χ^2/dof = 235/208; Fig. 3) could be obtained by fixing $N_{\rm H}$ to the Galactic value and adding a redshifted neutral absorption, $N_{{\rm H},z}$. This resulted in $\Gamma = 1.94 \pm 0.05$, $N_{{\rm H},z} = 6.8^{+1.8}_{-3.8} \times 10^{22}$ cm^{-2}, $z = 3.9 \pm 0.3$, and 0.2–10 keV observed flux $F_{\rm X} = 8.5 \times 10^{-13}$ ergs cm^{-2} s^{-1}. As shown in Figure 4, the redshift is not strongly constrained, its value being correlated with that of $N_{{\rm H},z}$. The best-fit values are only slightly dependent on the assumed Galactic $N_{\rm H}$ value: by varying it by ±30%, acceptable fits were always obtained with $\Gamma \sim 2$, while the 90% c.l. range of z and $N_{{\rm H},z}$ varied by less than 35%.

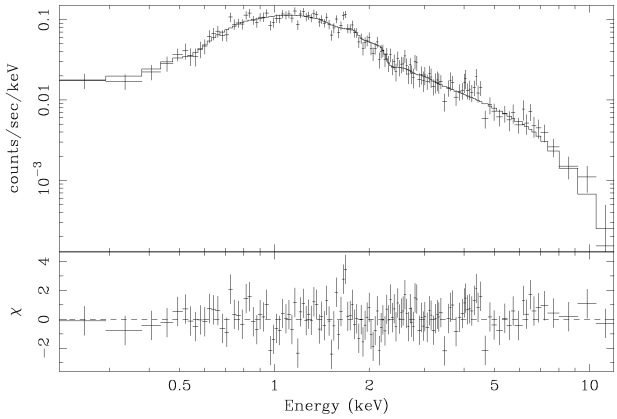

FIG. 3.—EPIC PN best-fit spectra of the afterglow of GRB 030227

Since the fit residuals of Figure 3 suggest the presence of possible lines in the spectrum, we tried to add Gaussian lines at different energies and with fixed widths, smaller than the instrumental resolution. The only possibly significant line was found at observed energy of $1.67^{+0.01}_{-0.03}$ keV. According to an F-test, this line is significant at the 3.2 σ level. However, such a probability value should be used with caution (Protassov et al. 2002), and we give it just to allow a comparison with other possible detections of lines reported for previous GRBs.

We also tried thermal models, both for the whole observation and for shorter time intervals, replacing the power-law component with a redshifted optically thin plasma model (MEKAL in XSPEC, with z linked to that of $N_{{\rm H},z}$). Keeping the elemental abundances fixed to the solar values resulted in unacceptable fits. Letting the abundances be free parameters, we obtained slightly better results (χ^2/dof = 260/207), with values of $N_{{\rm H},z}$ and z similar to the power-law case, and a temperature of ~25 keV. However, the corre-

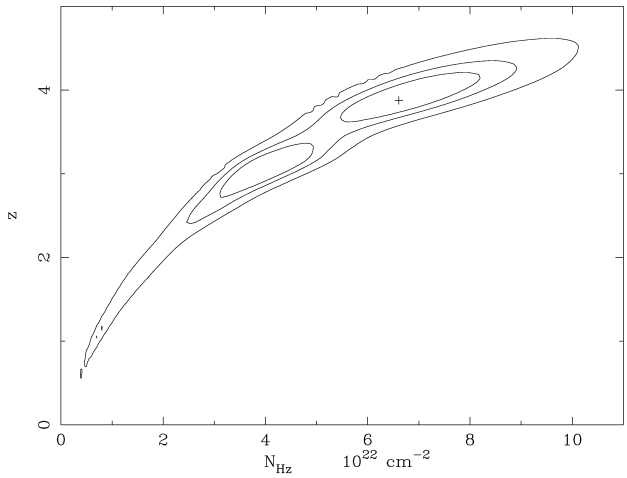

FIG. 4.—Confidence contours (68%, 90%, and 99% c.l.) of redshift and column density of the redshifted absorber from the fit of the whole PN data set.

sponding χ^2/dof values were always greater than in the power-law model.

Entirely consistent results were obtained with the MOS. As mentioned above, a short initial exposure was carried out only with the MOS, from 16:58 to 17:16 UT. These data do not provide enough statistics for a detailed spectral analysis, but they are consistent with the spectral parameters obtained for the rest of the observation. The corresponding flux is 1.34×10^{-12} ergs cm^{-2} s^{-1}.

4. DISCUSSION

The *INTEGRAL* data indicate that GRB 030227 belongs to the class of long GRBs. Its peak flux and fluence, converted to the 50–300 keV energy range used in the BATSE catalog, are, respectively, ~0.6 photons cm^{-2} s^{-1} and $\sim 7 \times 10^{-7}$ ergs cm^{-2} (these values slightly depend on the extrapolation; for example, a break in the spectrum at 120 keV to a slope of 2.5 would reduce them by 15%). About three-quarters of the GRBs in the fourth BATSE catalog (Paciesas et al. 1999) have a higher peak flux, indicating that GRB 030227 is quite faint. The possible evidence for a hard-to-soft spectral evolution in GRB 030227 suggests that such a trend, already observed in samples of brighter GRBs (Ford et al. 1995; Preece et al. 1998; Frontera et al. 2000), may also apply to relatively faint bursts.

GRB spectra usually show a curvature requiring more complex models than a single power law. A broken power law, with a smooth transition between the low-energy (α) and high-energy (β) slope, provides in most cases an adequate empirical description of the data (Band et al. 1993). By fitting such a function to our data, no improvement of the fit was obtained. A spectral break, if any, could occur outside the energy range over which we detected GRB 030227, most likely above ~100–200 keV as seen in most GRBs. Our photon index ~1.9 lies in the lower tail of the distribution of values of α (Preece et al. 2000), indicating that GRB 030227 is relatively soft. An extrapolation of its spectrum to lower energies leads to a ratio of fluences in the 6–30 to 30–400 keV ranges of 0.45 (or more if there is a high-energy break). This would qualify GRB 030227 as an X-ray–rich GRB (Heise et al. 2001; Barraud et al. 2003). In this context, it is interesting to note that its optical afterglow is particularly faint, $R \sim 23.3$ at $t - t_o = 12$ hr (Gorosabel et al. 2003), comparable to the dimmest GRB afterglows found so far.

The fading behavior of the source detected with EPIC and its positional coincidence with the optical transient qualify it as the X-ray afterglow of GRB 030227. Among the afterglows detected so far by *XMM-Newton*, this is the brightest and the one observed with the shortest delay after the prompt event ($t - t_o = 8$ hr). Its EPIC spectrum has the highest statistical quality among the afterglows detected to date with *XMM-Newton*. A power law with a redshifted absorber provides a statistically acceptable fit to the spectrum. We found tentative evidence for an emission line at 1.67 keV. If this line is due to Fe, as it has been suggested for similar features observed in other afterglows (see, e.g., Piro 2002), the implied redshift of ~2.7–3 (depending on the Fe ionization state) would be consistent with the value derived from the absorption. Other interpretations in terms of lighter elements are of course possible but somewhat arbitrary in the lack of an independent measure of z and/or other statistically significant lines.

Low-energy emission lines found in the initial part ($t - t_o \sim 11$–13 hr) of the GRB 011211 afterglow (Reeves et al. 2002, but see also Borozdin & Trudolyubov 2003) provide evidence for thermal emission from a plasma enriched in metals. Evidence for thermal emission in two other afterglows observed with *XMM-Newton*, GRB 010220 ($t - t_o \sim 15$ hr) and GRB 001025A ($t - t_o \sim 45$ hr), was reported by Watson et al. (2002a). On the other hand, the *XMM-Newton* spectra of the afterglow of GRB 020322 starting at $t - t_o \sim 15$ hr (Watson et al. 2002b) were adequately fitted with a power law. These results suggest that the presence of thermal components is not an ubiquitous property of all GRBs and/or it might be related only to some short-duration phases of the afterglows.

An upper limit to the redshift of $z \leq 3.5$ has been estimated from the absence of the onset of the Lyman forest blanketing in the optical data (Castro-Tirado et al. 2003b). This allows us to constrain the z-values derived by the X-ray spectral fitting (see Fig. 4), which is in any case greater than 1. The corresponding value of the local absorption $N_{H,z}$ of the order of a few times 10^{22} cm^{-2} supports the scenarios involving the occurrence of GRBs in regions of star formation (e.g., Galama & Wijers 2001).

Finally, we note that the rapid IBAS localization of GRB 030227 leading to the successful detection of its X-ray and optical afterglows, as well as the rate of ~1 GRB per month in the IBIS field of view observed so far, demonstrate that *INTEGRAL* will efficiently complement other satellites specifically devoted to GRB studies. We also expect that particularly interesting results will be obtained for a few bursts falling in the central part of the field of view, which is covered also by the *INTEGRAL* monitors operating in the optical (V band) and in the X-ray range (4.5–35 keV).

We thank the *XMM-Newton* staff for the prompt execution of the Target of Opportunity observation. The IBAS development has been funded by the Italian Space Agency. This research has been partially supported by the Spanish program AYA2002-0802 (including FEDER funds) and by Polish grant 2P03C00619p02 from KBN.

REFERENCES

Amati, L., et al. 2002, A&A, 390, 81
Band, D. L. 1993, ApJ, 413, 281
Barraud, C., et al. 2003, A&A, 400, 1021
Bazzano, A., & Paizis, A. 2002, GCN Circ. 1706 (http://gcn.gsfc.nasa.gov/gcn/gcn3/1706.gcn3)
Borkowski, J., Götz, D., & Mereghetti, S. 2003, GCN Circ. 1836 (http://gcn.gsfc.nasa.gov/gcn/gcn3/1836.gcn3)
Borozdin, K. N., & Trudolyubov, S. P. 2003, ApJ, 583, L57
Castro-Tirado, A., et al. 2003a, GCN Circ. 1904 (http://gcn.gsfc.nasa.gov/gcn/gcn3/1904.gcn3)
———. 2003b, A&A, submitted
Courvoisier, T., et al. 1999, Astrophys. Lett. Commun., 39, 355
Dean, A. J. 1983, Adv. Space Res., 3, 73
Ford, L. A. 1995, ApJ, 439, 307
Frontera, F., et al. 2000, ApJS, 127, 59
Galama, T. J., & Wijers, R. A. M. J. 2001, ApJ, 549, L209
Gorosabel, J., et al. 2003, GCN Circ. 1915 (http://gcn.gsfc.nasa.gov/gcn/gcn3/1915.gcn3)
Götz, D., Borkowski, J., & Mereghetti, S. 2003a, GCN Circ. 1895 (http://gcn.gsfc.nasa.gov/gcn/gcn3/1895.gcn3)
Götz, D., Mereghetti, S., & Borkowski, J. 2003b, GCN Circ. 1896 (http://gcn.gsfc.nasa.gov/gcn/gcn3/1896.gcn3)
Hartmann, D., & Burton, W. B. 1977, Atlas of Galactic Neutral Hydrogen (Cambridge: Cambridge Univ. Press)

Heise, J., in 't Zand, J., Kippen, R. M., & Woods, P. M. 2001, in Gamma-Ray Bursts in the Afterglow Era, ed. E. Costa, F. Frontera, & J. Hjorth (Heidelberg: Springer), 16
Lebrun, F., et al. 2001, in Proc. Fourth *INTEGRAL* Workshop, Exploring the Gamma-Ray Universe, ed. B. Battrick (ESA SP-459; Noordwijk: ESA), 591
Loiseau, N., et al. 2003, GCN Circ. 1901 (http://gcn.gsfc.nasa.gov/gcn/gcn3/1901.gcn3)
Mereghetti, S., Cremonesi, D., & Borkowski, J. 2001, in Gamma-Ray Bursts in the Afterglow Era, ed. E. Costa, F. Frontera, & J. Hjorth (Heidelberg: Springer), 363
Mereghetti, S., Götz, D., & Borkowski, J. 2002, GCN Circ. 1766 (http://gcn.gsfc.nasa.gov/gcn/gcn3/1766.gcn3)
———. 2003, GCN Circ. 1941 (http://gcn.gsfc.nasa.gov/gcn/gcn3/1941.gcn3)
Mereghetti, S., et al. 2001, in Proc. Fourth *INTEGRAL* Workshop, Exploring the Gamma-Ray Universe, ed. B. Battrick (ESA SP-459; Noordwijk: ESA), 513
Paciesas, W. S., et al. 1999, ApJS, 122, 465
Piro, L. 2002, preprint (astro-ph/0203275)
Preece, R. D., et al. 1998, ApJ, 496, 849
———. 2000, ApJS, 126, 19
Protassov, R., et al. 2002, ApJ, 571, 545
Reeves, J. N., et al. 2002, Nature, 416, 512
Ricker, G., et al. 2002, ApJ, 571, L127
Soderberg, A. M., et al. 2003, GCN Circ. 1907 (http://gcn.gsfc.nasa.gov/gcn/gcn3/1907.gcn3)
Strtlder, L., et al. 2001, A&A, 365, L18
Turner, M. J. L., et al. 2001, A&A, 365, L27
Ubertini, P., et al. 1999, Astrophys. Lett. Commun., 39, 331
van Paradijs, J., Kouveliotou, C., & Wijers, R. A. M. J. 2000, ARA&A, 38, 379
Vedrenne, G., et al. 1999, Astrophys. Lett. Commun., 39, 325
von Kienlin, A., et al. 2001, in Gamma-Ray Bursts in the Afterglow Era, ed. E. Costa, F. Frontera, & J. Hjorth (Heidelberg: Springer), 427
Watson, D., et al. 2002a, A&A, 393, L1
———. 2002b, A&A, 395, L41
Winkler, C., et al. 1999, Astrophys. Lett. Commun., 39, 309

A&A 409, 831–834 (2003)
DOI: 10.1051/0004-6361:20031128

Astronomy & Astrophysics

Observation of GRB 030131 with the INTEGRAL satellite⋆

D. Götz[1,2], S. Mereghetti[1], K. Hurley[3], S. Deluit[4], M. Feroci[5], F. Frontera[6,7], A. Fruchter[8], J. Gorosabel[8,16], D. H. Hartmann[9], J. Hjorth[10], R. Hudec[11], I. F. Mirabel[12,15], E. Pian[13], G. Pizzichini[7], P. Ubertini[5], and C. Winkler[14]

[1] Istituto di Astrofisica Spaziale e Fisica Cosmica – CNR, Sezione di Milano "G. Occhialini", Via Bassini 15, 20133 Milano, Italy
[2] Dipartimento di Fisica, Università degli Studi di Milano Bicocca, P.zza della Scienza 3, 20126 Milano, Italy
[3] UC Berkeley Space Sciences Laboratory, Berkeley CA 94720-7450, USA
[4] Integral Science Data Centre, Chemin d'Écogia 16, 1290 Versoix, Switzerland
[5] Istituto di Astrofisica Spaziale e Fisica Cosmica – CNR, via Fosso del Cavaliere 100, 00133 Roma, Italy
[6] Dipartimento di Fisica, Università di Ferrara, Via Paradiso 12, 44100 Ferrara, Italy
[7] Istituto di Astrofisica Spaziale e Fisica Cosmica – CNR, Sezione di Bologna, via Piero Gobetti 101, 40129 Bologna, Italy
[8] Space Telescope Science Institute, 3700 San Martin Drive, Baltimore, MD 21218, USA
[9] Department of Physics and Astronomy, Clemson University, Clemson, SC 29634-0978, USA
[10] Astronomical Observatory, University of Copenhagen, Juliane Maries Vej 30, 2100 Copenhagen, Denmark
[11] Astronomical Institute, Academy of Sciences of the Czech Republic, 251 65 Ondrejov, Czech Republic
[12] Service d'Astrophysique, CEA/Saclay, Orme des Merisiers, Bât. 709, 91191 Gif-sur-Yvette, France
[13] Osservatorio Astronomico di Trieste, Via GB Tiepolo 11, 34131 Trieste, Italy
[14] ESA-ESTEC, RSSD, Keplerlaan 1, 2201 AZ Nordwijk, The Netherlands
[15] Instituto de Astronomia y Fisica del Espacio / CONICET, cc67, suc 28. 1428 Buenos Aires, Argentina
[16] Instituto de Astrofísica de Andalucía (IAA-CSIC), PO Box 03004, 18080 Granada, Spain

Received 3 June 2003 / Accepted 23 July 2003

Abstract. A long Gamma-Ray Burst (GRB) was detected with the instruments on board the INTEGRAL satellite on January 31 2003. Although most of the GRB, which lasted ∼150 s, occurred during a satellite slew, the automatic software of the INTEGRAL Burst Alert System was able to detect it in near-real time. Here we report the results obtained with the IBIS instrument, which detected GRB 030131 in the 15 keV–200 keV energy range, and ESO/VLT observations of its optical transient. The burst displays a complex time profile with numerous peaks. The peak spectrum can be described by a single power law with photon index $\Gamma \simeq 1.7$ and has a flux of ∼2 photons cm^{-2} s^{-1} in the 20–200 keV energy band. The high sensitivity of IBIS has made it possible for the first time to perform detailed time-resolved spectroscopy of a GRB with a fluence of 7×10^{-6} erg cm^{-2} (20–200 keV).

Key words. gamma rays: bursts – gamma rays: observations

1. Introduction

Ever since their discovery (Klebesadel et al. 1973), Gamma-Ray Bursts (GRBs) have been a puzzling mystery, mostly because of their short durations and the apparent lack of counterparts at other wavelengths. A breakthrough in this field came thanks to the Italian-Dutch satellite *Beppo*SAX, which had the capability to localize the bursts' prompt emission with a precision of a few arcminutes within a few hours. This led to the discovery of the afterglow emission at lower energies, initially in X-rays (Costa et al. 1997) and subsequently at optical (van Paradijs et al. 1997) and radio (Frail et al. 1997) wavelengths, which allowed the redshift of these objects to be measured, and firmly established the cosmological nature of GRBs.

Due to the limited duration and the fading character of the afterglow emission, the prompt distribution of GRB coordinates to the scientific community is a high priority. After the end of the *Beppo*SAX mission this task has been accomplished mainly by HETE-2 (Ricker et al. 2002). INTEGRAL (Winkler et al. 1999), although not specifically designed as a GRB-oriented mission, can contribute to the rapid localization of the prompt emission of GRBs thanks to the INTEGRAL Burst Alert System (IBAS; Mereghetti et al. 2001). This software, running at the INTEGRAL Science Data Centre (ISDC; Courvoisier et al. 1999), is able to detect and localize GRBs

Send offprint requests to: D. Götz,
e-mail: diego@mi.iasf.cnr.it

⋆ Based on observations with INTEGRAL, an ESA project with instruments and science data centre funded by ESA member states (especially the PI countries: Denmark, France, Germany, Italy, Switzerland, Spain), Czech Republic and Poland, and with the participation of Russia and the USA, and on observations collected by the Gamma-Ray Burst Collaboration at ESO (GRACE) at the European Sourthern Observatory, Paranal, Chile (Programme 70.D-0523).

with a precision of a few arcminutes in a few seconds, and to distribute their coordinates in near real time over the Internet.

The high sensitivity of the INTEGRAL instruments also allows us to study in detail the prompt γ-ray emission of GRBs. This is particularly interesting for the faintest bursts, for which deep spectral studies were not possible up to now. For example, with the CGRO/BATSE instrument, time resolved spectroscopy was possible only for bursts with a fluence larger than $\sim 4 \times 10^{-5}$ ergs cm^{-2} (Preece et al. 1998).

On January 31 2003 at 07:38:49 UTC a GRB was detected in the field of view of the main instruments on board INTEGRAL: IBIS (Ubertini et al. 1999) and SPI (Vedrenne et al. 1999). Here we concentrate on the results obtained with IBIS, a coded mask imaging telescope based on two detectors, ISGRI and PICsIT, operating in the 15 keV–1 MeV and 170 keV–10 MeV energy ranges, respectively.

2. Detection and localization

GRB 030131 was discovered by IBAS (using IBIS/ISGRI data) on January 31 2003 at 07:39:10 UTC (~21 s after the beginning of the GRB, see below). The on-line automatic imaging analysis localized it to off-axis angles $Z = 10.1°$, $Y = -3.6°$, in the partially coded field of view (only ~23% of the detector was illuminated by the GRB). The GRB coordinates were not distributed automatically by IBAS because most of the burst occurred during a satellite slew (IBAS is disabled during satellite slews). In fact only the first ~20 s of this ~150 s long burst, during which the satellite attitude was stable and well known, were analyzed by IBAS, resulting in a low significance of the trigger. An off-line interactive analysis confirmed the reality of the event (Borkowski et al. 2003), but the reported error region radius was underestimated. A correct localization with an error radius of 5′ (Mereghetti et al. 2003a) was distributed only three days later.

By accumulating data over short time intervals and analyzing the corresponding images, we confirmed that the satellite slew started at 07:39:09 UTC, as indicated by the attitude data. We therefore used the first 20 s of the event, corresponding to the stable pointing period, to derive the GRB position $\alpha_{J2000} = 13^h\ 28^m\ 21^s$, $\delta_{J2000} = +30°\ 40'\ 33''$, with an error radius of 2.5′. Although the statistical error in these coordinates is only 1.6′, we conservatively added a systematic uncertainty of 2′, based on the results obtained in IBIS observations of sources with known positions. Our final position for GRB 030131 is consistent with the one reported earlier (Mereghetti et al. 2003a) and with the annulus derived with the IPN using Ulysses and IBIS/ISGRI data (see Fig. 1).

A provisional identification of an optical transient (OT) for GRB 030131 was reported by Fox et al. (2003a). The candidate OT, detected with the Palomar 48-inch Oschin telescope + NEAT Camera, had magnitude $R \sim 21.2$ at 3.62 hours after the burst, but it was much fainter and barely detectable ($R > 23.5$) ~26.8 hours after the burst at the 200-inch Hale telescope. Its coordinates, $\alpha_{J2000} = 13^h\ 28^m\ 22.29^s$, $\delta_{J2000} = +30°\ 40'\ 23.7''$, are 20″ from the center of the error circle derived here.

As a follow-up, we obtained a 3×300 s exposure in the V band using the European Southern Observatory Very Large Telescope (VLT) with the FORS1 instrument at a mean date of 13 February 09:11:54 UTC. The seeing was about 1″. There was no detectable object at the location of the candidate optical counterpart, with a 5 σ upper limit of $V > 26.4$.

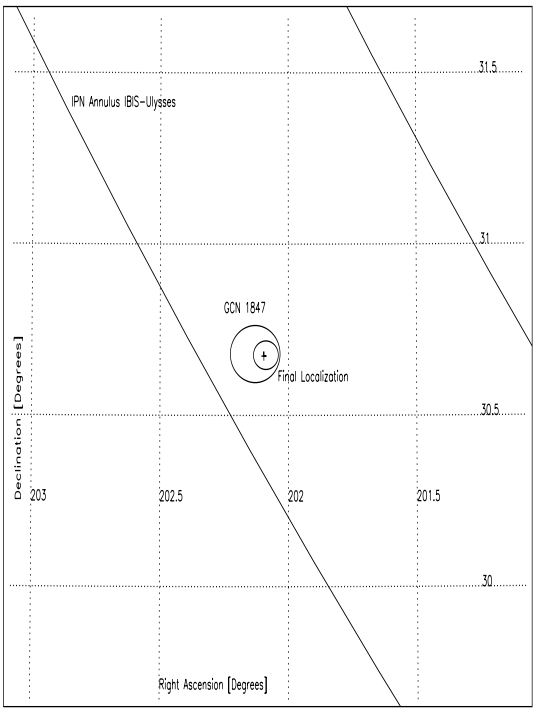

Fig. 1. Localizations of GRB 030131: the annulus obtained by the IPN is consistent with the localization given in Mereghetti et al. (2003a) (GCN 1847) and the one derived in this paper (the annulus obtained using SPI ACS and Ulysses is consistent with the one plotted but has a larger width). The cross indicates the position of the OT.

The marginal detection ~29 hours after the burst, with $B = 25.4 \pm 0.3$ (Gorosabel et al. 2003, but see also Henden 2003), and our VLT upper limit, confirm that this object is the OT of GRB 030131. Thus GRB 030131 is the first GRB detected with INTEGRAL with an associated optical counterpart.

3. Temporal and spectral analysis

We have analyzed IBIS/ISGRI single events, for which arrival time, energy deposit and interaction pixel of the detector are known for each event.

Figure 2 shows the light curves of GRB 030131 binned at 1 s resolution in different energy bands. The burst started at 07:38:49 UTC and lasted for about 150 s. The time profile shows several peaks (note that the small gaps are artifacts caused by satellite telemetry saturation). The T_{90} duration of the GRB in the 15–500 keV band is 124 s.

Since the GRB peaks during the satellite slew, we could not use the instrumental coordinates to extract the peak spectrum. Therefore we made an image selecting a time interval of 1 s around the GRB main peak ($t = 54$ s in Fig. 2). The high count rate at the peak allowed us to firmly establish the detector coordinates of the GRB even with this short integration time and thus to extract its peak spectrum. Since IBIS/ISGRI is a coded mask imaging instrument, the background can be estimated simultaneously with the source flux, using the Pixel Illumination Function (PIF; Skinner 1995). The spectra have

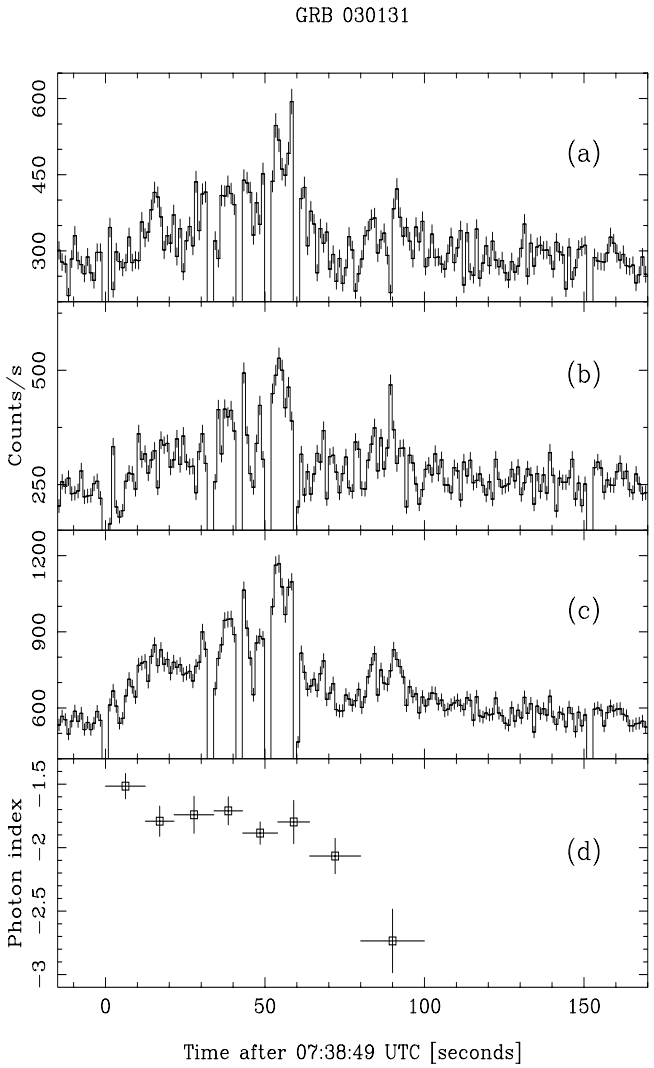

Fig. 2. IBIS/ISGRI light curve of GRB 030131 in various energy bands (**a**): 15–50 keV, **b**): 50–300 keV, **c**): 15–500 keV). The six data gaps are artifacts caused by satellite telemetry saturation. Four peaks can be identified, after ~15, ~40, ~55, ~85 s. The light curve has been corrected to take into account the varying fraction of the exposed instrument area during the satellite slew. Panel **d)** shows the spectral variation of the GRB with time.

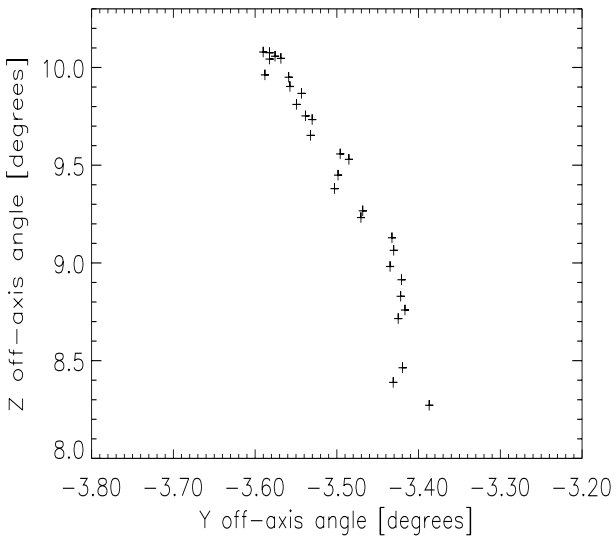

Fig. 3. Positions of GRB 030131 in detector coordinates as a function of time. Note the different scales of the two axes.

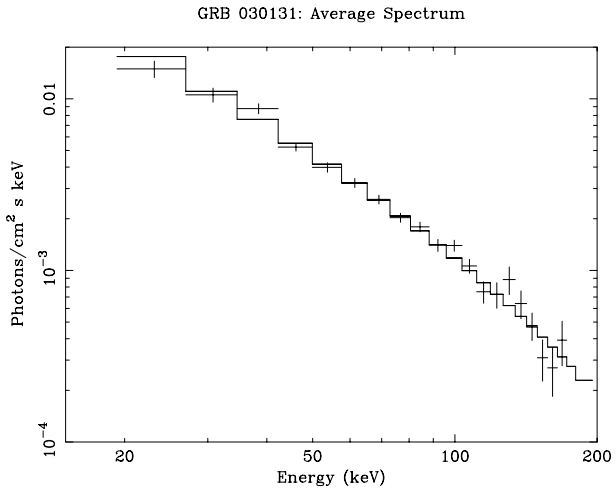

Fig. 4. Time averaged IBIS/ISGRI spectrum of GRB 030131. Data and best fit model are shown.

been extracted computing one PIF for each energy bin (128 linearly spaced bins have been used between 19 keV and 1 MeV). Since a fully calibrated spectral response matrix for sources at large off-axis angles is not yet available, we divided the count spectrum by the closest (in detector coordinates) count spectrum of the Crab Nebula. The resulting photon spectrum can be well fitted by a power law model (χ^2/d.o.f. = 8.66/8) with photon index $\Gamma = 1.73^{+0.16}_{-0.17}$ (90% confidence level). The flux is ~1.9 photons (~1.7×10^{-7} erg) cm^{-2} s^{-1} (~6.5 crab) in the 20–200 keV energy range.

To properly extract the total GRB flux and spectrum, we derived the GRB detector coordinates at various time intervals for the entire duration of the event. The first interval, corresponding to the stable pointing, lasts 20 s. The following 30 intervals last 3 s each and, finally, for the faint tail of the burst, four intervals with durations of 5, 5, 10 and 20 s were used. The coordinates as a function of time are shown in Fig. 3, where one can see the apparent drift of ~2° of the GRB in the IBIS field of view during the slew. To obtain the total (time averaged) spectrum, the 35 spectra extracted for the individual time intervals, corresponding to a net integration time of 147.2 s, were co-added. We derived the photon spectrum (shown in Fig. 4) in the same way that we did for the peak spectrum. The GRB is clearly detected up to 200 keV. In this case a single power law model does not provide a satisfactory fit (χ^2/d.o.f. = 39.84/18), indicating that a model which includes a spectral break would give a better representation of the data. A fit using the Band model (Band et al. 1993) yields a break energy $E_0 = 70 \pm 20$ keV, a low-energy power law index $\alpha = 1.4 \pm 0.2$ and a high-energy photon index $\beta = 3.0 \pm 1.0$ (χ^2/d.o.f. = 22.54/16). The fluence in the 20–200 keV band is ~73.8 photons cm^{-2} (7×10^{-6} erg cm^{-2}). To derive this value we have assumed that during the 4 central telemetry gaps the GRB had its average spectrum and intensity. Extrapolating the spectrum to the BATSE energy range (50–300 keV) we obtain a fluence of ~23 photons cm^{-2} (3.2×10^{-6} erg cm^{-2}). The values

of peak flux and fluence derived above are consistent within a factor of 2 with the ones measured with Ulysses. This indicates that our method does not suffer from large systematic errors and that the short telemetry gaps do not influence these values significantly.

We have also investigated the spectral evolution. As in the case of the peak spectrum, the data for the individual time intervals can be fitted with a single power law, without evidence for a spectral break. The photon index as a function of time is plotted in Fig. 2. A clear hard-to-soft evolution is seen. A hardening trend can also be seen corresponding to the rise of the second and third (main) peak with a softer spectrum for the latter peak. This correlation between light curve peaks and spectral hardening has already been reported in other bursts (e.g. Ford et al. 1995).

4. Discussion

The IBIS/ISGRI time-resolved spectroscopy of GRB 030131 is consistent with the overall hard-to-soft evolution observed with BATSE in many brighter GRBs, for which this kind of analysis was possible (e.g. Preece et al. 1998; Ford et al. 1995). The fluence of GRB 030131 is an order of magnitude smaller than those of the bursts studied by those authors, indicating that such spectral behaviour applies also to fainter GRBs. Clear evidence of this was also reported in the GRBs studied with *Beppo*SAX in the 2–700 keV energy range (e.g. Frontera et al. 2000; Frontera et al. 2003). While BATSE could better constrain the break energy and the high-energy slope of the Band function, thanks to its higher relative sensitivity above 200 keV, IBIS/ISGRI allows more detailed studies of the low-energy part of the spectrum for relatively low fluence GRBs.

In the framework of the internal fireball shock model (Rees & Mészáros 1994), and in particular of the Synchrotron Shock Model (Tavani 1996), the hard-to-soft evolution can be interpreted in two ways. The first possibility is a decrease of the magnetic field in the postshock region as a consequence of the postshock flow expansion; the second is a postshock decrease of the index of the particle distribution function as a consequence of strong cooling processes affecting the particle energy distribution for dynamical flow times larger than the radiating timescale. The two effects are not distinguishable in our case, since the time-resolved spectra do not have enough statistics to constrain a spectral break and hence a low-energy and a high-energy spectral index. The soft-to-hard evolution observed during the rise of the individual peaks, on the other hand, can be caused by an increase of the local magnetic field at the shock. Several authors reported that the duration of single pulses in GRB time histories is energy dependent (e.g. Link et al. 1993), with longer durations at lower energies, resulting in a hardening of the spectra before the peaks and a softening afterwards.

The optical transient associated with GRB 030131 indicates that we can classify it as an "optically dim" GRB. In fact it is as faint as (or even fainter than) the transient associated with GRB 030227, which is the only other INTEGRAL GRB with a firmly established optical conterpart, and was detected at $R \sim 23.3$ 12 hours after the burst (Mereghetti et al. 2003b). It is also comparable to GRB 021211. This event is also considered an optically dim burst since it was detected at $R \sim 18.2$ 1.3 hours after the prompt emission (Fox et al. 2003b) and was fainter than $R \sim 22.5$ after 12 hours (Klose et al. 2002). In addition GRB 030131 is located at much higher Galactic latitude ($b \simeq 81°$) which implies smaller foreground optical extinction. This indicates that, despite the efforts of observers, in some cases, optical follow-up with small telescopes is not an easy task, even less than 1 day after the burst (e.g Fynbo et al. 2001). The prompt localization of GRBs is hence a high priority in order to achieve a successful follow-up. The results on GRB 030501 (Beckmann et al. 2003) (an alert 30 s after the start of the GRB with an uncertainty of 4.4′; IBAS Alert 596) show that IBAS is now able to provide this service.

Acknowledgements. This research has been supported by the Italian Space Agency. KH is grateful for Ulysses support under JPL contract 958056, and for support of the IPN under NASA grant NAG5-12614. DHH acknowledges support by NASA. RH acknowledges the support by Prodex Project 14527.

References

Band, D. L., Matteson, J., Ford, L., et al. 1993, ApJ, 413, 281
Beckmann, V., Borkowski, J., Courvoisier, T. J.-L., et al. 2003, A&A, in press
Borkowski, J., Gotz, D., Mereghetti, S. Deluit, S., & Walter, R. 2003, GCN 1836
Costa, E., Frontera, F., Heise, J., et al. 1997, Nature, 387, 783
Courvoisier, T., et al. 1999, in Proc. of the 3rd INTEGRAL Workshop – Astro Lett. & Communications, 39, 355
Ford, L. A., Band, D. L., Matteson, J. L., et al. 1995, ApJ, 439, 307
Fox, D. W., Price, P. A., Herter, T., Appleton, P., & Cotter, G. 2003a, GCN 1857
Fox, D. W., Price, P. A., Soderberg, A. M., et al. 2003b, ApJ, 586, L5
Frail, D., Kulkarni, S. R., Nicastro, S. R., Feroci, M., & Taylor, G. B. 1997, Nature, 389, 261
Frontera, F., Amati, L., Costa, E., et al. 2000, ApJS, 127, 59
Frontera, F. et al. 2003, in preparation
Fynbo, J. U., Jensen, B. L., Gorosabel, J., et al. 2001, A&A, 369, 373
Gorosabel, J., Levan. A., Fruchter, A., et al. 2003, GCN 1866
Henden, A. 2003, GCN 1971
Klebesadel, R. W., Strong, I. B., & Olson, R. A. 1973, ApJ, 182, L85
Klose, S., Eisloeffel, J., Froebrich, D., et al. 2002, GCN 1739
Link, B., Esptein, R. I., & Priedhorski, W. C. 1993, ApJ, 408, L81
Mereghetti, S., et al. 2001, in Proc. of the 4th INTEGRAL Workshop, ESA-SP, 459, 513
Mereghetti, S., Produit, N., Borkowski, J., & Gotz, D. 2003a, GCN 1847
Mereghetti, S., Götz, D., Tiengo, A., et al. 2003b, ApJ, 590, L73
Preece, R. D., Pendleton, G. N., Briggs, M. S., et al. 1998, ApJ, 496, 849
Rees, M. J., & Mészáros, P. 1994, ApJ, 430, L93
Ricker, G., Hurley, K., Lamb, D., et al. 2002, ApJ, 571, L127
Skinner, G. K. 1995, Experimental Atronomy, 6/4, 1
Tavani, M. 1996, ApJ, 466, 768
Ubertini, P., Lebrun, F., Di Cocco, G., et al. 1999, in Proc. of the 3rd INTEGRAL Workshop – Astro Lett. & Communications, 39, 331
van Paradijs, J., Groot, P. J., Galama, T., et al. 1997, Nature, 386, 686
Vedrenne, G., Schönfelder, V., Albernhe, F., et al. 1999, in Proc. of the 3rd INTEGRAL Workshop – Astro Lett. & Communications, 39, 325
Winkler, C. 1999, in Proc. of the 3rd INTEGRAL Workshop – Astro Lett. & Communications, 39, 309

A&A 411, L291–L297 (2003)
DOI: 10.1051/0004-6361:20031289

Astronomy & Astrophysics

The INTEGRAL⋆ Burst Alert System

S. Mereghetti[1], D. Götz[1,2], J. Borkowski[3], R. Walter[3], and H. Pedersen[4]

[1] Istituto di Astrofisica Spaziale e Fisica Cosmica – CNR, Sezione di Milano "G.Occhialini", via Bassini 15, 20133 Milano, Italy
[2] Dipartimento di Fisica, Università degli Studi di Milano Bicocca, P.zza della Scienza 3, 20126 Milano, Italy
[3] Integral Science Data Centre, Chemin d'Écogia 16, 1290 Versoix, Switzerland
[4] Copenhagen University Observatory, Juliane Maries Vej 30, 2100 Copenhagen, Denmark

Received 7 July 2003 / Accepted 21 August 2003

Abstract. We describe the INTEGRAL Burst Alert System (IBAS): the automatic software for the rapid distribution of the coordinates of the Gamma-Ray Bursts detected by INTEGRAL. IBAS is implemented as a ground based system, working on the near-real time telemetry stream. During the first six months of operations, six GRB have been detected in the field of view of the INTEGRAL instruments and localized by IBAS. Positions with an accuracy of a few arcminutes are currently distributed by IBAS to the community for follow-up observations within a few tens of seconds of the event.

Key words. gamma rays: bursts

1. Introduction

For many years after their serendipitous discovery, Gamma-Ray Bursts (GRB) were relegated as a puzzling phenomenon in the field of high-energy astronomy. The real breakthrough in their understanding came with the discovery of X–ray (Costa et al. 1997), optical (van Paradijs et al. 1997), and radio (Frail et al. 1997) afterglows. This finally allowed to set a distance scale, proving that at least long (>2 s) GRB are located at cosmological distances and associated to the final evolutionary stages of massive stars (Stanek et al. 2003; Hjorth et al. 2003). These findings led to a renewed interest and to enormous developments in this field during the last few years (see, e.g., van Paradijs et al. 2000).

It is clear that the rapid derivation and distribution of accurate sky positions for GRB is crucial to successfully carry out such studies. Satellite missions specifically devoted to this, such as *HETE-2* (Ricker et al. 2003) and *Swift* (Gehrels 2001) have in fact been developed. Although INTEGRAL is a general γ-ray astronomy mission, not particularly optimized for GRB studies, it was soon realized that the unprecedented imaging performances of its IBIS instrument (Ubertini et al. 2003) could offer the possibility of rapid localization of the events observed by chance in its large field of view. It was therefore proposed to implement a "burst alert system" in order to allow rapid multi-wavelength follow-ups (Pedersen et al. 1997).

Compared to previous and current GRB localization facilities, IBAS represents a step forward. Error regions at the arcmin level were obtained by *BeppoSAX* (Costa 2000) with typical delays of one hour or more, related to the frequency (once per 96 min orbit) of the ground contacts. The Inter Planetary Network (IPN, Hurley et al. 2001) can provide error regions of a few tens of square arcmin, but after several hours (or even days). Real time localizations from CGRO/BATSE were distributed in the past with Bacodine (now called GCN, Barthelmy et al. 2001), but their typical uncertainty was of a few degrees. Currently, very nice results are being obtained with *HETE-2* (Ricker et al. 2003). The GRB positions derived on-board at the ∼degree level are available within a few seconds, and later (1–2 hours) refined down to a few arcmin, with a ground analysis.

A great advantage of the INTEGRAL mission is the continuous contact with the ground stations during the observations, made possible by its high orbit (3 days period). As shown below, IBAS is currently able to provide small error regions (∼4′ radius) within few tens of seconds from the GRB.

2. IBAS description

2.1. Overall architecture

The INTEGRAL Burst Alert System (IBAS) is the automatic software devoted to the rapid detection and localization of GRB (Mereghetti et al. 2001b). Contrary to most other γ-ray astronomy satellites, no on-board GRB triggering system is present

Send offprint requests to: S. Mereghetti,
e-mail: sandro@mi.iasf.cnr.it

⋆ INTEGRAL is an ESA project with instruments and science data centre funded by ESA member states (especially the PI countries: Denmark, France, Germany, Italy, Switzerland, Spain), Czech Republic and Poland, and with the participation of Russia and the USA.

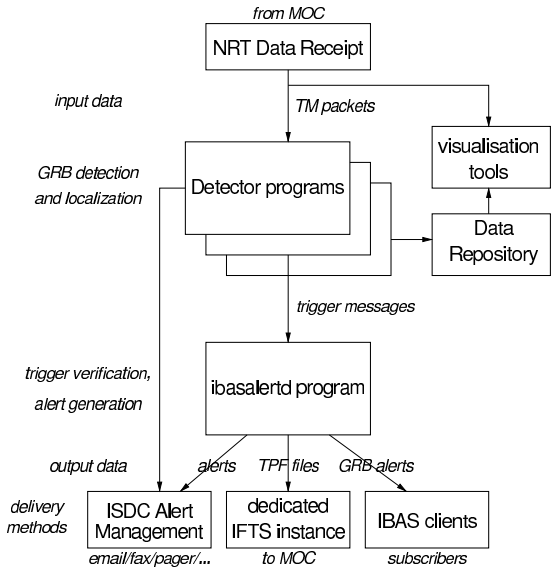

Fig. 1. Main components an interfaces of the IBAS software.

on INTEGRAL. Since the data are continuously transmitted without important delays, the search for GRB is done at the INTEGRAL Science Data Centre (ISDC, Courvoisier et al. 2003). The fact that IBAS is running on ground has some advantages: besides the availability of a larger computing power, a very important factor is the greater flexibility for what concerns software and hardware upgrades, with respect to systems operating on board satellites. To take full advantage of this flexibility, the IBAS software architecture has been designed in a modular way, which allows to plug-in various programs for the GRB search, based on different instruments and algorithms.

Figure 1 gives an overview of the IBAS software architecture. The telemetry, received at the ESA Mission Operation Center (MOC) in Darmstadt, is continuously transmitted to the ISDC on a 128 kbs dedicated line. As soon as the data reach the ISDC, they are processed by the Near Real Time Data Receipt Subsystem which extracts the relevant telemetry packets and, after some basics checks, feeds them into IBAS. IBAS comprises several independent *Detector Programs* runing in parallel. They have the task to trigger on possible GRB and to perform preliminary checks to filter out, as much as possible, spurious events. This architecture allows us to use in parallel different methods for the GRB detection, as well as to run several instances of the same *Detector Program* with different parameter settings (e.g. timescales, energy cuts, etc.) in order to increase the sensitivity for GRB with different properties.

Currently, programs based on two different algorithms using data from the ISGRI/IBIS detector are in use, plus one program to detect GRB seen by the anticoincidence shield of SPI (in this case no directional information is available). Other *Detector Programs* based on data from JEM-X and SPI are under development.

The trigger messages produced by the *Detector Programs* are then analyzed by the *Ibasalertd* program which combines them in order to extract the maximum information to decide on the reality of the GRB. The details of the logic of trigger confirmation can be defined in a very flexible way by means of a set of parameters involving significance of detection, tolerance for positional and temporal coincidence, etc. The *Ibasalertd* program also converts detector coordinates to sky positions based on the best available attitude information, verifies that the triggers are not due to known variable sources, and eventually distributes via Internet an *IBAS Alert Packet* containing the position of the GRB. When several trigger messages, received at slightly different times, refer to the same GRB, they are filtered by *Ibasalertd* in order to distribute new *Alerts Packets* only if relevant new information is available (e.g. an improved localization).

All the IBAS processes are multi-thread applications written in C or C++. They run as daemon processes, which means that they do not perform any terminal input/output and run in background. IBAS processes perform several subtasks in parallel, each one handled by a separate thread. With some unavoidable exception, the subtasks are independent and do not block each other.

As can be seen in Fig. 1, IBAS also comprises visualization and analysis tools which can be used for off-line examination of the data. In order to minimize the reaction time, the off-line analysis is based on data products directly saved by the IBAS programs.

Finally, all the IBAS programs interface with the ISDC Alert Management System, which is used by the ISDC operators and scientists on duty to monitor the correct functioning of the software and to react to possible problems and/or interesting scientific events.

2.2. Detector programs

Among the INTEGRAL instruments, IBIS is the most appropriate for GRB localization, thanks to its large field of view ($29° \times 29°$) and its capability to locate sources at the arcminute level (Gros et al. 2003). As mentioned above, IBAS localizations are based on two different programs using the data from the IBIS lower energy detector ISGRI (Lebrun et al. 2003).

Since imaging analysis is the most time consuming part of the algorithm, the first program performs a simple monitoring of the overall ISGRI counting rate. This is done by looking for significant excesses with respect to a running average, in a way similar to traditional triggering algorithms used on-board previous satellites. Different instances of this program are currently running with trigger timescales ranging from 2 ms to 5.12 s. The imaging analysis is done only when a significant counting rate excess is detected. Images are accumulated for different time intervals, deconvolved with very fast algorithms, and compared to the pre-burst reference images in order to detect the appearance of the GRB as a new source. This step is essential to eliminate many triggers due to instrumental effects and background variations which do not produce a point source excess in the reconstructed sky images.

The algorithm used in the second *Detector Program* is entirely based on image comparison. Images of the sky are continuously produced and compared with the previous ones to

search for new sources. With respect to the other program, this one has the advantage of being less affected by variability of the background or of other sources in the field of view. Currently, this program is sampling timescales from 10 to 40 s.

Finally a third kind of *Detector Program* is used to search for GRB detected by the Anti Coincidence System (ACS) of the SPI instrument. The available data consist of light curves with the overall ACS count rate binned at 50 ms resolution (von Kienlin et al. 2003a). Although no directional information is available, the resulting triggers can in principle be used by the *Ibasalertd* program to confirm low significance events seen in other instruments.

2.3. Distribution of the IBAS Alert Packets

IBAS *Alert Packets* with the GRB information are sent via Internet, using the UDP transport protocol. Each packet is 400 bytes long, and consists of several fields, the format and content of which is explained in detail in the documentation available at the ISDC web pages[1]. Different types of *Alert Packets* are distributed. Users can select which type(s) they want receive. Users interested in receiving the IBAS *Alert Packets* can also download a *Client Software*, written in standard C language and tested on the most popular operating systems, that allows them to receive the *Alert Packets* and to easily use their content, e.g. in the software commanding robot telescopes.

IBAS can send more than one packet for each GRB. After the first one (WAKEUP type) distributed with the shortest delay, one or more packets of type REFINED are sent automatically if a more precise localization becomes available. Finally, one or more packets of type OFFLINE can be sent manually after the interactive analysis of the data.

Since automated telescopes can exploit the a priori knowledge of the INTEGRAL pointing direction (e.g. to reduce the slew time in case of a GRB alert, to obtain reference images of the pre-GRB sky, to monitor the counterparts of INTEGRAL targets), IBAS is also sending packets containing updated pointing information each time a slew to a new direction begins. Test *Alert Packets* of each type are sent every 6 hours, to allow the IBAS users to check their software.

2.4. Automatic reconfiguration of the Optical Monitor Camera

INTEGRAL also carries an Optical Monitor Camera (OMC, Mas-Hesse et al. 2003), which consists of a 50 mm telescope covering the central $5° \times 5°$ region of the IBIS and SPI field of view. During normal operations, owing to the limited telemetry rate allocated to the OMC, only the data from a number of small pre-selected windows around sources of interest are recorded and transmitted to the ground. The *Ibasalertd Program* checks whether the derived GRB position falls within the OMC field of view. In such a case, the appropriate telecommand with the definition of a new window centered on the interesting region is generated and sent to the MOC to be uploaded to the satellite.

[1] http://isdc.unige.ch

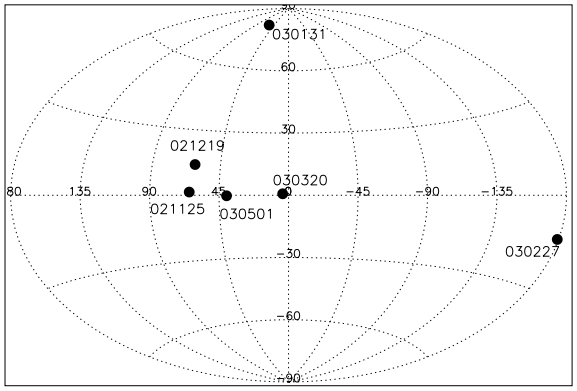

Fig. 2. Positions in Galactic coordinates of the six GRB localized so far by INTEGRAL. The large fraction of GRB at low Galactic latitudes reflects the non-uniform sky exposure obtained by INTEGRAL during the first months of the mission.

This will allow to quickly observe the GRB/afterglow emission in the optical band. The OMC observation will consist of several frames with integration times of 60 s to permit variability studies and to increase the sensitivity for very intense but short outbursts. The expected limiting magnitude is of the order of $V \sim 14$ for an integration time of 60 s at high Galactic latitudes.

3. IBAS performances

The IBAS programs have been running almost continuously since the launch of the INTEGRAL satellite. The first two months of operations were devoted to the setting of the many parameters involved in the GRB detection. Some changes in the algorithms were also required to adapt them to the in-flight data characteristics. Delivery of the *Alert Packets* to the external clients started on January 17, 2003. Since then it has always been enabled, except for the period from February 12 to 28 (during calibration observations of the Crab Nebula), and for a short interruption (4 hours) on April 23 (for hardware maintenance reasons).

Six GRB have been discovered to date in the field of view of IBIS (see Table 1 and Figs. 2 and 3). When a GRB is detected by IBAS with high significance, the *Alert Packet* with the corresponding coordinates is automatically delivered to all subscribed users. This actually happened so far only for GRB 030501. It would have also occurred for GRB 021219 and GRB 030227, but, as mentioned above, they were detected while the external delivery of alerts was switched off.

Possible GRB detected by IBAS with lower significance generate alerts reaching only the members of the IBAS Team, who quickly perform an analysis of the relevant data. If the GRB is confirmed an *Alert Packet* of type OFFLINE with the derived position is then distributed. This occurred for GRB 030131 and GRB 030320.

IBAS has also distributed a number of alerts which were subsequently found to be unrelated to GRB. They were retracted by OFFLINE packets and GCN circulars typically within a few tens of minutes. These false alerts had

Table 1. GRB in the IBIS Field of view.

GRB	Duration [s]	Delay[a] in position distribution internal/public	External delivery of IBAS *Alert Packets*	Peak Flux (20–200 keV) [ph $cm^{-2}s^{-1}$]	Peak Flux (20–200 keV) [erg $cm^{-2}s^{-1}$]	Fluence (20–200 keV) [erg cm^{-2}]	Ref.[b]
021125	25	–[c] / 0.9 days	OFF	22	2×10^{-6}	7.4×10^{-6}	1, 2
021219	6	10 s / 5 hr	OFF	3.7	3.5×10^{-7}	9×10^{-7}	3, 4
030131	150	21 s / 2 hr[d]	ON	1.9	1.7×10^{-7}	7×10^{-6}	5, 6
030227	20	35 s / 48 min	OFF	1.1	1.6×10^{-7}	7.5×10^{-7}	7, 8
030320	50	12 s / 6 hr	ON	5.7	5.4×10^{-7}	1.1×10^{-5}	9, 10
030501	40	30 s / 30 s	ON	2.7	3×10^{-7}	3×10^{-6}	11, 12

[a] Computed from the beginning of the GRB.
[b] References (for the first announcement and the first journal publication only): (1) Bazzano & Paizis (2002), (2) Malaguti et al. (2003), (3) Mereghetti et al. (2002), (4) Mereghetti et al. (2003d), (5) Borkowski et al. (2003), (6) Götz et al. (2003a), (7) Götz et al. (2003b), (8) Mereghetti et al. (2003a), (9) Mereghetti et al. (2003b), (10) von Kienlin et al. (2003b), (11) Mereghetti et al. (2003c), (12) Beckmann et al. (2003).
[c] The IBAS *Detector Programs* were in idle mode owing to the limited telemetry allocation for IBIS/ISGRI during this observation. See Ref. 2 for details.
[d] The localization of this GRB was complicated by the fact that it was detected while the satellite was performing a slew between two pointings. This also reduced its significance level below the threshold for immediate alert distribution. See Fig. 5 for the resulting error regions.

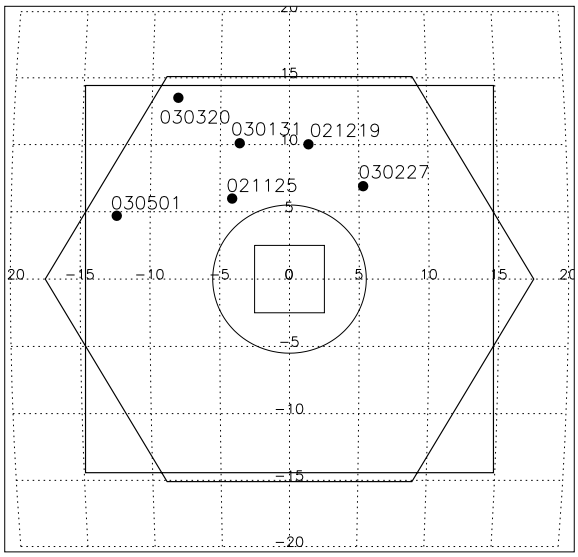

Fig. 3. Positions of the six GRB in the field of view of the INTEGRAL instruments: IBIS (large square), SPI (hexagon), JEM-X (circle) and OMC (small square). The scale is in degrees.

different origins. Each of them led to appropriate changes in the *Ibasalertd* input parameters and/or to modifications of the software in order to fix the problem. Most of the false alerts were caused by an unlucky combination of a very bright source in the field of view and some unexpected problem in the instruments and/or ground segment. In fact, bright (and/or variable) sources are not a problem for IBAS under normal conditions: all the triggers are cross-checked with a list of sky positions of known bright sources before being distributed. Obviously, this filter does not work if the wrong source coordinates are computed. To date this happened a few times, either because the imaging analysis failed due to some unexpected data configuration related to the instrument or because a wrong satellite attitude[2] was used to convert from instrumental to celestial coordinates.

Although in these months we have made considerable progress in the IBAS reliability, unexpected situations are by their nature difficult to deal with a priori and might generate other false alerts in the future. IBAS users have the possibility of trading off between speed of reaction time and reliability of the event by subscribing only to particular types of *Alert Packets*.

3.1. Time delay

The time performances of IBAS for what concerns the GRB detected so far are summarized in Table 1.

The time delay in the distribution of coordinates results from the sum of several factors. First of all there is a delay on board the satellite. This is variable and depends on the instrument. In the case of IBIS/ISGRI data the average delay is about 5 s, but it can be much longer for other instruments (e.g. approximately 20 s on average for the SPI ACS data, up to one minute for JEM-X data). Signal propagation to the ground station is negligible (maximum ~0.6 s), but some time is required before the data are received at the ISDC passing through the MOC. This is on average 3 s when the ESA ground station in Redu (Belgium) is used, or 6 s when the NASA Goldstone ground station is used.

[2] Specifically, problems arise whenever the satellite does not follow the planned timeline (e.g. due to a telecommand which failed or during manual recommanding). Since the attitude data from the star trackers are transmitted to the ISDC with a delay of a few minutes, IBAS must use the attitude predicted from the timeline whenever a trigger occurs shortly after the slew (i.e. about every hour, due to the dithering mode of observation).

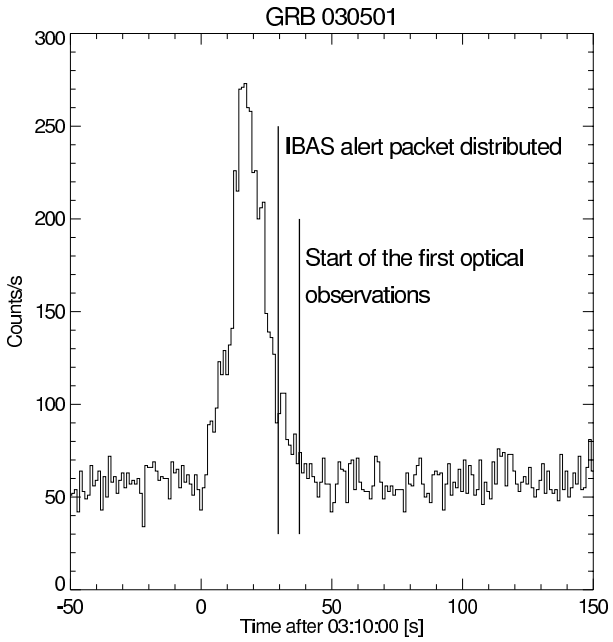

Fig. 4. Time performance of IBAS in the localization of GRB 030501, the GRB with the fastest positioning to date. The IBIS/ISGRI light curve refers to the 20–200 keV range. The two vertical lines indicate the time at which IBAS distributed the position with an error radius of 4.4′ and the start of the first observation of the field obtained with the TAROT automatic telescope (Boer & Klotz 2003).

The time to detect the GRB depends on the algorithm which triggers. The delay between the trigger time and the GRB onset is of course dependent on the intensity and time profile of the event. The IBAS simultaneous sampling in different timescales should ensure a minimum delay in most cases, however in practice a minimum of ~5 s is required to accumulate an image with sufficient statistics.

Finally, the conversion to sky coordinates, comparison with list of known variable sources, *Alert Packet* construction and delivery require less than about 2 s. Of course, the above numbers assume nominal condition, i.e. no telemetry gaps, no saturation of the allocated telemetry, no missing auxiliary data files, etc.

Thus, in many cases, we foresee to be able to generate alerts while the GRB is still ongoing. Indeed this has happened for GRB 030501, whose position with an uncertainty of only 4.4′ reached all the IBAS users only 30 s after the beginning of the GRB (Fig. 4). To our knowledge, such a combination of high speed and small error region was never achieved before in the localization of a GRB. Unfortunately, this GRB was located at low Galactic latitude in a region of very high interstellar absorption which prevented sensitive searches for counterparts (see Fig. 2).

3.2. Location accuracy

The source location accuracy (SLA) of coded mask imaging systems depends on the intrinsic angular resolution of the instrument and on the signal to noise ratio of the source. For sources detected with a high statistical significance the SLA can be a small fraction of the angular resolution. The angular resolution of IBIS/ISGRI is ~12′, but sources are typically located with an uncertainty of ~1–2′. For sources detected with a signal to noise ratio of ~30, the SLA is smaller than 30″ (90% confidence level).

For most of the time (except, e.g., during satellite slews) the INTEGRAL attitude accuracy is smaller than a few arcseconds (Walter et al. 2003). However, based on the data collected so far, it turns out that the current uncertainties in the relative alignment between the instruments and the satellite reference frame, lead to some differences between the derived and true positions of known sources. These differences depend on the position in the field of view, increasing at large off-axis angles. For IBIS/ISGRI these values range from 15″ on-axis to ~2.4′ at the border of the field of view.

For this reason, a conservative systematic error of 4′ is currently added in quadrature to the statistical error in the GRB positions distributed in the automatically delivered *Alert Packets*. Usually a better accuracy is obtained with the off-line analysis.

Figure 5 summarizes the performance in terms of localization accuracy obtained so far. Note that at the beginning of the mission the in-flight instrument misalignment was not calibrated yet. Therefore, error radii as large as 20′ or 30′ were given. The error regions obtained with the IPN, and the coordinates of the optical transients discovered for the two GRB for which prompt observations could be done, are also shown in the figure. Their agreement with the INTEGRAL positions confirms that the IBAS localizations are correct.

3.3. Sensitivity

The sensitivity of the IBIS/ISGRI detector is very close to that estimated before the INTEGRAL launch (Ubertini et al. 2003). Based on such expected sensitivity, we predicted a rate of GRB localizations with IBAS of about one per month (Mereghetti et al. 2001a), which seems to be confirmed by the results obtained so far.

A rough evaluation of the sensitivity to GRB can be derived as follows. The typical IBIS/ISGRI overall count rate in the energy range 15–200 keV used by one of the IBAS *Detector Programs* varies between about 400 and 800 counts s^{-1}, depending on the background conditions and on the presence of bright sources in the field of view. For a trigger time interval of 1 s and the current threshold value, a minimum net count rate of 120–170 counts s^{-1} is required to trigger (and to produce enough counts to locate the position in the deconvolved image). Assuming a typical GRB spectrum, such a count rate corresponds to a flux of ~0.14–0.22 photons cm^{-2} s^{-1} (20–200 keV). This applies to the central 9° × 9° of the IBIS field of view, where the full instrument effective area can be used. In the external part of the field of view, the so called partially coded region, the sensitivity is worse. This explains why the GRB discovered so far have relatively high peak fluxes compared to the above sensitivity (see Table 1 and Fig. 3).

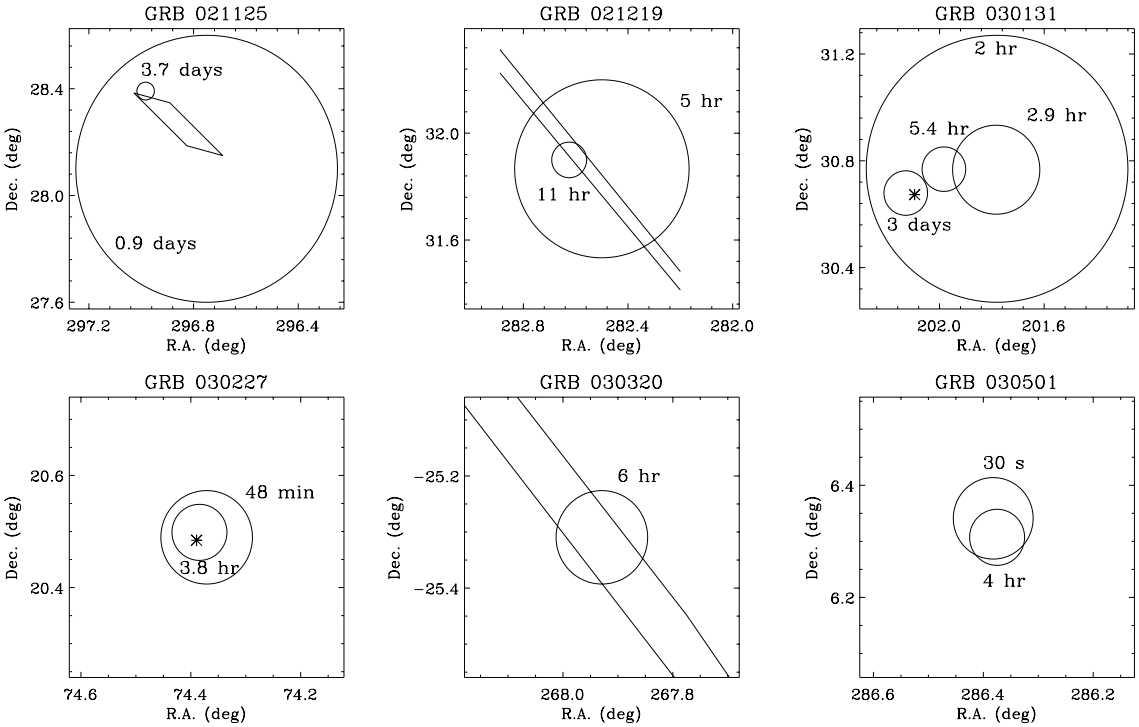

Fig. 5. Error regions distributed for the six GRB in the field of view of the INTEGRAL instruments, with the corresponding delays. Note the different scale of the three upper ($1° \times 1°$) and lower ($0.5° \times 0.5°$) panels. The parallelogram and the straight lines indicate error regions independently derived with the IPN (Hurley et al. 2002a; Hurley et al. 2002b; Hurley et al. 2003). The asterisks indicate the positions of the optical transients associated to GRB 030131 (Fox et al. 2003) and GRB 030227 (Castro-Tirado et al. 2003).

4. Conclusions

The results obtained in the first months of the INTEGRAL mission demonstrate that IBAS is working as expected. It can provide GRB positions with an accuracy of a few arcmin within few tens of seconds, at a rate of about one GRB per month. In addition, IBAS is distributing the light curves of about one GRB per day detected with the SPI ACS (von Kienlin et al. 2003a). These can be used to locate the bursts which are observed also by other satellites of the IPN.

It is remarkable that, after only two months from the start of in orbit operation of the instruments, IBAS was already functioning successfully, as demonstrated by the localization of GRB 021219. The results presented here, as summarized in Fig. 5 and Table 1, indicate that the IBAS capabilities, in terms of positional accuracy and speed of localization, have improved during the last few months. Although the location in the Galactic plane prevented deep studies of some of the IBAS GRB, successful observations of optical and X–ray afterglows have been obtained for GRB 030131 (Götz et al. 2003a) and GRB 030227 (Mereghetti et al. 2003a; Castro-Tirado et al. 2003).

It is expected that, as more experience is gained with the data and triggering algorithms, as well as by adding new *Detector Programs* using data from the other INTEGRAL instruments, the IBAS performances will improve also in terms of rate of GRB localizations.

Acknowledgements. The IBAS development has been supported by the Italian Space Agency. JB acknowledges the Polish State Committee for Scientific Research for grant number 2P03C00619p02. We thank the members of the INTEGRAL Science Working Team for their support of the IBAS activities, several useful suggestions, and the permission of using PV data for the testing of IBAS. Davide Cremonesi and Don Jennings gave an important contribution to the initial development of the IBAS software.

References

Barthelmy, S. D., Cline, T. L., & Butterworth, P. 2001, AIP Conf. Proc., 587, 213
Bazzano, A., & Paizis, A. 2002, GCN Circ., 1706
Beckmann, V., Borkowski, J., Courvoisier, T. J.-L., et al. 2003, 411, L327
Boer, M., & Klotz, A. 2003, GCN Circ., 2188
Borkowski, J., Götz, D., & Mereghetti, S. 2003, GCN Circ., 1836
Castro-Tirado, A. J., Gorosabel, J., Guziy, S., et al. 2003, 411, L315
Costa, E. 2000, AIP Conf. Proc., 526, 365
Costa, E., Frontera, F., Heise, J., et al. 1997, Nature, 387, 783
Courvoisier, T. J.-L., Walter, R., Beckmann, V., et al. 2003, 411, L53
Fox, D. W., Price, P. A., Heter, T., et al. 2003, GCN Circ., 1857
Frail, D. A., Kulkarni, S. L., Nicastro, S. R., et al. 1997, Nature, 389, 261
Gehrels, N. 2001, in Gamma-Ray Bursts in the Afterglow Era, ed. E. Costa, F. Frontera, & J. Hjorth (Berlin, Heidelberg: Springer), 357
Götz, D., Mereghetti, S., Hurley, K., et al. 2003a, A&A, in press
Götz, D., Borkowski, J., & Mereghetti, S. 2003b, GCN Circ., 1895
Gros, A., Goldwurm, A., Cadolle-Bel, M., et al. 2003, 411, L179

A&A 411, L307–L310 (2003)
DOI: 10.1051/0004-6361:20031155

Astronomy & Astrophysics

GRB 021125: The first GRB imaged by INTEGRAL⋆

G. Malaguti[1], A. Bazzano[2], V. Beckmann[3,4], A. J. Bird[5], M. Del Santo[2], G. Di Cocco[1], L. Foschini[1], P. Goldoni[6], D. Götz[7], S. Mereghetti[7], A. Paizis[3], A. Segreto[8], G. Skinner[9], P. Ubertini[2], and A. von Kienlin[10]

[1] Istituto di Astrofisica Spaziale e Fisica Cosmica (IASF) del CNR, Sezione di Bologna, via Gobetti 101, 40129 Bologna, Italy
[2] Istituto di Astrofisica Spaziale e Fisica Cosmica (IASF) del CNR, Sezione di Roma, via Fosso del Cavaliere 100, 00133 Roma, Italy
[3] INTEGRAL Science Data Centre, Chemin d'Écogia 16, 1290 Versoix, Switzerland
[4] Institut für Astronomie and Astrophysik, Universität Tübingen, Sand 1, 72076 Tübingen, Germany
[5] School of Physics and Astronomy, University of Southampton, Highfield, Southampton, SO17 1BJ, UK
[6] CEA Saclay, DSM/DAPNIA/SAp, 91191 Gif-sur-Yvette Cedex, France
[7] Istituto di Astrofisica Spaziale e Fisica Cosmica (IASF) del CNR, Sezione di Milano, via Bassini 15, 20133 Milano, Italy
[8] Istituto di Astrofisica Spaziale e Fisica Cosmica (IASF) del CNR, Sezione di Palermo, via U. La Malfa 153, 90146 Palermo, Italy
[9] Centre d'Étude Spatiale des Rayonnements, 9 avenue du Colonel Roche, 31028 Toulouse Cedex 4, France
[10] Max-Planck-Institut für Extraterrestrische Physik, Giessenbachstrasse, 85748 Garching, Germany

Received 14 July 2003 / Accepted 30 July 2003

Abstract. In the late afternoon of November 25th, 2002 a gamma–ray burst (GRB) was detected in the partially coded field of view (about 7.3° from the centre) of the imager IBIS on board the INTEGRAL satellite. The instruments on-board INTEGRAL allowed, for the first time, the observation of the prompt gamma-ray emission over a broad energy band from 15 to 500 keV. GRB 021125 lasted ~24 s with a mean flux of ~5.0 photons cm^{-2} s^{-1} in the 20–500 keV energy band, and a fluence of $\sim 4.8\times10^{-5}$ erg cm^{-2} in the same energy band. Here we report the analysis of the data from the imager IBIS and the spectrometer SPI.

Key words. gamma rays: burst – gamma rays: observations

1. Introduction

INTEGRAL is the ESA satellite dedicated to the astrophysics in the X– and γ–ray domain, launched on October 17th, 2002 (Winkler et al. 2003). It is composed of two main high–energy telescopes (IBIS, SPI) coupled with two monitors, one in the X–ray energy band (JEM–X, Lund et al. 2003) and the other working at optical wavelengths (OMC, Mas–Hesse et al. 2003). IBIS (Ubertini et al. 2003) has moderate energy resolution, and is optimized for fine imaging, with 12′ angular resolution, and $\leq$1′ point source location accuracy for $\geq 30\sigma$ detections (Gros et al. 2003) in a $9° \times 9°$ fully coded field of view. IBIS is composed of two layers: ISGRI (Lebrun et al. 2003) working in the energy band 15–1000 keV, and PICsIT (Di Cocco et al. 2003) operating from 175 keV to 10 MeV. The spectrometer SPI provides spectra with high energy resolution (3 keV at 1.7 MeV) in the energy band from 20 keV to 8 MeV (Vedrenne et al. 2003).

Just a few weeks after the launch, the INTEGRAL satellite started the in–orbit calibration observing Cyg X–1. On November 25th, 2002, the satellite was set up for a special observation with the PICsIT layer in the non–standard photon–by–photon mode, a reduced number of channels, and most of the satellite telemetry. This special configuration was required since PICsIT operates in an energy band where the background rate is very high (≈3500 counts/s on the whole detector) and the available telemetry is not sufficient to download all the data (for more details on the PICsIT modes of operation see Di Cocco et al. 2003) in photon-by-photon. So, to perform the calibration of PICsIT photon–by–photon mode it was necessary to limit the operative range at <500 keV and to strongly reduce the telemetry allocation to the other instruments (SPI, JEM–X, OMC were sending only housekeeping data to ground) and to the ISGRI layer of IBIS.

During this test, at 17:58:30 UTC a gamma–ray burst occurred in the partially coded field of view of IBIS (about 7.3°

Send offprint requests to: G. Malaguti,
e-mail: malaguti@bo.iasf.cnr.it

⋆ Based on observations with INTEGRAL, an ESA project with instruments and science data centre funded by ESA member states (especially the PI countries: Denmark, France, Germany, Italy, Spain, Switzerland), Czech Republic and Poland, and with the participation of Russia and the USA.

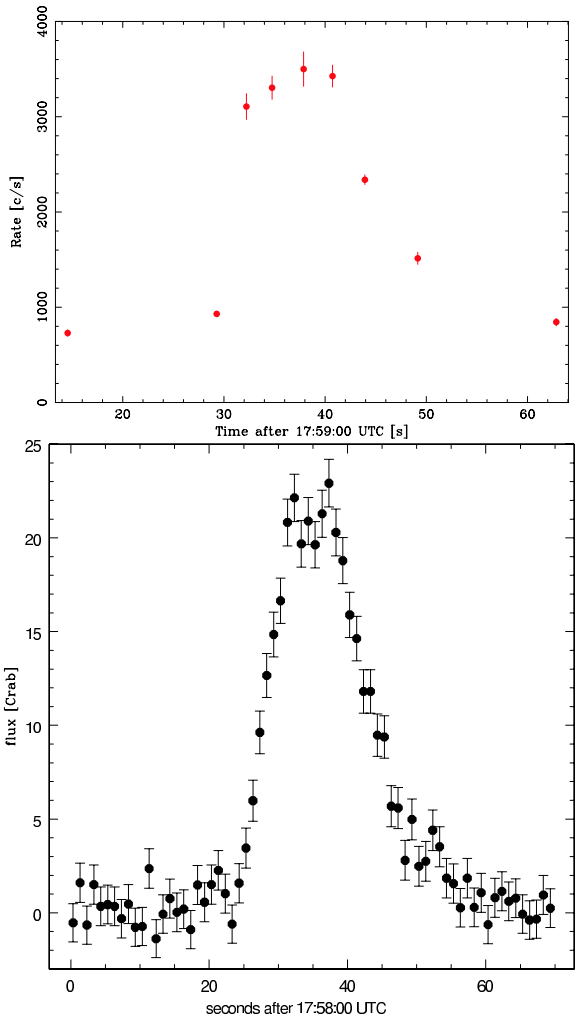

Fig. 1. GRB 021125 lightcurves: (*top*) IBIS/ISGRI lightcurve in the whole energy range, heavily affected by telemetry gaps; time starts from 17:58:00 UT. (*bottom*) SPI lightcurve (in Crab units) obtained from the detector count rates in the energy range 0.02–8 MeV, which are part of the scientific housekeeping data; time starts from 17:58:00 UT.

off–axis), and lasted about 24 s (Bazzano & Paizis 2002). The burst was soon confirmed by the InterPlanetary Network (IPN) composed of the satellites Ulysses, Mars Odyssey–HEND, and RHESSI (Hurley et al. 2002). Here we report on the analysis of the data from the INTEGRAL instruments.

2. Lightcurves

Lightcurves were available from IBIS and SPI instruments. For the former, the ISGRI detector data were strongly affected by telemetry reduction (data were available only for about 10% of time), so that the lightcurve has very few points (Fig. 1). Due to the restricted telemetry mode, SPI transmitted to ground only the science housekeeping data containing the detector's total count rates. In this case, the energy band is 20 keV–8 MeV, with a time resolution of 1 s (Fig. 1). The IBIS/PICsIT layer, although with a special amount of dedicated telemetry and a reduced number of channels, was influenced by telemetry gaps (about 62% of events were downloaded), clearly visible in Fig. 2. Moreover, only PICsIT single (i.e. events which deposit their energy in one pixel only) events were sent to ground, thus limiting the information for the high energy part of the spectrum.

Considering the duration of the GRB as the time when the count rate is more than 4σ above the background rate, we have that GRB 021125 was 24 s long in the energy range of IBIS/PICsIT, while it is 23 s according to SPI–ACS. For IBIS/ISGRI, because of the telemetry gaps, we have only a lower limit of 21 s.

The IBIS/PICsIT lightcurve (Fig. 2) in different energy bands shows the indication of a possible softening in the second part of the GRB. This is also consistent with the steep spectrum in the PICsIT energy range (see Sect. 4). On the other hand, the absence of detection above 500 keV could be due to the limited PICsIT energy range during this observation.

Table 1. Sky coordinates of the GRB 021125 as seen by the different instruments onboard INTEGRAL and by the IPN (3σ).

Instrument	RA (J2000)	Dec (J2000)	Error radius
IBIS/ISGRI	19:47:56	+28:23:28	2′
IBIS/PICsIT	19:47:51	+28:19:16	5′
SPI	19:47:55	+28:23:49	13′
IPN (centre)	19:47:25.93	+28:16:0.45	
IPN (corner 1)	19:46:49.27	+28:09:14.20	
IPN (corner 2)	19:47:47.73	+28:13:09.68	
IPN (corner 3)	19:47:37.78	+28:21:06.43	
IPN (corner 4)	19:48:36.40	+28:25:00.85	

3. Imaging

The fact that PICsIT was in photon–by–photon mode, allowed the extraction of the events in the time region around the burst and the subsequent deconvolution using the standard software IDAS[1]. The same occurred for IBIS/ISGRI, for which the photon–by–photon mode is already the standard operation mode and the only available. In addition, for ISGRI it was possible also to use the IBAS (INTEGRAL Burst Alert System, Mereghetti et al. 2003) off–line software, even though the special set up for PICsIT strongly reduced the available telemetry for ISGRI. Nevertheless, it was possible to obtain images also for ISGRI and to reconstruct the sky position. Only the scientific housekeeping and on board spectra data were available for SPI, because of the special configuration of INTEGRAL. However, these data allowed to obtain a deconvolved image, although with non–standard techniques.

The GRB coordinates as seen by INTEGRAL instruments and the IPN are shown in Table 1. Figure 3 shows the error boxes for IBIS/ISGRI (Gros & Produit 2002), IPN (Hurley et al. 2002), SPI, and IBIS/PICsIT.

[1] *INTEGRAL Data Analysis System*, available at `http://isdc.unige.ch/index.cgi?Soft+download`. See also Goldwurm et al. (2003).

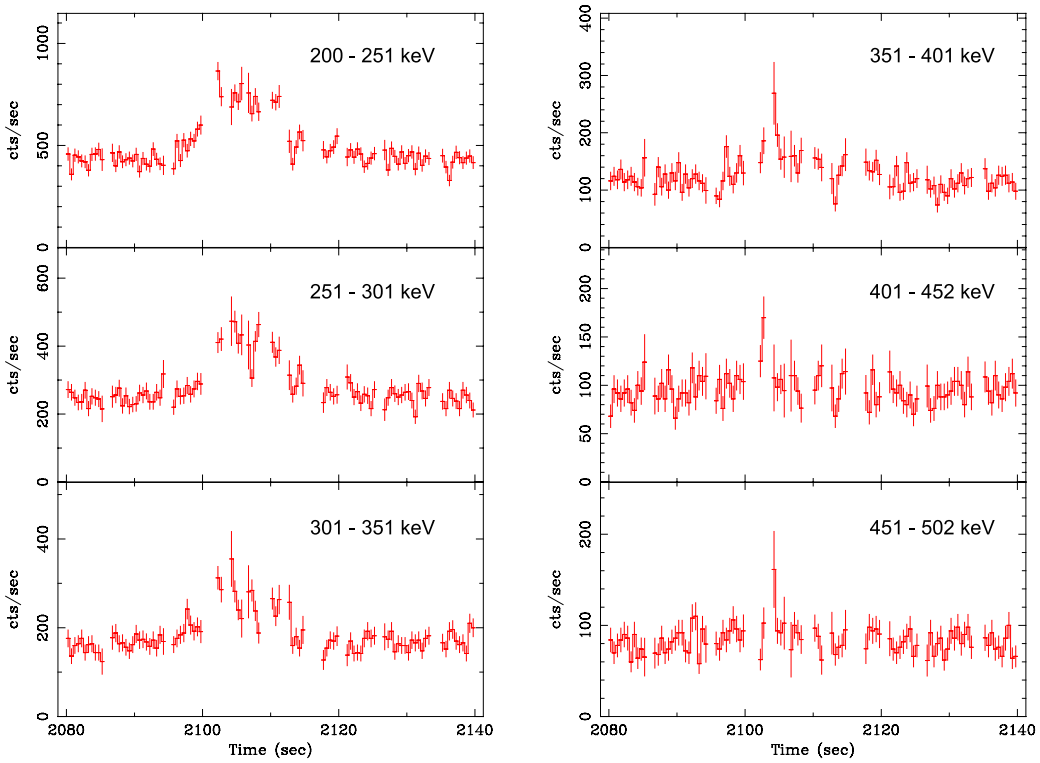

Fig. 2. GRB 021125: IBIS/PICsIT lightcurve for single events in different energy bands. Time starts from 17:23:50 UT.

The non-standard telemetry configuration of the instruments forced the IBAS[2] system to remain in idle mode. This, together with the fact that INTEGRAL was still in the PV phase, caused a delay in the release of the GRB coordinates of about one day, while the refined error box (with 2 arcmin uncertainty) was released only 3.7 days after the GRB. Therefore, the fact that no optical counterpart of GRB 021125 was found, could mean that the afterglow was below the actual sensitivities of ground telescopes.

4. Spectral analysis

IBIS is a coded mask detector and the photons of a single point source are spread all over the detector (e.g. Skinner 2002). The procedure of spectral extraction for ISGRI consists of the modelling of the illuminated mask by a point source of unitary flux, placed in the same sky coordinates of the GRB. Then, the model is fitted to the detected shadowgram in each energy channel to obtain the rate and error for each channel (see Goldwurm et al. 2003 for more details). The count spectra obtained by using this procedure, independently implemented in both ISGRI off–line scientific analysis and IBAS off–line software gave results in very good agreement.

The high PICsIT count rate during the burst (about 50% more than the background level) has allowed the use of a more direct procedure. The count spectrum of the GRB has been extracted by subtracting the background obtained from an empty field observation, and cleaning for the cosmic–rays induced events. This method implemented both in the Ground Support Equipement (GSE) and in the Instrument Specific Software (ISSW), has given results in good agreement.

The 20–500 keV time averaged spectrum from combined data of ISGRI and PICsIT, both corrected for intrinsic

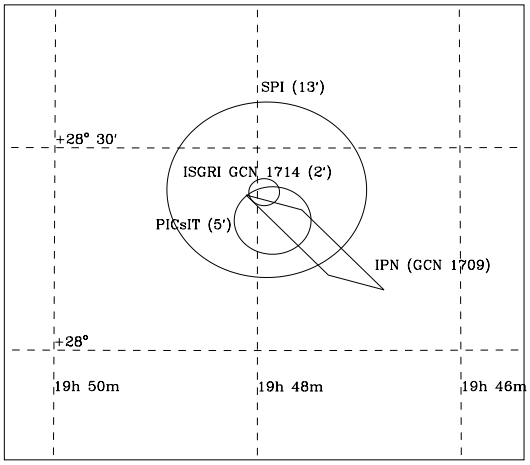

Fig. 3. Localisation uncertainties of the GRB 021125 from IBIS/ISGRI, IBIS/PICsIT, SPI, and the Interplanetary Gamma–Ray Burst Timing Network. For more details see Table 1.

[2] Normally, IBAS is triggered by the ISGRI layer, but in this case the limited data flow received from the detector telemetry did not allow the triggering.

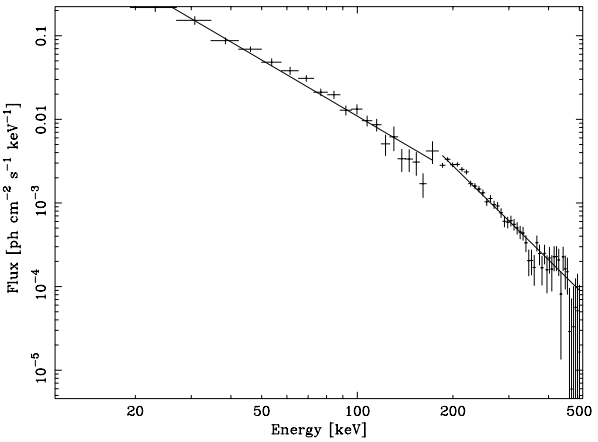

Fig. 4. IBIS photon spectrum of single events in the energy band 20–500 keV, fitted with the two power law models. The boundary between the two layers data is clearly visible.

detector deadtimes and telemetry gaps, is shown in Fig. 4. ISGRI refers to the energy range 20–180 keV, while PICsIT covers the range 175–500 keV. The low energy part of the spectrum (ISGRI) is well fitted with a power law model with $\Gamma \approx 2.2$, while the PICsIT part is fitted with a power law with $\Gamma \approx 3.7$. This difference in spectral indices between ISGRI and PICsIT could be the indication of a spectral break around 200 keV, but given the present uncertainties in the response of the two layers, it is not possible to clearly define the energy of the break. In any case, the estimated value would be in agreement with the statistical distribution of the energy break calculated by Preece et al. (2000) on the basis of about 5500 GRB observed with CGRO/BATSE. The apparent inconsistency between the ISGRI and PICsIT fluxes at 180–200 keV, is to be ascribed to the uncertainty in the ISGRI absolute flux measurement due to the large data loss caused by the 90% dead time during the GRB.

The average fluxes, corrected for intrinsic detector deadtimes and telemetry gaps, are 5.3 ± 0.6 ph cm^{-2} s^{-1}, and 0.25 ± 0.03 ph cm^{-2} s^{-1}, in the ISGRI and PICsIT energy bands, respectively. These correspond to 14 ± 2 Crab for ISGRI and 9 ± 1 Crab for PICsIT. The average flux obtained by SPI in the energy range 0.02–8 MeV is 9 ± 1 Crab, in agreement with IBIS. The fluence is approximately 5.1×10^{-5} erg cm^{-2} in the whole IBIS range.

As observed by Ulysses, the GRB had a duration of approximately 30 seconds, a 25–100 keV fluence of approximately 8.7×10^{-6} erg cm^{-2} and a peak flux of approximately 7.8×10^{-7}erg cm^{-2} over 0.50 seconds (Hurley et al. 2002).

5. Final remarks

GRB 021125 was the first GRB detected by INTEGRAL in the field of view of the IBIS imager. The sky coordinates reconstruction with IBIS and SPI are in agreement with each other, and consistent with the error box of the Interplanetary Network. The spectrum and lightcurve, obtained with independent methods, which gave consistent results, show an indication of a possible softening of the spectrum in the second part of the GRB.

GRB 021125 has shown the capabilities of the instruments on board the INTEGRAL satellite.

Acknowledgements. This work has been partially funded by the Italian Space Agency (ASI). LF acknowledges the hospitality of the INTEGRAL Science Data Centre (ISDC) during part of this work. AJB acknowledges funding by PPARC grant GR/2002/00446.

References

Bazzano, A., & Paizis, A. 2002, GCN 1706
Di Cocco, G., Caroli, E., Celesti, E., et al. 2003, A&A, 411, L189
Goldwurm, A., David, P., Foschini, L., et al. 2003, A&A, 411, L223
Gros, A., & Produit, N. 2002, GCN 1714
Gros, A., Goldwurm, A., Cadolle–Bel, M., et al. 2003, A&A, 411, L179
Hurley, K., Mazets, E., Golenetskiiet, S., et al. 2002, GCN, 1709
Lebrun, F., Leray, J. P., Lavocat, P., et al. 2003, A&A, 411, L141
Lund, N., Brandt, S., Budtz-Jorgensen, C., et al. 2003, A&A, 411, L231
Mas–Hesse, J. M., Giménez, A., Culhane, L., et al. 2003, A&A, 411, L261
Mereghetti, S., Götz, D., Borkowski, J., Walter, R., & Pedersen, H. 2003, A&A, 411, L291
Preece, R. D., Briggs, M. S., Mallozzi, R. S., et al. 2000, ApJS, 126, 19
Skinner, G. K. 2002, in The Gamma-Ray Universe, Proc. of the XXXVII Rencontres de Moriond, ed. A. Goldwurm, D. N. Neumann, & J. Tran Thanh Van (The Gioi Publ.), 423
Ubertini, P., Lebrun, F., Di Cocco, G., et al. 2003, A&A, 411, L131
Vedrenne, G., Roques, J.–P., Schönfelder, V., et al. 2003, A&A, 411, L63
Winkler, C., Courvoisier, T. J. L., Di Cocco, G., et al. 2003, A&A, 411, L1

A&A 411, L311–L314 (2003)
DOI: 10.1051/0004-6361:20031303

Astronomy & Astrophysics

GRB 021219: The first Gamma-Ray Burst localized in real time with IBAS⋆

S. Mereghetti[1], D. Götz[1,2], V. Beckmann[3,4], A. von Kienlin[5], P. Ubertini[6], A. Bazzano[6], L. Foschini[7], and G. Malaguti[7]

[1] Istituto di Astrofisica Spaziale e Fisica Cosmica – CNR, Sezione di Milano "G.Occhialini", via Bassini 15, 20133 Milano, Italy
[2] Dipartimento di Fisica, Università degli Studi di Milano Bicocca, P.zza della Scienza 3, 20126 Milano, Italy
[3] Integral Science Data Centre, Chemin d'Écogia 16, 1290 Versoix, Switzerland
[4] Institut für Astronomie und Astrophysik, Universität Tübingen, Sand 1, 72076 Tübingen, Germany
[5] Max Planck Institut für extraterrestrische Physik, Postfach 1312, 85741, Garching, Germany
[6] Istituto di Astrofisica Spaziale e Fisica Cosmica – CNR, Sezione di Roma, via Fosso del Cavaliere 100, 00133 Roma, Italy
[7] Istituto di Astrofisica Spaziale e Fisica Cosmica – CNR, Sezione di Bologna, via Gobetti 101, 40129 Bologna, Italy

Received 10 July 2003 / Accepted 26 August 2003

Abstract. On December 19, 2002, during the Performance and Verification Phase of INTEGRAL, a Gamma-Ray Burst (GRB) has been detected and localized in real time with the INTEGRAL Burst Alert System (IBAS). Here we present the results obtained with the IBIS and SPI instruments. The burst had a time profile with a single peak lasting about 6 s. The peak spectrum can be described by a single power law with photon index $\Gamma = 1.6 \pm 0.1$ and flux ~3.7 photons cm^{-2} s^{-1} (20–200 keV). The fluence in the same energy range is 9×10^{-7} erg cm^{-2}. Time resolved spectroscopy performed with IBIS/ISGRI shows a clear hard to soft evolution of the spectrum.

Key words. gamma rays: bursts – gamma rays: observations

1. Introduction

Although considerable progress in the understanding of Gamma-Ray Bursts (GRBs) has been made after the discovery of their afterglows at longer wavelengths (see, e.g., van Paradijs et al. 2000) the debate on their progenitors is still open. A model involving the core collapse of a massive star (e.g. Woosley 1993) seems to be favored for long GRBs and evidence for a Supernova-GRB association has been found recently (Stanek et al. 2003; Hjorth et al. 2003). The situation is more uncertain for what concerns short (<2 s) bursts, mostly because of the lack of counterparts at other wavelengths for this class of GRBs.

A multi-wavelength approach is crucial to the understanding of the complex nature of GRBs. The short duration of the prompt γ-ray emission and the fading character of the afterglow impose a rapid follow-up. This can be achieved only if the positions derived from the prompt emission are immediately distributed to the scientific community. The INTEGRAL satellite, although not built as a GRB-oriented mission, can contribute to this task thanks to the INTEGRAL Burst Alert System (IBAS; Mereghetti et al. 2003b). To date IBAS has successfully detected and located 5 GRBs, with increasing accuracy and decreasing delays (4.36′ error radius after 30 s for GRB 030501; IBAS Alert 596).

GRB 021219 is the first GRB detected in real time by IBAS. This occurred only two months after the launch of INTEGRAL, while the satellite was still in its performance and verification (PV) phase. During the PV phase, the external distribution of the IBAS alerts was not enabled yet. An internal alert message, produced only 10 s after the start of the burst, reached the members of the IBAS Localization Team and a GRB Coordinates Network (GCN) circular with a preliminary position could be issued 5 hours later, after a quick analysis to confirm the GRB (Mereghetti et al. 2002). Since during the PV phase the relative alignment between IBIS and the satellite star trackers was not well measured yet, an uncertainty of 20′ was attributed to the derived position. A refined position could be derived later

Send offprint requests to: S. Mereghetti,
e-mail: sandro@mi.iasf.cnr.it

⋆ Based on observations with INTEGRAL, an ESA project with instruments and science data centre funded by ESA member states (especially the PI countries: Denmark, France, Germany, Italy, Switzerland, Spain), Czech Republic and Poland, and with the participation of Russia and the USA.

(Götz et al. 2002), thanks to the presence of Cyg X-1 in the field of view.

Here we report on the results on GRB 021219 obtained with the IBIS (Ubertini et al. 2003) and SPI (Vedrenne et al. 2003) instruments. They are both coded mask imaging telescopes with a large field of view (29° × 29° IBIS, 36° diameter SPI). IBIS is based on two detectors, ISGRI (Lebrun et al. 2003) and PICsIT (Di Cocco et al. 2003), operating in the 15 keV–1 MeV and 175 keV–10 MeV energy ranges, respectively. SPI consists of 19 Ge detectors cooled at 85 K and works in the 20 keV–8 MeV range. The GRB was located outside the field of view of the two low energy monitoring instruments JEM-X (Lund et al. 2003) and OMC (Mas-Hesse et al. 2003).

2. Data analysis

2.1. IBIS

During this observation PICsIT provided images integrated on time intervals of several minutes, which cannot be used for the study of GRBs. Owing to the telemetry limitations at satellite level this is the standard operation mode of PICsIT. Useful data for GRB studies can be obtained by PICsIT when it is operated in photon-by-photon mode (as it occurred for GRB 021125, see Malaguti et al. 2003). Our results for GRB 021219 are therefore based only on data from the ISGRI detector.

We have analyzed ISGRI single interaction events, for which the arrival time, energy deposit and interaction pixel are known.

GRB 021219 has been detected at off-axis angles $Z = 1.38°$ and $Y = 10.02°$, in the partially coded field of view of IBIS, with a signal-to-noise ratio of 15.5 in the 15–100 keV band. The top panel of Fig. 2 shows the GRB light curve binned at 0.2 s intervals. It refers to the 15–500 keV band, and, to increase the signal to noise ratio, it has been extracted using only the pixels illuminated by the GRB for at least half of their surface. The GRB started at 07:33:55 UTC and had a T_{90} duration of 5.5 s. The time profile shows a single peak.

To derive an accurate position we selected a 15 s time interval starting at 07:33:55 UTC, obtaining $\alpha_{J2000} = 18^h50^m25^s$, $\delta_{J2000} = +31°56'23''$, with an uncertainty of 2′ radius. As shown in Fig. 1, this position is consistent with the one published earlier and with the annulus derived independently with the International Planetary Network (IPN, Hurley et al. 2002).

We have extracted the GRB peak spectrum (over a time interval of 1 s) using 128 linearly spaced bins between 19 keV and 1 MeV and then rebinned it to have at least 25 counts per channel. Since IBIS is a coded mask instrument, the background spectrum can be measured simultaneously to that of the target, by using the pixels not illuminated by the source. A fully calibrated response matrix for large off-axis angles is not available yet. Therefore, we divided the counts spectrum by the closest (in detector coordinates) spectrum of the Crab Nebula. The resulting photon spectrum (Fig. 3) is well described by a power law with photon index $\Gamma = 1.6 \pm 0.1$ and flux in the 20–200 keV band of 3.7 photons (3.5×10^{-7} erg) cm^{-2} s^{-1}.

The total (time averaged) spectrum has been obtained with the same technique and can be fitted by a power law with $\Gamma = 2.0 \pm 0.1$. The fluence in the 20–200 keV band (corrected for the telemetry gaps) is 9×10^{-7} erg cm^{-2}.

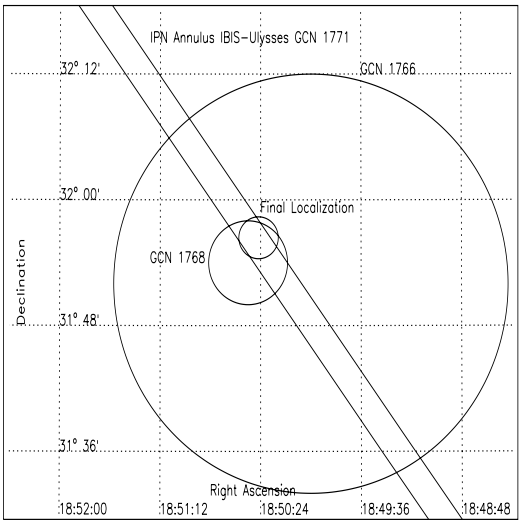

Fig. 1. Localizations of GRB 021219: the positions published earlier are consistent with the final one derived in this work, see text.

We have also investigated the spectral evolution with time. Four spectra of the duration of ∼1 s each have been extracted: one during the rising part of the GRB, one at the peak, and two during the decaying tail. All the spectra are well represented by a power law model. The corresponding photon indices, plotted in the lowest panel of Fig. 2, provide a significant evidence for a softening with time of the burst spectrum.

2.2. SPI

At the time of GRB 021219 the SPI instrument was in low-telemetry mode. Therefore, no single events have been transmitted to the ground in photon-by-photon mode. Only the events which occurred in several detectors (multiple events) and those analysed by the on-board pulse discriminator (PSD events) were kept. Due to this, there was no sensitivity below ∼200 keV. Still SPI transmitted to the ground the count-rates of all the events measured in each of the 19 Ge detectors in bins of 1 s (see middle panel of Fig. 2). For these events the information about the photon energy is lost and thus only a broad band count rate can be given. The background was determined using the data starting from 20 min before the burst occurrence. The peak flux and fluence have been then derived from the broad band count rate by comparison with the count rate measured for the Crab Nebula. This results in a peak flux of 10.7 ± 1.1 Crab at 07:33:56 UTC, which is consistent with the value obtained with IBIS/ISGRI. The values are consistent also for what concerns the fluence.

The imaging analysis of the SPI data, using a 3 s time interval starting at 07:33:55 UTC, yields a position $\alpha_{J2000} = 18^h49.3^m$, $\delta_{J2000} = +31°46.1'$, with an uncertainty of 30′ ($S/N = 8.5$) localizing the GRB 17.6′ from the IBIS/ISGRI position.

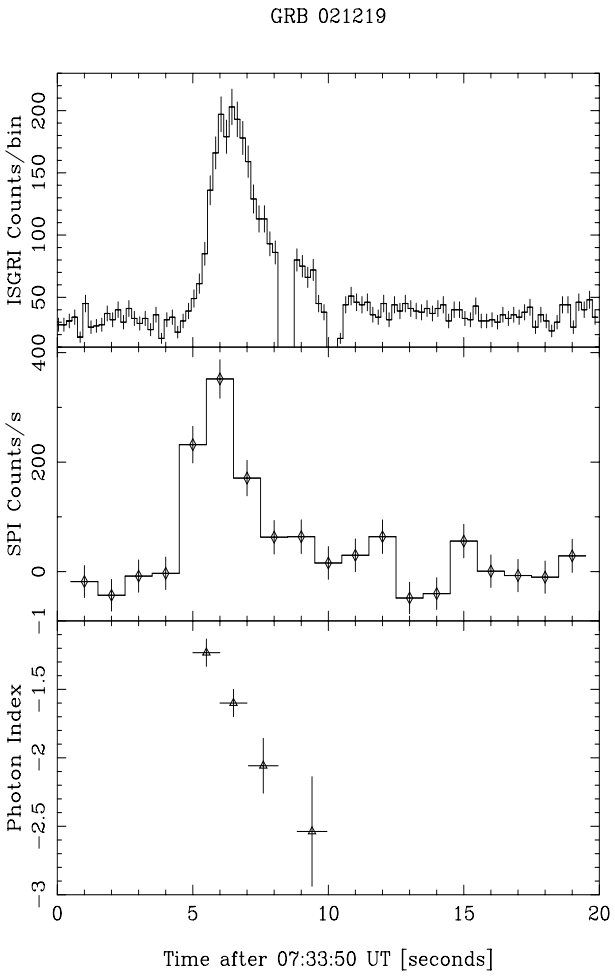

Fig. 2. *Upper panel*: IBIS/ISGRI light curve of GRB021219 in the 15–500 keV band binned over 0.2 s. The gaps are artifacs caused by satellite telemetry saturation. *Middle panel*: Background subtracted light curve of GRB 021219 measured with SPI. *Lower panel*: Spectral evolution of GRB 021219 with time. A clear hard-to-soft evolution is seen.

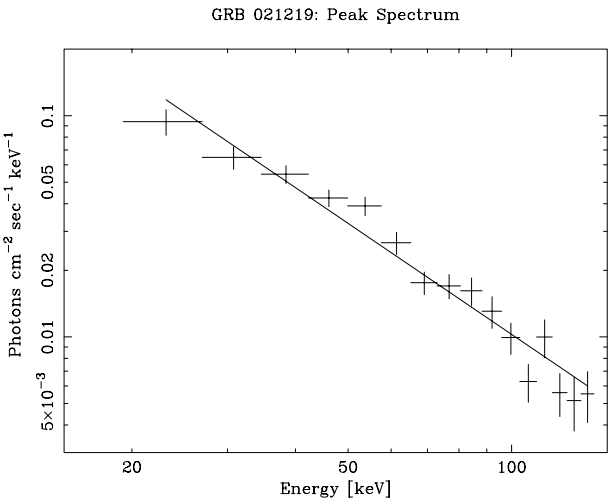

Fig. 3. Peak spectrum of GRB 021219 as measured with IBIS/ISGRI.

3. Discussion

GRB 021219 had a rather steep average spectrum, indicating that it can be considered an X-ray rich GRB. Usually GRB spectra are well described by a phenomenological model (Band et al. 1993) consisting of two power laws, one at low energies (with slope α) and one at high energies (with slope β), and a smooth break typically between about 100 and 400 keV (Preece et al. 2000). The fact that no break is seen in the spectrum of GRB 021219 up to 150 keV indicates that the break, if any, is outside our detection range. The value of the photon index ~2, compared to the ones typically observed in the BATSE sample $\langle\beta\rangle \sim 2.5$, suggests that we are observing the part of the spectrum above the break. We cannot exclude, however, that the break is at higher energies: this would qualify GRB 021219 even more as an X-ray rich GRB.

The time resolved spectroscopy performed with IBIS/ISGRI indicates a clear hard-to-soft spectral evolution. This is a common feature in many GRBs observed with previous satellites (e.g. Norris et al. 1986; Ford et al. 1995; Frontera et al. 2000).

No optical counterpart for this GRB has been reported, with limiting magnitudes of $R = 13.7$ at $t - t_0 \sim 7.5$ hours (Lipunov et al. 2002), $R = 18$ at $t - t_0 \sim 11$ hours, $I = 19.5$ at $t - t_0 \sim 18$ hours (Henden et al. 2002) and $R = 20.5$ at $t - t_0 \sim 34$ hours (Castro-Tirado et al. 2002). Observations in the radio band at 4.86 GHz (at $t - t_0 \sim 16$ hours) have not detected any new source down to a 4σ limit of 220 μJy (Berger et al. 2002).

The fact no optical transient has been detected indicates a "dark" or at least dim nature of this GRB. A similar behaviour has been noticed before in other X-ray rich events. For example, the X-ray rich GRB 021211 (Crew et al. 2003) was fainter than $R \sim 22.5$ 12 hours after the burst (Klose et al. 2002). The optical time history of this GRB is compatible with the upper limits reported above for GRB 021219.

4. Conclusions

The successful detection and localization of GRB 021219 only one month after IBIS activation, showed that IBAS is able to derive and distribute the position of the GRBs detected in the field of view of IBIS within a few tens of seconds.

The analysis of GRB 021219 reported here shows that IBIS/ISGRI is indicated for detailed spectral studies. In fact we have been able to obtain spectra integrated over only 1 s with good statistics, thus deriving the spectral shape of the GRB and its variation with time.

Acknowledgements. This research has been partially supported by the Italian Space Agency. LF acknowledges the hospitality of the ISDC during part of this work.

References

Band, D. L., Matteson, J., Ford, L., et al. 1993, ApJ, 413, 281
Berger, E., & Frail, D. A. 2002, GCN 1774
Castro-Tirado, A. J., et al. 2002, GCN 1775
Crew, G. B., Lamb, D. Q., Ricker, G. R., et al. 2003, ApJ submitted, [astro-ph/0303470]
Di Cocco, G., Caroli, E., Celesti, E., et al. 2003, A&A, 411, L189
Ford, L. A., Band, D. L., Matteson, J. L., et al. 1995, ApJ, 439, 307
Frontera, F., Amati, L., Costa, E., et al. 2000, ApJS, 127, 59
Götz, D., Favre, P., Mereghetti, S., & Borkowski, J. 2002, GCN 1768
Henden, A., Hambsch, J., & Broens, E. 2002, GCN 1773
Hjorth, J., Sollerman, J., Meller, P., et al. 2003, Nature, 423, 847
Hurley, K., Cline, T., Götz, D., et al. 2002, GCN 1771
Klose, S., Eisloeffel, J., Froebrich, D., et al. 2002, GCN 1739
Lebrun, F., Leray, J. P., Lavocat, P., et al. 2003, A&A, 411, L141
Lipunov, V., Krylov, A., Kornilov, V., et al. 2002, GCN 1770
Lund, N., Brandt, S., Budtz-Jørgensen, C., et al. 2003, A&A, 411, L231
Malaguti, G., Bazzano, A., Beckmann, V., et al. 2003, 411, L307
Mas-Hesse, J. M., Giménez, A., Culhane, L., et al. 2003, A&A, 411, L261
Mereghetti, S., Götz, D., & Borkowski, J. 2002, GCN 1766
Mereghetti, S., Götz, D., Tiengo, A., et al. 2003a, ApJ, 590, L73
Mereghetti, S., Götz, D., Borkowski, J., Walter, R., & Pedersen, H. 2003b, A&A, 411, L291
Norris, J. P., Share, G. H., Messina, D. C., et al. 1986, ApJ, 301, 213
Preece, R. D., Briggs, M. S., Mallozzi, R. S., et al. 2000, ApJS, 126, 19
Stanek, K. Z., Matheson, T., Garnavich, P. M., et al. 2003, ApJ, 591, L17
Ubertini, P., Lebrun, F., Di Cocco, G., et al. 2003, A&A, 411, L131
van Paradijs, J., Kouveliotou, C., & Wijers, R. A. M. J. 2000, ARA&A, 38, 379.
Vedrenne, G., Roques, J. P., Schönfelder, V., et al. 2003, A&A, 411, L63
Woosley, S. E., 1993, ApJ, 405, 273

A&A 411, L321–L325 (2003)
DOI: 10.1051/0004-6361:20031232

Astronomy & Astrophysics

INTEGRAL results on GRB 030320: A long gamma-ray burst detected at the edge of the field of view⋆

A. von Kienlin[1], V. Beckmann[2,3], S. Covino[8], D. Götz[4,5], G. G. Lichti[1], D. Malesani[9], S. Mereghetti[4], E. Molinari[8], A. Rau[1], C. R. Shrader[6,7], S. J. Sturner[6,7], and F. Zerbi[8]

[1] Max-Planck-Institut für extraterrestrische Physik, Giessenbachstrasse, 85748 Garching, Germany
[2] Institut für Astronomie und Astrophysik, Universität Tübingen, Sand 1, 72076 Tübingen, Germany
[3] INTEGRAL Science Data Centre, Chemin d'Écogia 16, 1290 Versoix, Switzerland
[4] Istituto di Astrofisica Spaziale e Fisica Cosmica – CNR, Sezione di Milano "G. Occhialini", via Bassini 15, 20133 Milano, Italy
[5] Dipartimento di Fisica, Università degli Studi di Milano Bicocca, P.zza della Scienza 3, 20126 Milano, Italy
[6] Code 661, NASA/Goddard Space Flight Center, Greenbelt, MD 20771, USA
[7] Universities Space Research Association, 7501 Forbes Blvd. #206, Seabrook, MD 20706, USA
[8] INAF / Brera Astronomical Observatory, via E. Bianchi 23807, Merate (LC), Italy
[9] International School for Advanced Studies (SISSA-ISAS), via Beirut 2–4, 34014 Trieste, Italy

Received 16 July 2003 / Accepted 8 August 2003

Abstract. GRB 030320 is the 5th gamma-ray burst (GRB) detected by INTEGRAL in the field of view (FoV). It is so far the GRB with the largest off-axis angle with respect to the INTEGRAL pointing direction, near to the edge of the FoV of both main instruments, IBIS and SPI. Nevertheless, it was possible to determine its position and to extract spectra and fluxes. The GRB nature of the event was confirmed by an IPN triangulation. It is a ~60 s long GRB with two prominent peaks separated by ~35 s. The spectral shape of the GRB is best represented by a single power law with a photon index $\Gamma \simeq 1.7$. The peak flux in the 20–200 keV band is determined to ~5.7 photons cm^{-2} s^{-1} and the GRB fluence to 1.1×10^{-5} erg cm^{-2}. Analysing the spectral evolution of the GRB, a "hard-to-soft" behaviour emerges. A search for an optical counterpart has been carried out, but none was found.

Key words. gamma-ray bursts – GRB – gamma-ray astronomy – INTEGRAL – SPI – IBIS

1. Introduction

Since their discovery more than thirty years ago (Klebesadel 1973) GRBs had evaded an understanding of their nature for about 20 years. This changed dramatically with the identification of the first GRB X-ray afterglow with a BeppoSAX observation (Costa et al. 1997). Since then it has been shown that at least the sources of long GRBs (lasting longer than 2 s) are located at cosmological distances. The observed fluxes revealed the enormous energy release of these events (van Paradijs et al. 2000) which is thought to be produced in asymmetric collapse of massive stars (Woosley 1993).

Here we report the detection of such an event by the two main instruments of INTEGRAL (Winkler et al. 2003) which have complementary performance characteristics. The imager IBIS (Ubertini et al. 2003) has an excellent angular resolution, whereas the spectrometer SPI (Vedrenne et al. 2003) is assigned to high-resolution spectroscopy, but has only modest imaging capabilities. The burst-detection capabilities of the INTEGRAL mission are achieved by the INTEGRAL burst alert system (IBAS: Mereghetti et al. 2003a; IBAS for SPI/ACS: von Kienlin et al. 2001), which scans the satellite telemetry in near-real time for GRBs at the INTEGRAL Science Data Centre (ISDC; Courvoisier et al. 2003).

2. Detection and localisation

On March 20, 2003 at 10:11:40 UTC, during the Galactic Centre Deep Exposure, a long GRB (~60 s) was detected at a large off-axis angle of 15.5°. This is near to one corner of the squared shaped IBIS FoV: 29° × 29° full width (SPI-FoV: ~35° full width).

Send offprint requests to: A. von Kienlin,
e-mail: azk@mpe.mpg.de

⋆ Based on observations with INTEGRAL, an ESA project with instruments and science data centre funded by ESA member states (especially the PI countries: Denmark, France, Germany, Italy, Switzerland, Spain), Czech Republic and Poland, and with the participation of Russia and the USA and on observations made with ESO telescopes at the La Silla Observatory under programme Id 71.D-0667(C).

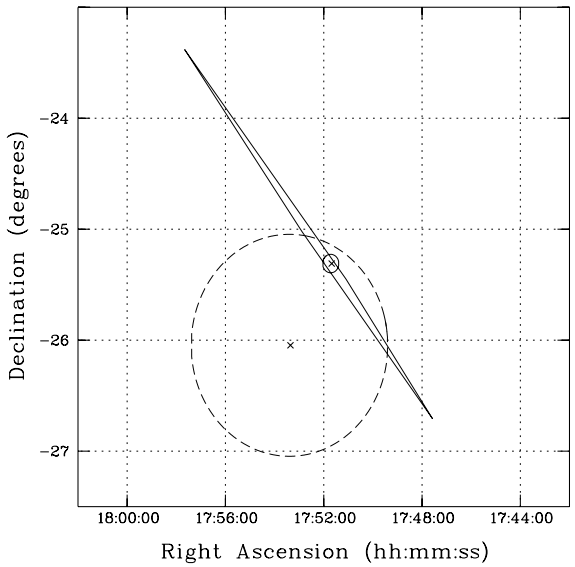

Fig. 1. Localisations of GRB 030320 showing the IBIS/ISGRI position (central cross) and error circle (solid line) of Mereghetti et al. (2003b). The IPN error box of Hurley et al. (2003b) and the derived SPI position with its 1° error circle (dashed line) are superimposed.

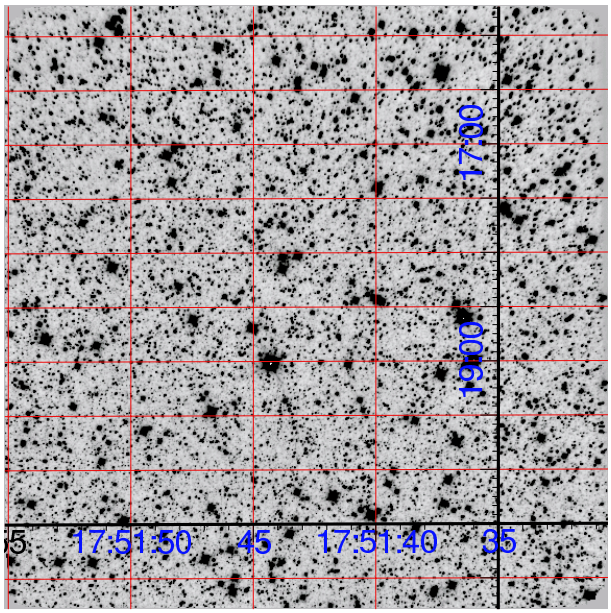

Fig. 2. ESO/NTT+SOFI image corresponding to the centre of the IBIS error circle derived here. The field is 5.5 × 5.5 arcmin wide. The 5 σ limiting magnitude is $Ks = 20.7$.

The GRB was detected by IBAS in near-real time in the data of ISGRI (Lebrun et al. 2001), the low-energy detector of IBIS. As the trigger had a low significance due to the position of the source on the edge of the FoV (only 3.7% of the detector was illuminated by the GRB) no prompt alert was distributed. An offline interactive analysis of the data confirmed that the trigger was due to an astrophysical source and allowed to determine and distribute a preliminary position 6.25 hours after the event (IBAS Alert 343; Mereghetti et al. 2003b). The preliminary derived position was $\alpha_{J2000} = 17^h51^m43^s$, $\delta_{J2000} = -25°18'34''$ with an uncertainty of 5′. In a further analysis of the entire GRB (UTC 10:11:36–10:12:40) in the 15–100 keV energy band the GRB was detected with a signal-to-noise ratio of $S/N \sim 15$. The derived error box had nearly the same centre $\alpha_{J2000} = 17^h51^m42^s$, $\delta_{J2000} = -25°18'44''$ but a smaller radius of 3′.

The GRB nature of the event was confirmed about one hour later by Konus, Mars Odyssey (HEND), and INTEGRAL/SPI-ACS via an IPN-annulus (Hurley et al. 2003a). By adding the information from Ulysses, Mars Odyssey (GRS), Konus-Wind and RHESSI to the above mentioned data, a small IPN error box was derived one day later (Hurley et al. 2003b).

SPI was only able to determine a rough position for the GRB in the energy interval between 100 keV and 1 MeV. At lower energies it was not possible to derive a position. One should notice that only 3 out of the 19 detectors of SPI's camera showed a substantial increase of the count rate, caused by the illumination of the GRB. By selecting two time intervals around the prominent peaks of emission (see below) from UTC 10:11:55 to 10:12:05 and 10:12:30 to 10:12:36 (in total 16 s), the derived SPI position is $\alpha_{J2000} = 17^h53.4^m$, $\delta_{J2000} = -26°2.8'$ with an uncertainty of 1° (S/N 7.2). This agrees within the error with the positions found by IBIS/ISGRI and IPN. Figure 1 shows a superposition of the IPN error box and the SPI- and IBIS/ISGRI-error circles.

The two monitoring instruments of INTEGRAL, the X-ray monitor JEM-X (Lund et al. 2003) and the optical camera OMC (Mas-Hesse et al. 2003), did not observe the event as it was outside their FoVs.

A search for an optical afterglow in the IBIS error circle was performed using the Wise-Observatory 1 m telescope 16.9 hours after the onset of the burst (Gal-Yam & Ofek 2003). This follow-up observation did not reveal any optical counterpart. R-band imaging under poor conditions did not show any new source down to a limiting magnitude of $R = 17.5$ mag.

We also performed two follow-up observations at ESO New Technology Telescope (NTT) using the SOFI camera. The first was made at 9.497 UT on the 21st of March (~23.3 hours after the GRB) with a Ks filter and had exposure of 30 min (see Fig. 2). The second was taken at 4.608 UT (~69.8 days after the GRB) on the 29th of May with the same filter and an exposure of 10 min. The difference image, although showing several variable sources, did not reveal a strong afterglow candidate.

The afterglow search was complicated by the burst location in the galactic plane. The foreground galactic hydrogen column density[1] of $N_H = (1.4 \pm 0.1) \times 10^{22}$ atoms/cm^2 in the direction of the burst results in an extinction of $A_V = (10.5 \pm 0.5)$ mag [$A_R = (7.85 \pm 0.35)$ mag]. This high extinction would have required an extraordinary intrinsically bright afterglow ($R_{int} < 10$ mag at the time of the Wise observations) in order to be detectable. This would be more than 5 mag brighter than the

[1] http://heasarc.gsfc.nasa.gov/cgi-bin/Tools/w3nh/w3nh.pl

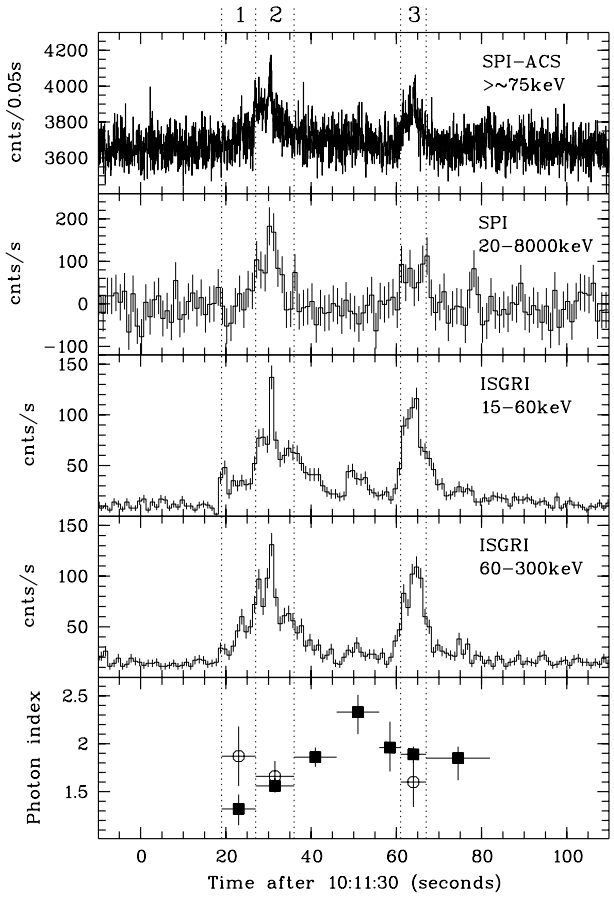

Fig. 3. Lightcurves of all INTEGRAL instruments which have seen GRB030320, from top to bottom: SPI-ACS overall veto count rate with 50 ms time resolution, SPI 1 s binned and IBIS/ISGRI in a soft (15–60 keV) and a hard (60–300 keV) energy range with 1 s binning. The bottom plot shows the evolution of photon index Γ [$f(E) = K \cdot (\frac{E}{1\mathrm{keV}})^{-\Gamma}$); K = photons/(keV cm^2 s) at 1 keV] for ISGRI (filled square) and SPI (XSPEC 12.0 results, open circle). The dotted lines mark the intervals 1–3 from Table 1.

very bright afterglow of GRB 030329 (Burenin et al. 2003) at the same time after the burst occurrence.

3. Temporal and spectral characteristics

Figure 3 shows the lightcurve for all INTEGRAL detectors which have observed GRB 030320. The lightcurves of ISGRI have been determined in two energy bands (15–60 keV and 60–300 keV) by using only the pixels that were illuminated by the GRB by at least half of their surface. The determination of a SPI lightcurve with a short time binning was only possible by using the 1 s count rates of the 19 Ge-detectors, which are normally used for science-housekeeping purposes. These values reflect the count rates of each detector in the broad SPI energy band from ~20 keV up to ~8 MeV. The SPI lightcurve in Fig. 3 was generated by summing the background-subtracted count rates. The background (~50 counts s^{-1} detector^{-1}) was determined from the SPI data before the burst occurrence over a duration of 40 min. The alternative method, which uses the time-tagged photon-by-photon SPI mode, with energy information for each photon, yielded insignificant results. With the anti-coincidence shield (ACS) of SPI the GRB was observed as an increase of the overall veto count rate. The effective area of the ACS is very small for sources observed within the field of view (von Kienlin et al. 2003a). For GRBs which occur outside the FoV of SPI the effective area of the ACS is however large, as it can be seen from the detection rate of ~0.8 GRBs/day (von Kienlin et al. 2003b). All lightcurves in Fig. 3 exhibit two prominent peaks during the ~60 s of prompt emission. A third peak is visible in the low-energy range of ISGRI, which is less significant at higher energies.

Spectra were extracted for characteristic intervals of the GRB lightcurve. The GRB spectrum was in all cases well represented by a single power-law model. The photon index and the source flux in the 20–200 keV energy range are listed for ISGRI and SPI in Table 1. For both instruments, the response for a source position near-to-zero coding is not yet well understood. For ISGRI the closest Crab observation was used for the calibration of the spectra. Any deficiencies of the SPI response at 15.5° off-axis angle is possibly the result of a not fully-representative mass model. Currently the off-axis effects of the response are assessed by using Crab observations, recorded during the payload-verification campaign, but the drawback of this method is the lack of Crab observations at such large off-axis angles.

The photon indices and fluxes listed in Table 1 for SPI were obtained by binning the photon-by-photon single and multiple events into six equally-spaced logarithmic energy bins in the 20 keV to 2 MeV range, for each of the listed time intervals. Spectral extraction was performed using SPIROS (SPI Iterative Removal of Sources; Skinner & Connell 2003), which takes the SPI photopeak effective area into account. Spectral model fitting was performed using XSPEC 11.2 and the off-diagonal response of SPI (SPI-RMF), as shown in the line $\mathrm{SPI}^{\mathrm{offd.}}_{11.2}$ of Table 1. For the background, all event data of the corresponding science window, with a duration of about 30 min, were used, but with the time of the GRB cut out (UTC 10:11:40–10:14:00). Table 1 lists the obtained photon indices and fluxes, when using XSPEC 11.2 only with a diagonal response (line $\mathrm{SPI}^{\mathrm{diag.}}_{11.2}$) too. Naturally one obtains a softer spectral shape with this method.

For comparison, the data were analysed using an alpha-test version of the XSPEC 12.0 software. This approach is distinct from the SPIROS method, in that the full diagonal plus off-diagonal response matrix is computed for each detector (and for each pointing direction, although here the GRB is contained within a single pointing) (Sturner et al. 2003; also Shrader et al. 2000). The detector-count spectra are then compared directly to the convolution of a photon model with, in this case, 19 response matrices, and a χ^2 minimisation is performed. This is, in principle, a more rigorous deconvolution procedure than the SPIROS method. However, the disadvantage is that the source and background must be simultaneously modelled whereas SPIROS reduces the problem to a single background subtracted spectrum and response matrix. A set of ancillary

Table 1. Photon indices and fluxes obtained by IBIS/ISGRI and SPI (by three different methods, see text) in 6 time intervals of the GRB. The quoted uncertainties are given for a 90% confidence range. For line $SPI_{12.0}$ it was only possible to quote the 90% confidence range approximately, because the calculation of uncertainty contours is not yet implemented in XSPEC 12.0.

Interval #		1	2	3	4	5	6
Position		before 1st peak	1st peak	2nd peak	max 1st peak	#1 + #2	full GRB
UTC 10 : _ : _		11:49–11:57	11:57–12:06	12:31–12:37	12:00–12:02	11:49–12:06	11:49–12:37
PhoIndex	ISGRI	$1.32\,^{0.15}_{-0.17}$	$1.56\,^{0.08}_{-0.07}$	$1.89\,^{0.09}_{-0.09}$	$1.62\,^{0.08}_{-0.09}$	$1.52\,^{0.08}_{-0.08}$	$1.69\,^{0.07}_{-0.08}$
	$SPI_{12.0}$	1.87 ± 0.31	1.66 ± 0.16	1.60 ± 0.26	1.01 ± 0.31	1.54 ± 0.15	1.51 ± 0.16
	$SPI^{offd.}_{11.2}$	$1.68\,^{0.67}_{-0.67}$	$0.94\,^{0.45}_{-0.87}$	$1.29\,^{0.45}_{-0.64}$	–	$1.28\,^{0.35}_{-0.48}$	$1.19\,^{0.29}_{-0.37}$
	$SPI^{diag.}_{11.2}$	$1.97\,^{0.71}_{-0.47}$	$1.40\,^{0.25}_{-0.28}$	$1.56\,^{0.36}_{-0.38}$	$1.03\,^{0.43}_{-0.50}$	$1.54\,^{0.24}_{-0.25}$	$1.57\,^{0.20}_{-0.20}$
20–200 keV Flux $\left[\frac{ph}{cm^2 s}\right]$	ISGRI	1.449	3.841	3.685	5.689	2.773	2.068
	$SPI_{12.0}$	3.08	4.35	3.53	3.14	3.24	2.11
	$SPI^{offd.}_{11.2}$	3.62	2.05	3.56	–	2.78	1.65
	$SPI^{diag.}_{11.2}$	4.40	4.45	4.95	4.13	4.11	2.82

response functions (ARFs), containing the energy, detector and angle-dependent effective area, were constructed for the GRB position and the burst spectrum was modelled in XSPEC 12.0 by fixing the background (derived by using the non-burst part of the observation). The obtained photon indices and fluxes are listed in the line $SPI_{12.0}$ of Table 1.

ISGRI single events have been used to derive photon indices and fluxes shown in the line "ISGRI" of Table 1. Thanks to the coded-mask design of the IBIS telescope, the source flux can be determined simultaneously with the background using the Pixel Illumination Function (PIF; Skinner 1995). The spectra have been extracted in 128 linearly-spaced energy bins between 19 keV and 1 MeV and were rebinned to have a signal-to-noise ratio larger than 3 in each channel. The photon spectra have then been obtained with the technique described above. In addition to the time intervals shown in Table 1 it was possible to obtain for ISGRI values of the photon index for the time intervals listed below:

Position:	Interval (UTC)	PhoIndex
decay of the 1st peak:	10:12:06–10:12:16	$1.859\,^{0.10}_{-0.10}$
small peak in between:	10:12:16–10:12:26	$2.329\,^{0.18}_{-0.23}$
rising of the 2nd peak:	10:12:26–10:12:31	$1.955\,^{0.28}_{-0.25}$
decay of the 2nd peak:	10:12:37–10:12:52	$1.849\,^{0.22}_{-0.22}$

With these ISGRI data it was possible to track the spectral evolution over the whole emission period, showing a general hard-to-soft evolution for the first peak up to the small peak between the two main peaks (Fig. 3 lower panel). During the second peak the spectrum hardens again (yet being softer compared to the first peak), but showing no evolution. The obtained ISGRI fluxes are reasonably correlated with the light curve.

The photon indices obtained with XSPEC 12.0 for SPI agree within the errors with the results obtained with ISGRI for interval 2, 3, 5 and 6, but reveals no spectral evolution. In contrast to the time between interval 2 and 3 (between to two main peaks) and after the last interval 3 (decay of the 2nd peak), it was possible to extract for SPI a spectrum for interval 1, although SPI's lightcurve did not show a rate increase. As expected the obtained photon index and flux do not agree well with the ISGRI values. A large discrepancy is observed for interval 4 (maximum of the 1st peak). SPI shows here a rather hard spectrum whereas for ISGRI the spectrum is even softer compared to interval 5. The SPI results have to be handled with care because for such a short 2 s interval, containing only a small number of counts in each energy bin, the determination of a spectrum is more difficult.

Comparing the results obtained with the three different methods used for the SPI data analysis, one can see that the XSPEC 12.0 derived photon indices yield the best agreement with the ISGRI data, although the same is valid for the SPIROS+XSPEC 11.2 results, using a diagonal response (line $SPI^{diag.}_{11.2}$ of Table 1), but these have a much broader confidence range. Second it should be noted that XSPEC 12.0 is using an off-diagonal response, which should represent the instrument much better.

The burst had a 20–200 keV peak flux (over 2 s) of $4.1\,^{1.3}_{-1.4} \times 10^{-7}$ erg cm^{-2} s^{-1} and 5.4×10^{-7} erg cm^{-2} s^{-1} and a 25–100 keV peak flux of $1.7\,^{0.9}_{-0.7} \times 10^{-7}$ erg cm^{-2} s^{-1} and 3.0×10^{-7} erg cm^{-2} s^{-1} measured with SPI and IBIS/ISGRI, respectively. These peak fluxes would place GRB 030320 in the top 25% of the BATSE peak flux distribution (Paciesas et al. 1999).

The gamma-ray fluence in the 20–200 keV band measured with SPI is $1.35\,^{0.21}_{-0.26} \times 10^{-5}$ erg cm^{-2}, consistent with 1.1×10^{-5} erg cm^{-2} from IBIS/ISGRI. The 25–100 keV fluence was $7.1\,^{1.6}_{-1.8} \times 10^{-6}$ erg cm^{-2} (SPI) and 6.5×10^{-6} erg cm^{-2} (ISGRI). Peak flux and fluence agree within a factor of two with the results obtained with Ulysses (Hurley et al. 2003b).

4. Conclusion

The analysis of GRB 030320 showed that INTEGRAL is still able to detect GRBs at the edge of its FoV. For this GRB a photon index of $\Gamma \simeq 1.7$ was derived for the prompt emission. The time resolved spectroscopy revealed a hard-to-soft transition of the spectrum during the 60 burst duration. Especially

IBIS/ISGRI showed a good performance in localisation and in the determination of the spectral evolution. The difficulties observed with SPI will hopefully improve with a better understanding of the response at the edge of the FoV.

Acknowledgements. The SPI project has been completed under the responsibility and leadership of CNES. We are grateful to ASI, CEA, CNES, DLR, ESA, INTA, NASA and OSTC for support. The SPI/ACS project is supported by the German "Ministerium für Bildung und Forschung" through DLR grant 50.OG.9503.0.

References

Burenin, R. A., Sunyaev, R. A., Pavlinsky, M. N., et al. 2003, Astron. Lett., accepted [astro-ph/0306137]
Coburn, W., & Boggs, S. E. 2003, Nature, 423, 415
Costa, E., Frontera, F., Heise, J., et al. 1997, Nature, 387, 783
Courvoisier, T. J.-L., Walter, R., Beckmann, V., et al. 2003, A&A, 411, L53
Gal-Yam, A., & Ofek, E. O. 2003, GCN, 1946
Hurley, K., Cline, T., Mitrofanov, I., et al. 2003a, GCN, 1942
Hurley, K., Cline, T., Mitrofanov, I., et al. 2003b, GCN 1943
Klebesadel, R., Strong, I., & Olsen, R. 1973, ApJ, 182, L85
Lebrun, F. 2001, in Proc. 4th INTEGRAL Workshop, ESA SP 459, 591
Lund, N., Brandt, S., Budtz-Jorgensen, C., et al. 2003, A&A, 411, L231
Mas-Hesse, M., Gimenez, A., Culhane, L., et al. 2003, A&A, 411, L261
Mereghetti, S., Götz, D., Borkowski, J., et al. 2003a, A&A, 411, L291
Mereghetti, S., Götz, D., Borkowski, J., et al. 2003b, GCN, 1941
Paciesas, W. S., Meegan, C. A., Pendleton, G. N., et al. 1999, ApJS, 122, 465
van Paradijs, J., Kouveliotou, C., & Wijers, R. A. M. J. 2000, ARA&A, 38, 379
Shrader, C., Sturner, S., & Teegarden, B. 2000, Proc. The Fifth Compton Symp., AIP CP-510
Skinner, G. K. 1995, Experimental Astronomy, 6/4, 1
Skinner, G. K., & Connell, P. H. 2003, A&A, 411, L123
Sturner, S., Shrader, C. R., Weidenspointner, W., et al. 2003, A&A, 411, L81
Ubertini, P., Lebrun, F., Di Cocco, G., et al. 2003, A&A, 411, L131
Vedrenne, G., Roques, J.-P., Schönfelder, V., et al. 2003, A&A, 411, L63
von Kienlin, A., Arend, N., & Lichti, G. G. 2001, in Proc. of the International GRB workshop held in Rome (Springer), 427
von Kienlin, A., Arend, N., Lichti, G. G., et al. 2003, in SPIE Conf. Proc. 4851, X-ray and Gamma-ray Telescopes and Instruments for Astronomy, 1336
von Kienlin, A., Beckmann, V., Rau, A., et al. 2003, A&A, 411, L299
Winkler, C., Courvoisier, T. J.-L., Di Cocco, G., et al. 2003, A&A, 411, L1
Woosley, S. E. 1993, ApJ, 405, 273

A&A 411, L327–L330 (2003)
DOI: 10.1051/0004-6361:20031075

Astronomy & Astrophysics

Time resolved spectroscopy of GRB 030501 using INTEGRAL⋆

V. Beckmann[1,2], J. Borkowski[2], T. J.-L. Courvoisier[2,3], D. Götz[4], R. Hudec[5], F. Hroch[2,5], N. Lund[6], S. Mereghetti[4], S. E. Shaw[2,7], A. von Kienlin[8], and C. Wigger[9]

[1] Institut für Astronomie und Astrophysik, Universität Tübingen, Sand 1, 72076 Tübingen, Germany
[2] INTEGRAL Science Data Centre, Chemin d'Écogia 16, 1290 Versoix, Switzerland
[3] Geneva Observatory, 51 chemin des Maillettes, 1290 Sauverny, Switzerland
[4] Istituto di Astrofisica Spaziale e Fisica Cosmica, CNR v. Bassini 15, 20133 Milano, Italy
[5] Astronomical Institute, Academy of Sciences of the Czech Republic, 25165 Ondrejov, Czech Republic
[6] Danish Space Research Institute, Juliane Maries Vej 30, 2100, Copenhagen, Denmark
[7] School of Physics and Astronomy, University of Southampton, Southampton, SO17 1BJ, UK
[8] Max-Planck-Institut für extraterrestrische Physik, Giessenbachstrasse, 85748 Garching, Germany
[9] Paul Scherrer Institut, 5232 Villingen, Switzerland

Received 28 May 2003 / Accepted 26 June 2003

Abstract. The gamma-ray instruments on-board INTEGRAL offer an unique opportunity to perform time resolved analysis on GRBs. The imager IBIS allows accurate positioning of GRBs and broad band spectral analysis, while SPI provides high resolution spectroscopy. GRB 030501 was discovered by the INTEGRAL Burst Alert System in the ISGRI field of view. Although the burst was fairly weak (fluence $F_{20\text{–}200\,\mathrm{keV}} \simeq 3.5 \times 10^{-6}$ erg cm^{-2}) it was possible to perform time resolved spectroscopy with a resolution of a few seconds. The GRB shows a spectrum in the 20–400 keV range which is consistent with a spectral index $\Gamma = -1.8$. No emission line or spectral break was detectable in the spectrum. Although the flux seems to be correlated with the hardness of the GRB spectrum, there is no clear soft to hard evolution seen over the duration of the burst. The INTEGRAL data have been compared with results from the Ulysses and RHESSI experiments.

Key words. gamma rays: bursts – gamma rays: observations

1. Introduction

Gamma Ray Bursts (GRBs) were discovered by chance in the late 1960s by the Vela experiments (Klebesadel et al. 1973). They have been proven to be extragalactic in origin after a successful identification of an X-ray afterglow by BeppoSAX (GRB 970508; Piro et al. 1998) with an optical counterpart at redshift $z = 0.835$ (Metzger et al. 1997). Even though we are now rather confident that long GRBs are related to massive explosions in distant galaxies, there are still many open questions remaining. First, whether GRBs are related to Supernova explosions, and also, what the connection to the star formation phenomenon is. Another crucial point is the exact mechanism by which GRBs can produce an energy output of $>10^{52}$ ergs (under the assumption that the emission is isotropic, which is probably not true). Prompt observation of GRBs in several energy ranges is essential to obtain high quality data for the study of these rapidly fading objects. Although GRBs were not one of the main targets for the scientific program of INTEGRAL (Winkler et al. 2000), the two main gamma-ray instruments, the imager IBIS (Ubertini et al. 1999) and the spectrometer SPI (Vedrenne et al. 1999), offer great capabilities for studying the prompt emission of GRBs when they occur in the field of view. Since the field of view is about 29 degrees, one gamma-ray burst per month is expected to be observed. This rate has been confirmed so far by the six bursts in the field of view between November 2002 and May 2003: GRB 021125 (Bazzano & Paizis 2002), GRB 021219 (Mereghetti et al. 2002), GRB 030131 (Borkowski et al. 2003), GRB 030227 (Mereghetti et al. 2003a), GRB 030320 (Mereghetti et al. 2003b), and GRB 030501 (Mereghetti et al. 2003c). In addition, the anticoincidence shield (ACS) of SPI can be used as an all-sky monitor for GRBs (von Kienlin et al. 2003).

During the last three bursts in the field of view, both SPI and IBIS, were in full operational mode, allowing time resolved spectral analysis.

2. INTEGRAL observation

GRB 030501 was detected on 1st May 2003 at 03:10:18 UT with data from the low energy detector of the IBIS instrument,

Send offprint requests to: V. Beckmann,
e-mail: Volker.Beckmann@obs.unige.ch

⋆ Based on observations with INTEGRAL, an ESA project with instruments and science data centre funded by ESA member states (especially the PI countries: Denmark, France, Germany, Italy, Switzerland, Spain), Czech Republic and Poland, and with the participation of Russia and the USA.

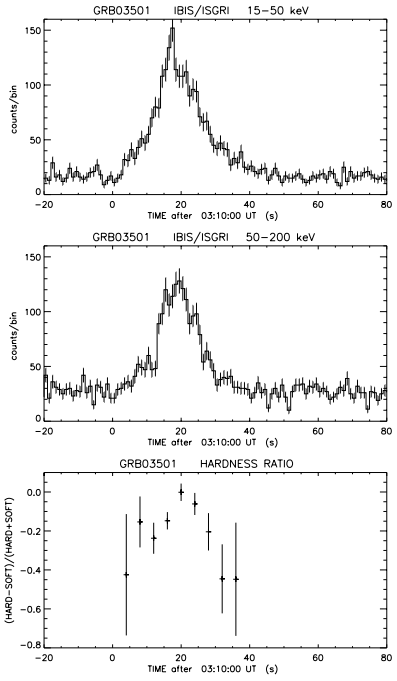

Fig. 1. Top panels: ISGRI lightcurves in the soft and hard band, respectively. IBAS triggered the GRB alert, within half a minute from the burst start, based on the ISGRI data. Bottom panel: hardness ratio evolution derived from the ISGRI countrates.

the Integral Soft Gamma Ray Imager (ISGRI; Lebrun et al. 2001), which consists of 128 × 128 CdTe crystals sensitive in the energy range 15–300 keV. ISGRI uses the coded mask technique and offers an instrumental resolution of ∼12 arcmin over the field of view of 29° × 29°. The source location precision depends on the brightness of the source, and is about 1 arcmin for sources with a detection significance of 10σ. The GRB was detected in the ISGRI data by the INTEGRAL Burst Alert System (IBAS; Mereghetti et al. 2001), which automatically determines the position and time of events which occur in the IBIS field of view. The IBAS alert was distributed approximately 30 s after the burst start time with a positional uncertainty of only 4 arcmin (Mereghetti et al. 2003c). The ISGRI lightcurve, is shown in Fig. 1.

A later analysis, performed off-line, on the ISGRI data revealed a position of (J2000.0) $19^h05^m30^s$, $+6°18^m26^s$ with an uncertainty of ∼3 arcmin (Mereghetti et al. 2003c). The gamma-ray burst had a duration of 40 s. Data from the spectrometer SPI were also analysed at the INTEGRAL Science Data Centre (ISDC; Courvoisier et al. 1999; Beckmann 2002). SPI is designed for high spectral resolution (FWHM of 2.5 keV at 1 MeV) in the energy range 20–8000 keV, which is achieved by 19 cooled germanium detectors. A coded mask with 128 elements provides an instrumental spatial resolution of 2.8 degrees. The position accuracy for point sources can be <5 arcmin (for a source with $S/N = 100$). The position for GRB 030501 extracted from the SPI data is (J2000.0) 19^h07^m, $+6°25^m$ (±21 arcmin), which is 19 arcmin off the position detected by ISGRI. As the GRB falls into the partially coded field of view, the low position accuracy of SPI is not surprising, as only part of the detector plane (5 out of 19 detectors) is in fact illuminated by the event.

The peak gamma ray flux, $f_{20\text{–}200\,\mathrm{keV}}$, in the 20–200 keV band measured by SPI in a 2 s bin starting at 03:10:20 UTC is 2.8 ± 0.4 photons cm^{-2} s^{-1}. This is consistent with ISGRI where $f_{20\text{–}200\,\mathrm{keV}} = 2.7 \pm 1.2$ photons cm^{-2} s^{-1} was measured in a 1 s bin starting at 03:10:18.4 UTC, reaching the peak about 1 s before it occurs in the SPI data. The fluence, $F_{20\text{–}200\,\mathrm{keV}}$, measured for the GRB by both instruments in the same band and integrated over the full burst visibility period is also consistent:

$$\begin{aligned} \text{SPI: } F_{20\text{–}200\,\mathrm{keV}} &= 39.3 \pm 2.5 \text{ photons cm}^{-2} \\ &= 3.7 \pm 0.2 \times 10^{-6} \text{ erg cm}^{-2} \\ \text{ISGRI: } F_{20\text{–}200\,\mathrm{keV}} &= 37.5 \pm 12.5 \text{ photons cm}^{-2} \\ &= 3 \pm 1 \times 10^{-6} \text{ erg cm}^{-2} \end{aligned}$$

The GRB was also observed by the Ulysses experiment (Hurley et al. 2003). Due to the weakness of the detection the reported fluence, in the 25–100 keV band, is uncertain by about a factor of two, but this is still consistent with the measurements made by the INTEGRAL instruments:

$$\begin{aligned} \text{SPI: } F_{25\text{–}100\,\mathrm{keV}} &\simeq 2.0 \times 10^{-6} \text{ erg cm}^{-2} \\ \text{ISGRI: } F_{25\text{–}100\,\mathrm{keV}} &\simeq 1.5 \times 10^{-6} \text{ erg cm}^{-2} \\ \text{ULYSSES: } F_{25\text{–}100\,\mathrm{keV}} &\simeq 1.1 \times 10^{-6} \text{ erg cm}^{-2}. \end{aligned}$$

The ∼30% uncertainty on ISGRI fluence is dominated by systematic errors on the response of the instrument at large off-axis angles. We note however a good agreement with the SPI value, which confirms the value obtained with ISGRI. The overall spectrum of the burst based on SPI data is shown in Fig. 2. The GRB occurred in a pointed observation of 1800 s length. The background emission was estimated from this pointing, but excluding the time when the GRB occurred. The GRB is detectable up to at least 200 keV in both the ISGRI and SPI[1] data. A single power law represents the SPI data well, resulting in a photon index of $\Gamma = -1.88 \pm 0.10$. A more complicated model (e.g. a broken power law or a Band model; Band et al. 1993) does not improve the fit, thus no spectral break is detectable. This result is consistent with the spectral slope of $\Gamma = -1.75 \pm 0.10$ derived from ISGRI data. For the ISGRI data the background can be estimated at the same time as the source flux, using the Pixel Illumination Function (PIF). Spectra are extracted computing one PIF for each energy bin (128 linearly spaced bins have been used).

There was a marginal detection of the GRB by the SPI-ACS (Hurley et al. 2003). The low countrate of this GRB is expected in the ACS data, as the effective area for events in the field of view of SPI is small for the ACS, which shields the spectrograph from the sides and from its back (von Kienlin et al. 2003).

[1] A detailed description how to perform the extraction of a GRB from SPI data can be found at
`http://isdc.unige.ch/Instrument/spi/pages/usermanual.html`

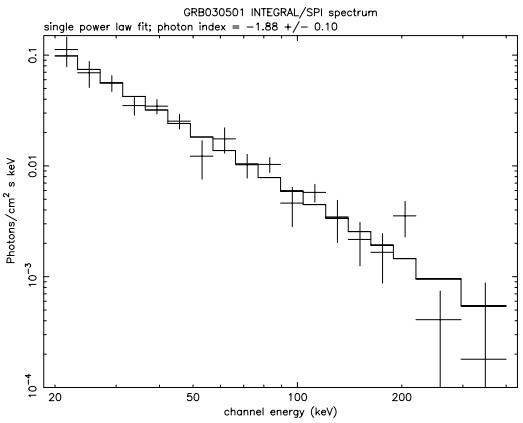

Fig. 2. GRB spectrum in the range 20–400 keV, taken from the SPI data over 20 seconds after the burst occurance.

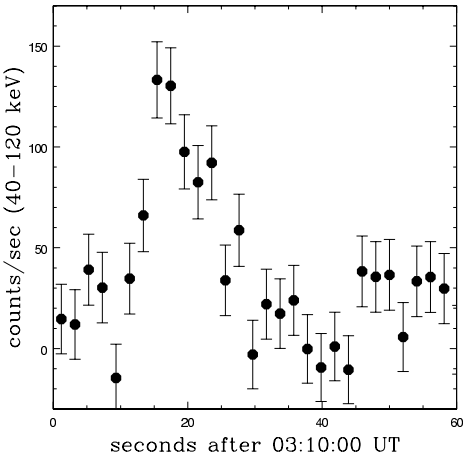

Fig. 3. Lightcurve of GRB 030501 measured by the spectrograph of RHESSI.

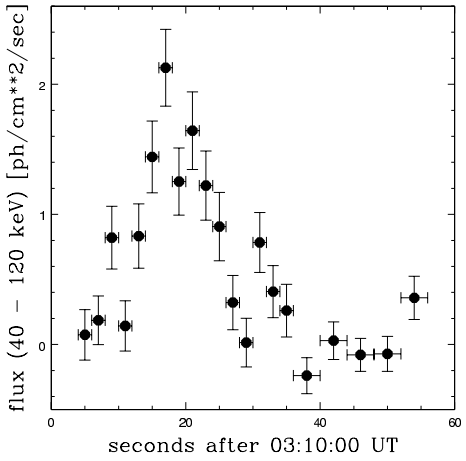

Fig. 4. Lightcurve of GRB 030501 in the same energy band as the RHESSI data, taken from INTEGRAL/SPI.

The combination of Ulysses and INTEGRAL data also allowed triangulation of the GRB event by the 3rd Interplanetary Network (IPN). The result is consistent with the ISGRI position (Hurley et al. 2003). The INTEGRAL X-ray (JEM-X) and optical (OMC) monitors were unable to provide any additional information since the GRB was located well outside of the respective fields of view of these instruments.

3. Comparison with RHESSI observation of GRB 030501

GRB 030501 has also been seen by the spectrometer of the Ramaty High Energy Solar Spectroscopic Imager (RHESSI), which is a NASA Small Explorer satellite designed to study hard X-rays and gamma-rays from solar flares (Lin et al. 2002). The instrument consists of 9 germanium detectors, each of volume 300 cm^3, that cover an energy range of 3 keV to 17 MeV, with an energy resolution of about 3 keV (FWHM) at 1 MeV (Smith et al. 2002). The detector uses a Rotation Modulation Collimator (RMC) system for high resolution imaging of solar flares. The germanium detectors are only lightly shielded. Above about 60 keV, they have a significant response to photons from any direction in the sky. Thus, RHESSI is a sensitive GRB detector, and as such it is part of the IPN.

The lightcurve of GRB 030501 as seen by RHESSI in the 40–120 keV band is shown in Fig. 3. The peak photon flux measured is $f_{70-200keV} \simeq 0.55 \pm 0.17$ photons cm^{-2} s^{-1}, and the fluence over the 20 s burst duration is $F_{70-200keV} \simeq 2.1 \pm 0.6 \times 10^{-6}$ erg cm^{-2}.

4. Time resolved results on GRB 030501

Although the burst is comparably weak, the sensitivity of ISGRI and SPI allows the study of the lightcurve of the prompt emission. We show the SPI lightcurve in the same energy band as for RHESSI in Fig. 4. The peak flux is reached ~10 s after the burst started. Spectra were extracted from the SPI data, in 5 logarithmically binned energy bands between 20 and 400 keV. For ISGRI the data have been binned in order to have at least 25 counts per bin. XSPEC 11.2 was used to fit a single power law to the data in time bins of 2–10 s over a period of 30 s after the burst started.

The results are shown in Fig. 5. The spectrum starts apparently rather steep, but then immediately has a photon index of $\Gamma \simeq -1.5$ as the flux increases. Before the GRB is below the instrumental sensitity, it apparently softens again. In the ISGRI data there is evidence of hardness intensity correlation as seen in other GRBs before (e.g. Ford et al. 1995). This is consistent with the SPI data, though the statistic is not high enough to constrain the results. No clear spectral evolution is seen in the data. The hardness ratio evolution in the RHESSI data show a similar trend to the one seen in ISGRI (Fig. 1), though the error bars are larger.

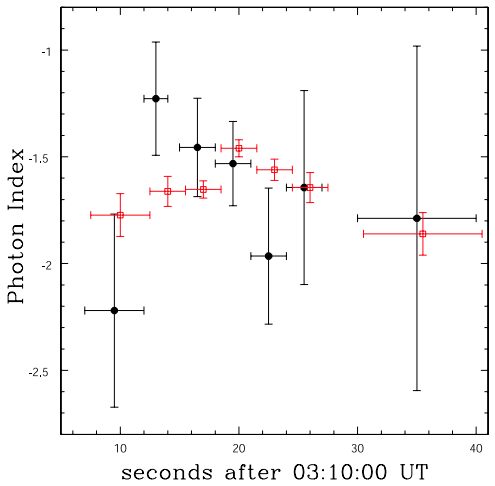

Fig. 5. Evolution of the spectral slope of a single power law, fitted to the ISGRI (open squares) and SPI (filled circles) data of GRB 030501. The ISGRI data points have been shifted by +0.5 s for better visibility. The definition of the photon index is $f_\nu \propto \nu^\Gamma$.

5. Discussion

Optical follow up observation has not revealed an optical counterpart to this GRB (Boer & Klotz 2003; Fox 2003; Rumjantsev et al. 2003). Using the 1 m Wise telescope in comparison with POSS-II E photographic plates, the magnitude of the optical counterpart 16.5 hours after the prompt emission can be limited to $R \geq 20.0$ mag (Ofek et al. 2003). Also analysis of optical observations carried out with the automatic 25 cm TAROT telescope shortly after the burst occurrence (i.e. within 15 min) shows no optical counter part with $R \leq 18.0$ mag (Klotz & Boer 2003).

With a Galactic latitude of only 0.2 degree and an estimated extinction of $E(B-V) \sim 15$, identification of an optical counterpart is indeed difficult, if not impossible.

As no break in the spectrum was detected in either the SPI or the ISGRI data, it can be assumed that the peak energy of this long GRB is either $E_{\rm peak} \lesssim 30$ keV or $E_{\rm peak} \gtrsim 200$ keV. Since a very low peak energy is rather unlikely (see Preece et al. 2000), we assume a spectral break above 200 keV. GRB 030501 shows a similar spectral behaviour to bursts studied before (e.g. GRB 921207; Ghirlanda et al. 2002) but is about a factor ~10 weaker than the bursts where time resolved spectroscopy has been possible with data from previous missions.

The comparison with the RHESSI data shows that this experiment is also a powerful tool in the detection and spectral analysis of GRBs. Especially for GRBs, which are not in the field of view of the INTEGRAL main instruments SPI and IBIS, RHESSI provides sufficient spectral and timing resolution (16 μs) to study those events, as the RHESSI spectrograph is a non-shielded all-sky monitoring instrument.

This GRB demonstrates the great capabilities of INTEGRAL and the software package, provided by the ISDC in collaboration with the instrument teams. The time lag between GRB occurrence and providing detailed spectral and timing analysis is less than half a day.

Acknowledgements. RH and FH acknowledge the support provided by the ESA Prodex Project 14527. JB was supported by the Polish grant 2P03C00619p02 from KBN and SS by PPARC grant GR/K/94867.

References

Band, D. L., Matteson, J. L., & Ford, L. A. 1993, ApJ, 413, 281
Bazzano, A., & Paizis, A. 2002, GCN, 1706
Beckmann, V. 2002, Proc. XXII Moriond Astroph. Meet., 417 [astro-ph/0206506]
Boer, M., & Klotz, A. 2003, GCN, 2188
Borkowski, J., Götz, D., & Mereghetti, S., 2003, GCN, 1836
Courvoisier, T., Poletta, M., & Türler, M. 1999, Astron. Lett. Comm., 39, 355
Ford, L. A., Band, D. L., Matteson, J. L., et al. 1995, ApJ, 439, 307
Fox, D. 2003, GCN, 2189
Ghirlanda, G., Celotti, A., & Ghisellini, G. 2002, A&A, 393, 409
Hurley, K., von Kienlin, A., Lichti, G. et al., 2003, GCN, 2187
Klebesadel, R. W., Strong, I. B., & Olson, R.A. 1973, ApJ, 182, L85
Klotz, A., & Boer, M. 2003, GCN, 2224
Lebrun, F. 2001, in Proc. 4th INTEGRAL Workshop, ESA SP, 459, 591
Lin, R. P., Dennis, B. R., Hurford, G. J., et al. 2002, Sol. Phys., 210, 3
Mereghetti, S., Cremonesi, D.I., & Borkowski, J. 2001, in Proc. 4th INTEGRAL Workshop, ESA SP, 459, 513
Mereghetti, S., Götz, D., & Borkowski, J. 2002, GCN, 1766
Mereghetti, S., Götz, D., Tiengo, A., Beckmann, V. et al., 2003a, ApJL, in press [astro-ph/0304477]
Mereghetti, S., Götz, D., & Borkowski, J. 2003b, GCN, 1941
Mereghetti, S., Götz, D., Borkowski, J., et al. 2003c, GCN, 2183
Metzger, M. R., Djogovski, S. G., Kulkarni, S. R. et al., 1997, Nature, 387, 879
Ofek, E. O., Choi, Y.-J., Gal-Yam, A., et al. 2003, GCN, 2201
Piro, L., Amati, L., Antonelli, L. A. et al., 1998, A&A, 331, L41
Preece, R. D., Briggs, M. S., Mallozzi, R. S., et al. 2000, ApJS, 126, 19
Rumyantsev, V., Pavlenko, E., & Pozanenko, A., 2003, GCN, 2202
Smith, D. M., Lin, R. P., Turin, P., et al. 2002, Sol. Phys., 210, 33
Ubertini, P., Lebrun, F., di Cocco, G., et al., 1999, Astron. Lett. Comm., 39, 331
Vedrenne, G., Schönfelder, V., Albernhe, F., et al., 1999, Astron. Lett. Comm., 39, 325
von Kienlin, A., Arend, N., Lichti, G. G., et al. 2003, SPIE Conf. Proc., 4851 [astro-ph/0302139]
Winkler, C., & Hermsen, W. 2000, AIP Conf. Proc., 510, 676

A&A 417, L45–L48 (2004)
DOI: 10.1051/0004-6361:20040080

Astronomy & Astrophysics

Spectral evolution of weak bursts from SGR 1806–20 observed with INTEGRAL⋆

D. Götz[1,2], S. Mereghetti[1], I. F. Mirabel[3,4], and K. Hurley[5]

[1] Istituto di Astrofisica Spaziale e Fisica Cosmica – CNR, Sezione di Milano "G. Occhialini", via Bassini 15, 20133 Milano, Italy
[2] Dipartimento di Fisica, Università degli Studi di Milano Bicocca, P.zza della Scienza 3, 20126 Milano, Italy
[3] Service d'Astrophysique, CEA/Saclay, Orme des Merisiers, Bât. 709, 91191 Gif-sur-Yvette, France
[4] Instituto de Astronomia y Fisica del Espacio / CONICET, cc67, suc 28, 1428 Buenos Aires, Argentina
[5] UC Berkeley Space Sciences Laboratory, Berkeley CA 94720-7450, USA

Received 28 January 2004 / Accepted 29 February 2004

Abstract. We report on bursts from the Soft Gamma-Ray Repeater SGR 1806–20 detected with INTEGRAL in October 2003, during a period of moderate activity of the source. The spectral and temporal properties of 21 short bursts are consistent with those found in previous observations, even if these bursts are among the faintest observed in the 15–200 keV range from this source. During some of the bursts a clear spectral evolution is visible. The data also show, for the first time, evidence for a hardness-intensity anti-correlation within SGR 1806–20 bursts.

Key words. gamma rays: bursts – gamma rays: observations – pulsars: general – stars: individual: SGR 1806-20

1. Introduction

Soft Gamma-ray Repeaters (SGRs) are a class of peculiar high-energy sources discovered through their recurrent emission of soft γ-ray bursts. These bursts have typical durations of ~0.1 s and luminosities in the range 10^{39}–10^{42} ergs s^{-1} (see Hurley 2000 for a review of this class of objects). The bursting activity and the persistent emission observed in the ~0.5–10 keV energy range are generally explained in the framework of the "Magnetar" model (e.g. Duncan & Thompson 1992; Thompson & Duncan 1995), as caused by a highly magnetized ($B \sim 10^{15}$ G) slowly rotating ($P \sim 5$–8 s) neutron star.

SGR 1806–20 is one of the most active Soft Gamma-ray Repeaters. Here we report new observations of this source obtained with the INTEGRAL satellite in October 2003 during a period of bursting activity (Götz et al. 2003a; Hurley et al. 2003; Mereghetti et al. 2003b; Götz et al. 2003b). These data have two advantages compared to previous observations in the soft γ-ray energy range of bursts from this source. First, they have been obtained with an imaging instrument, thus we can exclude that the bursts originate from a different source in the field. Second, they have a good sensitivity and time resolution which allows us to study the spectral evolution of relatively faint bursts.

2. Observations and data analysis

The region of SGR 1806–20 was observed by INTEGRAL (Winkler et al. 2003) between October 8 and 15 2003 as part of the Core Program deep observation of the Galactic Centre, yielding an exposure of about ~480 ks on the source. Several bursts from the direction of SGR 1806–20 were detected in near real time by the INTEGRAL Burst Alert System (IBAS, Mereghetti et al. 2003a), using data from the IBIS instrument (Ubertini et al. 2003). IBIS, a coded mask telescope with a large field of view (29° × 29°), comprises two detector layers: ISGRI (15 keV–1 MeV, Lebrun et al. 2003) and PICsIT (170 keV–10 MeV, Labanti et al. 2003). Only ISGRI data are relevant here, since PICsIT does not have enough time resolution for the study such short bursts.

In total, 21 bursts were detected by the IBAS programs. By means of images accumulated over the time intervals corresponding to the individual bursts, we can be confident that all of them originated from SGR 1806–20. In fact, the derived coordinates are all within 2′ from the well known position of SGR 1806–20 (Kaplan et al. 2002), while the 90% confidence error circle is typically of the order of 2.5′. In particular, the bursts positions are not consistent with the possible SGR 1808–20 (Lamb et al. 2003) recently discovered at 15′ from SGR 1806–20.

Send offprint requests to: D. Götz, e-mail: diego@mi.iasf.cnr.it

⋆ Based on observations with INTEGRAL, an ESA project with instruments and science data centre funded by ESA member states (especially the PI countries: Denmark, France, Germany, Italy, Switzerland, Spain), Czech Republic and Poland, and with the participation of Russia and the USA.

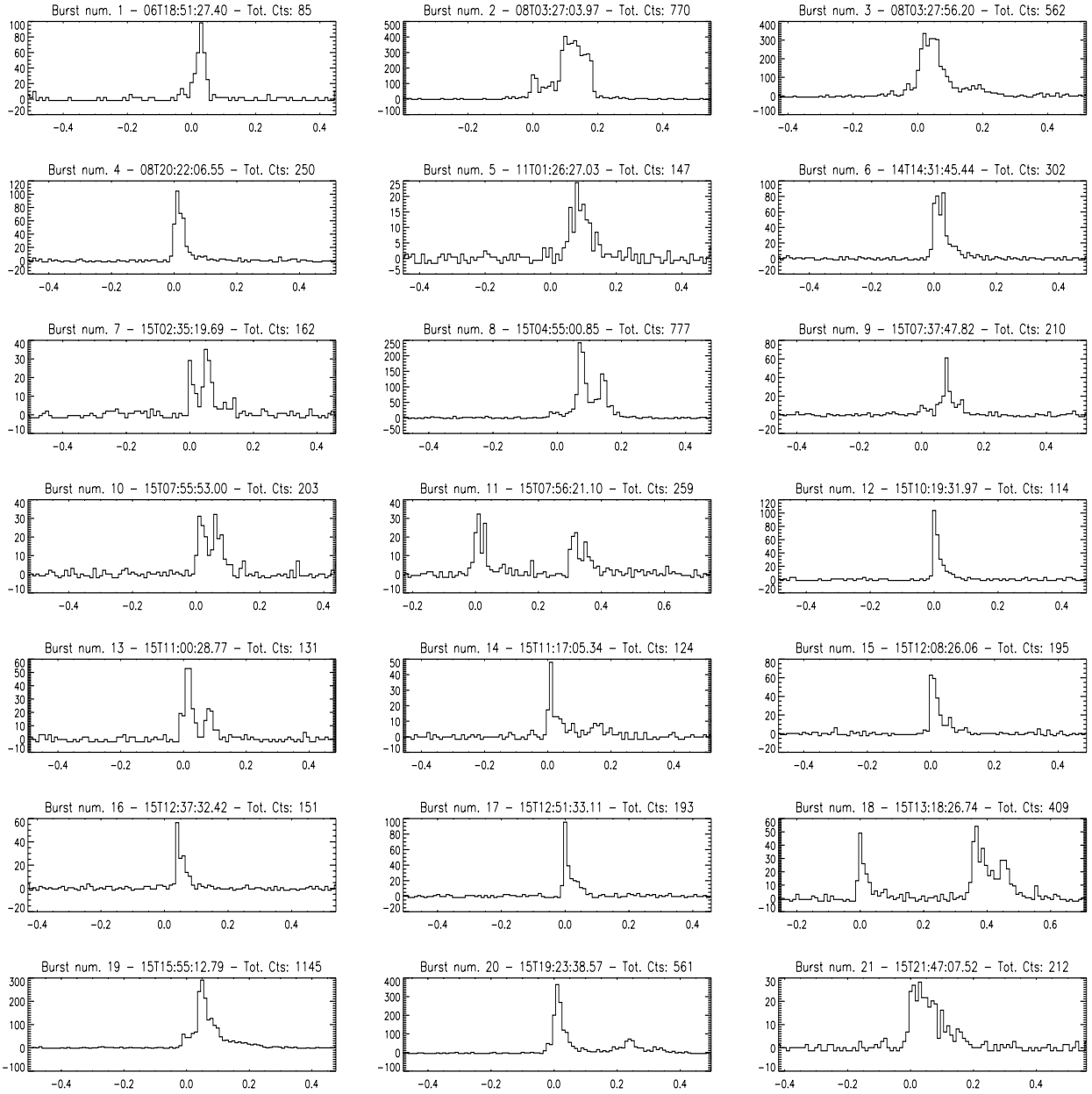

Fig. 1. IBIS/ISGRI background subtracted light curves of the SGR 1806–20 bursts in the 15–100 keV range. Each panel corresponds to a time interval of one second and the time bins are of 10 ms. Units of the axes are time in seconds and vignetting corrected counts per bin. Time 0 corresponds to the the starting time of the T_{90} computation and is reported on top of each panel together with the total number of net counts.

The background subtracted light curves of the bursts, binned at 10 ms, are shown in Fig. 1. In order to increase the signal-to-noise-ratio, they were extracted from ISGRI pixels illuminated by the source for at least half of their surface and selecting counts in the 15–100 keV energy range (most of the bursts had little or no signal at higher energy). The bursts were detected at various off-axis angles, ranging from 2.5 to 13.3 degrees, corresponding to a variation of 80% in the instrument effective area. The light curves shown in Fig. 1 have been corrected for this vignetting effect. The total number of net counts actually recorded for each burst is indicated in the corresponding panel.

The light curves shown in Fig. 1 have shapes typical for SGR bursts. From the light curves we determined the T_{90} duration of each burst (i.e. the time during which 90% of the total burst counts are accumulated). The T_{90} values range typically from ~0.1 to ~0.2 s for single peaked bursts and can be as long as ~0.6 seconds for double peaked bursts. In fact the T_{90} values of these bursts include the "interpulse" period. Some bursts are preceded by a small precursor.

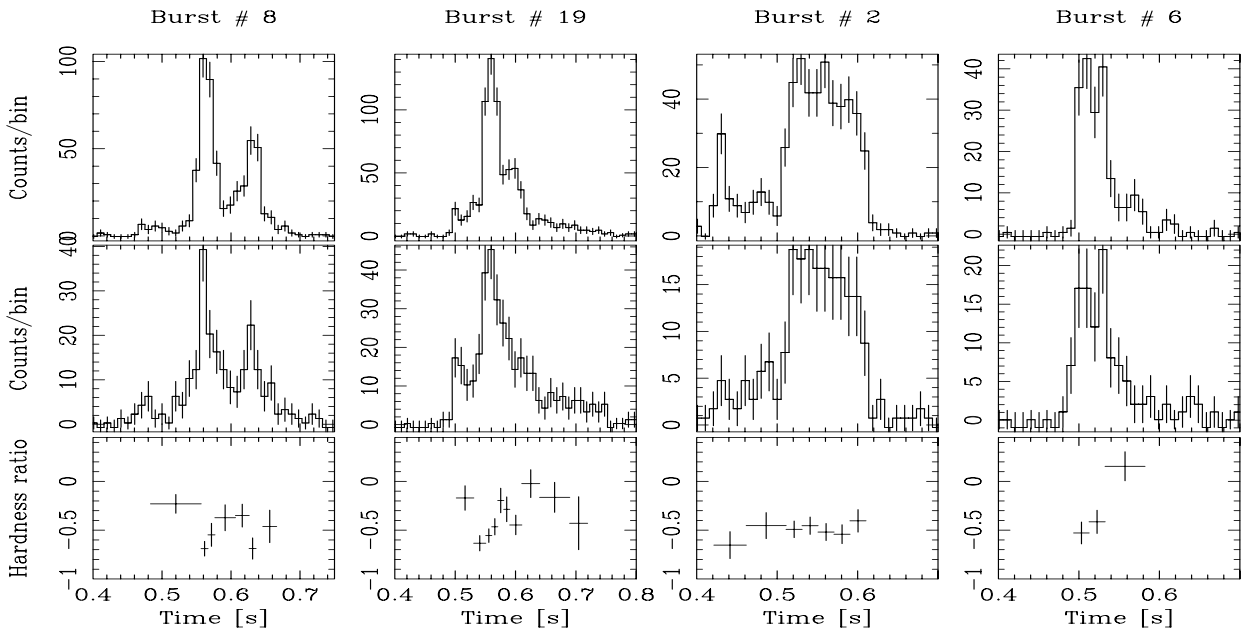

Fig. 2. 15–40 keV light curve (*top panels*), 40–100 keV light curve (*middle panels*), time resolved hardness ratio (*bottom panels*) for four bursts with good statistics. The time resolved hardness ratio for bursts number 8, 19, 6 is inconsistent with a constant value at ~3.5σ level.

The peak flux and fluence for each burst were first derived in counts units from the light curves of Fig. 1, and then converted to physical units adopting a constant conversion factor derived from the spectral analysis of the brightest bursts (see next section). The resulting 15–100 keV peak fluxes and fluences are respectively in the range $(4–50) \times 10^{-7}$ erg cm^{-2} s^{-1} (Δt = 10 ms) and $(2–60) \times 10^{-8}$ erg cm^{-2}. Within the large uncertainties, the fluence distribution is consistent with the power law slope found by Göğüş et al. (2000). Many of these bursts are among the faintest ever detected from SGRs at these energies.

2.1. Spectral properties

For the bursts with more than 500 net counts we could perform a detailed spectral analysis. The 15–200 keV spectra, integrated over the whole duration of each burst, were well fitted by an Optically Thin Thermal Bremsstrahlung (OTTB) model, yielding temperatures in the range from 32 to 42 keV. We tried other models, like a power law or a black body, but they were clearly ruled out.

Adopting a temperature kT = 38 keV (consistent with the average spectra of the brightest bursts) we derived a conversion factor of 1 count s^{-1} = 1.5×10^{-10} erg cm^{-2} s^{-1} (15–100 keV), which we adopted for all the bursts.

To investigate the time evolution of the burst spectra we computed hardness ratios, defined as $HR = (H - S)/(H + S)$, based on the background subtracted counts in the ranges 40–100 keV (H) and 15–40 keV (S). The time resolved HR values were computed for all the bursts with more than 200 net counts (i.e. for 12 bursts of our sample). The duration of the individual time bins were chosen in order to have at least 80 net counts in the total ($H + S$) band.

Some bursts show a significant spectral evolution, while others, particularly those with a "flat topped" profile, do not. Some examples are given in Fig. 2. While several bursts show a soft-to-hard evolution (e.g. number 6), others show a more complex evolution (eg. number 19).

We investigated the variation of the hardness ratio versus intensity (I). Considering all the time bins of all the bursts (see Fig. 3), we find a hardness-intensity anti-correlation. The linear correlation coefficient of the data plotted in Fig. 3 has a chance probability P smaller than 10^{-3} of being due to uncorrelated data. According to an F-test, the data are significantly (~5.2σ) better described by a linear fit ($HR = 0.45 - 0.22 \times \log(I)$) than by a constant value. The exclusion of the three "flat topped" bursts from the fit does not affect the statistical significance of the anti-correlation.

We also find an hardness-fluence anti-correlation over the entire fluence range of our bursts, although with a smaller statistical significance ($P = 5 \times 10^{-3}$), which is consistent with our hardness-intensity anti-correlation and also with the results obtained with *RXTE* data at lower energies (Göğüş et al. 2001).

3. Discussion

Previous studies indicated weak or no spectral evolution for SGR bursts (e.g. Fenimore et al. 1994; Kouveliotou et al. 1987). Up to now indication for a hard-to-soft evolution has been reported only for a single burst from SGR 1806–20 (Strohmayer & Ibrahim 1998) and for a precursor to a long burst (3.5 s) from SGR 1900+14 (Ibrahim et al. 2001). The same kind of spectral evolution has also been reported for a ~9 s long burst from SGR 0526–66

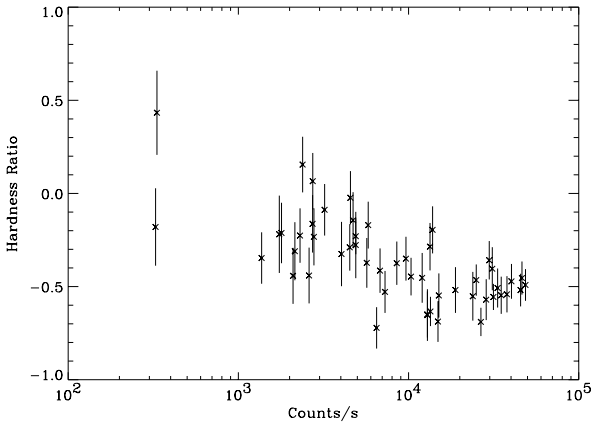

Fig. 3. Hardness-Intensity plot of the time resolved hardness ratios of the 12 bursts with the best statistics. The hardness ratio is defined as $(H-S)/(H+S)$, where H and S are the background subtracted counts in the ranges 40–100 keV and 15–40 keV respectively. The count rates are corrected for the vignetting and refer to the 15–100 keV range.

(Golenetskii et al. 1987): the softening trend is seen in the first three of the four spectra extracted, while the last one is as hard as the first one. In our sample we do not find evidence for this kind of evolution.

On the other hand, soft-to-hard evolution has been seen with the BATSE instrument for two peculiar bursts very likely originating from SGR 1900+14 (Woods et al. 1999). These two bursts were quite different from the usual bursts, both in terms of duration (lasting ~1 s), and spectral hardness (kT of the order of 100 keV).

In the framework of the magnetar model (Duncan & Thompson 1992), short (~0.1 s) SGR bursts are usually described as the radiation originating from the cooling of an optically thick pair-photon plasma. This plasma is generated in the neutron star magnetosphere by an Alfvén pulse, which is triggered by a sudden shift in the magnetospheric footpoints driven by a fracture in the neutron star crust (Thompson & Duncan 1995). This model is able to explain the time histories and energetics of the typical SGR bursts, and predicts that the effective temperature of the spectra should vary weakly during the bursts, owing to the constancy of the photospheric energy flux. No detailed predictions are available concerning more complex spectral evolution as we observe in some of the bursts. For example the model does not account for the presence of a soft precursor as observed in burst number 2 (see Fig. 2).

Our results indicate that a hardness-intensity anti-correlation (which in many bursts manifests itself as a soft-to-hard time evolution) is present in bursts from SGR 1806–20 which are not particularly long, nor spectrally hard and not at all very energetic. It is interesting to note that this correlation is opposite to what found for the bursts emitted from 1E 2259+586 (Gavrill et al. 2004), which although have lower fluences than the ones we measure.

Acknowledgements. This research has been supported by the Italian Space Agency.

References

Duncan, R. C., & Thompson, C. 1992, ApJ, 392, L9
Fenimore, E. E., Laros, J. G., & Ulmer, A. 1994, ApJ 432, 742
Gavrill, F. P., Kaspi, V. M., & Woods, P. M. 2004, ApJ, in press, [arXiv:astro-ph/0310852]
Göğüş, E., Woods, P. M., Kouveliotou, C., et al. 2000, ApJ, 532, L21
Göğüş, E., Kouveliotou, C., Woods, P. M., et al. 2001, ApJ, 558, 228
Golenetskii, S. V., Aptekar, R. L., Gur'yan, Y. A., et al. 1987, Sov. Astron. Lett., 13, 166
Götz, D., Mereghetti, S., Beck, M., & Mirabel, I. F. 2003a, GCN, 2408
Götz, D., Mereghetti, S., Beck, M., & Mirabel, I. F. 2003b, GCN, 2419
Hurley, K. 2000, in 5th Hunstville Symp. on Gamma-Ray Bursts, ed. R. M. Kippen, R. S. Mallozzi, & G. F. Fishman (New York: AIP), AIP Conf. Proc., 526, 763
Hurley, K., Cline, T., Mazets, E., & Golenetskii, S. 2003, GCN, 2414
Kaplan, D. L., Fox, D. W., Kulkarni, S. R., et al. 2002, ApJ, 564, 935
Kouveliotou, C., Norris, J. P., Cline, T. L., et al. 1987, ApJ, 322, L21
Ibrahim, A. I., Strohmayer, T. E., Woods, P. M., et al. 2001, ApJ, 558, 237
Labanti, C., Di Cocco, G., Ferro, G., et al. 2003, A&A, 411, L149
Lamb, D., Graziani, C., Shirasaki, Y., et al. 2003, GCN, 2351
Lebrun, F., Leray, J. P., Lavocat, P., et al. 2003, A&A, 411, L141
Mereghetti, S., Götz, D., Borkowski, J., Walter, R., & Pedersen, H. 2003a, A&A, 411, L291
Mereghetti, S., Götz, D., Beck, M., & Mirabel, I. F. 2003b, GCN, 2415
Strohmayer, T., & Ibrahim, A. 1998, in Fourth Hunstville Symp. on Gamma-Ray Bursts, ed. C. A. Meegan, R. D. Preece, & T. M. Koshut (Woodbury: AIP), AIP Conf. Proc., 428, 947
Thompson, C., & Duncan, R. C. 1995, MNRAS, 275, 255
Ubertini, P., Lebrun, F., Di Cocco, G., et al. 2003, A&A, 411, L131
Winkler, C, Courvoisier, T. J.-L., Di Cocco G., et al. 2003, A&A, 411, L1
Woods, P. M., Kouveliotou, C., van Paradijs, J., et al. 1999, ApJ, 527, L47

THE ASTROPHYSICAL JOURNAL, 609:L5–L8, 2004 July 1

SN 2003lw AND GRB 031203: A BRIGHT SUPERNOVA FOR A FAINT GAMMA-RAY BURST

D. MALESANI,[1] G. TAGLIAFERRI,[2] G. CHINCARINI,[2,3] S. COVINO,[2] M. DELLA VALLE,[4] D. FUGAZZA,[2] P. A. MAZZALI,[5,6] F. M. ZERBI,[2] P. D'AVANZO,[2] S. KALOGERAKOS,[2,7] A. SIMONCELLI,[2,7] L. A. ANTONELLI,[8] L. BURDERI,[8] S. CAMPANA,[2] A. CUCCHIARA,[2,7] F. FIORE,[8] G. GHIRLANDA,[2] P. GOLDONI,[9] D. GÖTZ,[3,10] S. MEREGHETTI,[10] I. F. MIRABEL,[9,11] P. ROMANO,[2] L. STELLA,[8] T. MINEZAKI,[12] Y. YOSHII,[12] AND K. NOMOTO[6]

Received 2004 April 14; accepted 2004 May 21; published 2004 May 27

ABSTRACT

Optical and near-infrared observations of the gamma-ray burst GRB 031203, at $z = 0.1055$, are reported. A very faint afterglow is detected superposed onto the host galaxy in our first infrared *JHK* observations, carried out ~9 hr after the burst. Subsequently, a rebrightening is detected in all bands, peaking in the *R* band about 18 rest-frame days after the burst. The rebrightening closely resembles the light curve of a supernova like SN 1998bw, assuming that the GRB and the SN went off almost simultaneously, but with a somewhat slower evolution. Spectra taken close to the maximum of the rebrightening show extremely broad features as in SN 1998bw. The determination of the absolute magnitude of this SN (SN 2003lw) is difficult owing to the large and uncertain extinction, but likely this event was brighter than SN 1998bw by 0.5 mag in the *VRI* bands, reaching an absolute magnitude $M_V = -19.75 \pm 0.15$.

Subject headings: gamma rays: bursts — supernovae: individual (SN 2003lw)

Online material: color figures

1. INTRODUCTION

In recent years, an extensive optical and near-infrared (NIR) follow-up of gamma-ray bursts (GRBs) has revealed a physical connection between a fraction of long-duration GRBs and core-collapse supernovae (SNe). First, SN 1998bw was discovered spatially and temporally coincident with GRB 980425 (Galama et al. 1998; Kulkarni et al. 1998). This event, however, was rather different from classical, cosmological GRBs, being severely underenergetic and lacking an optical afterglow. Then, SN 2003dh was detected in the afterglow of GRB 030329 (Stanek et al. 2003; Hjorth et al. 2003). Both SNe showed broad bumps in their spectra, indicating very large expansion velocities (up to 30,000 km s^{-1}), and were extremely bright. These highly energetic SNe are often designed as hypernovae (e.g., Iwamoto et al. 1998). Finally, bumps in the light curves of several afterglows, peaking ~20 days after the GRB, have been interpreted as being due to SNe outshining the afterglow light, based on their brightness, temporal evolution, and colors (e.g., Bloom et al. 1999; Garnavich et al. 2003). The bumps resemble the light curve of SN 1998bw, with a certain scatter in the brightness and rise time (e.g., Zeh et al. 2004). Spectroscopic confirmation that the bump of GRB 021211 has an SN spectrum (SN 2002lt; Della Valle et al. 2003) supports this conclusion. These observations indicate that the GRB/SN association is common.

GRB 031203 was discovered by *INTEGRAL* on 2003 December 3.91769 UT (Götz et al. 2003), with a duration of ~30 s and a peak flux of 1.3×10^{-7} ergs cm^{-2} s^{-1} (20–200 keV; Mereghetti & Götz 2003). The precise and fast dissemination of the GRB coordinates by the *INTEGRAL* burst alert system (Mereghetti et al. 2003) facilitated an effective search for the afterglow. We also immediately activated our Target of Opportunity program at ESO, starting NIR observations at the New Technology Telescope (NTT) 7 hr after the GRB (Zerbi et al. 2003). The X-ray and radio afterglows were soon discovered (Santos-Lleo & Calderon 2003; Frail 2003). A compact galaxy, located at a consistent position, was proposed to be the GRB host galaxy by Prochaska et al. (2003). The redshift was $z = 0.1055 \pm 0.0001$ (Prochaska et al. 2003, 2004), making GRB 031203 the second closest burst after GRB 980425 at $z = 0.0085$ (Galama et al. 1998). Vaughan et al. (2004) discovered a scattered, expanding X-ray halo that was due to the reflection of the burst and/or early afterglow light from Galactic dust grains, thus providing an (indirect) measurement of the X-ray flux at the earliest stages after the burst onset.

Given the low redshift of this event, the isotropic-equivalent burst energy is extremely low,[13] $E_{iso} \sim 3 \times 10^{49}$ ergs (20–2000 keV; Watson et al. 2004; Prochaska et al. 2004), well below the standard reservoir of $\sim 2 \times 10^{51}$ ergs of normal GRBs (Frail et al. 2001; Bloom et al. 2003). Only GRB 980425 (Galama et al. 1998) and XRF 020903 (Sakamoto et al. 2004) were less energetic.

Based on photometric monitoring of the host galaxy, several groups have reported evidence of an SN associated with GRB 031203 (Bersier et al. 2004; Thomsen et al. 2004; Cobb et al.

[1] International School for Advanced Studies (SISSA-ISAS), via Beirut 2-4, I-34014 Trieste, Italy.
[2] INAF–Osservatorio Astronomico di Brera, via E. Bianchi 46, I-23807 Merate (Lc), Italy.
[3] Università degli studi di Milano-Bicocca, Dipartimento di Fisica, Piazza delle Scienze 3, I-20126 Milan, Italy.
[4] INAF–Osservatorio Astronomico di Arcetri, Largo E. Fermi 5, I-50125 Florence, Italy.
[5] INAF–Osservatorio Astronomico di Trieste, via G. Tiepolo 11, I-34131 Trieste, Italy.
[6] Department of Astronomy, School of Science, University of Tokyo, Bunkyo-ku, Tokyo 113-0033, Japan.
[7] Università degli Studi di Milano, Dipartimento di Fisica, via Celoria 16, I-20133 Milan, Italy.
[8] INAF–Osservatorio Astronomico di Roma, via di Frascati 33, I-00040 Monteporzio Catone (Rome), Italy.
[9] CEA Saclay, DSM/DAPNIA/Service d'Astrophysique, F-91191, Gif sur Yvette, France.
[10] Istituto di Astrofisica Spaziale e Fisica Cosmica/CNR, Sezione di Milano, via Bassini 15, I-20133 Milan, Italy.
[11] Instituto de Astronomia y Fisica del Espacio, CC 67, Suc 28, 1428 Capital Federal, Argentina.
[12] Institute of Astronomy, School of Science, University of Tokyo, 2-21-1 Osawa, Mitaka, Tokyo 181-0015, Japan.

[13] We adopt a cosmology with $H_0 = 71$ km s^{-1} Mpc^{-1}, $\Omega_m = 0.27$, and $\Omega_\Lambda = 0.73$ (*WMAP* results). At $z = 0.1055$, the luminosity distance is $D = 477$ Mpc, and the distance modulus is $\mu = 38.42$ mag.

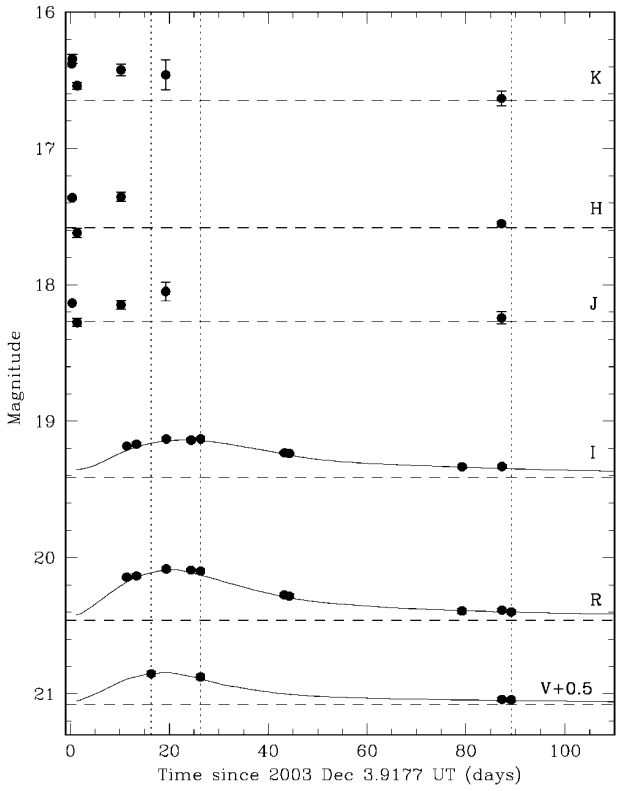

FIG. 1.—Optical and NIR light curves of GRB 031203 (*circles*). Error bars indicate the amount of relative errors only (Table 1). The solid curves show the evolution of SN 1998bw (Galama et al. 1998; McKenzie & Schaefer 1999), rescaled at $z = 0.1055$, stretched by a factor 1.1, extinguished with $E_{B-V} = 1.1$, and brightened by 0.5 mag. The dashed lines indicate the host galaxy contribution. The vertical dotted lines mark the epochs of our spectra. [*See the electronic edition of the Journal for a color version of this figure.*]

2004; Gal-Yam et al. 2004). After the ultimate confirmation, coming from spectroscopic observations and reported by our group (Tagliaferri et al. 2004), the IAU named this event SN 2003lw.

2. OBSERVATIONS AND DATA REDUCTION

Photometry.—We observed the field of GRB 031203 ≈7 hr after the trigger, to search for the NIR afterglow, using SofI on the ESO NTT. Subsequent imaging with ISAAC on the ESO VLT showed a varying source coincident with the putative host galaxy of GRB 031203: the total flux had dimmed in the *J*, *H*, and *K* filters by a few tenths of a magnitude (see Fig. 1). We therefore started a campaign to monitor the light curve of the event, searching for an SN rebrightening. The observing log is presented in Table 1.

Image reduction and analysis were performed following the standard procedures, by means of both aperture photometry and point-spread function (PSF)–matched image subtraction. To avoid saturation from a nearby bright star, the exposure time was always kept short. In some cases, occulting bars were used to cover the bright star (showing that the effect was negligible). Optical and NIR photometry were calibrated against Landolt standard stars and the Two Micron All Sky Survey, respectively. To focus on the issue of variability, in Table 1 we list just the relative photometry with respect to a reference epoch. We should also note that the host galaxy spectrum is dominated by prominent emission lines. This may lead to relatively large offsets when comparing results from other instruments, owing to unavoidable small differences in the filter profiles and CCD efficiencies.

TABLE 1
SUMMARY OF PHOTOMETRIC OBSERVATIONS

UT Start	Seeing (arcsec)	Instrument	Band	Magnitude[a]
2003 Dec 20.247	0.3	FORS2	*V*	−0.023 ± 0.020
2003 Dec 30.250	0.5	FORS1	*V*	**20.37 ± 0.05**
2004 Feb 29.193	0.7	FORS1	*V*	0.165 ± 0.012
2004 Mar 02.064	0.7	FORS1	*V*	0.169 ± 0.015
2003 Dec 15.314	0.6	FORS1	*R*	**20.14 ± 0.03**
2003 Dec 17.284	0.7	FORS1	*R*	−0.009 ± 0.016
2003 Dec 23.295	0.5	FORS1	*R*	−0.060 ± 0.016
2003 Dec 28.296	0.6	FORS1	*R*	−0.051 ± 0.010
2003 Dec 30.241	0.5	FORS1	*R*	−0.044 ± 0.013
2004 Jan 16.171	0.8	FORS1	*R*	0.130 ± 0.013
2004 Jan 17.185	0.5	FORS1	*R*	0.139 ± 0.014
2004 Feb 21.101	0.7	FORS1	*R*	0.248 ± 0.019
2004 Feb 29.198	0.7	FORS1	*R*	0.242 ± 0.012
2004 Mar 02.069	0.6	FORS1	*R*	0.255 ± 0.016
2003 Dec 15.321	0.5	FORS1	*I*	**19.18 ± 0.03**
2003 Dec 17.291	0.6	FORS1	*I*	−0.014 ± 0.015
2003 Dec 23.300	0.4	FORS1	*I*	−0.052 ± 0.013
2003 Dec 28.301	0.6	FORS1	*I*	−0.044 ± 0.015
2003 Dec 30.245	0.4	FORS1	*I*	−0.052 ± 0.009
2004 Jan 16.177	0.6	FORS1	*I*	0.050 ± 0.008
2004 Jan 17.179	0.6	FORS1	*I*	0.054 ± 0.007
2004 Feb 21.107	0.5	FORS1	*I*	0.151 ± 0.013
2004 Feb 29.203	0.8	FORS1	*I*	0.150 ± 0.013
2003 Dec 04.288	0.9	SofI	*J*	**18.13 ± 0.034**
2003 Dec 05.258	0.5	ISAAC	*J*	0.143 ± 0.030
2003 Dec 15.140	1.1	SofI	*J*	0.014 ± 0.032
2003 Dec 24.191	1.0	SofI	*J*	−0.084 ± 0.069
2004 Feb 28.111	0.5	ISAAC	*J*	0.110 ± 0.045
2003 Dec 04.300	0.9	SofI	*H*	**17.36 ± 0.042**
2003 Dec 05.271	0.5	ISAAC	*H*	0.257 ± 0.035
2003 Dec 14.148	0.9	SofI	*H*	−0.006 ± 0.033
2004 Feb 28.104	0.5	ISAAC	*H*	0.190 ± 0.019
2003 Dec 04.204	0.9	SofI	*K*	**16.38 ± 0.036**
2003 Dec 04.312	0.8	SofI	*K*	−0.036 ± 0.033
2003 Dec 05.267	0.5	ISAAC	*K*	0.161 ± 0.025
2003 Dec 14.154	0.8	SofI	*K*	0.046 ± 0.044
2003 Dec 23.188	1.0	SofI	*K*	0.082 ± 0.107
2004 Feb 28.095	0.5	ISAAC	*K*	0.255 ± 0.055
2003 Dec 24.507	1.5	MAGNUM	*I*	19.16 ± 0.03
2004 Jan 06.447	1.4	MAGNUM	*I*	19.16 ± 0.03
2003 Dec 24.503	1.1	MAGNUM	*K*	16.61 ± 0.04
2004 Jan 06.445	1.1	MAGNUM	*K*	16.58 ± 0.04

[a] Magnitudes are given relative to the boldface epoch.

Additional *K* and *I* photometry was acquired with the 2 m Multicolor Active Galactic Nuclei Monitoring (MAGNUM) telescope of the University of Tokyo (Yoshii et al. 2003), located in the Hawaii Islands. Although the different shape of the MAGNUM and ESO *I* filters (particularly critical due to the presence of the bright Hα line in the blue filter wing) makes it difficult to compare the results, the data are in good agreement (Table 1). For consistency, these data are not plotted in Figure 1.

Spectroscopy.—Moderate-resolution spectra (FWHM ≈ 10 Å) were taken with the VLT on 2003 December 20 (FORS2), 2003 December 30 (FORS1), and 2004 March 1 (FORS1). Flux calibration was achieved by observing spectrophotometric stars. After comparing synthetic magnitudes calculated from our spectra with the photometry, we introduced a correction to account for light loss outside the slit. To ensure a sound relative calibration between the spectra, we also checked that the fluxes of the host galaxy emission lines did not vary. A detailed discussion of the spectroscopy and of the host galaxy will be presented elsewhere (G. Chincarini et al. 2004, in preparation [hereafter C04]).

3. RESULTS AND DISCUSSION

In Figure 1, we show the light curves of GRB 031203. Early-time NIR photometry shows a dimming in all bands between

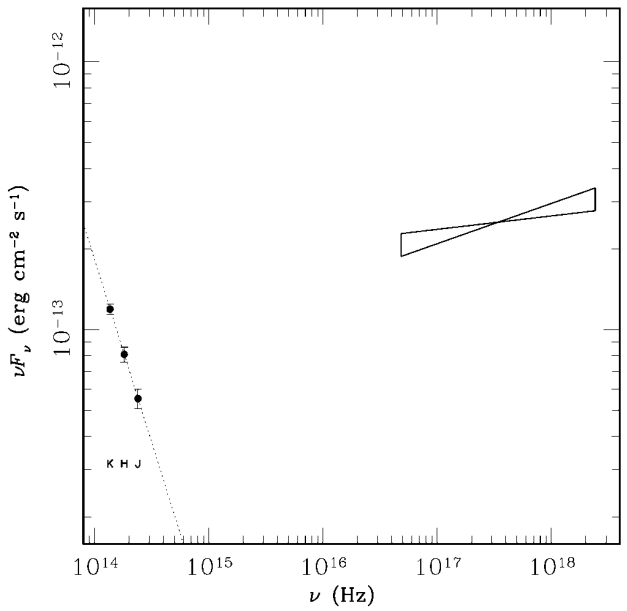

FIG. 2.—Spectral energy distribution of the afterglow of GRB 031203 on 2003 December 4.3 UT (9 hr after the trigger). The NIR values are calculated from our data by subtracting the host contribution and assuming $E_{B-V} = 1.1$. The NIR spectral index is $\beta = 2.36 \pm 0.02$ ($F_\nu \propto \nu^{-\beta}$). The X-ray spectrum is from Watson et al. (2004; reported at $t = 9$ hr using the X-ray decay slope), who find $N_H = 8.8 \times 10^{21}$ cm^{-2} and $\beta_X = 0.90 \pm 0.05$. [*See the electronic edition of the Journal for a color version of this figure.*]

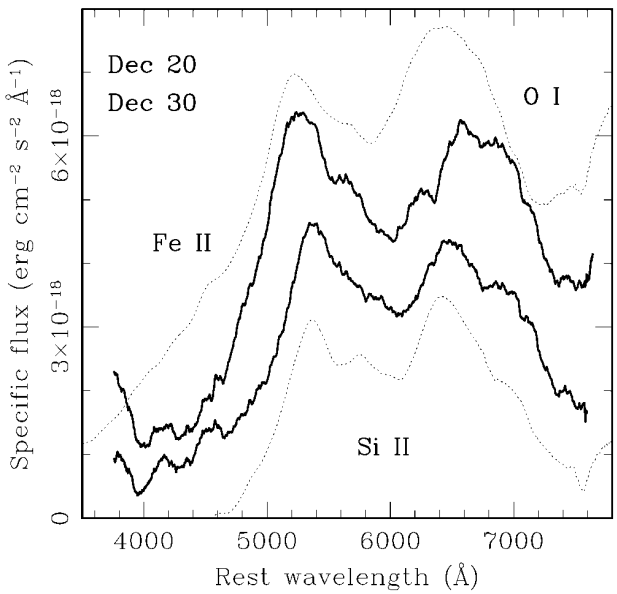

FIG. 3.—Spectra of SN 2003lw, taken on 2003 December 20 and 30 (*solid lines*), smoothed with a boxcar filter 250 Å wide. Dotted lines show the spectra of SN 1998bw (from Patat et al. 2001), taken on 1998 May 9 and 19 (13.5 and 23.5 days after the GRB, or 2 days before and 7 days after the *V*-band maximum, respectively), extinguished with $E_{B-V} = 1.1$ and a Galactic extinction law (Cardelli et al. 1989). The spectra of SN 1998bw were vertically displaced for presentation purposes. [*See the electronic edition of the Journal for a color version of this figure.*]

the first and second night after the GRB. This is confirmed by PSF-matched image subtraction. We believe that we have seen the NIR afterglow of GRB 031203. The magnitudes are $J = 20.60 \pm 0.09$, $H = 19.05 \pm 0.07$, and $K = 17.56 \pm 0.05$ (9 hr after the GRB), obtained by subtracting the host contribution. Cobb et al. (2004) have *I*-band observations at similar epochs, and they do not report evidence of variability. However, extrapolation to the visible region yields $I \sim 23.4$, quite a faint value when compared to the host luminosity $I \approx 19.4$. Little contribution from the afterglow is seen in our measurement of December 5, implying a quick decay between the two nights [$F(t) \propto t^{-\alpha}$, with $\alpha \gtrsim 2$]. However, there is no variation between the two *K*-band observations of the first night (separated by 2.6 hr), suggesting a break in the light curve or a bumpy behavior. In Figure 2, we compare the spectrum in the NIR and X-ray regions (Watson et al. 2004). A discontinuity is apparent, indicating a different origin for the emission in the two bands. The X-ray component has a much harder spectrum and a slower decay ($\alpha = 0.55 \pm 0.05$). Interestingly, Watson et al. (2004) infer a fast decay of the early-time X-ray afterglow, consistent with our NIR value ($\alpha \gtrsim 1.7$). In the standard model of afterglows (e.g., Sari et al. 1998), a fast decay is consistent with a soft spectrum blueward of the peak frequency.

A few days after the GRB, a rebrightening is apparent in all optical/NIR bands. The rebrightening amounts to ≈30% of the total flux and is coincident with the center of the host galaxy to within 0.″1 (≈200 pc at $z = 0.1055$). For comparison, we show in Figure 1 the *VRI* light curves of SN 1998bw (Galama et al. 1998; McKenzie & Schaefer 1999), placed at $z = 0.1055$ and dereddened with $E_{B-V} = 1.1$ (see below). Interpolation of the *UBVRI* data was performed in order to estimate the fluxes of SN 1998bw at the frequencies corresponding to the observed bands. Even after correcting for cosmological time dilation, the light curve of SN 2003lw is broader than that of SN 1998bw and requires an additional stretching factor of ≈0.9 to match the *R* and *I* bands. Near the peak, the light curve is rather flat, resembling the hypernova SN 1997ef (Iwamoto et al. 2000) more than SN 1998bw. The *R*-band maximum is reached on approximately 2003 December 24 (~18 comoving days after the GRB). We note that the details of the light-curve shape are sensitive to the removal of the host contribution. This may explain the different finding of Cobb et al. (2004), who find a longer rise, and Thomsen et al. (2004), who need no stretch. Assuming a light-curve shape similar to SN 1998bw, which had a rise time of 16 days in the *V* band, our data suggest an explosion time nearly simultaneous with the GRB. However, given that SN 2003lw was not strictly identical to SN 1998bw, and as we lack optical data in the days immediately following the GRB, a lag of a few days cannot be ruled out. Type Ic SNe usually reach *V*-band maximum in ~12–20 days, the brightest events showing a slower evolution (see, e.g., Fig. 2 of Mazzali et al. 2002).

A precise determination of the absolute magnitude of the SN is made difficult by the uncertain, and significant, extinction. C04 and Prochaska et al. (2004) constrain the average combined Galactic and host extinction to be $E_{B-V} \approx 1.1$ based on the Balmer ratios of the host galaxy. Given the good spatial coincidence of the SN with the center of the host, such a value is likely a good estimate for the SN extinction. We also adopt a Galactic extinction law (Cardelli et al. 1989) with $R_V = 3.1$. With the assumed reddening, SN 2003lw appears brighter than SN 1998bw by 0.5 mag in the *V*, *R*, and *I* bands. The absolute magnitudes of SN 2003lw are hence $M_V = -19.75 \pm 0.15$, $M_R = -19.9 \pm 0.08$, and $M_I = -19.80 \pm 0.12$. Thomsen et al. (2004), using *I*-band data, also found that SN 2003lw was brighter than SN 1998bw by ~0.55 mag, in full agreement with our result. Cobb et al. (2004), however, found a comparable luminosity for the two SNe; this discrepancy is entirely due to the lower extinction they assume.

Figure 3 shows the spectra of the rebrightening on 2003 December 20 and 30 (14 and 23 rest-frame days after the GRB,

respectively), after subtracting the spectrum taken on 2004 March 1 (81 rest-frame days after the GRB). This assumes that the latter spectrum contains only a negligible contribution from the SN, which is confirmed by the photometry (Fig. 1). The spectra of SN 2003lw are remarkably similar to those of SN 1998bw obtained at comparable epochs (shown as dotted lines in Fig. 3; from Patat et al. 2001). Both SNe show very broad absorption features, indicating large expansion velocities. Thus, we tentatively classify SN 2003lw as a hypernova. The main absorptions are identified in Figure 3 as in SN 1998bw, following Iwamoto et al. (1998). The velocity of the Si II line in SN 2003lw is apparently smaller than in SN 1998bw. The broad peaks near 5300 and 6600 Å are probably the emission components of P Cygni profiles due to the blending of several lines. There is evolution between the two epochs: the bluer bump is observed at longer wavelengths in the second spectrum and is slightly narrower. Moreover, the shape of the redder peak is different in the two epochs. Both peaks appear at redder wavelengths than in SN 1998bw. Detailed modeling of the spectra will be presented elsewhere (P. A. Mazzali et al. 2004, in preparation).

By modeling the X-ray dust echo, Watson et al. (2004) concluded that GRB 031203 was an X-ray flash (XRF); however, the prompt emission data do not confirm this hypothesis (S. Sazonov et al. 2004, in preparation). This event, like GRB 980425 (Pian et al. 2000), seems therefore to violate the correlation between the isotropic-equivalent gamma-ray energy $E_{\rm iso}$ and the peak spectral energy E_p (Amati et al. 2002; Lamb et al. 2003). In fact, assuming $E_{\rm iso} \sim 1.5 \times 10^{50}$ ergs (1–10,000 keV; Watson et al. 2004), the Amati et al. (2002) relation would imply $E_p \sim 10$ keV, a value indicating an XRF nature for GRB 031203. This is in contrast with *INTEGRAL* data. Of course, this issue will be settled only after a thorough analysis of the prompt emission spectra.

The afterglow of GRB 031203 was very weak, the faintest ever detected in the optical/NIR. Extrapolation in the R band yields a luminosity ~200 times fainter than the dimmest afterglow discovered so far (GRB 021211; Fox et al. 2003; Pandey et al. 2003). The detection of the SN optical light implies that an extreme dust obscuration was not the reason for such faintness. Given also the low redshift of the event, this example shows that some optical afterglows may escape detection just because they are faint (e.g., Fynbo et al. 2001; Lazzati et al. 2002; De Pasquale et al. 2003).

GRB 031203, together with GRB 980425 at $z = 0.085$, were very dim events, perhaps jets observed far from their axes (e.g., Maeda et al. 2002; Yamazaki et al. 2003). Being so faint, they would have been likely missed at cosmological distances. Since the volume they sample is much smaller than that probed by classical, distant GRBs with $\langle z \rangle \approx 1$, the rate of these events could be much larger. As noted by Thomsen et al. (2004), this would increase the detection rate for the *Swift* satellite (Gehrels et al. 2004). More rapid and efficient observations, also soon feasible thanks to *Swift*, will allow one to make a detailed study of this largely unexplored class of events.

GRB 031203 was quite similar to GRB 980425, even if overall more powerful. Both events consisted in a single, underenergetic pulse. Their afterglows were very faint or absent in the optical and showed a very slow decline in the X-ray (Pian et al. 2000; Watson et al. 2004). Finally, they were both accompanied by a powerful hypernova.

The data presented in this work were obtained with ESO telescopes under programmes 072.D-0480 and 072.D-0137. We are grateful to the ESO staff and in particular to M. Billeres, O. Hainaut, S. Hubrig, R. Johnson, C. Lidman, G. Marconi, and T. Szeifert. F. Patat is warmly acknowledged for providing the SN 1998bw data. D. M. thanks L. Ballo for useful discussions. This work was supported by contract ASI/I/R/390/02 of the Italian Space Agency for the Italian *Swift* Project, by the Italian Ministry for University and Research, and by the Italian National Institute for Astrophysics (INAF). We thank the anonymous referee for useful suggestions and a prompt reply.

REFERENCES

Amati, L., et al. 2002, A&A, 390, 81
Bersier, D., et al. 2004, GCN Circ. 2544, http://gcn.gsfc.nasa.gov/gcn3/2544.gcn3
Bloom, J. S., et al. 1999, Nature, 401, 453
Bloom, J. S., Frail, D. A., & Kulkarni, S. R. 2003, ApJ, 594, 674
Cardelli, J. A., Clayton, G. C., & Mathis, J. S. 1989, ApJ, 345, 245
Cobb, B. E., Baylin, C. D., van Dokkum, P. G., Buxton, M. M., & Bloom, J. S. 2004, ApJ, 608, L93
Della Valle, M., et al. 2003, A&A, 406, L33
De Pasquale, M., et al. 2003, ApJ, 592, 1018
Fox, D. W., et al. 2003, ApJ, 586, L5
Frail, D. A., et al. 2001, ApJ, 562, L55
Frail, D. A. 2003, GCN Circ. 2473, http://gcn.gsfc.nasa.gov/gcn3/2473.gcn3
Fynbo, J. U., et al. 2001, A&A, 369, 373
Galama, T. J., et al. 1998, Nature, 395, 670
Gal-Yam, A., et al. 2004, ApJ, submitted (astro-ph/0403608)
Garnavich, P. M., et al. 2003, ApJ, 582, 924
Gehrels, N., et al. 2004, ApJ, in press (astro-ph/0405233)
Götz, D., Mereghetti, S., Beck, M., Borkowski, J., & Mowlavi, N. 2003, GCN Circ. 2459, http://gcn.gsfc.nasa.gov/gcn3/2459.gcn3
Hjorth, J., et al. 2003, Nature, 423, 847
Iwamoto, K., et al. 1998, Nature, 395, 672
———. 2000, ApJ, 534, 660
Kulkarni, S. R., et al. 1998, Nature, 395, 663
Lamb, D. Q., Donaghy, T. Q., & Graziani, C. 2003, ApJ, submitted (astro-ph/0312634)
Lazzati, D., Covino, S., & Ghisellini, G. 2002, MNRAS, 330, 583
Maeda, K., Nakamura, T., Nomoto, K., Mazzali, P. A., Patat, F., & Hachisu, I. 2002, ApJ, 565, 405
Mazzali, P. A., et al. 2002, ApJ, 572, L61
McKenzie, E. H., & Schaefer, B. E. 1999, PASP, 111, 964
Mereghetti, S., & Götz, D. 2003, GCN Circ. 2460, http://gcn.gsfc.nasa.gov/gcn3/2460.gcn3
Mereghetti, S., Götz, D., Borkowski, J., Walter, R., & Pedersen, H. 2003, A&A, 411, L291
Pandey, S. B., et al. 2003, A&A, 408, L21
Patat, F., et al. 2001, ApJ, 555, 900
Pian, E., et al. 2000, ApJ, 536, 778
Prochaska, J. X., Chen, H. W., Hurley, K., Bloom, J. S., Graham, J. R., & Vacca, W. D. 2003, GCN Circ. 2475, http://gcn.gsfc.nasa.gov/gcn3/2475.gcn3
Prochaska, J. X., et al. 2004, ApJ, in press (astro-ph/0402085)
Sakamoto, T., et al. 2004, ApJ, 602, 875
Santos-Lleo, M., & Calderon, P. 2003, GCN Circ. 2464, http://gcn.gsfc.nasa.gov/gcn3/2464.gcn3
Sari, R., Piran, T., & Narayan, R. 1998, ApJ, 497, L17
Stanek, K. Z., et al. 2003, ApJ, 591, L17
Tagliaferri, G., et al. 2004, IAU Circ. 8308
Thomsen, B., et al. 2004, A&A, 419, L21
Vaughan, S., et al. 2004, ApJ, 603, L5
Watson, D., et al. 2004, ApJ, 605, L97
Yamazaki, R., Yonetoku, D., & Nakamaura, T. 2003, ApJ, 594, L79
Yoshii, Y., et al. 2003, ApJ, 592, 467
Zeh, A., Klose, S., & Hartmann, D. H. 2004, ApJ, in press (astro-ph/0311610)
Zerbi, F. M., et al. 2003, GCN Circ. 2471, http://gcn.gsfc.nasa.gov/gcn3/2471.gcn3

Appendix B

IBAS Alert Packets Description

The Alert Packet is an array of bytes with the following structure (from Borkowski et al. (2002)):

offset (bytes)	size (bytes)	type	label	comment
0	4	int	IBAS_ID	magic number, fixed value : 1229078867 == 'IBAS'
4	4	int	PID	ibasalertd process ID. Used by **ibasalertd** to demultiplex client responses
8	4	int	SEQNUM	sequence number. Used by **ibasalertd** to demultiplex client responses
12	4	int	HANDLE	Client handle. Used by **ibasalertd** to demultiplex client responses
16	2	int	PKT_TYPE	1 = POINTDIR 2 = SPIACS 3 = WAKUEP 4 = REFINED 5 = OFFLINE
18	2	int	TEST_FLAG	Identifies test alerts 0 : normal alert packet 1 : test alert packet

offset (bytes)	size (bytes)	type	label	comment
20	4	int	PKT_NUMBER	Sequential numbering of all the packets that are sent out by IBAS. The numbering is different for the different types and also for test and real packets. The numbering sequences are not reset when IBAS restarts
24	24	time	PKT_TIME	UTC of packet generation in the format : YYYY-MM-DDThh:mm:ss.ffff. Not to be confused with the GRB time
48	4	int	ALERT_NUMBER	Incremental number assigned to each (potential) GRB. ALERT_NUMBERs are unique, i.e. IBAS keeps track of counting after each restart. Negative numbers are reserved to test packets (TEST_FLAG=1) generated both before and during operations.
52	4	int	ALERT_SUBNUM	always 0 for PKT_TYPE=3 1,2,...N for PKT_TYPE=4 N+1 (N+2,..) for PKT_TYPE=5
56	8	real	NX_POINT_RA	Direction of the next pointing. Right Ascension (J2000) in degrees of S/C X axis.
64	8	real	NX_POINT_DEC	Direction of the next pointing. Declination (J2000) in degrees of S/C X axis.
72	24	time	NX_POINT_TIME	Start time of the next pointing. UTC in format : YYYY-MM-DDThh:mm:ss.ffff
96	24	time	GRB_TIME	UTC of GRB trigger in the format YYYY-MM-DDThh:mm:ss.ffff . This value can change in packet types 4 and 5 following a more detailed analysis of the data.
120	8	real	GRB_TIME_ERR	accuracy of GRB timing information (seconds). This is usually the sum of the time bin size used for image reconstruction and the propagation delay. It is expected that packets of type 5 (OFFLINE) will be corrected for propagation delays.

offset (bytes)	size (bytes)	type	label	comment
128	8	real	GRB_RA	Right Ascension (J2000) in degrees of derived burst position
136	8	real	GRB_DEC	Declination (J2000) in degrees of derived burst position
144	8	real	GRB_POS_ERR	Radius of error region in arcmin. This should be the TBD% c.l. error, but in practice it is difficult to calibrate it a priori. A circular error region should be valid for all events. If this is not the case, new fields with the corners of the error box will be defined.
152	8	real	GRB_SIGMA	Statistical significance of the GRB detection. Difficult to univocally associate it with a well defined probability, but it should give an idea of the event reality. The exact content and meaning of this field depends on the packet type (and possibly on the value of DET_FLAGS) Details shall be specified later.
160	8	real	GRB_TIMESCALE	Timescale on which the alert was generated. The exact content depends on packet type: Type 2 : light curve binning Types 3,4: SIT or IMIT that triggered Type 5 : a TBD measure of GRB length
168	8	real	POINT_RA	Right Ascension (J2000) in degrees of S/C X axis at the time of the GRB note: current format does not provide roll angle information - this should be added
176	8	real	POINT_DEC	Declination (J2000) in degrees of S/C X axis at the time of the GRB note: current format does not provide roll angle information - this should be added
184	4	int	DET_FLAGS	bit-flags giving some info on the processes that triggered. Exact content is PKT_TYPE dependent and still TBD

offset (bytes)	size (bytes)	type	label	comment
188	4	int	ATT_FLAGS	bit-flags giving info on the satellite status during GRB detection and attitude used in computations Exact content is PKT_TYPE dependent and still TBD.
192	4	int	MULT_POS	In some cases it might happen that more than one position is derived. 0 : if this is the only one or the most likely 1,2,... : for other positions
196	102	string	COMMENT	ASCII string with a comment (if any)
298	100	undef	SPARE	not used
398	2	byte	CRC16	control sum - this sum is computed by **ibasalertd** and checked by ibc_api_listen function.

Note that :

- the total size of each IBAS Alert Packet is exactly 400 bytes.
- all multibyte fields have standard network byte order. The standard network byte order is BIG ENDIAN: the MOST significant byte is sent first (or at the lowest memory address). When constructing packet with alert, before sending it, IBAS converts all fields from host's native byte order into standard network byte order. Applications receiving such packets must do reverse transformation. This is facilitated by using the IBAS Client API library routines that will do the necessary byte swapping.
- real numbers are in IEEE Standard 754 Floating Point format. This format is natively supported by the large majority of systems (including PC's, Macintoshes, SPARCs).
- items in the packet are packed, that is the are no extra spare bytes between them (besides those described in this document).

Some fields in the packet are not used for some packet types. The table below gives details :

label	POINTDIR	SPIACS	WAKEUP	REFINED	OFFLINE
IBAS_ID	X	X	X	X	X
PID	X	X	X	X	X
SEQNUM	X	X	X	X	X
HANDLE	X	X	X	X	X
PKT_TYPE	X	X	X	X	X
TEST_FLAG	X	X	X	X	X
PKT_NUMBER	X	X	X	X	X
PKT_TIME	X	X	X	X	X
ALERT_NUMBER	-	X	X	X	X
ALERT_SUBNUM	-	-	X	X	X
NX_POINT_RA	X	-	-	-	-
NX_POINT_DEC	X	-	-	-	-
NX_POINT_TIME	X	-	-	-	-
GRB_TIME	-	X	X	X	X
GRB_TIME_ERR	-	X	X	X	X
GRB_RA	-	-	X	X	X
GRB_DEC	-	-	X	X	X
GRB_POS_ERR	-	-	X	X	X
GRB_SIGMA	-	X	X	X	X
GRB_TIMESCALE	-	X	X	X	X
POINT_RA	-	-	X	X	X
POINT_DEC	-	-	X	X	X
DET_FLAGS	-	X	X	X	X
ATT_FLAGS	-	X	X	X	X
MULT_POS	-	-	X	X	X
COMMENT	X	X	X	X	X
SPARE	X	X	X	X	X
CRC16	X	X	X	X	X

Bibliography

Akerlof, C., Balsano, R., Barthelemy, S., Bloch, J., Butterworth, P., Casperson, D., Cline, T., Fletcher, S., Frontera, F., Gisler, G., Heise, J., Hills, J., Kehoe, R., Lee, B., Marshall, S., McKay, T., Miller, R., Piro, L., Priedhorsky, W., Szymanski, J., & Wren, J. 1999, Nature, 398, 400

Amati, L., Astone, P., Bassan, M., Bonifazi, P., Carelli, P., Coccia, E., Cosmelli, C., Costa, E., Fafone, V., Feroci, M., Frasca, S., Frontera, F., Longo, F., Mauceli, E., Minenkov, Y., Modena, I., Modestino, G., Moleti, A., Orlandini, M., Pallottino, G. V., Piro, L., Pizzella, G., Preger, B., Salemi, F., Terenzi, R., & Visco, M. 1999, A&AS, 138, 605

Amati, L., Frontera, F., Tavani, M., in't Zand, J. J. M., Antonelli, A., Costa, E., Feroci, M., Guidorzi, C., Heise, J., Masetti, N., Montanari, E., Nicastro, L., Palazzi, E., Pian, E., Piro, L., & Soffitta, P. 2002, A&A, 390, 81

Amati, L., Frontera, F., Vietri, M., in't Zand, J. J. M., Soffitta, P., Costa, E., Del Sordo, S., Pian, E., Piro, L., Antonelli, L. A., Fiume, D. D., Feroci, M., Gandolfi, G., Guidorzi, C., Heise, J., Kuulkers, E., Masetti, N., Montanari, E., Nicastro, L., Orlandini, M., & Palazzi, E. 2000, Science, 290, 953

Antonelli, L. A., Piro, L., Vietri, M., Costa, E., Soffitta, P., Feroci, M., Amati, L., Frontera, F., Pian, E., Zand, J. J. M. i., Heise, J., Kuulkers, E., Nicastro, L., Butler, R. C., Stella, L., & Perola, G. C. 2000, ApJ, 545, L39

Aptekar, R. L., Frederiks, D. D., Golenetskii, S. V., Il'inskii, V. N., Mazets, E. P., Pal'shin, V. D., Butterworth, P. S., & Cline, T. L. 2001, ApJS, 137, 227

Arras, P., Cumming, A., & Thompson, C. 2004, ApJ, 608, L49

Band, D., Matteson, J., Ford, L., Schaefer, B., Palmer, D., Teegarden, B., Cline, T., Briggs, M., Paciesas, W., Pendleton, G., Fishman, G., Kouveliotou, C., Meegan, C., Wilson, R., & Lestrade, P. 1993, ApJ, 413, 281

Barraud, C., Olive, J.-F., Lestrade, J. P., Atteia, J.-L., Hurley, K., Ricker, G., Lamb, D. Q., Kawai, N., Boer, M., Dezalay, J.-P., Pizzichini, G., Vanderspek, R., Crew, G., Doty, J., Monnelly, G., Villasenor, J., Butler, N., Levine, A., Yoshida, A., Shirasaki, Y., Sakamoto, T., Tamagawa, T., Torii, K., Matsuoka, M., Fenimore, E. E., Galassi, M., Tavenner, T., Donaghy, T. Q., Graziani, C., & Jernigan, J. G. 2003, A&A, 400, 1021

Barthelmy, S. 2002, GRB Circular Network, 1529, 1

Barthelmy, S. D., Butterworth, P., Cline, T. L., Gehrels, N., Fishman, G. J., Kouveliotou, C., & Meegan, C. A. 1995, Ap&SS, 231, 235

Bazzano, A. & Paizis, A. 2002, GRB Circular Network, 1706, 1

Beckmann, V., Borkowski, J., Courvoisier, T. J.-L., Götz, D., Hudec, R., Hroch, F., Lund, N., Mereghetti, S., Shaw, S. E., von Kienlin, A., & Wigger, C. 2003, A&A, 411, L327

Berger, E., Kulkarni, S. R., Bloom, J. S., Price, P. A., Fox, D. W., Frail, D. A., Axelrod, T. S., Chevalier, R. A., Colbert, E., Costa, E., Djorgovski, S. G., Frontera, F., Galama, T. J., Halpern, J. P., Harrison, F. A., Holtzman, J., Hurley, K., Kimble, R. A., McCarthy, P. J., Piro, L., Reichart, D., Ricker, G. R., Sari, R., Schmidt, B. P., Wheeler, J. C., Vanderppek, R., & Yost, S. A. 2002, ApJ, 581, 981

Berger, E., Kulkarni, S. R., & Frail, D. A. 2003, ApJ, 590, 379

Berger, E., Thompson, I., & Krzeminski, W. 2004, GRB Circular Network, 2680, 1

Blandford, R. D. & Znajek, R. L. 1977, MNRAS, 179, 433

Bloom, J. S., Frail, D. A., & Kulkarni, S. R. 2003, ApJ, 594, 674

Bloom, J. S., Frail, D. A., & Sari, R. 2001, AJ, 121, 2879

Bloom, J. S., Kulkarni, S. R., & Djorgovski, S. G. 2002a, AJ, 123, 1111

Bloom, J. S., Kulkarni, S. R., Djorgovski, S. G., Eichelberger, A. C., Cote, P., Blakeslee, J. P., Odewahn, S. C., Harrison, F. A., Frail, D. A., Filippenko, A. V., Leonard, D. C., Riess, A. G., Spinrad, H., Stern, D., Bunker, A., Dey, A., Grossan, B., Perlmutter, S., Knop, R. A., Hook, I. M., & Feroci, M. 1999, Nature, 401, 453

Bloom, J. S., Kulkarni, S. R., Price, P. A., Reichart, D., Galama, T. J., Schmidt, B. P., Frail, D. A., Berger, E., McCarthy, P. J., Chevalier, R. A., Wheeler, J. C., Halpern, J. P., Fox, D. W., Djorgovski, S. G., Harrison, F. A., Sari, R., Axelrod, T. S., Kimble, R. A., Holtzman, J., Hurley, K., Frontera, F., Piro, L., & Costa, E. 2002b, ApJ, 572, L45

Boer, M. & Klotz, A. 2003, GRB Circular Network, 2188, 1

Boggs, S. E. & Coburn, W. 2003, ArXiv Astrophysics e-prints

Borgonovo, L. & Ryde, F. 2001, ApJ, 548, 770

Borkowski, J., Götz, D., Mereghetti, S., Deluit, S., & Walter, R. 2003, GRB Circular Network, 1836, 1

Borkowski, J., Mereghetti, S., Cremonesi, D., Aarendt, N., & Götz, D. 2002, IBAS-ADD 2.4, http://isdc.unige.ch/doc/tec/ADD/IBAS/IBAS-2-4/ibas_add-2-4.ps.gz

Brainerd, J. J. 1994, in AIP Conf. Proc. 307: Gamma-Ray Bursts, 346–+

Breitfellner, M. G., Munuera, P., & Martos, A. 2004, GRB Circular Network, 2530, 1

Burenin, R. A., Vikhlinin, A. A., Gilfanov, M. R., Terekhov, O. V., Tkachenko, A. Y., Sazonov, S. Y., Churazov, E. M., Sunyaev, R. A., Goldoni, P., Claret, A., Goldwurm, A., Paul, J., Roques, J. P., Jourdain, E., Pelaez, F., & Vedrenne, G. 1999, A&A, 344, L53

Butler, N., Dullighan, A., Ford, P., Monnelly, G., Ricker, G., Vanderspek, R., Hurley, K., & Lamb, D. 2002, GRB Circular Network, 1415, 1

Castro-Tirado, A. J., Gorosabel, J., Guziy, S., Reverte, D., Castro Cerón, J. M., de Ugarte Postigo, A., Tanvir, N., Mereghetti, S., Tiengo, A., Buckle, J., Sagar, R., Pandey, S. B., Mohan, V., Masetti, N., Mannucci, F., Feltzing, S., Lundstrom, I., Pedersen, H., Riess, C., Trushkin, S., Vílchez, J., Lund, N., Brandt, S., Martínez Núñez, S., Reglero, V., Pérez-Ramírez, M. D., Klose, S., Greiner, J., Hjorth, J., Kaper, L., Pian, E., Palazzi, E., Andersen, M. I., Fruchter, A., Fynbo, J. P. U., Jensen, B. L., Kouveliotou, C., Rhoads, J., Rol, E., Vreeswijk, P. M., Wijers, R. A. M. J., & van den Heuvel, E. 2003, A&A, 411, L315

Cheng, B., Epstein, R. I., Guyer, R. A., & Young, C. 1996, Nature, 382, 518

Chevalier, R. A. & Li, Z. 1999, ApJ, 520, L29

Chornock, R., Foley, R. J., Filippenko, A. V., Papenkova, M., & Weisz, D. 2003, GRB Circular Network, 2131, 1

Cline, D. B., Matthey, C., & Otwinowski, S. 2003, Astroparticle Physics, 18, 531

Cline, T., Frederiks, D. D., Golenetskii, S., Hurley, K., Kouveliotou, C., Mazets, E., & van Paradijs, J. 2000, ApJ, 531, 407

Cobb, B. E., Bailyn, C. D., van Dokkum, P. G., Buxton, M. M., & Bloom, J. S. 2004, ApJ, 608, L93

Coburn, W. & Boggs, S. E. 2003, Nature, 423, 415

Cocchi, M., Bazzano, A., Natalucci, L., Ubertini, P., Heise, J., Kuulkers, E., Muller, J. M., & in't Zand, J. J. M. 2000, A&A, 357, 527

Cohen, E., Katz, J. I., Piran, T., Sari, R., Preece, R. D., & Band, D. L. 1997, ApJ, 488, 330

Colpi, M., Geppert, U., & Page, D. 2000, ApJ, 529, L29

Connaughton, V. 2002, ApJ, 567, 1028

Costa, E., Frontera, F., Heise, J., Feroci, M., in 't Zand, J., Fiore, F., Cinti, M. N., dal Fiume, D., Nicastro, L., Orlandini, M., Palazzi, E., Rapisarda, M., Zavattini, G., Jager, R., Parmar, A., Owens, A., Molendi, S., Cusumano, G., Maccarone, M. C., Giarrusso, S., Coletta, A., Antonelli, L. A., Giommi, P., Muller, J. M., Piro, L., & Butler, R. C. 1997, Nature, 387, 783

Courvoisier, T. J.-L., Walter, R., Beckmann, V., Dean, A. J., Dubath, P., Hudec, R., Kretschmar, P., Mereghetti, S., Montmerle, T., Mowlavi, N., Paltani, S., Preite Martinez, A., Produit, N., Staubert, R., Strong, A. W., Swings, J.-P., Westergaard, N. J., White, N., Winkler, C., & Zdziarski, A. A. 2003, A&A, 411, L53

Covino, S., Lazzati, D., Ghisellini, G., Saracco, P., Campana, S., Chincarini, G., di Serego, S., Cimatti, A., Vanzi, L., Pasquini, L., Haardt, F., Israel, G. L., Stella, L., & Vietri, M. 1999, A&A, 348, L1

De Luca, A., Götz, I., & Campana, S. 2004, GRB Circular Network, 2670, 1

De Pasquale, M., Piro, L., Perna, R., Costa, E., Feroci, M., Gandolfi, G., Zand, J. i., Nicastro, L., Frontera, F., Antonelli, L. A., Fiore, F., & Stratta, G. 2003, ApJ, 592, 1018

Dezalay, J. P., Lestrade, J. P., Barat, C., Talon, R., Sunyaev, R., Terekhov, O., & Kuznetsov, A. 1996, ApJ, 471, L27+

Dickey, J. M. & Lockman, F. J. 1990, ARA&A, 28, 215

Dingus, B. L. & Catelli, J. R. 1998, in Abstracts of the 19th Texas Symposium on Relativistic Astrophysics and Cosmology, held in Paris, France, Dec. 14-18, 1998. Eds.: J. Paul, T. Montmerle, and E. Aubourg (CEA Saclay).

Djorgovski, S. G., Frail, D. A., Kulkarni, S. R., Bloom, J. S., Odewahn, S. C., & Diercks, A. 2001, ApJ, 562, 654

Draine, B. T. 2003, ApJ, 598, 1026

Duncan, R. C. & Thompson, C. 1992a, ApJ, 392, L9

—. 1992b, ApJ, 392, L9

Ehle, M., Gonzalez-Riestra, R., & Gonzalez-Garcia, B. 2004, GRB Circular Network, 2508, 1

Eichler, D., Livio, M., Piran, T., & Schramm, D. N. 1989, Nature, 340, 126

Fenimore, E. E. & Cannon, T. M. 1978, Appl. Opt., 17, 337

Fenimore, E. E., Evans, W. D., Klebesadel, R. W., Laros, J. G., & Terrell, J. 1981, Nature, 289, 42

Fenimore, E. E., in 't Zand, J. J. M., Norris, J. P., Bonnell, J. T., & Nemiroff, R. J. 1995, ApJ, 448, L101+

Fenimore, E. E., Laros, J. G., & Ulmer, A. 1994, ApJ, 432, 742

Fenimore, E. E., Madras, C. D., & Nayakshin, S. 1996, ApJ, 473, 998

Feroci, M., Caliandro, G. A., Massaro, E., Mereghetti, S., & Woods, P. M. 2004, ApJ, 612, 408

Feroci, M., Frontera, F., Costa, E., Amati, L., Tavani, M., Rapisarda, M., & Orlandini, M. 1999, ApJ, 515, L9

Feroci, M., Hurley, K., Duncan, R. C., & Thompson, C. 2001, ApJ, 549, 1021

Feroci, M., Mereghetti, S., Woods, P., Kouveliotou, C., Costa, E., Frederiks, D. D., Golenetskii, S. V., Hurley, K., Mazets, E., Soffitta, P., & Tavani, M. 2003, ApJ, 596, 470

Fishman, G. J., Meegan, C. A., Wilson, R. B., Brock, M. N., Horack, J. M., Kouveliotou, C., Howard, S., Paciesas, W. S., Briggs, M. S., Pendleton, G. N., Koshut, T. M., Mallozzi, R. S., Stollberg, M., & Lestrade, J. P. 1994, ApJS, 92, 229

Ford, L. A., Band, D. L., Matteson, J. L., Briggs, M. S., Pendleton, G. N., Preece, R. D., Paciesas, W. S., Teegarden, B. J., Palmer, D. M., Schaefer, B. E., Cline, T. L., Fishman, G. J., Kouveliotou, C., Meegan, C. A., Wilson, R. B., & Lestrade, J. P. 1995, ApJ, 439, 307

Fox, D. B., Kaplan, D. L., Cenko, B., Kulkarni, S. R., & Nechita, A. 2003a, GRB Circular Network, 2323, 1

Fox, D. W., Yost, S., Kulkarni, S. R., Torii, K., Kato, T., Yamaoka, H., Sako, M., Harrison, F. A., Sari, R., Price, P. A., Berger, E., Soderberg, A. M., Djorgovski, S. G., Barth, A. J., Pravdo, S. H., Frail, D. A., Gal-Yam, A., Lipkin, Y., Mauch, T., Harrison, C., & Buttery, H. 2003b, Nature, 422, 284

Frail, D. A., Kulkarni, S. R., Nicastro, S. R., Feroci, M., & Taylor, G. B. 1997, Nature, 389, 261

Frail, D. A., Kulkarni, S. R., Sari, R., Djorgovski, S. G., Bloom, J. S., Galama, T. J., Reichart, D. E., Berger, E., Harrison, F. A., Price, P. A., Yost, S. A., Diercks, A., Goodrich, R. W., & Chaffee, F. 2001, ApJ, 562, L55

Frail, D. A., Waxman, E., & Kulkarni, S. R. 2000, ApJ, 537, 191

Freedman, D. L. & Waxman, E. 2001, ApJ, 547, 922

Frontera, F., Amati, L., Costa, E., Muller, J. M., Pian, E., Piro, L., Soffitta, P., Tavani, M., Castro-Tirado, A., Dal Fiume, D., Feroci, M., Heise, J., Masetti, N., Nicastro, L., Orlandini, M., Palazzi, E., & Sari, R. 2000, ApJS, 127, 59

Fruchter, A. S., Pian, E., Thorsett, S. E., Bergeron, L. E., González, R. A., Metzger, M., Goudfrooij, P., Sahu, K. C., Ferguson, H., Livio, M., Mutchler, M., Petro, L., Frontera, F., Galama, T., Groot, P., Hook, R., Kouveliotou, C., Macchetto, D., van Paradijs, J., Palazzi, E., Pedersen, H., Sparks, W., & Tavani, M. 1999, ApJ, 516, 683

Fruchter, A. S., Pian, E., Thorsett, S. E., Gonzalez, R., Sahu, K. C., Mutchler, M., Frontera, F., Galama, T. J., Groot, P. J., Hook, R., Kouveliotou, C., Livio, M., Macchetto, F. D., van Paradijs, J., Palazzi, E., Petro, L., & Tavani, M. 1998, in American Institute of Physics Conference Series, 509–+

Fryer, C. L. & Woosley, S. E. 1998, ApJ, 502, L9+

Fryer, C. L., Woosley, S. E., Herant, M., & Davies, M. B. 1999, ApJ, 520, 650

Fynbo, J. P. U., Jakobsson, P., Möller, P., Hjorth, J., Thomsen, B., Andersen, M. I., Fruchter, A. S., Gorosabel, J., Holland, S. T., Ledoux, C., Pedersen, H., Rhoads, J., Weidinger, M., & Wijers, R. A. M. J. 2003, A&A, 406, L63

Fynbo, J. P. U., Möller, P., Thomsen, B., Hjorth, J., Gorosabel, J., Andersen, M. I., Egholm, M. P., Holland, S., Jensen, B. L., Pedersen, H., & Weidinger, M. 2002, A&A, 388, 425

Fynbo, J. U., Jensen, B. L., Gorosabel, J., Hjorth, J., Pedersen, H., Møller, P., Abbott, T., Castro-Tirado, A. J., Delgado, D., Greiner, J., Henden, A., Magazzù, A., Masetti, N., Merlino, S., Masegosa, J., Østensen, R., Palazzi, E., Pian, E., Schwarz, H. E., Cline, T., Guidorzi, C., Goldsten, J., Hurley, K., Mazets, E., McClanahan, T., Montanari, E., Starr, R., & Trombka, J. 2001, A&A, 369, 373

Göğüş , E., Woods, P. M., Kouveliotou, C., van Paradijs, J., Briggs, M. S., Duncan, R. C., & Thompson, C. 1999, ApJ, 526, L93

Göğüş, E., Kouveliotou, C., Woods, P. M., Thompson, C., Duncan, R. C., & Briggs, M. S. 2001, ApJ, 558, 228

Göğüş, E., Woods, P. M., Kouveliotou, C., van Paradijs, J., Briggs, M. S., Duncan, R. C., & Thompson, C. 2000, ApJ, 532, L121

Gal-Yam, A., Fox, D., Berger, E., & Wyatt, P. 2004, GRB Circular Network, 2555, 1

Galama, T. J., Vreeswijk, P. M., van Paradijs, J., Kouveliotou, C., Augusteijn, T., Bohnhardt, H., Brewer, J. P., Doublier, V., Gonzalez, J.-F., Leibundgut, B., Lidman, C., Hainaut, O. R., Patat, F., Heise, J., in 't Zand, J., Hurley, K., Groot, P. J., Strom, R. G., Mazzali, P. A., Iwamoto, K., Nomoto, K., Umeda, H., Nakamura, T., Young, T. R., Suzuki, T., Shigeyama, T., Koshut, T., Kippen, M., Robinson, C., de Wildt, P., Wijers, R. A. M. J., Tanvir, N., Greiner, J., Pian, E., Palazzi, E., Frontera, F., Masetti, N., Nicastro, L., Feroci, M., Costa, E., Piro, L., Peterson, B. A., Tinney, C., Boyle, B., Cannon, R., Stathakis, R., Sadler, E., Begam, M. C., & Ianna, P. 1998, Nature, 395, 670

Garnavich, P. M., Stanek, K. Z., Wyrzykowski, L., Infante, L., Bendek, E., Bersier, D., Holland, S. T., Jha, S., Matheson, T., Kirshner, R. P., Krisciunas, K., Phillips, M. M., & Carlberg, R. G. 2003, ApJ, 582, 924

Gavriil, F. P., Kaspi, V. M., & Woods, P. M. 2002, Nature, 419, 142

Gendre, B., Piro, L., & De Pasquale, M. 2004, ArXiv Astrophysics e-prints, astro-ph/0407613

Ghisellini, G. & Celotti, A. 1999, ApJ, 511, L93

Ghisellini, G., Lazzati, D., & Covino, S. 2001, in Gamma-ray Bursts in the Afterglow Era, 288–+

Ghisellini, G., Lazzati, D., Rossi, E., & Rees, M. J. 2002, A&A, 389, L33

Giblin, T. W., van Paradijs, J., Kouveliotou, C., Connaughton, V., Wijers, R. A. M. J., Briggs, M. S., Preece, R. D., & Fishman, G. J. 1999, ApJ, 524, L47

Goldwurm, A., David, P., Foschini, L., Gros, A., Laurent, P., Sauvageon, A., Bird, A. J., Lerusse, L., & Produit, N. 2003, A&A, 411, L223

Golenetskii, S., Aptekar, R., Mazets, E., Pal'shin, V.and Frederiks, D., & T., C. 2004a, GRB Circular Network, 2769, 1

Golenetskii, S., Aptekar, R., Mazets, E., Pal'Shin, V., Frederiks, D., Cline, T., Rau, A., von Kienlin, A., & Lichti, G. 2004b, GRB Circular Network, 2665, 1

González, M. M., Dingus, B. L., Kaneko, Y., Preece, R. D., Dermer, C. D., & Briggs, M. S. 2003, Nature, 424, 749

Goodman, J. 1997, New Astronomy, 2, 449

Gottesman, S. R. & Fenimore, E. E. 1989, Appl. Opt., 28, 4344

Götz, D., Borkowski, J., & Mereghetti, S. 2003a, GRB Circular Network, 1895, 1

Götz, D. & Mereghetti, S. 2003, in XXII Moriond Astrophysics Meeting, The Gamma Ray Universe, 521, astro-ph/0205071

Götz, D., Mereghetti, S., Beck, M., Borkowski, J., & Mowlavi, N. 2003b, GRB Circular Network, 2459, 1

Götz, D., Mereghetti, S., Beck, M., Borkowski, J., Shaw, S., & Mowlavi, N. 2004a, GRB Circular Network, 2525, 1

Götz, D., Mereghetti, S., Beck, M., & Mirabel, F. 2003c, GRB Circular Network, 2408, 1

—. 2003d, GRB Circular Network, 2419, 1

Götz, D., Mereghetti, S., Borkowski, J., Beck, M., & Shaw, S. 2004b, GRB Circular Network, 2560, 1

Götz, D., Mereghetti, S., Hurley, K., Deluit, S., Feroci, M., Frontera, F., Fruchter, A., Gorosabel, J., Hartmann, D. H., Hjorth, J., Hudec, R., Mirabel, I. F., Pian, E., Pizzichini, G., Ubertini, P., & Winkler, C. 2003e, A&A, 409, 831

Götz, D., Mereghetti, S., & Mirabel, F. 2004c, GRB Circular Network, 2764, 1

—. 2004d, GRB Circular Network, 2760, 1

Götz, D., Mereghetti, S., Mirabel, I. F., & Hurley, K. 2004e, A&A, 417, L45

Götz, D., Mereghetti, S., Mirabel, I. F., Hurley, K., Brandt, S., Lund, N., Ubertini, P., Del Santo, M., Costa, E., Feroci, M., Castro-Tirado, A., Gimenez, A., Atteia, J. ., Boer, M., Cline, T., Frontera, F., Pizzichini, G., von Kienlin, A., Gougus, E., Kouveliotou, C., Finger, M., Thompson, C., Pedersen, H., & van der Klis, M. 2004f, ArXiv Astrophysics e-prints, astro-ph/0405135

Götz, D., Mereghetti, S., & Mowlavi, N. 2004g, GRB Circular Network, 2690, 1

Götz, D., Mereghetti, S., Mowlavi, n., Borkowski, J., & Beck, M. 2004h, GRB Circular Network, 2634, 1

—. 2004i, GRB Circular Network, 2640, 1

Granot, J., Piran, T., & Sari, R. 1999, ApJ, 513, 679

Gros, A., Goldwurm, A., Cadolle-Bel, M., Goldoni, P., Rodriguez, J., Foschini, L., Del Santo, M., & Blay, P. 2003, A&A, 411, L179

Guetta, D. & Granot, J. 2003, Physical Review Letters, 90, 201103

Guetta, D., Piran, T., & Waxman, E. 2003, ArXiv Astrophysics e-prints, astro-ph/0311488

Harrison, F. A., Bloom, J. S., Frail, D. A., Sari, R., Kulkarni, S. R., Djorgovski, S. G., Axelrod, T., Mould, J., Schmidt, B. P., Wieringa, M. H., Wark, R. M., Subrahmanyan, R., McConnell, D., McCarthy, P. J., Schaefer, B. E., McMahon, R. G., Markze, R. O., Firth, E., Soffitta, P., & Amati, L. 1999, ApJ, 523, L121

Heise, J., in't Zand, J., Kippen, R. M., & Woods, P. M. 2001, in Gamma-ray Bursts in the Afterglow Era, 16–+

Heyl, J. S. & Hernquist, L. 1998, MNRAS, 300, 599

Heyl, J. S. & Kulkarni, S. R. 1998, ApJ, 506, L61

Hjorth, J., Sollerman, J., Møller, P., Fynbo, J. P. U., Woosley, S. E., Kouveliotou, C., Tanvir, N. R., Greiner, J., Andersen, M. I., Castro-Tirado, A. J., Castro Cerón, J. M., Fruchter, A. S., Gorosabel, J., Jakobsson, P., Kaper, L., Klose, S., Masetti, N., Pedersen, H., Pedersen, K., Pian, E., Palazzi, E., Rhoads, J. E., Rol, E., van den Heuvel, E. P. J., Vreeswijk, P. M., Watson, D., & Wijers, R. A. M. J. 2003, Nature, 423, 847

Hurley, K. 1994, Nature, 372, 652

Hurley, K. 2000, in AIP Conf. Proc. 526: Gamma-ray Bursts, 5th Huntsville Symposium, 763–+

Hurley, K., Berger, E., Castro-Tirado, A., Castro Cerón, J. M., Cline, T., Feroci, M., Frail, D. A., Frontera, F., Masetti, N., Guidorzi, C., Montanari, E., Hartmann, D. H., Henden, A., Levine, S. E., Mazets, E., Golenetskii, S., Frederiks, D., Morrison, G., Oksanen, A., Moilanen, M., Park, H.-S., Price, P. A., Prochaska, J., Trombka, J., & Williams, G. 2002a, ApJ, 567, 447

Hurley, K., Cline, T., Mazets, E., Barthelmy, S., Butterworth, P., Marshall, F., Palmer, D., Aptekar, R., Golenetskii, S., Il'Inskii, V., Frederiks, D., McTiernan, J., Gold, R., & Trombka, J. 1999a, Nature, 397, 41

Hurley, K., Cline, T., Mazets, E., & Golenetskii, S. 2003a, GRB Circular Network, 2414, 1

Hurley, K., Cline, T., Mitrofanov, I., Anfimov, D., Kozyrev, A., Litvak, M., Sanin, A., Boynton, W., Fellows, C., Harshman, K., Shinohara, C., & Starr, R. 2002b, GRB Circular Network, 1727, 1

Hurley, K., Cline, T., Mitrofanov, I., Anfimov, D., Kozyrev, A., Litvak, M., Sanin, A., Boynton, W., Fellows, C., Harshman, K., Shinohara, C., Starr, R., Mazets, E., & Golenetskii, S. 2002c, GRB Circular Network, 1728, 1

Hurley, K., Cline, T., Mitrofanov, I., Anfimov, D., Kozyrev, A., Litvak, M., Sanin, A., Boynton, W., Fellows, C., Harshman, K., Shinohara, C., Starr, R., Ricker, G., Atteia, J.-L., Kawai, N., Lamb, D., Woosley, S., Doty, J., Vanderspek, R., Villasenor, J., Crew, G., Monnelly, G., Butler, N., Jernigan, J. G., Levine, A., Martel, F., Morgan, E., Prigozhin, G., Braga, J., Manchanda, R., Pizzichini, G., Shirasaki, Y., Graziani, C., Matsuoka, M., Tamagawa, T., Torii, K., Sakamoto, T., Yoshida, A., Fenimore, E., Galassi, M., Tavenner, T., Donaghy, T., Boer, M., Olive, J.-F., & Dezalay, J.-P. 2002d, GRB Circular Network, 1402, 1

Hurley, K., Kouveliotou, C., Woods, P., Cline, T., Butterworth, P., Mazets, E., Golenetskii, S., & Frederics, D. 1999b, ApJ, 510, L107

Hurley, K., Sari, R., & Djorgovski, S. G. 2003b, ArXiv Astrophysics e-prints, astro-ph/0211620

Ibrahim, A. I., Strohmayer, T. E., Woods, P. M., Kouveliotou, C., Thompson, C., Duncan, R. C., Dieters, S., Swank, J. H., van Paradijs, J., & Finger, M. 2001, ApJ, 558, 237

Iwamoto, K., Mazzali, P. A., Nomoto, K., Umeda, H., Nakamura, T., Patat, F., Danziger, I. J., Young, T. R., Suzuki, T., Shigeyama, T., Augusteijn, T., Doublier, V., Gonzalez, J.-F., Boehnhardt, H., Brewer, J., Hainaut, O. R., Lidman, C., Leibundgut, B., Cappellaro, E., Turatto, M., Galama, T. J., Vreeswijk, P. M., Kouveliotou, C., van Paradijs, J., Pian, E., Palazzi, E., & Frontera, F. 1998, Nature, 395, 672

Jones, P. B. 2003, ApJ, 595, 342

Königl, A. & Granot, J. 2002, ApJ, 574, 134

Kaplan, D. L., Fox, D. W., Kulkarni, S. R., Gotthelf, E. V., Vasisht, G., & Frail, D. A. 2002, ApJ, 564, 935

Kaspi, V. M., Gavriil, F. P., Woods, P. M., Jensen, J. B., Roberts, M. S. E., & Chakrabarty, D. 2003, ApJ, 588, L93

Katz, J. I. & Piran, T. 1997, ApJ, 490, 772

Kehoe, R., Akerlof, C., Balsano, R., Barthelmy, S., Bloch, J., Butterworth, P., Casperson, D., Cline, T., Fletcher, S., Gisler, G., Hurley, K., Kippen, M., Lee, B., Marshall, S., McKay, T., Rykoff, E., Smith, D., Vestrand, T., & Wren, J. 2001, ApJ, 554, L159

Kippen, R. M., Woods, P. M., Heise, J., in't Zand, J., Preece, R. D., & Briggs, M. 2002, APS Meeting Abstracts, 6003

Klebesadel, R. W., Strong, I. B., & Olson, R. A. 1973, ApJ, 182, L85+

Klotz, A., Boër, M., & Atteia, J. L. 2003, A&A, 404, 815

Kouveliotou, C., Eichler, D., Woods, P. M., Lyubarsky, Y., Patel, S. K., Göğüş, E., van der Klis, M., Tennant, A., Wachter, S., & Hurley, K. 2003, ApJ, 596, L79

Kouveliotou, C., Koshut, T., Briggs, M. S., Pendleton, G. N., Meegan, C. A., Fishman, G. J., & Lestrade, J. P. 1996, in American Institute of Physics Conference Series, 42–+

Kouveliotou, C., Meegan, C. A., Fishman, G. J., Bhat, N. P., Briggs, M. S., Koshut, T. M., Paciesas, W. S., & Pendleton, G. N. 1993, ApJ, 413, L101

Kulkarni, S. R., Frail, D. A., Wieringa, M. H., Ekers, R. D., Sadler, E. M., Wark, R. M., Higdon, J. L., Phinney, E. S., & Bloom, J. S. 1998, Nature, 395, 663

Kumar, P. 2000, ApJ, 538, L125

Kumar, P. & Piran, T. 2000, ApJ, 535, 152

Labanti, C., Di Cocco, G., Ferro, G., Gianotti, F., Mauri, A., Rossi, E., Stephen, J. B., Traci, A., & Trifoglio, M. 2003, A&A, 411, L149

Lamb, D., Graziani, C., Shirasaki, Y., Atteia, J. L., Barraud, C., Hurley, K., Crew, G., Kawai, N., Ricker, G., & Woosley, S. 2003, GRB Circular Network, 2351, 1

Lamb, D. Q. & Reichart, D. E. 2000, ApJ, 536, 1

Laros, J. G., Fenimore, E. E., Klebesadel, R. W., Atteia, J.-L., Boer, M., Hurley, K., Niel, M., Vedrenne, G., Kane, S. R., Kouveliotou, C., Cline, T. L., Dennis, B. R., Desai, U. D., Orwig, L. E., Kuznetsov, A. V., Sunyaev, R. A., & Terekhov, O. V. 1987, ApJ, 320, L111

Lazzati, D., Covino, S., & Ghisellini, G. 2002, MNRAS, 330, 583

Lazzati, D., Rossi, E., Ghisellini, G., & Rees, M. J. 2004, MNRAS, 347, L1

Lebrun, F., Leray, J. P., Lavocat, P., Crétolle, J., Arquès, M., Blondel, C., Bonnin, C., Bouère, A., Cara, C., Chaleil, T., Daly, F., Desages, F., Dzitko, H., Horeau, B., Laurent, P., Limousin, O., Mathy, F., Mauguen, V., Meignier, F., Molinié, F., Poindron, E., Rouger, M., Sauvageon, A., & Tourrette, T. 2003, A&A, 411, L141

Lenters, G. T., Woods, P. M., Goupell, J. E., Kouveliotou, C., Göğüş, E., Hurley, K., Frederiks, D., Golenetskii, S., & Swank, J. 2003, ApJ, 587, 761

Li, W., Filippenko, A. V., Chornock, R., & Jha, S. 2003, ApJ, 586, L9

Liang, E. & Kargatis, V. 1996, Nature, 381, 49

Lin, R. P., Dennis, B. R., Hurford, G. J., Smith, D. M., Zehnder, A., Harvey, P. R., Curtis, D. W., Pankow, D., Turin, P., Bester, M., Csillaghy, A., Lewis, M., Madden, N., van Beek, H. F., Appleby, M., Raudorf, T., McTiernan, J., Ramaty, R., Schmahl, E., Schwartz, R., Krucker, S., Abiad, R., Quinn, T., Berg, P., Hashii, M., Sterling, R., Jackson, R., Pratt, R., Campbell, R. D., Malone, D., Landis, D., Barrington-Leigh, C. P., Slassi-Sennou, S., Cork, C., Clark, D., Amato, D., Orwig, L., Boyle, R., Banks, I. S., Shirey, K., Tolbert, A. K., Zarro, D., Snow, F., Thomsen, K., Henneck, R., Mchedlishvili, A., Ming, P., Fivian, M., Jordan, J., Wanner, R., Crubb, J., Preble, J., Matranga, M., Benz, A., Hudson, H., Canfield, R. C., Holman, G. D., Crannell, C., Kosugi, T., Emslie, A. G., Vilmer, N., Brown, J. C., Johns-Krull, C., Aschwanden, M., Metcalf, T., & Conway, A. 2002, Sol. Phys., 210, 3

Lipunov, V. M., Postnov, K. A., & Prokhorov, M. E. 2001, Astronomy Reports, 45, 236

Lithwick, Y. & Sari, R. 2001, ApJ, 555, 540

Lund, N., Budtz-Jørgensen, C., Westergaard, N. J., Brandt, S., Rasmussen, I. L., Hornstrup, A., Oxborrow, C. A., Chenevez, J., Jensen, P. A., Laursen, S., Andersen, K. H., Mogensen, P. B., Rasmussen, I., Omø, K., Pedersen, S. M., Polny, J.,

Andersson, H., Andersson, T., Kämäräinen, V., Vilhu, O., Huovelin, J., Maisala, S., Morawski, M., Juchnikowski, G., Costa, E., Feroci, M., Rubini, A., Rapisarda, M., Morelli, E., Carassiti, V., Frontera, F., Pelliciari, C., Loffredo, G., Martínez Núñez, S., Reglero, V., Velasco, T., Larsson, S., Svensson, R., Zdziarski, A. A., Castro-Tirado, A., Attina, P., Goria, M., Giulianelli, G., Cordero, F., Rezazad, M., Schmidt, M., Carli, R., Gomez, C., Jensen, P. L., Sarri, G., Tiemon, A., Orr, A., Much, R., Kretschmar, P., & Schnopper, H. W. 2003, A&A, 411, L231

Lyubarsky, Y., Eichler, D., & Thompson, C. 2002, ApJ, 580, L69

Lyubarsky, Y. E. 2002, MNRAS, 332, 199

Lyutikov, M. 2003, MNRAS, 346, 540

MacFadyen, A. I. & Woosley, S. E. 1999, ApJ, 524, 262

Magliocchetti, M., Ghirlanda, G., & Celotti, A. 2003, MNRAS, 343, 255

Malaguti, G., Bazzano, A., Beckmann, V., Bird, A. J., Del Santo, M., Di Cocco, G., Foschini, L., Goldoni, P., Götz, D., Mereghetti, S., Paizis, A., Segreto, A., Skinner, G., Ubertini, P., & von Kienlin, A. 2003, A&A, 411, L307

Malesani, D., Tagliaferri, G., Chincarini, G., Covino, S., Della Valle, M., Fugazza, D., Mazzali, P. A., Zerbi, F. M., D'Avanzo, P., Kalogerakos, S., Simoncelli, A., Antonelli, L. A., Burderi, L., Campana, S., Cucchiara, A., Fiore, F., Ghirlanda, G., Goldoni, P., Götz, D., Mereghetti, S., Mirabel, I. F., Romano, P., Stella, L., Minezaki, T., Yoshii, Y., & Nomoto, K. 2004, ApJ, 609, L5

Mallozzi, R. S., Paciesas, W. S., Pendleton, G. N., Briggs, M. S., Preece, R. D., Meegan, C. A., & Fishman, G. J. 1995, ApJ, 454, 597

Mallozzi, R. S., Pendleton, G. N., Paciesas, W. S., Preece, R. D., & Briggs, M. S. 1998, in American Institute of Physics Conference Series, 273–+

Marsden, D. & White, N. E. 2001, ApJ, 551, L155

Mas-Hesse, J. M., Giménez, A., Culhane, J. L., Jamar, C., McBreen, B., Torra, J., Hudec, R., Fabregat, J., Meurs, E., Swings, J. P., Alcacera, M. A., Balado, A., Beiztegui, R., Belenguer, T., Bradley, L., Caballero, M. D., Cabo, P., Defise, J. M., Díaz, E., Domingo, A., Figueras, F., Figueroa, I., Hanlon, L., Hroch, F., Hudcova, V., García, T., Jordan, B., Jordi, C., Kretschmar, P., Laviada, C., March, M., Martín, E., Mazy, E., Menéndez, M., Mi, J. M., de Miguel, E., Muñoz, T., Nolan, K., Olmedo, R., Plesseria, J. Y., Polcar, J., Reina, M., Renotte, E., Rochus, P., Sánchez, A., San Martín, J. C., Smith, A., Soldan, J., Thomas, P., Timón, V., & Walton, D. 2003, A&A, 411, L261

Masetti, N., Palazzi, E., Rol, E., Pian, E., & Pompei, E. 2004, GRB Circular Network, 2515, 1

Matheson, T., Garnavich, P. M., Stanek, K. Z., Bersier, D., Holland, S. T., Krisciunas, K., Caldwell, N., Berlind, P., Bloom, J. S., Bolte, M., Bonanos, A. Z., Brown, M. J. I., Brown, W. R., Calkins, M. L., Challis, P., Chornock, R., Echevarria, L., Eisenstein, D. J., Everett, M. E., Filippenko, A. V., Flint, K., Foley, R. J., Freedman, D. L., Hamuy, M., Harding, P., Hathi, N. P., Hicken, M., Hoopes, C., Impey, C., Jannuzi, B. T., Jansen, R. A., Jha, S., Kaluzny, J., Kannappan, S., Kirshner, R. P., Latham, D. W., Lee, J. C., Leonard, D. C., Li, W., Luhman, K. L., Martini, P., Mathis, H., Maza, J., Megeath, S. T., Miller, L. R., Minniti, D., Olszewski, E. W., Papenkova, M., Phillips, M. M., Pindor, B., Sasselov, D. D., Schild, R., Schweiker, H., Spahr, T., Thomas-Osip, J., Thompson, I., Weisz, D., Windhorst, R., & Zaritsky, D. 2003, ApJ, 599, 394

Mazets, E. P., Aptekar, R. L., Butterworth, P. S., Cline, T. L., Frederiks, D. D., Golenetskii, S. V., Hurley, K., & Il'Inskii, V. N. 1999a, ApJ, 519, L151

Mazets, E. P., Cline, T. L., Aptekar', R. L., Butterworth, P. S., Frederiks, D. D., Golenetskii, S. V., Il'Inskii, V. N., & Pal'Shin, V. D. 1999b, Astronomy Letters, 25, 635

Mazets, E. P., Golentskii, S. V., Ilinskii, V. N., Aptekar, R. L., & Guryan, I. A. 1979, Nature, 282, 587

Mazzali, P. A., Deng, J., Tominaga, N., Maeda, K., Nomoto, K., Matheson, T., Kawabata, K. S., Stanek, K. Z., & Garnavich, P. M. 2003, ApJ, 599, L95

McBreen, S., Quilligan, F., McBreen, B., Hanlon, L., & Watson, D. 2001, A&A, 380, L31

Meegan, C. A., Fishman, G. J., Wilson, R. B., Horack, J. M., Brock, M. N., Paciesas, W. S., Pendleton, G. N., & Kouveliotou, C. 1992, Nature, 355, 143

Mereghetti, S., Cremonesi, D., Feroci, M., & Tavani, M. 2000, A&A, 361, 240

Mereghetti, S., Cremonesi, D. I., & Borkowski, J. 2001, in ESA SP-459: Exploring the Gamma-Ray Universe, 513–+

Mereghetti, S., Götz, D., Beck, M., & Borkowski, J. 2004a, GRB Circular Network, 2551, 1

—. 2004b, GRB Circular Network, 2613, 1

Mereghetti, S., Götz, D., Beck, M., Borkowski, J., & Shaw, S. 2004c, GRB Circular Network, 2505, 1

Mereghetti, S., Götz, D., Beck, M., & Mirabel, F. 2003a, GRB Circular Network, 2415, 1

Mereghetti, S., Götz, D., Beck, M., Shaw, S., Lubinski, P., & Borkowski, J. 2004d, GRB Circular Network, 2670, 1

Mereghetti, S., Götz, D., Beckmann, V., von Kienlin, A., Ubertini, P., Bazzano, A., Foschini, L., & Malaguti, G. 2003b, A&A, 411, L311

Mereghetti, S., Götz, D., Borkowski, J., Beck, M., Shaw, S., & Walter, R. 2004e, GRB Circular Network, 2572, 1

Mereghetti, S., Götz, D., Borkowski, J., Beck, M., von Kienlin, A., & Lund, N. 2004f, ArXiv Astrophysics e-prints, astro-ph/0404019

Mereghetti, S., Götz, D., Borkowski, J., Paizis, A., Beckmann, V., & Turler, M. 2003c, GRB Circular Network, 1941, 1

Mereghetti, S., Götz, D., Borkowski, J., Shaw, S., & Courvoisier, T. 2003d, GRB Circular Network, 2183, 1

Mereghetti, S., Götz, D., Borkowski, J., Walter, R., & Pedersen, H. 2003e, A&A, 411, L291

Mereghetti, S., Götz, D., Borkowski, J.and Beck, M., & Mirabel, F. 2004g, GRB Circular Network, 2763, 1

Mereghetti, S., Götz, D., & Borkowsky, J. 2002, GRB Circular Network, 1766, 1

Mereghetti, S., Götz, D., & Hurley, K. 2003f, GRB Circular Network, 2377, 1

Mereghetti, S., Götz, D., Mowlavi, N., Shaw, S., & Hurley, K. 2004h, GRB Circular Network, 2647, 1

Mereghetti, S., Götz, D., Tiengo, A., Beckmann, V., Borkowski, J., Courvoisier, T. J.-L., von Kienlin, A., Schoenfelder, V., Roques, J. P., Bouchet, L., Ubertini, P., Castro-Tirado, A., Lebrun, F., Paul, J., Lund, N., Mas-Hesse, J. M., Hermsen, W., Hartog, P. R. d., & Winkler, C. 2003g, ApJ, 590, L73

Metzger, M. R., Djorgovski, S. G., Kulkarni, S. R., Steidel, C. C., Adelberger, K. L., Frail, D. A., Costa, E., & Frontera, F. 1997, Nature, 387, 878

Molkov, S., Hurley, K., Lutovinov, A., & Sunyaev, R. 2004, The Astronomer's Telegram, 325, 1

Moran, L., Mereghetti, S., Götz, D., Hanlon, L., von Kienlin, A., McBreen, B., Tiengo, A., Preece, R., Williams, O. R., Bennet, K., Kippen, R. M., McBreen, S., & McGlynn, S. 2004, A&A, 333, 333

Murakami, T., Tanaka, Y., Kulkarni, S. R., Ogasaka, Y., Sonobe, T., Ogawara, Y., Aoki, T., & Yoshida, A. 1994, Nature, 368, 127

Nakar, E. & Piran, T. 2002, MNRAS, 331, 40

—. 2003, ApJ, 598, 400

Nakar, E., Piran, T., & Granot, J. 2003, New Astronomy, 8, 495

Narayan, R., Paczynski, B., & Piran, T. 1992, ApJ, 395, L83

Narayan, R., Piran, T., & Kumar, P. 2001, ApJ, 557, 949

Neckel, T., Klare, G., & Sarcander, M. 1980, A&AS, 42, 251

Norris, J. P., Marani, G. F., & Bonnell, J. T. 2000, ApJ, 534, 248

Norris, J. P., Nemiroff, R. J., Bonnell, J. T., Scargle, J. D., Kouveliotou, C., Paciesas, W. S., Meegan, C. A., & Fishman, G. J. 1996, ApJ, 459, 393

Olive, J.-F., Hurley, K., Dezalay, J.-P., Atteia, J.-L., Barraud, C., Butler, N., Crew, G. B., Doty, J., Ricker, G., Vanderspek, R., Lamb, D. Q., Kawai, N., Yoshida, A., Shirasaki, Y., Sakamoto, T., Tamagawa, T., Torii, K., Matsuoka, M., Fenimore, E. E., Galassi, M., Tavenner, T., Donaghy, T. Q., & Graziani, C. 2003, in AIP Conf. Proc. 662: Gamma-Ray Burst and Afterglow Astronomy 2001: A Workshop Celebrating the First Year of the HETE Mission, 82–87

Paczynski, B. 1991, Acta Astronomica, 41, 257

—. 1992, Acta Astronomica, 42, 145

—. 1998, ApJ, 494, L45+

Panaitescu, A. & Kumar, P. 2001, ApJ, 560, L49

Patel, S., Kouveliotou, C., Mereghetti, S., Gotz, D., Lund, N., Chenevez, J., Ubertini, P., Levan, A., van den Heuvel, E., & Hurley, K. 2004, GRB Circular Network, 2655, 1

Pendleton, G. N., Paciesas, W. S., Briggs, M. S., Mallozzi, R. S., Koshut, T. M., Fishman, G. J., Meegan, C. A., Wilson, R. B., Harmon, A. B., & Kouveliotou, C. 1994, ApJ, 431, 416

Pendleton, G. N., Paciesas, W. S., Briggs, M. S., Preece, R. D., Mallozzi, R. S., Meegan, C. A., Horack, J. M., Fishman, G. J., Band, D. L., Matteson, J. L., Skelton, R. T., Hakkila, J., Ford, L. A., Kouveliotou, C., & Koshut, T. M. 1997, ApJ, 489, 175

Pian, E., Amati, L., Antonelli, L. A., Butler, R. C., Costa, E., Cusumano, G., Danziger, J., Feroci, M., Fiore, F., Frontera, F., Giommi, P., Masetti, N., Muller, J. M., Nicastro, L., Oosterbroek, T., Orlandini, M., Owens, A., Palazzi, E., Parmar, A., Piro, L., in't Zand, J. J. M., Castro-Tirado, A., Coletta, A., Dal Fiume, D., Del Sordo, S., Heise, J., Soffitta, P., & Torroni, V. 2000, ApJ, 536, 778

Pian, E., Giommi, P., Amati, L., Costa, E., Danziger, J., Feroci, M., Fiocchi, M. T., Frontera, F., Kouveliotou, K., Masetti, N., Nicastro, L., & Palazzi, E. 2003, ArXiv Astrophysics e-prints, astro-ph/0304521

Piran, T. 2004, ArXiv Astrophysics e-prints, astro-ph/0405503

Piran, T., Kumar, P., Panaitescu, A., & Piro, L. 2001, ApJ, 560, L167

Piro, L. 2001, in Gamma-ray Bursts in the Afterglow Era, 97–+

Piro, L. 2004, ArXiv Astrophysics e-prints, astro-ph/0402638

Piro, L., Amati, L., Antonelli, L. A., Butler, R. C., Costa, E., Cusumano, G., Feroci, M., Frontera, F., Heise, J., in 't Zand, J. J. M., Molendi, S., Muller, J., Nicastro, L., Orlandini, M., Owens, A., Parmar, A. N., Soffitta, P., & Tavani, M. 1998, A&A, 331, L41

Piro, L., Frail, D. A., Gorosabel, J., Garmire, G., Soffitta, P., Amati, L., Andersen, M. I., Antonelli, L. A., Berger, E., Frontera, F., Fynbo, J., Gandolfi, G., Garcia, M. R., Hjorth, J., Zand, J. i., Jensen, B. L., Masetti, N., Møller, P., Pedersen, H., Pian, E., & Wieringa, M. H. 2002, ApJ, 577, 680

Piro, L., Garmire, G., Garcia, M., Stratta, G., Costa, E., Feroci, M., Mészáros, P., Vietri, M., Bradt, H., Frail, D., Frontera, F., Halpern, J., Heise, J., Hurley, K., Kawai, N., Kippen, R. M., Marshall, F., Murakami, T., Sokolov, V. V., Takeshima, T., & Yoshida, A. 2000, Science, 290, 955

Potekhin, A. Y. & Yakovlev, D. G. 2001, A&A, 374, 213

Preece, R. D., Briggs, M. S., Giblin, T. W., Mallozzi, R. S., Pendleton, G. N., Paciesas, W. S., & Band, D. L. 2002, ApJ, 581, 1248

Preece, R. D., Briggs, M. S., Mallozzi, R. S., Pendleton, G. N., Paciesas, W. S., & Band, D. L. 1998, ApJ, 506, L23

—. 2000, ApJS, 126, 19

Price, P. A., Fox, D. W., Kulkarni, S. R., Peterson, B. A., Schmidt, B. P., Soderberg, A. M., Yost, S. A., Berger, E., Djorgovski, S. G., Frail, D. A., Harrison, F. A., Sari, R., Blain, A. W., & Chapman, S. C. 2003, Nature, 423, 844

Ramirez-Ruiz, E. & Fenimore, E. E. 2000, ApJ, 539, 712

Reeves, J. N., Watson, D., Osborne, J. P., Pounds, K. A., O'Brien, P. T., Short, A. D. T., Turner, M. J. L., Watson, M. G., Mason, K. O., Ehle, M., & Schartel, N. 2002, Nature, 416, 512

Reglero, V., Sánchez, F., Rodrigo, J., Velasco, T., Gasent, J. L., Chato, R., Alamo, J., Burgos, J. A., Suso, J., Blay, P., Martínez, S., Doñate, M., Reina, M., Sabau, D., Ruiz-Urien, I., Santos, I., Zarauz, J., & Vázquez, J. 2001, in ESA SP-459: Exploring the Gamma-Ray Universe, 619–622

Reichart, D. E. 1999, ApJ, 521, L111

Reichart, D. E. & Price, P. A. 2002, ApJ, 565, 174

Rhoads, J. E. 1999, ApJ, 525, 737

Rideout, R. M. & Skinner, G. K. 1996, A&AS, 120, 579

Rossi, E., Lazzati, D., & Rees, M. J. 2002, MNRAS, 332, 945

Ruderman, M. 1975, New York Academy Sciences Annals, 262, 164

Rutledge, R. E. & Fox, D. B. 2004, MNRAS, 350, 1288

Rutledge, R. E. & Sako, M. 2003, MNRAS, 339, 600

Sakamoto, T., Lamb, D. Q., Graziani, C., Donaghy, T. Q., Suzuki, M., Ricker, G., Atteia, J., Kawai, N., Yoshida, A., Shirasaki, Y., Tamagawa, T., Torii, K., Matsuoka, M., Fenimore, E. E., Galassi, M., Doty, J., Vanderspek, R., Crew, G. B., Villasenor, J., Butler, N., Prigozhin, G., Jernigan, J. G., Barraud, C., Boer, M., Dezalay, J., Olive, J., Hurley, K., Levine, A., Monnelly, G., Martel, F., Morgan, E., Woosley, S. E., Cline, T., Braga, J., Manchanda, R., Pizzichini, G., Takagishi, K., & Yamauchi, M. 2004, ArXiv Astrophysics e-prints, astro-ph/0409128

Sako, M., Harrison, F., & Rutledge, R. 2004, ArXiv Astrophysics e-prints, astro-ph/0406210

Sari, R. & Piran, T. 1997, ApJ, 485, 270

Sari, R., Piran, T., & Halpern, J. P. 1999, ApJ, 519, L17

Sari, R., Piran, T., & Narayan, R. 1998, ApJ, 497, L17+

Sazonov, S., Lutovinov, A., & Sunyaev, R. 2004, Nature, 430, 646

Shaviv, N. J. & Dar, A. 1995, ApJ, 447, 863

Shemi, A. 1994, MNRAS, 269, 1112

Skinner, G. 1995, Experimental Astronomy, 6, 1

Skinner, G. & Connell, P. 2003, A&A, 411, L123

Soderberg, A. M., Kulkarni, S. R., Berger, E., Fox, D. W., Sako, M., Frail, D. A., Gal-Yam, A., Moon, D. S., Cenko, S. B., Yost, S. A., Phillips, M. M., Persson, S. E., Freedman, W. L., Wyatt, P., Jayawardhana, R., & Paulson, D. 2004, Nature, 430, 648

Soderberg, A. M., Price, P. A., Fox, D. W., Kulkarni, S. R., Djorgovski, S. G., Berger, E., Harrison, F., Yost, S., Hamuy, M., Shectman, S., Mirabal, N., & Halpern, J. 2002, GRB Circular Network, 1554, 1

Sommer, M., Bertsch, D. L., Dingus, B. L., Fichtel, C. E., Fishman, G. J., Harding, A. K., Hartman, R. C., Hunter, S. D., Hurley, K., Kanbach, G., Kniffen, D. A., Kouveliotou, C., Lin, Y. C., Mattox, J. R., Mayer-Hasselwander, H. A., Michelson, P. F., von Montigny, C., Nolan, P. L., Schneid, E., Sreekumar, P., & Thompson, D. J. 1994, ApJ, 422, L63

Stanek, K. Z., Garnavich, P. M., Kaluzny, J., Pych, W., & Thompson, I. 1999, ApJ, 522, L39

Stanek, K. Z., Matheson, T., Garnavich, P. M., Martini, P., Berlind, P., Caldwell, N., Challis, P., Brown, W. R., Schild, R., Krisciunas, K., Calkins, M. L., Lee, J. C., Hathi, N., Jansen, R. A., Windhorst, R., Echevarria, L., Eisenstein, D. J., Pindor, B., Olszewski, E. W., Harding, P., Holland, S. T., & Bersier, D. 2003, ApJ, 591, L17

Strüder, L., Briel, U., Dennerl, K., Hartmann, R., Kendziorra, E., Meidinger, N., Pfeffermann, E., Reppin, C., Aschenbach, B., Bornemann, W., Bräuninger, H., Burkert, W., Elender, M., Freyberg, M., Haberl, F., Hartner, G., Heuschmann, F., Hippmann, H., Kastelic, E., Kemmer, S., Kettenring, G., Kink, W., Krause, N., Müller, S., Oppitz, A., Pietsch, W., Popp, M., Predehl, P., Read, A., Stephan, K. H., Stötter, D., Trümper, J., Holl, P., Kemmer, J., Soltau, H., Stötter, R., Weber, U., Weichert, U., von Zanthier, C., Carathanassis, D., Lutz, G., Richter, R. H., Solc, P., Böttcher, H., Kuster, M., Staubert, R., Abbey, A., Holland, A., Turner, M., Balasini, M., Bignami, G. F., La Palombara, N., Villa, G., Buttler, W., Gianini, F., Lainé, R., Lumb, D., & Dhez, P. 2001, A&A, 365, L18

Strohmayer, T. E., Fenimore, E. E., Murakami, T., & Yoshida, A. 1998, ApJ, 500, 873

Taylor, G. B., Frail, D. A., & Fox, D. 2001, GRB Circular Network, 1122, 1

Terrell, J., Evans, W. D., Klebesadel, R. W., & Laros, J. G. 1980, Nature, 285, 383

Thompson, C. & Duncan, R. C. 1995, MNRAS, 275, 255

—. 1996, ApJ, 473, 322

—. 2001, ApJ, 561, 980

Thompson, C., Lyutikov, M., & Kulkarni, S. R. 2002, ApJ, 574, 332

Tiengo, A., Mereghetti, S., & de Luca, A. 2004, GRB Circular Network, 2548, 1

Totani, T. 1997, ApJ, 486, L71+

Trümper, J. & Schönfelder, V. 1973, A&A, 25, 445

Turner, M. J. L., Abbey, A., Arnaud, M., Balasini, M., Barbera, M., Belsole, E., Bennie, P. J., Bernard, J. P., Bignami, G. F., Boer, M., Briel, U., Butler, I., Cara, C., Chabaud, C., Cole, R., Collura, A., Conte, M., Cros, A., Denby, M., Dhez, P., Di Coco, G., Dowson, J., Ferrando, P., Ghizzardi, S., Gianotti, F., Goodall, C. V., Gretton, L., Griffiths, R. G., Hainaut, O., Hochedez, J. F., Holland, A. D., Jourdain, E.,

Kendziorra, E., Lagostina, A., Laine, R., La Palombara, N., Lortholary, M., Lumb, D., Marty, P., Molendi, S., Pigot, C., Poindron, E., Pounds, K. A., Reeves, J. N., Reppin, C., Rothenflug, R., Salvetat, P., Sauvageot, J. L., Schmitt, D., Sembay, S., Short, A. D. T., Spragg, J., Stephen, J., Strüder, L., Tiengo, A., Trifoglio, M., Trümper, J., Vercellone, S., Vigroux, L., Villa, G., Ward, M. J., Whitehead, S., & Zonca, E. 2001, A&A, 365, L27

Ubertini, P., Lebrun, F., Di Cocco, G., Bazzano, A., Bird, A. J., Broenstad, K., Goldwurm, A., La Rosa, G., Labanti, C., Laurent, P., Mirabel, I. F., Quadrini, E. M., Ramsey, B., Reglero, V., Sabau, L., Sacco, B., Staubert, R., Vigroux, L., Weisskopf, M. C., & Zdziarski, A. A. 2003, A&A, 411, L131

Usov, V. V. 1992, Nature, 357, 472

van Paradijs, J., Groot, P. J., Galama, T., Kouveliotou, C., Strom, R. G., Telting, J., Rutten, R. G. M., Fishman, G. J., Meegan, C. A., Pettini, M., Tanvir, N., Bloom, J., Pedersen, H., Nordgaard-Nielsen, H. U., Linden-Vornle, M., Melnick, J., van der Steene, G., Bremer, M., Naber, R., Heise, J., in 't Zand, J., Costa, E., Feroci, M., Piro, L., Frontera, F., Zavattini, G., Nicastro, L., Palazzi, E., Bennet, K., Hanlon, L., & Parmar, A. 1997, Nature, 386, 686

van Putten, M. H. P. M. & Levinson, A. 2001, ApJ, 555, L41

Vaughan, S., Willingale, R., O'Brien, P. T., Osborne, J. P., Reeves, J. N., Levan, A. J., Watson, M. G., Tedds, J. A., Watson, D., Santos-Lleó, M., Rodríguez-Pascual, P. M., & Schartel, N. 2004, ApJ, 603, L5

Vedrenne, G., Roques, J.-P., Schönfelder, V., Mandrou, P., Lichti, G. G., von Kienlin, A., Cordier, B., Schanne, S., Knödlseder, J., Skinner, G., Jean, P., Sanchez, F., Caraveo, P., Teegarden, B., von Ballmoos, P., Bouchet, L., Paul, P., Matteson, J., Boggs, S., Wunderer, C., Leleux, P., Weidenspointner, G., Durouchoux, P., Diehl, R., Strong, A., Cassé, M., Clair, M. A., & André, Y. 2003, A&A, 411, L63

Vietri, M. & Stella, L. 1998, ApJ, 507, L45

—. 1999, ApJ, 527, L43

von Kienlin, A., Beckmann, V., Covino, S., Götz, D., Lichti, G. G., Malesani, D., Mereghetti, S., Molinari, E., Rau, A., Shrader, C. R., Sturner, S. J., & Zerbi, F. 2003a, A&A, 411, L321

von Kienlin, A., Beckmann, V., Rau, A., Arend, N., Bennett, K., McBreen, B., Connell, P., Deluit, S., Hanlon, L., Hurley, K., Kippen, M., Lichti, G. G., Moran, L., Preece, R., Roques, J.-P., Schönfelder, V., Skinner, G., Strong, A., & Williams, R. 2003b, A&A, 411, L299

Watson, D., Hjorth, J., Levan, A., Jakobsson, P., O'Brien, P. T., Osborne, J. P., Pedersen, K., Reeves, J. N., Tedds, J. A., Vaughan, S. A., Ward, M. J., & Willingale, R. 2004, ApJ, 605, L101

Watson, D., Reeves, J. N., Hjorth, J., Jakobsson, P., & Pedersen, K. 2003, ApJ, 595, L29

Watson, D., Reeves, J. N., Osborne, J., O'Brien, P. T., Pounds, K. A., Tedds, J. A., Santos-Lleó, M., & Ehle, M. 2002, A&A, 393, L1

Waxman, E. 1997, ApJ, 485, L5+

Wijers, R. A. M. J., Bloom, J. S., Bagla, J. S., & Natarajan, P. 1998, MNRAS, 294, L13

Wijers, R. A. M. J. & Galama, T. J. 1999, ApJ, 523, 177

Winkler, C., Courvoisier, T. J.-L., Di Cocco, G., Gehrels, N., Giménez, A., Grebenev, S., Hermsen, W., Mas-Hesse, J. M., Lebrun, F., Lund, N., Palumbo, G. G. C., Paul, J., Roques, J.-P., Schnopper, H., Schönfelder, V., Sunyaev, R., Teegarden, B., Ubertini, P., Vedrenne, G., & Dean, A. J. 2003, A&A, 411, L1

Woods, P. M., Kouveliotou, C., Göğüş, E., Finger, M. H., Feroci, M., Mereghetti, S., Swank, J. H., Hurley, K., Heise, J., Smith, D., Frontera, F., Guidorzi, C., & Thompson, C. 2003, ApJ, 596, 464

Woods, P. M., Kouveliotou, C., Göğüş, E., Finger, M. H., Swank, J., Smith, D. A., Hurley, K., & Thompson, C. 2001, ApJ, 552, 748

Woods, P. M., Kouveliotou, C., Gogus, E., Patel, S., Hurley, K., & Swank, J. 2004, The Astronomer's Telegram, 313, 1

Woods, P. M., Kouveliotou, C., van Paradijs, J., Briggs, M. S., Hurley, K., Göğüş, E., Preece, R. D., Giblin, T. W., Thompson, C., & Duncan, R. C. 1999a, ApJ, 527, L47

Woods, P. M., Kouveliotou, C., van Paradijs, J., Hurley, K., Kippen, R. M., Finger, M. H., Briggs, M. S., Dieters, S., & Fishman, G. J. 1999b, ApJ, 519, L139

Woods, P. M. & Thompson, C. 2004, ArXiv Astrophysics e-prints, astro-ph/0406133

Woosley, S. E. 1993, ApJ, 405, 273

Yakovlev, D. G., Kaminker, A. D., Gnedin, O. Y., & Haensel, P. 2001, Phys. Rep., 354, 1

Yoshida, A., Namiki, M., Otani, C., Kawai, N., Murakami, T., Ueda, Y., Shibata, R., & Uno, S. 1999, A&AS, 138, 433

Zhang, B. & Mészáros, P. 2002, ApJ, 571, 876